Tor Arne Hammer

Deformations, strain capacity and cracking of concrete in plastic and early hardening phases

Thesis for the degree doctor philosophiae

Trondheim, November 2007

Norwegian University of Science and Technology
Faculty of Engineering Science and Technology
Department of Structural Engineering

NTNU

NTNU
Norwegian University of Science and Technology

Thesis for the degree doctor philosophiae

Faculty of Engineering Science and Technology
Department of Structural Engineering

ISBN 978-82-471-5191-4 (printed version)
ISBN 978-82-471-5207-2 (electronic version)
ISSN 1503-8181

Doctoral theses at NTNU, 2007:234

Printed by NTNU-trykk

Executive summary and conclusions

Field observation reveals that cracking of free concrete surfaces in the period before and during setting, may appear at two basically different ages: Minutes after surface finishing, here called "**plastic phase**" and at some hours after surface finishing, here called "**early hardening phase**". This has been verified by tests in the present work by investigating the deformations and strain capacities in both phases, as well as the crack initiation and propagation.

In the **plastic phase**, the rate of water evaporation relative to the permeability of the concrete (i.e. the ability to transport water to the surface) is the dominating factor. It follows that the "critical" evaporation rate decreases with decreasing permeability, e.g. concretes with relatively low permeability, i.e. with relatively low water-to-powder ratios (like HSC and SCC) have low critical rates.

When the evaporation rate is high relative to the permeability, an important point is the very early formation of capillary tension of pore water (meniscus system) at the surface, which appears as a skin formation. It results in shrinkage of the skin ("plastic shrinkage"), but probably more important, in very low strain capacity of the skin. The latter suggests that deformations caused by differential settlement (as results of reinforcement bars or cross section shifts) and even relatively small external deformations (e.g. formwork movement) may then result in cracking. Furthermore, the skin formation, and thus high cracking risk, may in practise appear before any curing aid is applied.

It is suggested that cracks initiate by emptying of surface cavities (or coarse surface pores): Such cavities will empty (if not already empty) before the pores between the cement grains. Then, there is no meniscus left to restrain the cavities, and they will open as the shrinkage continues.

The fact that both deformation and strain capacity are result of capillary tension of the pore water, suggests that pore water pressure (e.g. as measured in the present work) can be used as a single measure to assess the cracking risk in the plastic phase.

Cracking in the **early hardening phase**, may be assessed as for hardened concrete, e.g. from the stress-tensile strength ratio, where the stress is result of the restrained drying shrinkage and thermal dilation (autogenous shrinkage may contribute in very low w/b systems).

A promising methodology has been developed to measure deformation, tensile strain capacity, stress generation and tensile strength evolution in the early hardening phase, and the results confirm that the period is critical for cracking. It is shown that the deformation of surfaces in this period caused by moderate drying (here exposed to 20 ºC and 50 % RH) combined with a moderate cooling (here approximately 5 °C), generate restraining stress that may exceed the tensile strength, and thus, generate failure.

Trondheim, 1 November 2007

Acknowledgement

This work was made possible by the funding from the Research Council of Norway and the financial and professional support form the partners of the NOR-IPACS project: Selmer ASA (now Skanska Norge AS), Elkem ASA Materials, Fesil ASA, the Norwegian Public Roads Administration, Norcem AS and the professional support from NTNU (the Norwegian Institute of Science and Technology) as well as the suppleness and encouragement of my employer, SINTEF.

I am sincerely grateful to Erik J. Sellevold for his always presence for discussions, catching enthusiasm and fruitful critique. I want to give a special gratitude to Øyvind Bjøntegaard for excellent co-operation and to Ove Loraas for the lab. assistance and help in constructing experimental equipment, and to Harald Justnes for the many professional discussions.
And thanks to Odny for being so patient …..

Summary

Background, aim and strategy
Experience has revealed that concretes with relative low water to binder ratios, commonly referred to as high strength concrete or high performance concrete (HSC or HPC), are susceptible to cracking in the early ages. This is particularly true for large horizontal surfaces (e.g. bridge decks) in the time before and during setting in particular, commonly referred to as "**plastic cracking**."

There are a number of investigations on the measurement of plastic shrinkage as driving force for cracking. However, I have found few investigations, on the tensile strain capacity and on fundamental approaches to understand crack propagation. These conclude that the tensile strain capacity is very high in the first hours of age and that it goes through a minimum value in the period around final set. This appears to be in disagreement with practical experience and other investigations on qualitative studies of plastic shrinkage cracking, which say that cracking may occur minutes after placing/finishing. In fact, field observation reveals that cracking may appear at two basically different ages: Minutes after surface finishing, here called "**plastic phase**" and at some hours after surface finishing, here called "**early hardening phase**". Furthermore, the inconsistency that cracking apparently occurred regardless of curing procedures underlines the need for more fundamental studies of the problem.

The aim of the present work was to contribute to understanding the mechanism(s) of cracking of horizontal surfaces in the period between placing/finishing and early hardening of the concrete, and HSC/HPC/SCC in particular. A specific aim is to explain the apparent disagreement between results from field experience and qualitative studies as mentioned above.

The work includes identification of measurable concrete properties influencing the risk of "plastic shrinkage cracking" as well as development of experimental systems to measure these properties. Also, it includes identification of the important mix design parameters and investigation of the influence of exposure conditions.

The present fundamental approach to the cracking problem is to separate the issue into the dual concept of "load and capacity". The load is the strain or stress generated by deformations in the concrete, and the capacity is the tensile strain capacity or tensile strength of the concrete.

Driving forces to cracking
The driving forces to cracking in the plastic and early hardening age are deformations caused by self generated **volume change** and any **externally imposed deformation**. The latter may originate from unwanted movement of the concrete after placing/finishing caused by e.g. formwork movement (settlement, vibration, etc.) or from gentle flow of a sloping slab (e.g. parking places, bridge decks, road pavements) which may occur if the concrete has high viscosity and low yield shear strength. The volume change that appears after casting is mainly result of:

- autogenous deformation, AD, (resulting from chemical shrinkage, CS),
- evaporation and
- temperature changes

The volume change is basically a volumetric deformation, but from a practical point of view it is convenient to consider linear deformations, commonly referred to as “plastic settlement” and “plastic shrinkage”. The shrinkage-settlement ratio changes basically from 0 to 1 in the period, as the stiffness of the paste changes from that of a liquid to that of a solid in the hardening age (with isotropic properties).

Evaporation is the most important driving force. A meniscus system forms at the top surface when evaporation rate exceeds bleeding rate. It results in capillary tension in the pore water which appears as contraction forces between the particles resulting in increased settlement and shrinkage. This is a geometry controlled system which means that the deformation rate increases with decreasing spacing between particles at a given evaporation rate. It follows that w/b and fineness of the particle system are the important material parameters (and more important than the chemistry of the binder).

An important point is the very early formation of capillary tension and subsequent shrinkage at the top surface, which appears as a skin formation, which typically occurs in systems where the permeability is low (e.g. low w/b) relative to the evaporation rate. This may be “the driving force” for cracking in the liquid phase.

The early age as considered here, is divided in three consecutive phases:

1. “**Liquid phase”**: Until formation of mineral skeleton caused by the hydration, or until formation of a meniscus system formed by evaporation, i.e. until paste/mortar/concrete can support its own weight (point of self-support, PSS). It is the phase when AD equals chemical shrinkage, CS, and manifests it self in settlement, only (i.e. no horizontal deformation).

2. **“Semi-liquid phase”**: Until significant stiffness starts to develop, i.e. around initial setting time. The start of the phase is associated with time when pore water pressure becomes tension and horizontal deformation (shrinkage) starts to develop. The phase coincides probably with the time when the paste/mortar/concrete can be brought back to liquid phase with agitation.

3. **“Early hardening phase”**: Through final setting and the following few hours. The phase is associated with significant stiffness development and minimum strain capacity of the hardening paste/mortar/concrete.

Liquid phase plus semi-liquid phase equals plastic phase.

AD may constitute the main contributor to settlement (the only one if there is no air expulsion, bleeding, evaporation or thermal dilation). The rate of AD is of course influenced by the hydration rate of the cement and by the use of accelerating or retarding admixtures, but the paste (and cement) composition is considered to be of minor importance with respect to AD as driving force to cracking in the liquid phases, because of the dominating influence of evaporation.

Later, in the semi-liquid phase, when the hydration has created a skeleton with stiffness that needs a higher force than that caused by gravity to collapse, AD becomes significantly lower

than CS and new empty pore space occurs as expansion of existing air voids and/or formation of new pores. Accordingly, the settlement rate is significantly reduced. This diversion point appears to occur much earlier in linear test methods than in the widely used volumetric "condom test method". The reason can be that CS generates a vacuum effect in the condom, which constitutes an additional force to the gravitational force, and which therefore results in compaction for a longer time. The surrounding air in the linear test, releases the vacuum effect and allows water to suck in from the surface (i.e. emptying of surface pores as the "formation of new empty pore space"). It follows that linear (and non air tight) measurement is better suited for evaluation of the practical consequence of AD, i.e. on settlement of equivalent mortars or concretes. Deviation point from condom test may be used as a rough measure for final setting time of pastes (but the relation to Vicat-measure is not clear).

AD is often expansion in the semi-liquid phase and early hardening phase (seen in both settlement and "shrinkage") caused by re-absorption of bleed water/chemical reactions (which of course contributes to reduce cracking tendency). The expansion is seldom observed in condom-test (probably because it is overshadowed by the vacuum effect). Air voids in the paste (e.g. formed by the use of air entraining admixture) seems to increase AD in the liquid phase. It is suggested, but not verified, that the reasons could be lower stiffness of the pastes with air and/or capillary tension of pore water caused by menisci formed by the air voids. Anyway, AD is considered not to be an important contributor to the driving force to cracking in the semi-liquid phase either, because it is small relative to strain capacity and other deformations. But AD may be an important contributor to contraction in the early hardening age of mortars or concretes with very low w/b-ratios, because the strain capacity then is very low, independent of degree of evaporation.

Temperature changes may influence evaporation and give thermal deformation: If the concrete surface is insufficiently protected, decreasing temperature of surrounding air may contribute to increased evaporation. It is because the vapour pressure decreases with temperature, and thus, results in larger difference between the vapour pressure of the surrounding air and that over the pore water meniscus. And opposite, a lower concrete temperature than air temperature reduces evaporation. Thermal contraction is particularly important in the early hardening age, when the tensile strain capacity is at its minimum.

Experimental system for testing of deformations and pore water pressure

The "Dilation Rig" is built on a triple 100 mm cube mould of steel, which makes preparation, testing and demoulding simple. The height and thickness when used for concrete is 100 mm and the length is 280 mm. The dimension is a compromise, i.e. small enough for easy handling, but still large enough to represent a concrete body. The friction is prevented by the use of two plastic sheets with talk powder in between, between the concrete and the mould.

The shrinkage is measured as the horizontal movement of two "nails" placed centric in both ends of the specimen. The settlement is measured as the vertical movement of two circular plastic meshes with diameter of 50 mm, placed on the top surface. The pore water pressure is measured by a pressure transducer connected to a water filled tube with inner diameter of 3 mm. Two tubes are placed vertically in the concrete with the ends normally at 5 mm and 50 mm depths, respectively. Wind may be applied by the use of a fan connected to a channel. The whole system is placed on a balance in order to determine the evaporation in test with drying. Hence, deformations, pore water pressure, evaporation and temperature can be measured on the same sample. This is important because there is a consistent relationship between these measures, which is used to verify the individual results.

Experimental system for testing of strain capacity
The "Tension Rig" was constructed based on a previously developed design in Japan. The equipment is simple, in principle; a direct tension test of a supported body with easy deformation application and load recording. The length of the specimen is 490 mm and the square cross section is 100 mm in the area of deformation measurement, which is equal to the cross section in the companion deformation rig.

The rig consists of one base frame with displacement and loading device, and four moulds which can easily be pushed in and pulled out of the frame. The end plates have grips made of threaded steel bolts 100 mm in length, and it is connected to the load cell by two ball bolts, with an adjustable tension rod in between, to minimize the influence of any eccentricities. The deformation is applied on both sides, using step motors with controllers to control the deformation rate, and which is connected to the loads cells via linear bearings. The deformation is recorded over 200 mm on the middle of the specimen, with the use of two inductive displacement transducers (IDT), in a rack fixed to the base frame. During testing, the IDTs are connected to 1x10x100 mm steel plates in the concrete.

The system gives load-deformation correlation until ultimate load (failure). In the plastic phase however, the stiffness is still to low to generate significant load. The strain at first crack, is then determined visually by observing the surface during testing at a given strain rate (ε/unit time) and record the time (t) at which the first crack appears. Then, the strain capacity (ε_t) can be calculated simply as (ε/unit time) · (t).

Crack risk assessment
The work confirms that there are two critical periods for plastic cracking. The two periods "**Plastic phase"** and "**Early hardening phase"** was investigated separately. The load (deformation) has the same origin in the two periods, but the strain capacity and the cracking mechanisms seem to be basically different.

In the **plastic phase**, the strain capacity seems to be related to whether or not the meniscus system has been established: If not established (i.e. if evaporation rate is lower than bleeding rate), the concrete acts like a liquid and the strain capacity is then "infinite". If established (i.e. if evaporation rate exceeds bleeding rate) the concrete seems to act like a stiff body with a very low strain capacity (probably in the order of magnitude of 100 μstrain). This is probably because the geometry controlled meniscus system means that the particles are locked in position and can not move more than that caused by the evaporation. If any external deformation is applied, or if the body it is restrained during the evaporation, the body is prone to crack. Cracks probably initiate at inhomogeneities, like cavities and aggregate-paste interfaces where the menisci-particle structure is "weak" and may act as wall effect.

If the permeability of the mass is sufficiently low to prevent water flow to the surface, the surface will dry faster and form a stiff body (skin) on top, with a liquid beneath. This may happen during the first minutes of drying, and is probably the main reason why low permeable systems (i.e. low water to powder ratio systems like in HSC and SCC) are more vulnerable to such cracking.

Since pore water measurement easily reveals when the menisci system occur, it is a good tool in the assessment cracking risk in the "plastic age".

A promising methodology has been developed to measure deformation, tensile strain capacity, stress generation and tensile strength evolution, in order to assess the risk of cracking in the **early hardening phase**.

It is shown that the deformation of surfaces in this period caused by moderate drying (here exposed to 20 ºC and 50 % RH) combined with a moderate cooling (here approximately 5 °C), generate restraining stress that may exceed the tensile strength, and thus, generate failure. The influence of mix design was not investigated explicitly, and I think it is still a question if a reduction of w/b makes the concrete more vulnerable to cracking in this period. It is however, definitely yes if the w/b is very low, because autogenous shrinkage then may contribute to the stress generating contraction. Use of shrinkage reducing admixtures, internal curing (e.g. LWA) and air pores may contribute to reduce the shrinkage in both these cases.

The results indicate that crack risk assessment from stress/strength is more reliable than using strain/strain capacity.

Table of Contents

Executive Summary and Conclusions

Acknowledgement

Summary

1. Introduction 1
1.1 Background and motivation 1
1.2 Aim and limitation of this work 2

2. Fundamental Approach and Strategy 3
Plastic Age 3
Early Hardening Age 4

3. Deformations - the Driving Forces to Cracking 5
3.1 Introduction 5
3.2 Autogenous deformation of paste - origin, significance and testing 6
3.2.1 Origin and significance 6
3.2.2 Measuring techniques for volume change of cement based pastes 6
3.2.3 Chemical shrinkage versus autogenous deformation – transition from a liquid to a solid 11
3.2.4 Influence of bleeding 17
3.3 Autogenous deformation - influence of paste composition 20
3.3.1 General 20
3.3.2 Influence of cement type 20
3.3.3 Influence of w/c 23
3.3.4 Influence of silica fume and fly ash 24
3.3.5 Influence of admixtures 24
3.3.6 Influence of air voids 25
3.3.7 Influence of aggregates 28
3.3.8 Conclusion – influence of paste composition on early age autogenous deformation 28
3.4 Volume change caused by evaporation 30
3.4.1 General 30
3.4.2 Influence of permeability 32
3.5 Volume change due to temperature changes 32
3.6 Summary - the driving forces to cracking 34

4. Development of Experimental System for Testing of Settlement, Shrinkage, Pore Water Pressure and Water loss due to Evaporation 37
4.1 Introduction and test systems found in the literature 37
4.2 Requirements and Description 40
4.3 Repeatability 43
4.3.1 General 43
4.3.2 Evaporation rate 44
4.3.3 Temperature evolution 46
4.3.4 Settlement 47
4.3.5 Shrinkage 53
4.3.6 Pore water pressure 56

4.3.7 Relationship between the measures 59
4.3.8 Conclusion – repeatability 71

5. Deformations - influence of mix design and execution 73
5.1 General 73
5.2 Influence of w/b 73
5.2.1 Sealed condition 73
5.2.2 Exposed to 50 % RH (0 m/s) 75
5.2.3 Conclusion – influence of w/b on deformations 81
5.3 Influence of cement type 82
5.3.1 Exposed to 50 % RH and 0 m/s 82
5.3.2 Exposed to 50 % RH and 5 m/s 87
5.4 Influence of water reducing admixtures 90
5.5 Influence of silica fume 94
5.6 Influence of shrinkage reducing admixture (SRA) 98
5.7 Influence of internal water source 101
5.8 Influence of air content 105
5.9 Self compacting concrete 108
5.10 Influence of initial concrete temperature 112

6. Tensile Strain and Stress Capacity: State-of-the-art, Test Methods and Hypothesis. 116
6.1 State-of-the-art and white spots 116
6.2 Influence of drying on strain and stress capacity 122
6.3 Test methods 123

7. Development of the "Tension Rig" - for Testing of Strain Capacity and Tensile Strength 127
7.1 Basis and design 127
7.2 Deformation and Load Control 130
7.2.1 Deformation 130
7.2.2 Load 133
7.3 Friction 134
7.4 Casting and testing procedure 136
7.5 Stress/strain 137
7.6 Summary 139

8. Crack Risk Assessment in the Plastic Age 140
8.1 Determination of strain capacity 140
8.2 Tests 142
8.2.1 Tension tests 142
8.2.2 Tests on restrained specimens 143
8.2.3 Conclusion 144

9. Crack Risk Assessment in the Early Hardening Age 147
9.1 General 147
9.2 Influence of autogenous deformation 147
9.3 Influence of drying and cooling 150
9.3.1 Experimental program 150
9.3.2 Testing 150
9.4 Results and discussion 152
9.4.1 Setting time 152
9.4.2 Uniaxial Tensile Strength and Strain Capacity 152
9.4.3 Deformation 154

9.4.4 Stress generation 154
9.5 Conclusion 156
10. References 157

APPENDIX Materials and Recipes

1. Introduction

1.1 Background and motivation

Both national and international experience have revealed that concretes commonly referred to as high strength or high performance concrete (HSC or HPC), i.e. with relatively low water/binder ratios, are susceptible to cracking in the early ages. This is particularly true for large horizontal surfaces (e.g. bridge decks) in the initial phase (before and during setting) in particular, commonly referred to as "**plastic cracking**."

The field experience from bridge construction in Norway concerning early age cracking of this kind of concrete in the period between 1989 and 1993 has been summarised by Kompen (1994). His final remarks were:

> *"The plastic cracking phenomenon is regarded the most serious problem met in using low w/b-ratio concrete. There are serious worries that this phenomenon will jeopardise the quality improvements intended by the use of low w/b concretes.*
>
> *By observation in the field and fullscale trials a lot of experience has been gained on how to reduce cracking to a more acceptable level. Understanding of the mechanisms involved has, however, not reached such a level that this cracking can be completely avoided in every construction work. Consequently, it is strongly recommended that research should continue on early age cracking problem, to develop both basic understanding and practical measures."*

It should be added that the Public Roads Administration have now developed, despite all the setbacks met, a casting/curing/protection procedure that practically eliminates plastic cracking of bridge decks (communication with Kompen, 2006). The topic has gained new interest recently, as self-compacting concrete (SCC) seems to be susceptible to plastic cracking.

A literature survey on plastic shrinkage and plastic shrinkage induced cracks has been performed by Radocea in 1992. He concluded that even if it has been investigated by many researchers the last decades, no generally accepted theory could be found in the literature. This is confirmed by the literature reviewed in the present work.

There are a large number of investigations on qualitative studies of plastic shrinkage cracking in terms of visual observation of crack propagation, often combined with measurement of evaporation. Many tests have been performed using a method developed at NTNU/SINTEF by Johansen and Dahl (1993) (NORDTEST-method NT Build 433), where wind is blown over a fresh concrete surface restrained between two concentric steel rings. The results on the effects of w/b, the cement type, paste content, amount and type of plasticizers + superplasticizers and aggregate grading seems to correspond well with the practical experience (Kompen, 1994 and Bjøntegaard et al, 1998). However, such results alone are not sufficient to contribute significantly to the fundamental understanding of the problem (Bjøntegaard et al, 1998).

Also, there are a number of investigations on the measurement of plastic shrinkage as driving force for cracking, but there are very few investigations on the tensile strain capacity and on

fundamental approaches to understand crack propagation. They conclude that the tensile strain capacity is very high in the first hours of age and that it goes through a minimum value in the period around final set. This appears to be in disagreement with the conclusion of Kompen (1994) and in other investigations on qualitative studies of plastic shrinkage cracking, which say that cracking often occurs minutes after placing/ finishing.

Another field observation is that cracking may appear at two basically different ages (Kompen, 1994): Minutes after surface finishing, and at some hours after surface finishing.

Furthermore, the observation that cracking may occur apparently regardless of curing procedures demonstrates the need of more fundamental studies of the problem.

1.2 Aim and limitation of this work

The aim is to contribute to understanding the mechanism(s) of cracking in the period between placing/finishing and early hardening of horizontal surface of concrete, and HSC/HPC/SCC in particular. A specific aim is to explain the apparent disagreement between results from field experience and qualitative studies concluding that cracking often occurs minutes after placing/finishing, and results from stress/strain tests that the tensile strain capacity is very high, and thus, not detrimental with respect to cracking in the same time period.

The work includes identification of the concrete properties influencing the risk of cracking and development of an experimental system for determination of these properties. Also, it includes identification of the important mix design and execution parameters.

2. Fundamental Approach and Strategy

The present fundamental approach to the cracking problem is to separate the issue into the dual concept of "load and capacity". The load is the strain or stress generated by deformations in the concrete, and the capacity is the tensile strain capacity or tensile strength of the concrete.

The work is divided in four main tasks:

1. To identify deformation types and their relative importance. Since the deformations originate as volume change in the cement based paste, this part of the work was mainly concentrated on cement pastes. How volume change manifests itself in linear deformation (settlement and horizontal length change) over time is considered, as are the influences of admixtures and aggregates used in concretes (chapter 3). This work consists of both literature survey and own experiments.

2. To find suitable test methods for determination of deformations and tensile strain capacity of concrete (chapters 4, 6 and 7). This work includes both literature survey and own experiments.

3. To investigate the influences of some important material properties and of exposure conditions on deformations of typical Norwegian concretes (chapter 5). This work is mainly own experiments.

4. To investigate the influence of exposure conditions on the tensile strain capacity and crack initiation (chapters 8 and 9). This work is mainly own experiments.

Task 4 was split in two since the experience shows that cracking may appear during two different ages (Kompen, 1994):

- Minutes after surface finishing, i.e. when the concrete is still **plastic**
- Several hours after surface finishing, i.e. in period of setting/**early hardening**

The load (deformations) was considered to have the same origin in the two periods. But the capacity and cracking mechanism were considered to be basically different, and therefore investigated separately for the two periods "**Plastic age"** and "**Early hardening age"** (chapters 8 and 9). The approach to investigate the two is given here:

Plastic Age

The phenomenon of plastic shrinkage was described by Wittmann (1976): If the rate of evaporation exceeds the rate of bleeding, the concrete surface dries out and water menisci form near the surface. This leads to capillary tension of pore water, and thus, contraction forces between particles. Since capillary tension of pore water is considered a fundamental parameter in plastic shrinkage, the tests were supported by pore water pressure measurements (PWP), see section 4.3.6.

An important conclusion from field experience of HSC was that cracking occurred, apparently, even if the surface was applied "best practice" protection against evaporation (Kompen, 1994). The **first step** was, therefore, to investigate the deformations and strain

capacity under moisture sealed conditions or moderate drying conditions (which can simulate the consequence of the small evaporation that may occur in spite best practice protection).

Results from the first step confirmed that the tensile strain capacity, defined as strain at maximum stress, in moisture sealed conditions is very high for HSC as it is for NSC in the first hours of age. They also showed that the deformations of the concretes in the same period were considerably lower than the strain capacity, and thus, harmless with respect to cracking, see chapters 5 and 8. Any externally imposed deformations (i.e. unwanted movement of formwork or flow of concrete), is also considered to be harmless relative to the high strain capacity.

These conclusions do not comply with the experience saying that "cracking occurred irrespective of procedure" (Kompen, 1994). It suggests that "the best curing practice" is not always sufficient to prevent external drying. The **second step** was therefore to investigate deformations under exposure to drying, see chapter 5. The results showed that the deformations were still rather small compared with the tensile strain capacity measured under sealed conditions. It suggests that the strain capacity is also influenced by drying, since cracks do occur.

The **third step** was therefore to find the strain capacity of HSC when exposed to drying. At first, no influence of external drying was observed, as the load-deformation curves were not significantly changed from those found at sealed condition, see chapter 8. But eye observations of the surface revealed hair cracks shortly after start of the test corresponding to a strain of less than $200 \cdot 10^{-6}$, only, see chapter 8.

Early Hardening Age

The strategy was to identify deformations in the period, and then demonstrate that such deformations are large enough to act as driving forces to cracking, by testing the stress generation in a fully restraint concrete, and compare it with the measured tensile strength.

The experimental work is based on a family of concretes that were developed and used in the Norwegian joint industry projects with financial support from the Norwegian Research Council, "NOR-IPACS" (1996 – 2000) and "NOR-CRACK" (2000 - 2004) of which the present work was a part. The "basic" concrete is a typical Norwegian concrete for marine bridges (w/b = 0.40). Recipes and information about the material used are given in the APPENDIX.

3. Deformations - the Driving Forces to Cracking

3.1 Introduction

The driving forces are deformations caused by self generated **volume change** and any **externally imposed deformation**. The latter may originate from unwanted movement of the concrete after placing/finishing caused by e.g. formwork movement (settlement, vibration, etc.) or from gentle flow of a sloping slab (e.g. parking places, bridge decks, road pavements) which may occur if the concrete has high viscosity and low yield shear strength. The influence of these other sources is briefly discussed together with the discussion of strain capacity.

The volume change in the plastic and early hardening age is the sum of:

- Autogenous deformation (AD) resulting from chemical shrinkage (CS)
- Air expulsion
- Bleeding water on the top surface (acting in the plastic age)
- Water loss driven by evaporation (in addition to any bleed water)
- Deformation caused by re-absorption of bleed water (acting in late plastic age and in early hardening age)
- Thermal dilation due to heat of hydration and/or external sources

I consider the role of air evacuation to be of less importance in the time beyond finishing of the surface. I.e. I assume that the expulsing occurs under agitation, i.e. under mixing, transportation and casting. The other driving forces are discussed in following sections.

Except for thermal dilation, the volume change of aggregate is considered to be insignificant here. However, aggregate may have some secondary effects: Aggregate particles may constitute internal water reservoirs, and the fines may influence bleeding. Therefore, the various volume changes listed above is firstly discussed with respect to volume change of **the cement based paste**, and secondly with respect to the influence of aggregates.

The volume change is basically a volumetric deformation, but from a practical point of view it is convenient to consider linear deformations, commonly referred to as “plastic settlement” and “plastic shrinkage”. The terms are adopted here and refer to settlement as the vertical deformation and shrinkage as the horizontal one.

The shrinkage-settlement ratio changes basically from 0 to 1 in the period, as the stiffness of concrete changes from that of a liquid in the early plastic age (all volume change seen as settlement, only) to that of a solid in the hardening age (with isotropic properties). The transition from liquid to solid has caused discussions between researchers, in particular because different measuring methods for AD appear to indicate quite different ages of the transition. This is a fundamental feature resulting from the hydration of early age paste-mortar-concrete, and is thus paid some attention in this chapter. The transition is obviously influenced by evaporation, which is shown in chapter 5.

3.2 Autogenous deformation of paste - origin, significance and testing

3.2.1 Origin and significance

Autogenous Deformation (AD) is the bulk volume change resulting from the **chemical shrinkage (CS)** associated with hydration of cement (plus any pozzolans). As long as the paste behaves like a liquid, gravity makes AD equal CS. Later, when the hydration has created a skeleton with stiffness that needs a higher force than that caused by gravity to collapse, AD becomes lower than CS and empty pores are being formed in the paste. This is further discussed in section 3.2.3. Normally, the deviation occurs within a few hours of age, and corresponds in principle to the point in time when the settlement rate flattens out and horizontal deformation starts. So, from a practical point of view AD before deviation point is seen as part of plastic settlement. Apparently, it may constitute the main contributor to settlement (the only one if there is no air expulsion, bleeding, evaporation or thermal dilation). An example: Fig. 3.5 shows that AD is approximately 0.2 cm^3/hg cement between 1 hour and the deviation point (3 hours). It corresponds to a volume change, i.e. settlement, of 800 μstrain of a concrete with 400 kg/m^3 cement. In addition comes the volume change in the time before one hour of age. Fig. 5.2 (section 5.3) shows that the settlement of a concrete with the same cement type and w/b (0.30) is approximately the same, i.e. 800 μstrain in the same period of time (1-3 hours of age). Even if the hydration rate is lower in the concrete due to use of lignosulphonate based water reducer with retarding side effect, it suggests that AD (CS) may be an important contributor to settlement.

Powers (1948) found that the chemical shrinkage of Portland Cement hydration is 25.4 % of the chemically bound water and that the chemically bound water constitute 25 % at 100 % degree of hydration. Hence, the chemical shrinkage corresponds to approximately 6 % of amount of reacted cement ($0.25 \bullet 0.25 \bullet \alpha \bullet C$, α is degree of hydration and C is cement content). CS in the above example corresponds approximately to 0.6 % at the deviation point, suggesting that degree of hydration is approximately 10 %, already (in fact a bit higher since the first hour is left out).

It is shown by Bjøntegaard (2000) that AD may be an important contributor to shrinkage in the early hardening age, also, see section 9.2.

From a practical point of view, the time before casting is not much of interest because AD of concrete will “disappear” during mixing, transportation and casting. Moreover, concretes are normally made with water reducing admixtures (WRA) which often retard hydration (i.e. significantly delays setting time), see section 3.3.5. AD of equivalent pure cement pastes without WRA should therefore be evaluated on a time scale shifted to shorter times.

3.2.2 Measuring techniques for volume change of cement based pastes

3.2.2.1 General

Many authors have reported on volume changes of cement based pastes in terms of CS and AD. When it comes to the plastic and early hardening age, the most used test methods in recent years are quite similar. As will be seen, the pore water pressure is a good tool to describe the volume change evolution in early age concrete, and is therefore included among the test methods described here.

3.2.2.2 Measuring techniques for chemical shrinkage

The recently most used method to find the total chemical shrinkage is as follows: A small amount of paste is filled in a glass tube, Erlenmeyer flask, etc. The rest of the volume is filled with water. The volume change is recorded as the reduction of the water level in the system (Geiker 1984, Justnes et al, 1994). The flasks are placed in a temperature controlled water bath. The method has proven to be reliable, and it may be started at a short time after mixing (less than 15 minutes).

The method is based on the assumption that the pores, when created, fills with water. This is true in most cases because the thickness of the paste samples is small (i.e. maximum 10 mm), at least in the first day(s) of age. Geiker (1984) investigated the influence of time, w/c and thickness on the reliability of the method. Fig. 3.1 shows CS versus time for paste with w/c = 0.30. As can be seen the curves representing various paste thicknesses up to 5.5 cm coincide until approximately 20 hours. Hence, the method gives the true chemical shrinkage in the time period and for the w/b- ratios considered in the present report. The deviation points implies deficient pore filling and may thus be used to find the validity of the method with respect to maximum thickness and time as well as minimum w/c.

Another type of methods is based on weighing of the amount of water needed to re-fill a water filled closed container with a sealed paste-mortar sample. The sealing may be rubber membrane (Setter and Roy, 1978), plastic sheets (Ziegeldorf and Hilsdorf, 1989) or oil (Slate and Matheus, 1967).

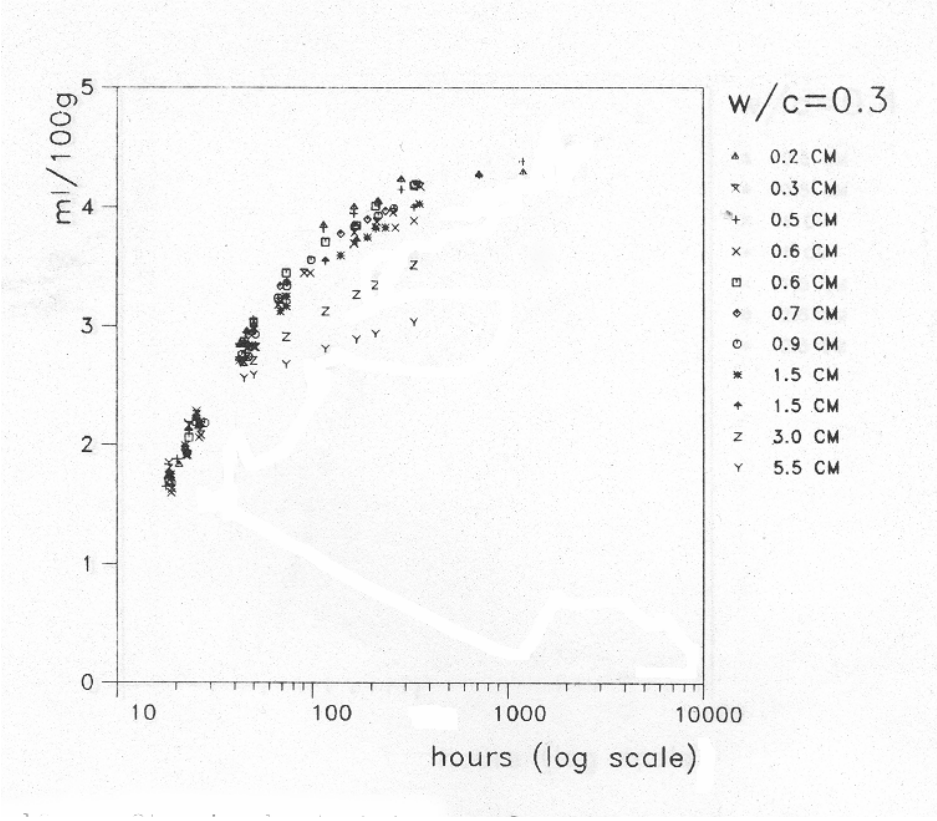

Fig. 3.1 Chemical shrinkage of pastes with various thicknesses (Geiker, 1984)

3.2.2.3 Measuring techniques for volumetric autogenous deformation

The most common way of measuring AD is presently to observe the change in buoyancy of a sample in an elastic bag (usually a condom, which has given the name “the condom method”). The sample volume is usually in the range of 100 – 200 ml. The condom is filled in gentle way in order to not rupture the condom and to avoid cavities. It is closed with a non soaking thread and silicon paste. The condom is in principle placed in water on a non-absorbing basket fixed to a balance. The weight is recorded continuously or in intervals. Temperature control is taken care of by the continuous immersion in water.

The method allows any bleed water to lay on the surface. The subsequent re-absorption will be observed as an extra contraction. Setter and Roy (1978) demonstrated this “false autogenous shrinkage” due to bleeding by measuring the volume change of two similar pastes, sealed in rubber balloon, one with removing the bleeding water after the end of bleeding and the other without removing. The results are seen in Fig 3.2. The false shrinkage has been confirmed by Justnes et al (1994).

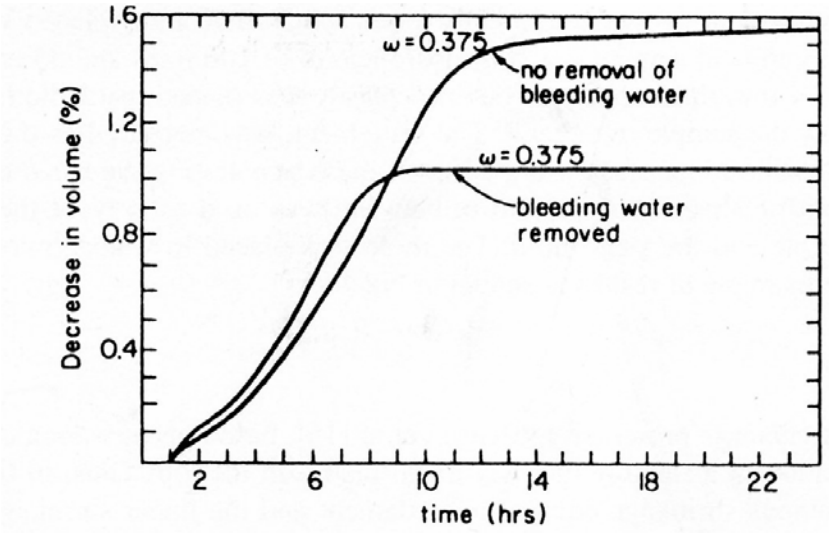

Fig. 3.2 Effect of removal of bleeding water on autogenous shrinkage (Setter and Roy, 1978)

In order to avoid bleeding, the condom can be rotated. The effect of rotation is discussed by Justnes et al (1994), and the procedure has proven to give good correlation with the chemical shrinkage method over short times. More sophisticated set ups have been built, allowing a continuous weight recording under simultaneous rotation (Barcelo et al, 1999).

Another method for pastes and fine mortars based on the buoyancy principle, is presented by Paulini (1992). The sample is here placed in a plastic case with an elastic sheet on top, instead of a rubber balloon. In principle, the method measures the same as the rubber balloon method (provided that the elastic sheet with joints is water tight) in the initial phase. Thus, the absorption of possible bleeding water will be observed as an extra shrinkage. Temperature control is taken care of by the continuous immersion in water.

Ziegeldorf and Hilsdorf (1980) also demonstrated that the geometry of the sample is

important in this respect: The bleeding increases with increasing height and, thus, the time of re-absorption increases, too.

An important point is the fact that the elastic materials used are not always water tight. The consequences are considered to be insignificant in the plastic and early hardening age, since the errors constitute rather small values taken in to consideration the high values of AD and the relatively short time considered.

The un-tightness was demonstrated by simply recording the weight of a water filled condom placed in air by time. The results showed a water loss driven by the low RH in the surrounding air (approximately 30 % RH), as shown in Fig 3.3. The diffusion coefficient for the material was calculated from the results, to be $2.1 \cdot 10^{-13}$ kg/(m·Pa·s), which is rather high.

The influence of the un-tightness has been investigated by Barcelo et al (1999) and Lura and Jensen (2005). They confirmed the high permeability leading to water transport through the membrane driven by decreasing RH in the paste. It contributes to slow down the evolution rate of RH, and thus AD. But it also contributes to increased weight of the sample which appears as reduced buoyancy, and thus, shrinkage. Furthermore, they showed that the material absorbs water which corresponds to typically 20 mg for a condom. The weight change of the sample in the condom is typically 500 mg in time before the deviation point. Thus, the water absorption of the condom is considered not to be significant up to the deviation point. After that the AD slope is very small, and correspondingly strongly influenced by leakage.

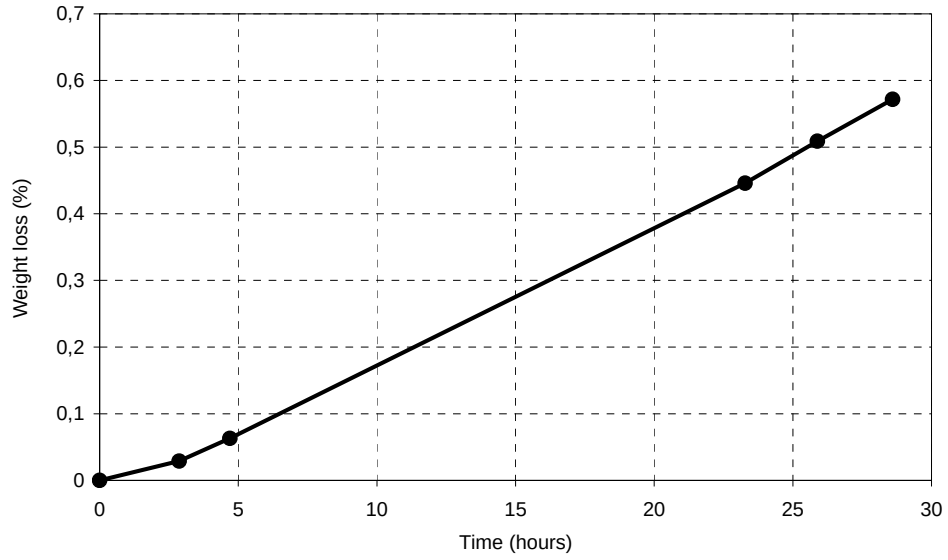

Fig. 3.3 Loss of water through a water filled condom placed in air of approximately 30 % RH.

3.2.2.4 Measuring techniques for linear autogenous deformation

Analogous to plastic settlement and plastic shrinkage of concrete, AD of pastes may be divided in settlement and shrinkage, respectively. Most tests methods found in the literature

are designed for measuring the autogenous and/or drying shrinkage from the time **beyond** setting.

A common feature for test methods designed for the plastic phase and the early hardening age, is that the specimens stay in the mould during testing. The friction between the specimen and the mould may, in combination with the low stiffness of the paste-mortar-concrete in this phase, hinder the movement of the specimen. The efforts to prevent the friction differ in the test methods: In some methods the mould surface is treated with oil, wax or asphalt, while other tests use double set of plastic with talcum in between or sheets of Teflon between the specimen and the mould. The third group uses flexible tubes, i.e. corrugated tubes of metal, plastic or rubber to prevent the friction. Metal discs and oil film has also been used as under-layer for pastes cast in thin plastic sheets.

Obviously, the features are the same for methods used for paste measurements and used for concrete measurements, and the literature survey shows that some authors use the same method for paste, mortar and/or concrete. A more detailed discussion of test methods is therefore given in connection with development of the method used in the present work (chapter 4).

However, there is one method which is basically different from the others, and that is a paste dilatometer described by Jensen (1993), where the paste is poured into corrugated plastic tubes. The method is specially design for the determination of the “hardening phase” autogenous shrinkage of pastes and fine mortars. The corrugation makes the system sufficiently flexible to allow shrinkage recording in the initial phase too, but the author does not trust the results in this phase due to the possible lack of contact between the transducers and the paste and some stiffness of the tube. In principle, if the contact and tube stiffness problems are solved, the method should give a reliable linear autogenous shrinkage measurement in the time after the paste-mortar is self-supporting (see section 3.2.3). The deformation development often starts with an expansion, which probably is due to the hydrostatic pressure of the “liquid” paste, pressing out the transducers. The method may allow bleeding water to lay on the surface, which may influence the deformation (see section 3.2.4). The author has however not to my knowledge reported such influence, i.e. like swelling due re-absorption of bleed water. The temperature control is taken care of by placing the whole system in a temperature controlled oil bath.

Most of the experiments on pastes in the present work were done using the rig described in chapter 4, but with a cross section of 50x50 mm, and submerged in water to avoid significant temperature rise from heat of hydration.

3.2.2.5 Measurement of pore water pressure

Measurement of pore water pressure, e.g. as developed by Radocea (1992), is a good tool to achieve independent support of the results from the linear measurements. Initially, the pressure at a given point corresponds to the hydrostatic pressure of the liquid paste-mortar-concrete given by the height and the density. The pressure decreases with time as result of the formation of a "self-supporting" body, see section 3.2.3. At the time when the concrete is able to support its own weight, the pressure corresponds to the water pressure at the depth of measuring. It follows that the horizontal component of the shrinkage should appear at this time. The further development is a decreasing pressure, i.e. increasing pore water tension due

to the vacuum and/or meniscus formation, caused by the chemical shrinkage and any external drying, see the following sections. Consequently, this method is suited to verify the **"point of self-support"**, shortened to **"PSS"**. Any measured "horizontal shrinkage" at times before this point is then erroneous (e.g. due to "false" movement of the measuring points, see section 4.2). Furthermore, if a horizontal deformation is not measured from this time, it may be a result of friction. Consequently, the method is a tool for checking of the linear measure test method.

The set up used here is adopted from Radocea (1992). A principle sketch is shown in Fig 3.4. A pressure transducer is connected to a water filled steel tube with inner diameter of 3 mm. The water used is boiled and then cooled in order to reduce any dissolved air in the water that may influence the pore water pressure evolution (air bubbles act as relaxing cavities). The tube is placed vertically with the tip at different depths below the top surface of the paste or concrete, see Fig 3.4.

The pressure transducer measures the difference between absolute pressure at the depth of measurement and atmospheric pressure. Furthermore, in order to allow an easier observation of PSS and pore water tension regardless of measuring depth, the pressure is given as the measured value minus the hydrostatic water pressure at the depth of measurement, referred to as **"apparent pore water pressure"** or simply **"PWP"**. I.e. PWP equals zero at PSS, and negative PWP-values represent pore water tension.

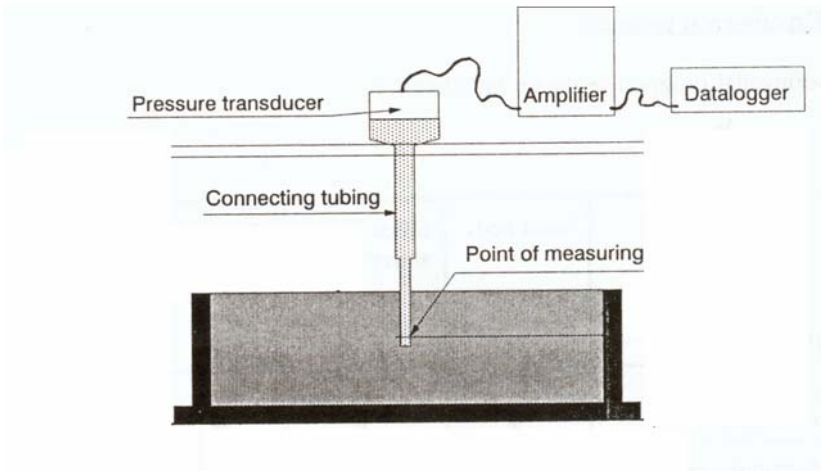

Fig. 3.4 Principle sketch of set up for measurement of pore water pressure (Radocea, 1992)

3.2.3 Chemical shrinkage versus autogenous deformation – transition from a liquid to a solid

3.2.3.1 Theory

As mention in 3.2.1, AD is the bulk volume change resulting from CS. Many authors have confirmed that AD equals CS in the time period when the paste has a fluid like behaviour. At a certain point in time the particles start to support each other, due to decrease of particle spacing which is result of water consumption caused by hydration, and growth on particle surfaces. This point in time when rate of AD, according to the given method, and rate of CS become different, is called **"deviation point"**, see Fig. 3.5.

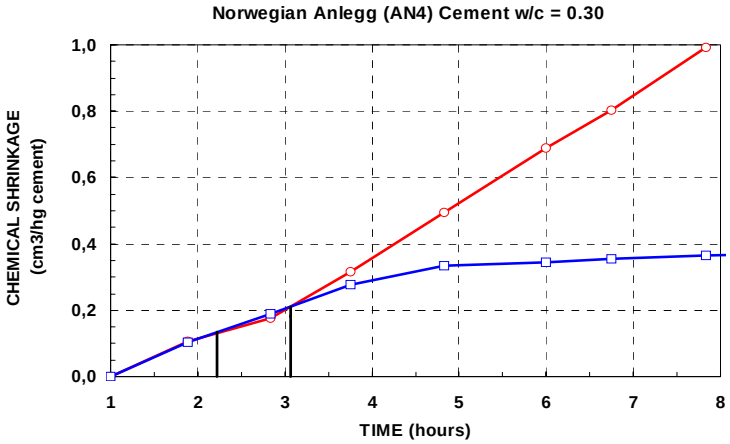

Fig. 3.5 Chemical shrinkage (red/circles) and autogenous shrinkage (blue/squares) of a cement paste with w/c = 0.30, plus initial and finale setting (vertical lines) by Vicat needle (after Justnes et al, 2000.)

The deviation point is obviously related to the time of setting, but of course the setting it self is not uniquely defined. Justnes et al (2000) investigated the correlation between the deviation point and setting times according to the Vicat-test. Fig 3.5 shows an example where the deviation point coincides fairly well with final setting occurring at 3.1 hours, according to the Vicat-test (initial setting time was at 2.3 hours). They showed also that initial setting always occurred before the deviation point, while final setting sometimes occurred before, sometimes concurrently and sometimes shortly after. It appears that setting times increased more with increasing w/b (0.3 – 0.5) and decreasing cement fineness (370 to 290 m^2/kg Blain) than the deviation point did.

As CS continues regardless of paste stiffness, empty pore space is being created in the paste and the rate of AD decreases rapidly until it reaches a rather constant rate seen in the present scale, at approximately 5 hours of age for the this paste, see Fig. 3.5.

Barcelo et al. (2001) have done similar measurements, but with a set up that probably allows a more accurate recording of AD. They found that the AD and CS of a w/c = 0.28 paste start to diverge approximately 40 minutes after casting, already (corresponding to approx. a CS of 0.25 mm^3/g in Fig 3.6), which coincides with the point where a "mineral skeleton" is formed according to an ultrasonic test. However, the AD rate does not deviate much from the CS rate until CS reaches approximately 3 mm^3/g (corresponding to approx. 3 hours of age), see Fig 3.6, implying that the skeleton is very soft until then. This early skeleton formation agrees with the observation that the deviation point occurs much earlier in linear measurements, see Fig. 3.7, as reported by Barcelo et al (2001), also.

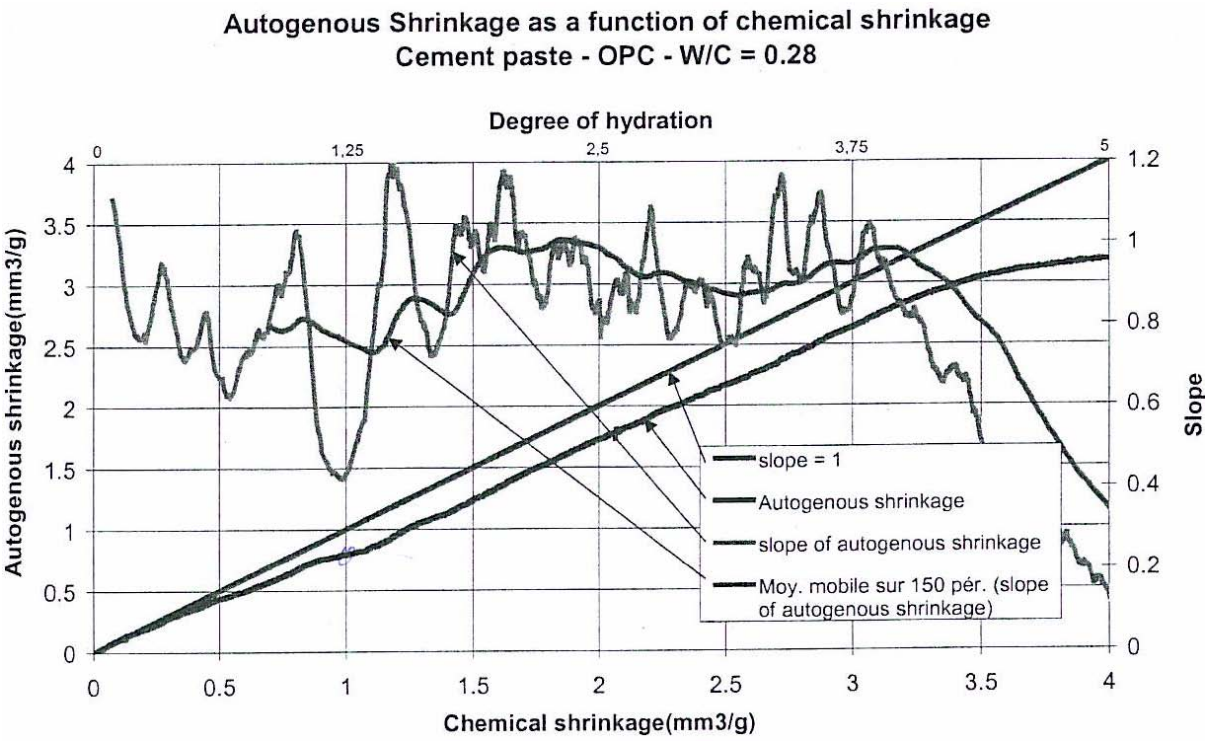

Fig. 3.6 Chemical shrinkage and autogenous shrinkage of a cement paste with w/c = 0.28 (Barcelo et al, 2001)

In order to explain the apparent disagreement between deviation points in linear/non air tight tests and volumetric/air tight tests, it seems sensible to start with the question how "empty pores" arise, since they occur apparently in the plastic stage in the linear test? In an ideal model with cement paste in an air tight box with stiff walls, and where all space between dense cement particles is filled with water that contains no air and may flow freely, the air space must originate from **vacuum** (cavitation - occurrence of vapor filled pores), since there is no water menisci present to create capillary tension of pore water. It means that the point where AD deviates from CS (i.e. when the first empty pore arises) should correspond to a pore water pressure equal to the vapor pressure of water at the given temperature. It is 2.3 KPa (0.023 atm.), only, of pure water at 20 ^{o}C. As the CS rate is close to constant in this period of time, one should expect a rather constant rate of pore water pressure decrease until cavitation. Then, further water consumption (CS) leads to growth in the volume of the vapor filled pores. The system is geometry controlled in that as degree of hydration increases the pores decreases in size (as their total volume increases) as does the menisci, and tension increases.

It follows that this ideal system is controlled by **vacuum** from the beginning and by **capillary tension** in the time beyond cavitation.

The condition described above does not occur in practice: The linear test does not constitute an air tight system and the condom does not constitute a stiff box. PWP in the condom equals then basically the pressure outside the bag (plus the hydrostatic pressure of the cement paste at the point of measuring). As a skeleton is formed CS builds up tension of pore water (vacuum effect). The pore water tension may be considered as an additional load to the load caused by gravitation, which makes the body deform at higher stiffness (i.e. higher degree of

hydration). **It would result in a longer time of full deformation of the paste, i.e. longer time until deviation point.** The pore water tension pulls on the bag wall which in turn wants to deform between the outer particles. Such deformation is probably possible to some extent since the bag wall has negligible stiffness and thickness of approximately 0.05 mm, only. The bag wall deformation allows some surface water to move inwards, to "refill" CS. At some point in time, as the curvature of the surface water between particles becomes smaller, the bag wall is no longer able to follow, the refill of CS is prevented, and more important, the skeleton forms its own "stiff wall". Consequently, empty pores form internally, basically as vacuum, at the vapor pressure of water at the given temperature. As mentioned above the vapor pressure of pure water at 20 ^{o}C is 2.3 KPa, corresponding to PWP of -97.7 KPa, increasing with temperature (the vapor pressure of pore water is lower since it is polluted by various salts).

In most **linear tests** there is air between the paste and the sealing against moisture exchange. Hence, the sample is surrounded by air of 100 % RH instead of an elastic bag. Then, as a skeleton is formed and CS builds up tension of pore water in the interior of the sample, surface water is free to be sucked in. The result will be surface cavities, i.e. the first "empty pores". It follows that the dimension and permeability may influence the deviation point of samples in non air tight conditions: In samples with low thickness/high permeability water may flow from the surface pores to the internal at sufficient rate to relax the vacuum effect (giving early deviation point). High thickness/low permeability may prevent sufficient "refill" of the internal. Consequently, the internal may experience an "air tight condition", which is expected to result in delayed deviation point.

Another important point in both air tight and non air tight tests is that there are probably always some air bubbles/cavities in the paste which may simply expand to reduce pore water tension. This is expected to result in earlier occurrence of the deviation point (see also sections 3.3.6 and 5.9).

It follows from the discussion above that there may be three consecutive phases:

1. "**Liquid phase"**: Until formation of mineral skeleton, i.e. until paste/mortar/concrete can support its own weight (point of self-support, PSS). It is the phase when AD equals chemical shrinkage, CS, and manifests it self in settlement, only (i.e. no horizontal deformation).

2. **"Semi-liquid phase"**: Until significant stiffness starts to develop, i.e. around initial setting time. The start of the phase is associated with time when pore water pressure becomes tension and horizontal deformation (shrinkage) starts to develop. The phase coincides probably with the time when the paste/mortar/concrete can be brought back to liquid phase with agitation.

3. **"Early hardening phase"**: Through final setting and the following few hours. The phase is associated with significant stiffness development and minimum strain capacity of the hardening paste/mortar/concrete.

Liquid phase plus semi-liquid phase equals plastic phase, as defined in chapter 2.

3.2.3.2 Tests

A set of tests were run in order to support the above discussed theory, using a pure cement paste of "Norcem Anlegg" and with w/c = 0.30, known to have insignificant bleeding. CS was found by the "Erlenmeyer" method, AD by the condom method and by the dilation rig (see section 4.2). In addition PWP was measured both in a "dummy" condom placed in water and in the beam in the dilation rig.

As can be seen in Fig 3.7, the "air tight" volumetric AD found by the condom method ("volumetric AD"), follows CS for approximately 2 hours and then bends rather smoothly. The "non air tight" volumetric AD found as the sum of deformations in the three directions, i.e. settlement and 2 times shrinkage, follows CS less than half an hour, only, and then turns rather abrupt into expansion for a couple of hours. The expansion of approximately 100 μstrain is result of the temperature rise of 4 °C between 2 and 6 hours of age plus the chemical/physical swelling as discussed in next section. Assuming that the strain difference between the two of about 5000 μstrain after leveling out, corresponds to the volume of empty surface pores, as suggested above, it means that the thickness of the outer layer with empty pores is 0.12 mm (calculated from the volume and surface area of the 280x50x50 mm sample and w/c of 0.30).

Barcelo et al (2001) found the same principle discrepancy between linear and volumetric measurements using similar methods.

Surface drying (water loss to the interior) is supported by the fact that the surface of the beam in the dilation rig looks dry already at early age, even though of course protected from evaporation (with plastic sheet).

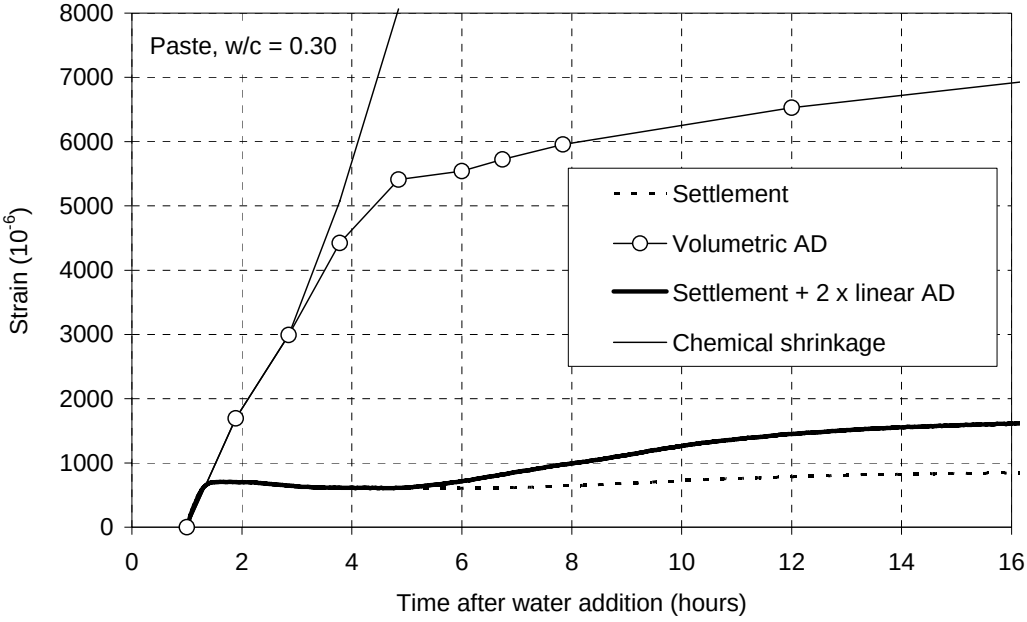

Fig 3.7 Chemical shrinkage, autogenous shrinkage from the condom method (volmetric) and from the dilation rig (settlement and linear AD) of a cement paste with w/c = 0.30

Note that the age of approximately 1.5 hours when **linear** AD deviates from CS, coincides fairly well with the age when the PWP becomes zero, both indicating point of self-support, PSS (section 3.2.2.5), see Figs 3.8 and 3.9.

As suggested in the previous section, the vacuum effect builds up pore water tension in the condom. Hence, it is expected that pore water tension in the condom test is higher than that in the beam test in the time between PSS and deviation point. This is not clear at first sight on Figs. 3.8 and 3.9 because the pressure in the condom is compression for a long time, caused by the stretching of the condom which results in a confinement of approximately 1 KPa, see Figs 3.8 and 3.9. It is therefore not evident how PSS can be seen from PWP in the condom, but it appears to be at approximately 2 hours since the typical knee-point is seen at that age. Assuming that PSS is at 2 hours of age (condom), the following slight decrease of PWP indicates pore water tension. Then, it can be seen that pore water tension decreases faster in the condom than in the beam in the time shortly after PSS, as suggested. The difference is small, but remember that the paste is still rather soft, and thus, can not generate much stress (note that a later PSS and earlier bending of PWP into the steep part than in the beam, is probably result of lower temperature in the condom; approximately 20 ^{o}C (submerged in water), while it in the beam increased from 23 to 24.5 ^{o}C at 4 hours of age).

The condom deviation point in Fig. 3.7 appears to be at 3-4 hours, which is just before PWP turns into the steep part. The “knee-point”, i.e. when the AD has reached low rate, coincides with the time when PWP has reached its high rate, as expected.

The results support the hypotheses that the presence of surrounding air is of vital importance in the discussion of the relationship between CS and AD in the period before and during setting.

Also, it can be seen that rate of "Volumetric AD” (condom) becomes slightly higher than the rate of “Settlement + 2 times linear AD” in the time beyond the swelling period, i.e. in the hardening period. It is probably result of water penetrating the condom as discussed earlier.

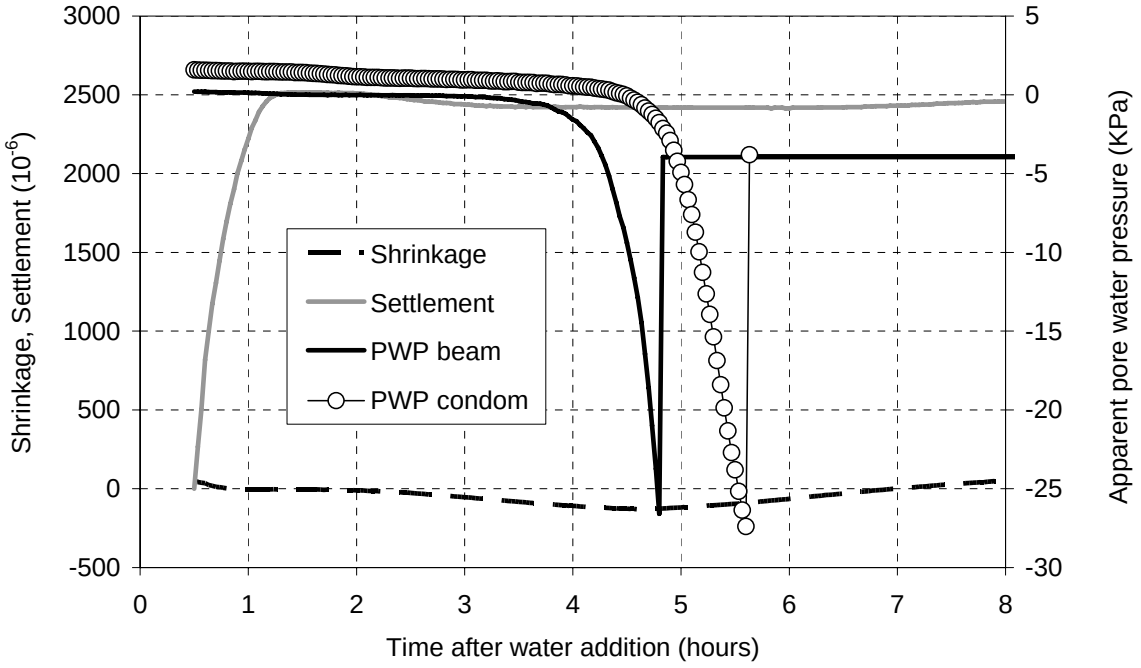

Fig 3.8 Autogenous settlement and shrinkage together with and apparent pore water pressure (PWP) measured on the same sample ("beam") and in a condom

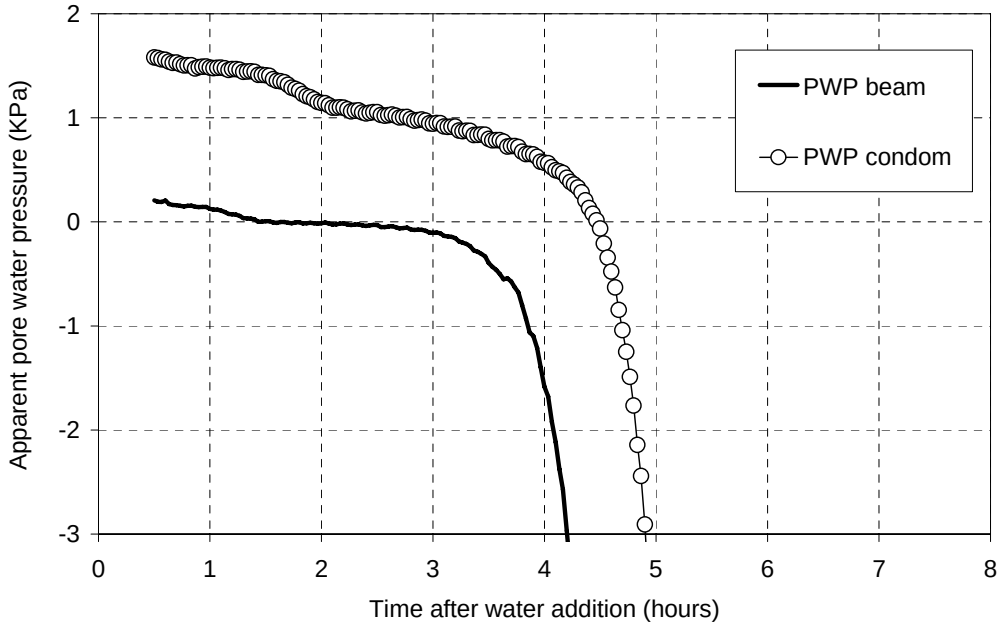

Fig 3.9 Apparent pore water pressure (PWP) as in Fig. 3.8, but enlarged

3.2.4 Influence of bleeding

Regardless of the external condition, any bleeding may give additional volume change depending on how the volume change is considered/measured. Bleeding stops at PSS at the latest, in nature. In a volumetric test, e.g. by use of the condom method, bleeding will not

result in additional shrinkage in the bleeding period, but will in the subsequent period when the bleed water re-absorbs, see section 3.2.2.3. In a linear test, bleeding will appear as an additional settlement, if the measuring support on surface is designed to follow the solid. It follows that bleeding will not appear as additional volume change if the support floats on the bleed water. However, in contrast to the volumetric method, the re-absorption of bleed water will give swelling in the period beyond PSS, increasing in amount and time with increasing amount of bleeding as discussed below. The practical consequence of this depends of course on whether or not the bleed water allows to evaporate. If not allowed or if the evaporation rate is equal to or lower than the bleeding rate, the volume change will probably not constitute a driving force to cracking. On the contrary, the expansion may contribute to the opposite. The consequence if evaporation rate exceeds bleeding rate, and thus, bleeding water becomes a part of the total amount of water evaporated, is discussed in the next chapter

Reasons for the early age swelling (seen both in settlement and shrinkage) have been discussed by several authors. Some assign it to chemical reactions others to absorption of bleed water. Barcelo et al. (2001) have surveyed expansion mechanisms and found that growth of ettringite or portlandite, or even C-S-H formation have been suggested as causes for the expansion. A plausible hypothesis is then that there are two counteracting mechanisms: A physical grid of particles and reaction products on the surface of the particles which pushes them apart and thus results in expansion, and consumption of water (CS) which result in bulk contraction. Then the net result will be expansion if CS is being refilled with water (externally or internally). It is commonly known that cement paste or concrete when continuously cured in water from the time of casting swells as result of adsorption of water by the gel (water molecules act against the cohesive forces and tend to force the gel particles further apart). However, water is not always available in the whole cross section, e.g. in pastes/concretes with low w/c, i.e. where the permeability is too low to allow water transport to the interior. The net result may in fact be shrinkage in spite of water curing (see for instance Acker, 2004).

Bleed water may be seen as water curing (see also role of water absorbed in the aggregates in section 5.8). Fig. 3.10 shows that the time and magnitude of the swelling of pastes decreases with decreasing w/c and with addition of silica fume, both leading to reduced bleeding. Bjøntegaard (2000) demonstrated that increasing amount of water have the same effect on concrete, see Fig. 3.11.

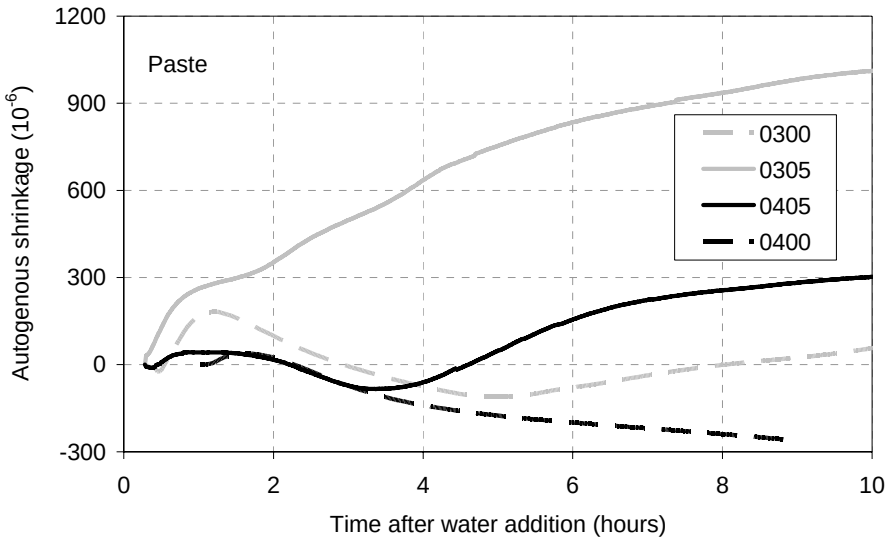

Fig. 3.10 Autogenous shrinkage of cement pastes with w/b = 0.30 and 0.40 both with and without 5 % silica fume (own results)

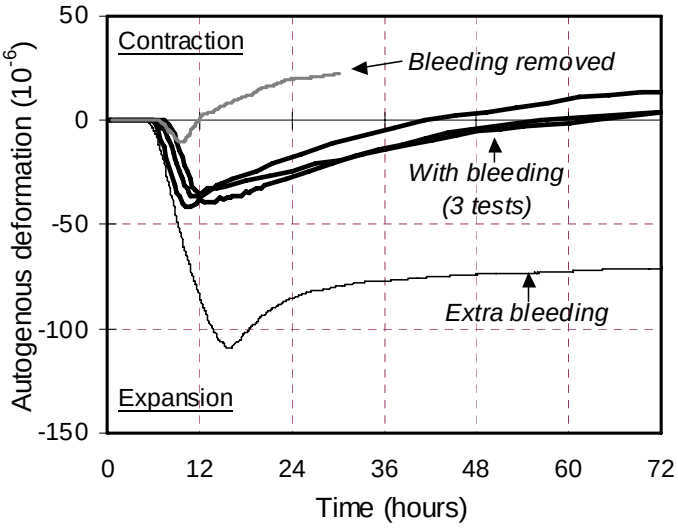

Fig. 3.11 Autogenous shrinkage of a concrete with w/b = 0.40 with 5 % silica fume and with "Bleeding" ("natural bleeding"), "Bleeding removed" (sucked up externally), and with "Extra bleeding" (extra water added on top) (Bjøntegaard, 2000.)

3.3 Autogenous deformation - influence of paste composition

3.3.1 General

It follows from the previous section that the main contribution from AD in the plastic and early hardening ages, is to settlement in the time when the mortar/concrete is “liquid” (i.e. before point of self-support), and that AD then equals CS. The influence of paste composition is therefore discussed with respect to AD and/or CS up to the deviation point, mainly.

3.3.2 Influence of cement type

At a given temperature, the rate and magnitude of hydration, given in unit weight of chemically bound water per unit weight of cement, is influenced by the fineness and composition of cement. The latter because the pure cement is composed of 4 clinker minerals having different hydration rates and CS: C_3S, C_2S, C_3A and C_4AF, where C = CaO, S = SiO_2, A = Al_2O_3, and F = Fe_2O_3. Typical cement compositions are given in Table 3.1 (Justnes et al, 1999). There are shrinkage-giving reactions within the first minutes associated with salt dissolution and recrystallisation of calcium sulphate (gypsum) from hemihydrate to dihydrate. The shrinkage of salt dissolutions in the form of alkalies like KOH and NaOH has been measured to be rather low; in the range of 0.1 – 0.2 ml/100 g cement, and the shrinkage from recrystallisation of calcium sulphate has been measured to be 4 ml/g reacted hemihydrate (Justnes 1999). The calcium sulphate content is typically 3 - 6 % of total cement weight, and not all of it will react in this initial stage. Thus, the shrinkage corresponds probably to less than 0.2 ml/100 g cement. Anyway, these volume changes are considered to be insignificant from a practical point of view since they take place before concrete is cast.

It is commonly known that the C_3A and C_3S are the two minerals most active in the early age, the ettringite formation from C_3A dominating first and C_3S dominating later.

Kjellsen and Lagerblad (2006) has demonstrated from calorimetry-measurements that the C_3S-hydration is practically absent until approximately 3 hours of age (depends of course of the fineness). It can therefore be assumed that CS in the first few hours of age is generated from C_3A-hydration. Justnes et al (1999) tested CS (according to a method described in chapter 3.2.2.2) of a number of pastes with cements having different characteristics in terms of composition and fineness, see table 3.1. The results are shown in Figs 3.12 and 3.13. The results did not show any distinct correlation with the cement characteristics, but the cements with the highest C_3A content and highest fineness are among those with highest CS. This is more distinct at the earliest ages (Fig. 3.12) than at the later ages (Fig 3.13), which supports that C_3A-hydration dominates at the earliest ages. Furthermore, the high CS rate at 10 minutes implies (by extrapolation) that a considerably amount of the ettringite formation of these cements has taken place in the time before 10 minutes of age.

The latter may be supported by comparing measured and calculated CS. The volume change, $\Delta V = \Sigma V_{reactants} - V_{product}$, associated with the chemical reactions of the clinker phases, can be calculaterd when knowing the density and molar weight of reactants and products of chemical reaction:

$V = m/\rho = n/M/\rho$, where

m = mass of reactant or product
ρ = density of mass of reactant or product
n = number of moles of reactant or product
M = molar wass of reactant or product

The calculation gives the total CS from each reaction. Such calculation has been done by Justnes et al (1999), and is as follows for ettringite formation:

	C_3A +	$3\ C\bar{S}H_2$ +	26 H =	$C_6A\bar{S}_3H_{32}$
M (g/mol)	270.2	172.17	18.02	1255.26
n (mmol)	3.7	1.91	1.73	4.64
m (gram)	1.00	11.10	96.20	3.70
ρ (g/ml)	3.03	2.32	0.998	1.78
V (ml)	0.33	0.82	1.73	2.61

ΔV = (0.33 + 0.82 +1.73) - 2.61 = **-0.27 ml/g C_3A**

The cements given in Table 1 have C_3A contents between 0.5 and 7.9 % of total cement weight. Then, the **calculated** CS from C_3A-hydration corresponds $0.27 \cdot 0.5/100 \cdot 100$ = **0.14 ml/100 g cement**, and $0.27 \cdot 7.9/100 \cdot 100$ = **2.13 ml/100 g cement**, respectively. Fig. 3.1 show that the **measured** CS is always lower than the calculated CS ones, for the high C_3A-contents in particular. The latter suggests that most of the ettringite formation has taken place in the time before 10 minutes of age (which is supported by the results given in Fig. 3.13, in that the CS rate at 10 minutes of age is high), and/or that hydration of the other minerals, starts earlier than anticipated when blended in the cement where a number of ions are present.

Table 3.1 Cement characteristics (Justnes et al, 1999)

Characteristics	A	B	C	D	E	F	G	H	I	J
Alkalis (%)	1.04	1.05	1.13	1.06	0.94	0.57	0.51	0.55	0.57	0.59
C_3S (%)	57.4	56.3	57.0	46.9	55	48.0	53	53.6	59.5	61.2
C_2S (%)	16.4	15.6	16.0	24.4	19	28.7	24	25.0	18.2	16.9
C_3A (%)	7.9	6.4	6.9	7.8	6.2	5.6	5.0	0.5	1.0	1.3
C_4AF (%)	6.6	11.2	11.0	10.0	10.8	10.2	10.3	15.1	14.9	14.5
$C\bar{S}$ (%)	5.8	6.2	5.1	4.6	5.2	4.5	5.2	3.7	3.7	3.0
Fineness (m^2/kg Blaine)	461	438	309	361	358	413	418	305	290	303

Similar calculations can be done for the other minerals, all showing **shrinkage** (Justnes et al, 1999. However, "external shrinkage" (AD) tests often show **expansion** in the semi-liquid and early hardening age as discussed in section 3.2.4, possibly explained by growth of crystals pushing particles apart, and assuming that the space created from CS fills with water (e.g. bleed water) and/or air.

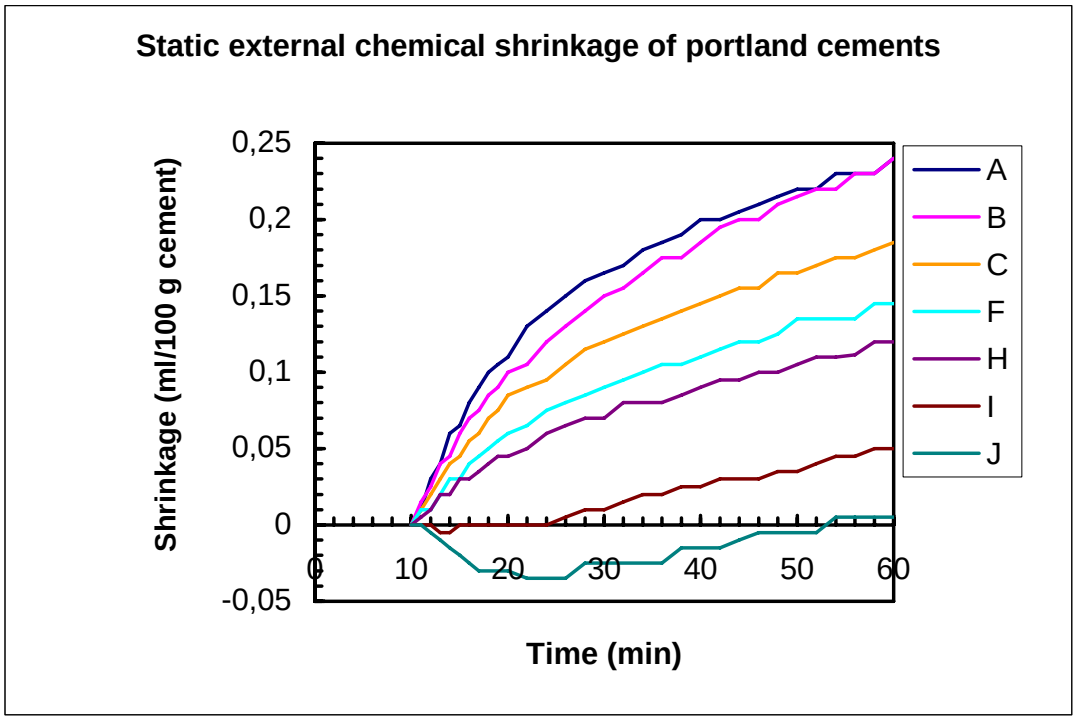

Fig. 3.12 Autogenous deformation ("Static external chemical shrinkage) development for different Portland cement pastes with w/c= 0.40 from 10 to 60 minutes of age 26 (Justnes et al, 1999)

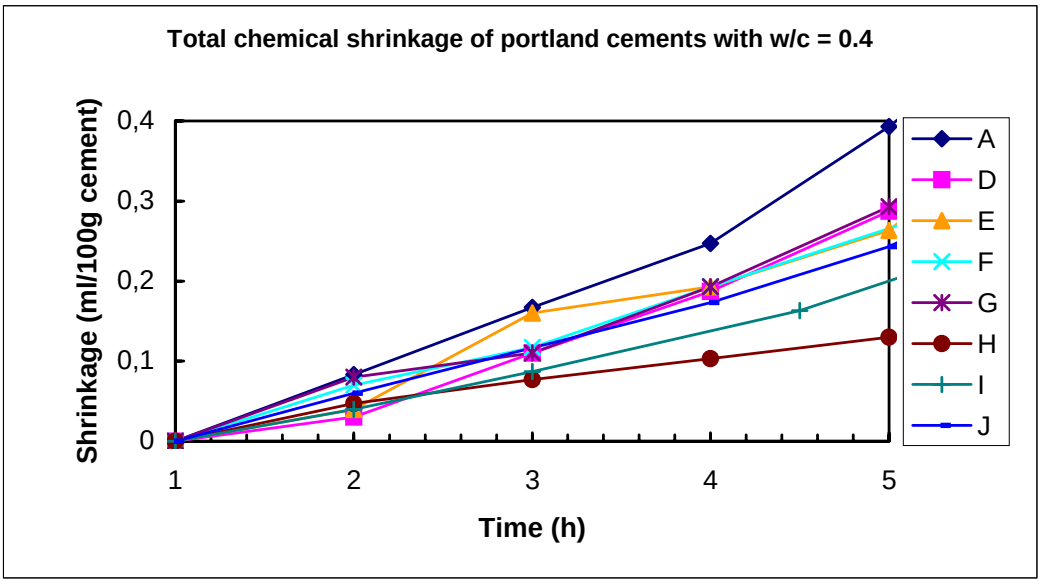

Fig. 3.13 Chemical shrinkage development for different Portland cement pastes (see Table 3.1), with w/c = 0.40 from 1 to 5 h of age (Justnes et al, 1999).

The influence of cement composition will not be further discussed here. The interesting finding is that AD/CS may be anything between slight expansion and considerable shrinkage within the first hour depending on cement type, which from a practical point of view may be important with respect to settlement. However, one may expect that these earliest age differences between cements appear during mixing, transportation and casting. In the rest of the "liquid time" (end of main settlement), the influence of cement type is probably not as significant, but differences in hydration rate does influence settlement. There is no distinct correlation with the cement characteristics, although the cements with the highest C_3A content and highest fineness are among those with highest CS. Note that cement composition may influence settlement through the influence on bleeding (a part of settlement), also, and that high C_3A content and high fineness reduces bleeding (and thus settlement). Consequently, the cement composition, and C_3A-content in particular, is not always the main key to the predict AD with respect to the practical influence on settlement.

3.3.3 Influence of w/c

Ziegeldorf and Hilsdorf (1980) investigated CS (unsealed samples) and AD (sealed samples) of cement pastes with different w/c-ratios, by the use of a water filled dilatometer. They found that CS is not significantly influenced by w/c, see Fig. 3.14, but, the point where AD deviates from CS is influenced by w/c, as seen. This is confirmed later by Geiker (1984) and Justnes et al (1994).

Note that AD follows CS, in Fig. 3.14, for several days for the pastes with the highest w/c. This seems out of the ordinary and may be result of re-absorption of bleed water (increasing with increasing w/c), which gives a false AD as discussed in section 3.2.4.

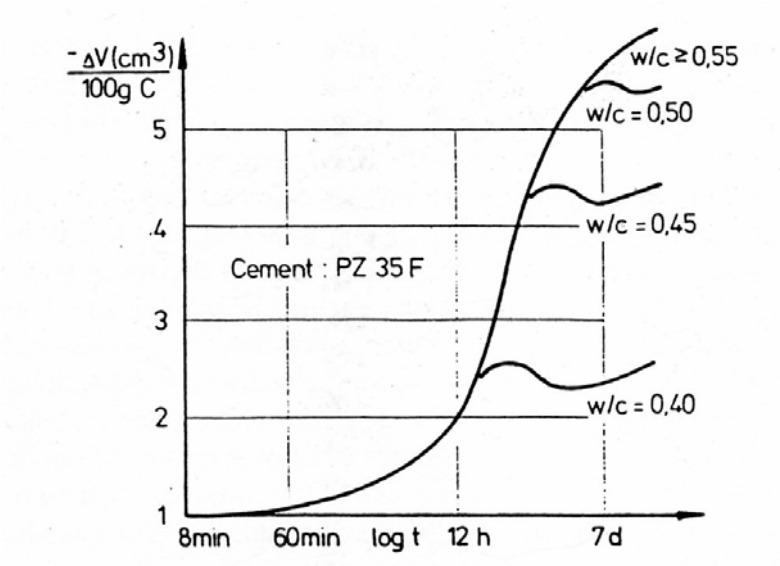

Fig. 3.14 Chemical shrinkage and autogenous shrinkage (coincides until the "deviation points) of pastes with various w/c (Ziegeldorf and Hilsdorf, 1980)

3.3.4 Influence of silica fume and fly ash

It seems that normal amounts of silica fume (less than approximately 10 % as replacement for cement weight) do not influence early age CS rate significantly (Justnes et al, 1999). It follows that the efficiency factor of silica fume regarding early age CS is close to one. Other pozzolanes like fly ash is known to contribute little to early age hydration, and thus, CS. Results given by Justnes et al (1999) confirm it and show no significant contribution of fly ash to early age CS, neither on the deviation point. Consequently, the efficiency factor of fly ash with respect to early age CS is close to zero.

3.3.5 Influence of admixtures

Since CS is driven by hydration, admixtures influencing hydration is of interest. These are mainly accelerators and retarders or water reducing admixtures (WRA) with retarding side effect, mainly. An example is given in Fig 3.15 showing that the retarding side effect of lignosulphonate based WRA (LS) delays CS, compared with the melamine based WRA (SMF) which did not have significant influence (Justnes et al, 2000) (results from before 1 hour of age are not given). Also, the results indicate that LS gives delayed deviation point.

Another group of active admixtures are shrinkage reducing admixtures, SRA, which reduces surface tension of water and with that reduces PWP, and thus, shrinkage. This is confirmed in section 5.8 by tests on concretes.

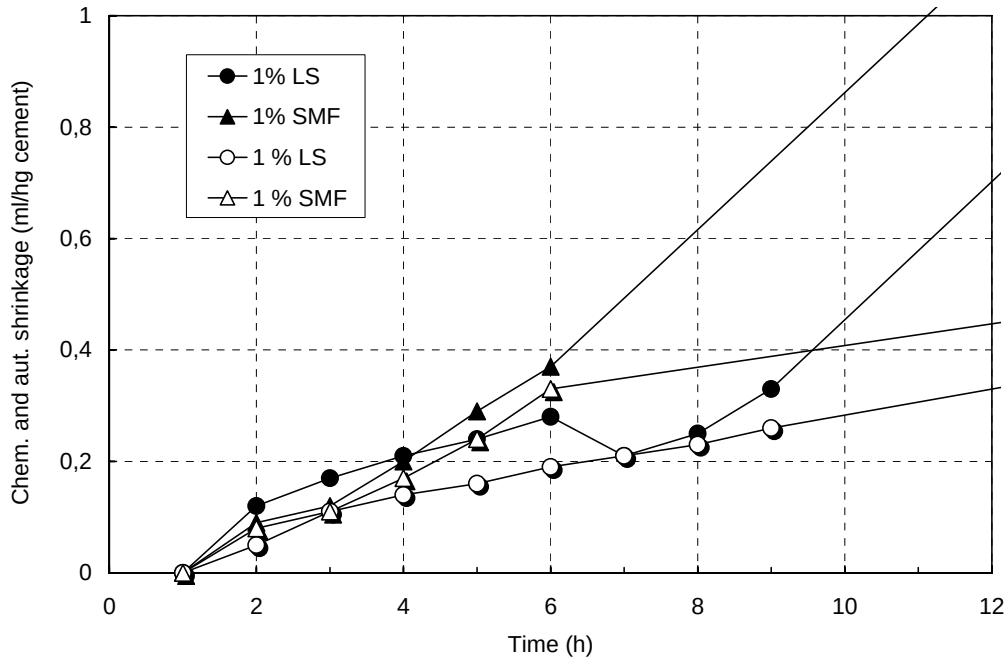

Fig. 3.15 Chemical (filled markers) and autogenous shrinkage (open markers) of cement pastes with different water reducing admixtures. "Norcem Anlegg"and w/c =0.40 (Justnes et al, 2000)

3.3.6 Influence of air voids

Cement paste contain very little air compared with equivalent mortars and concrete. In fact, the amount of air pores in the paste varies from “zero” in pure paste, to typically 20 % when in concrete with air entraining agent (AEA). Air voids may act as buffer for PWP, and thus volume change, i.e. they may expand with decreasing PWP as long as it is controlled by vacuum effects and the stiffness of the paste-mortar-concrete is low. Therefore, air pores may play an important role in the early age volume change.

The following was done in order to demonstrate the influence of air pores on AD: PWP and AD (condom method) was measured on two cement pastes both with an Ordinary Portland cement (“Norcem Standard”) and w/c = 0.35, one with air entraining admixture (AEA) in order to generate air pores. It turned out to be difficult to generate a stable air pore system in the cement paste, and even a dosage of 10 times the normal one did not give more than 5 % air (the target was 15 – 20 %). The paste showed sufficient fluidity to allow good compaction during filling. The pastes did not show bleeding, and thus, AD test was performed without rotation. The water was boiled and then cooled to room temperature prior to mixing, in order to evacuate any entrapped air in the water. The pastes were mixed in a 5 liter Hobart kitchen mixer. When mixing the paste without AEA, the mixer was placed in a tank under vacuum in order to avoid entrapping air during mixing.

From each paste, two condoms were filled carefully in order to avoid entrapped air bubbles, one to measure AD and the other to measure PWP. The tube of the PWP device was placed in the condom and then the condom was tightened thoroughly as the one without the tube, with a waxed thread and silicon.

Tests on paste without AEA were repeated once and tests on paste with AEA were repeated four times. The results show some scatter between repetitions, see Figs. 3.16 and 3.17, which is discussed later. The apparent influence of air pores on autogenous deformation (AD) is (compare Figs. 3.16 and 3.17):

- Higher rate of AD before the knee point
- Earlier arrival of the knee point
- Higher AD
- Lower rate of AD beyond the knee point

Similar observations were made when testing concretes with and without AEA, see section 5.9

CS was not measured in the present investigation, but an indicative CS is taken from an investigation with similar cement and w/c performed by Justnes et al (2000), and shown in Figs. 3.16 and 3.17. It seems that AD of the pastes without AEA coincides with CS in a short period of time only, which supports the results of Barcelo et al. (2001) showing that AD deviates from CS 40 minutes after casting only, see section 3.2.3.1. However, AD of pastes with AEA follows CS nearly to the knee-point. Since the time of coincidence depends on the stiffness evolution of the paste, it is tempting to suggest that it is partly result of lower stiffness of the paste due to the presence of air voids. Another theory is that the air voids are small and spherical and set up a meniscus system (see section 3.4.1), which causes contraction. This is discussed further in section 5.8. A third theory is that air voids form in the paste-condom interface and compress due to the tension of the condom, and/or suck into the

paste to refill CS. Both will result in reduced outer volume, and thus, appear as increased AD. However, the fact that increased AD was found in "non-condom" concrete tests, too, indicates that the latter theory does not represent the main reason for higher AD when using AEA. This is further discussed in section 5.8, along with the practical consequences of it.

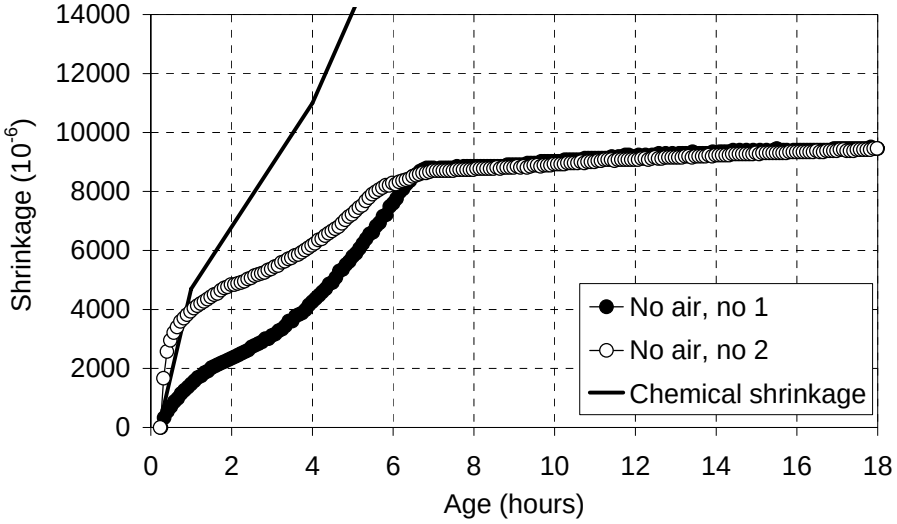

Fig. 3.16 Autogenous deformation (shrinkage) of paste without air entraining admixture. Chemical shrinkage is taken from Justnes et al (2000)

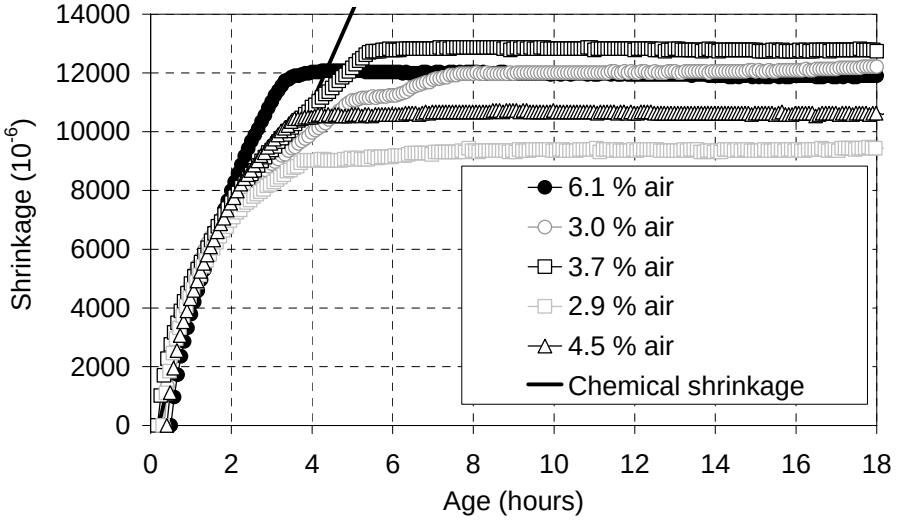

Fig. 3.17 Autogenous deformation (shrinkage) of paste with air entraining admixture. Chemical shrinkage is taken from Justnes et al (2000)

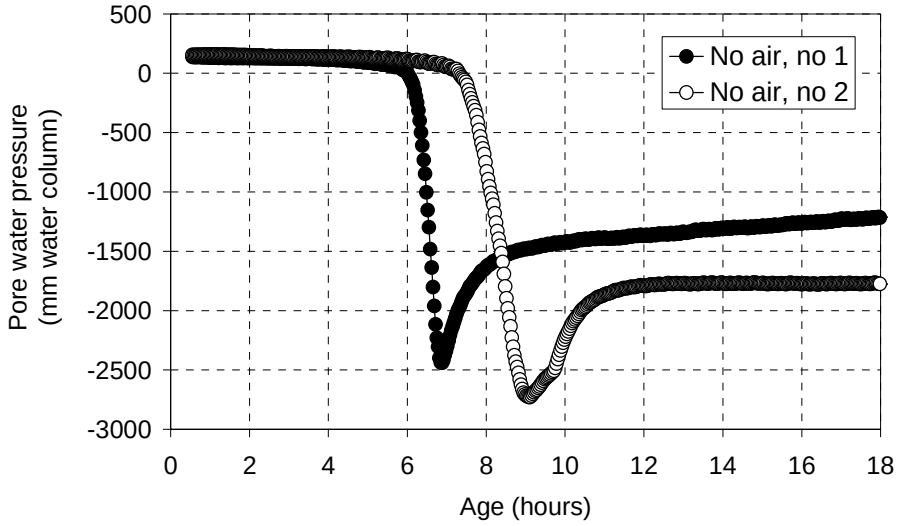

Fig. 3.18 Pore water pressure of paste without air entraining admixture.

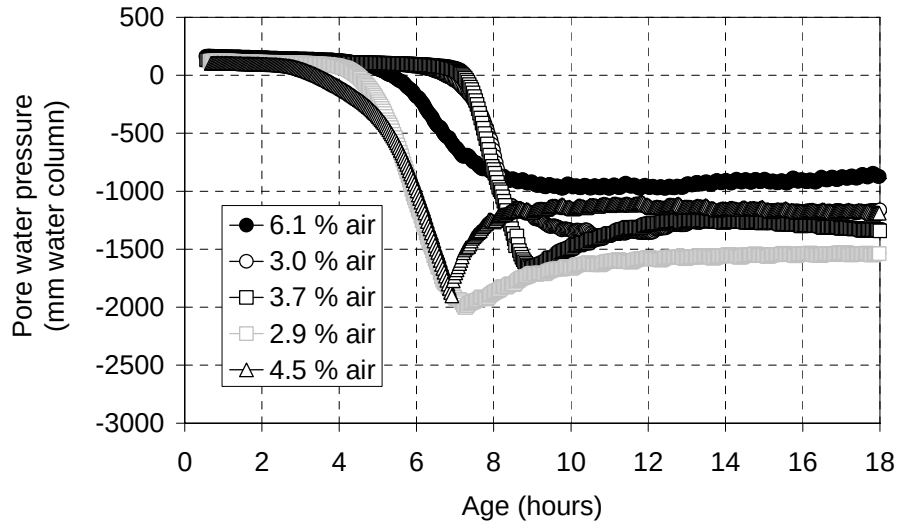

Fig. 3.19 Pore water pressure of paste with air entraining admixture.

The scatter observed may be related to inaccuracy in measurement, but also to the differences in air content. The influence of the air content is not systematic, neither on CS nor on PWP. But the time of the CS and PWP "kneepoints" seem to coincide as expected: Pastes with 2.9 and 4.5 % air have the earliest kneepoints in both measurements and pastes with 3.0 and 3.7 % have the latest kneepoints in both measurements (compare Figs. 3.16-3.17 with 3.18-3.19). The paste with 6.0 % air has an atypical PWP development compared to that of the other pastes. Also, it can be seen that the two pastes with the highest air content showed a smoother transition of the PWP from the horizontal part to the steep part, while all showed rather abrupt knee-points in the AD measurements. More data is needed to verify the influence of air pores on AD and PWP, in the time before the knee-point in particular.

Note that PWP of "No air, no 1" (Fig. 3.18) was measured in a rather small water container which probably caused insufficient cooling, and thus, a temperature rise in the sample. This would in turn caused faster hydration, which may explain both earlier bending off of and

higher PWP rate, as seen. The “zero-point” of PWP is here considered as the pressure difference from atmospheric pressure minus the hydrostatic pressure of water at the point of measurement (i.e. depth from the surface). As can be seen in Figs. 3.18 and 3.19, PWP is slightly higher than zero. This is probably the pressure exerted from stretching of the condom when filling it with paste.

Another feature is that AD of the pastes without AEA increases distinctly in the time **beyond the knee-point**, as expected, while AD of the pastes with AEA does not. This is probably directly caused by the buffer effect of the air pores: The vacuum effect drives the PWP downwards, but the air pores releases the pressure through expansion. The result is reduced rate of PWP accompanied with reduced AD rate.

3.3.7 Influence of aggregates

Justnes et al (1999) measured CS of paste with natural filler or fine sand (0-2 mm), and found no significant influence on CS nor the deviation point. The materials used are similar to those used in the present work.

It is commonly known that aggregates may contribute to reduced AD of hardened concrete through its function as internal water reservoir (release of absorbed water) and as restraint (aggregates having higher stiffness than the paste). Both are considered to be insignificant in the plastic age because the paste is sufficiently soft to freely deform around aggregate particles and the capillary force needed to suck out water absorbed in the aggregate is still absent or too low. In the early hardening age, PWP becomes significant and the cement paste may therefore suck some absorbed water from the aggregates, which contributes to reduce shrinkage. This is further discussed in section 5.8.

Secondary effects of introducing aggregates are that bleeding decreases and that air pores come along. The influence of bleeding and air pores is discussed in sections 3.2.4 and 3.2.6, respectively. See also section 5.9 regarding the influence of air pores.

The influence of aggregates may be investigated by simply comparing results from testing of a concrete and the equivalent matrix, where the matrix is the cement paste with the admixtures and the aggregate fines. It is a challenge of course to obtain the same air content and air void distribution as well as the same bleeding in the two. Such a comparison was not done here.

3.3.8 Conclusion – influence of paste composition on early age autogenous deformation

The main contribution of autogenous shrinkage (AD) to deformations in the plastic and early hardening phase is to settlement while the paste is still liquid, which coincides with the time when AD equals chemical shrinkage (CS). Note, however, that in systems with very low w/b (< 0.30) AD may constitute a significant contribution to the deformation in the early hardening age, too.

Cement type: CS may be anything between slight expansion and considerable shrinkage within the first hour of age depending on cement chemistry and fineness. It does not seem to be any distinct correlation with the cement characteristics, although the cements with the

highest C_3A content and highest fineness are among those with highest CS. One may expect that most of these earliest age differences are of less practical importance since they occur during mixing, transportation and casting. However, there are differences in hydration rate between cements beyond this point, which will directly influence the rate of settlement in the rest of the liquid phase.

w/c: CS rate is not significantly influenced by w/c, but the point where AD deviates from CS decreases with decreasing w/c.

Pozzolana: Normal amounts of silica fume (less than approximately 10 % as replacement for cement weight) do not seem to influence early age CS rate significantly. It follows that the efficiency factor of silica fume regarding early age CS is close to one. Other pozzolanes like fly ash is known to contribute little to early age hydration, and thus, CS.

Admixtures: Since CS is driven by hydration, admixtures influencing hydration is of interest. These are mainly accelerators and retarders or water reducing admixtures (WRA) with retarding side effect, mainly. It follows that the rate of CS and AD are influenced as well as the deviation point between CS and AD.

Air voids
Air voids formed by air entraining admixture (AEA) influences AD by:

- Higher rate of AD before the knee point
- HigherAD
- Earlier arrival of the knee point
- Lower rate of AD beyond the knee point

The three first points can be result of lower stiffness of the paste due to the presence of air voids, and/or of that the air voids constitute a meniscus system that leads to increased contraction. The last point is probably directly caused by the buffer effect of the air pores: The vacuum effect drives the PWP downwards, but the air pores releases the pressure through expansion.

Filler and aggregates: It is commonly known that aggregates may contribute to reduced AD of hardened concrete through its function as internal water reservoir (release of absorbed water) and as restraint. Both are considered to be insignificant in the plastic age because the paste is sufficiently soft to freely deform around aggregate particles and the capillary force needed to suck out water absorbed in the aggregate is still absent or too low. In the early hardening age, PWP becomes significant and the cement paste may therefore suck some absorbed water from the aggregates, which contributes to reduce AD. Natural filler or fine sand (0-2 mm) does not seem to influence on AD significantly. A secondary effect of introducing aggregates is that air pores come along, and which influence AD as mentioned above, and that bleeding decreases.

3.4 Volume change caused by evaporation

3.4.1 General

As pointed out in chapter 3.1, the water loss can be seen as the sum of water loss due to bleeding driven by gravity and water loss driven by evaporation. The nature of volume change caused by evaporation is that it equals the volume of water evaporated as long as there is a flat water surface on top, i.e. when **evaporation rate is equal to or lower than bleeding rate**, and that the sample is always water saturated. It has been pointed out by Radocea (1992) that rate of evaporation from the surface of fresh concrete is fairly constant during the first few hours of age, referring to several authors.

If **evaporation rate is higher than the bleeding rate**, the water surface will move down between the particles. This will cause two effects, which are thoroughly discussed by Radocea (1992):

1) The volume of evaporated water will of course be recorded as a weight loss, but the equivalent deformation (settlement and shrinkage) will not be recorded. Thus, there will appear a discrepancy between measured and true volume change due to evaporation, corresponding to the volume of empty space between top particles, see chapter 4.
2) Due to the surface tension of water, the water surfaces will curl and become menisci, which again introduce capillary tension in the water bounded by the menisci, according to the Laplace equation. This is an important point which is discussed in the following:

Formation of menisci leads to capillary tension of the pore water. This may be expressed by the Laplace equation for cylindrical pores, assuming that that the contact angle is zero:

$$\Delta P = 2\sigma/r \qquad \text{(eq. 3.1)}$$

where ΔP is the capillary tension in the pore water given as the difference in vapour pressure of the air and in the water, σ is the surface tension of water, and r is the meniscus radius. σ of pure water is 0.073 N/m according to physical reference books, but Jensen (1993) found it to be 0.055 N/m for a typical pore fluid. r is influenced by particle spacing and the contact angel between water and solid. Cement and fines from aggregate are known to have high wetting ability which gives a contact angel close to zero, and thus, a rather low r. It follows that r is at the same order of magnitude as the spacing between the cement/fines particles, and that the capillary tension is controlled by the geometry between the particles, i.e. particle spacing, mainly.

Consequently, capillary tension increases with decreasing particle spacing, at a given evaporation rate.

Firstly, the evaporation will be observed as increased settlement. Secondly, Wittmann (1976) showed that the capillary tension causes contraction forces between the particles resulting in particles moving towards horizontally, also, i.e. horizontal movement (shrinkage) occurs. He also confirmed by tests the relationship between shrinkage and pore water pressure. The same relationship was later confirmed by Radocea (1992). The horizontal movement starts earlier at the top than in the interior because decreasing permeability by time prevents more and

more water transport to the surface. This results in a progressively thickening zone developing from top downward (Powers, 1968). It is confirmed by own tests, where shrinkage of concrete was measured at the top (0 - 5 mm) and at 50 mm depth, see Fig 3.20 (see section 4.3 for description of the test method). Also, it can be seen that PWP turns into tension at the same points in time, as expected. This "skin" formation is supported by eye observation and by "finger pressure feeling" on the surface, and is typical for low w/b concretes, as experienced in situ. Consequently, in such cases PSS is influenced by the meniscus system, rather than particle contact it self, and may arrive quite early at the top surface.

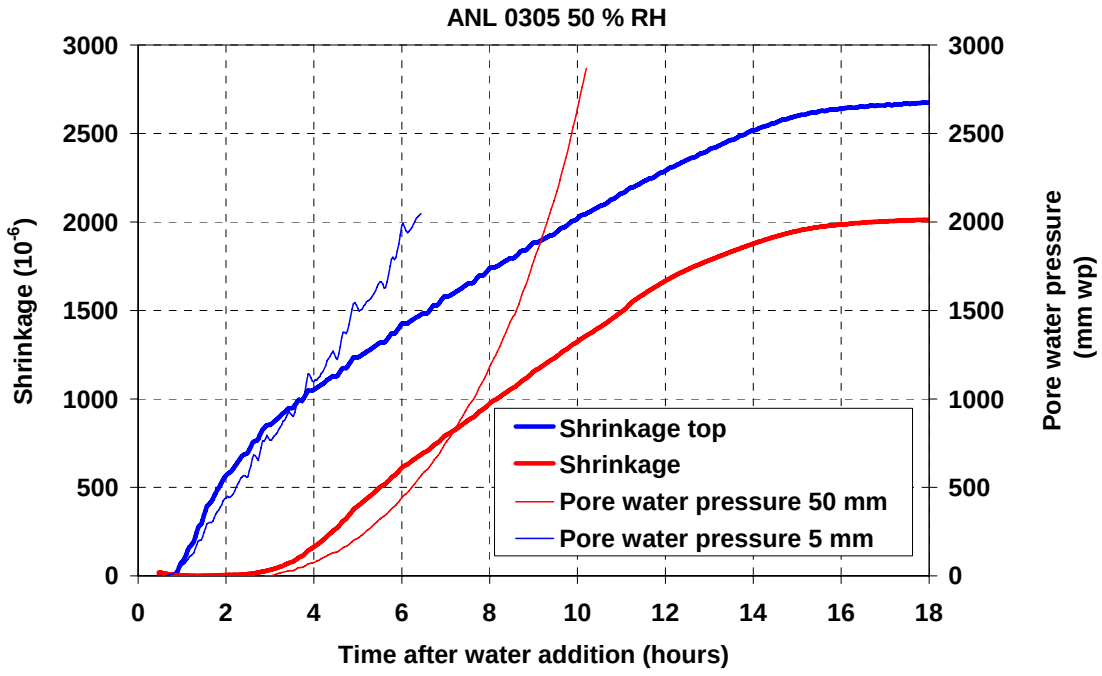

Fig 3.20 Shrinkage and apparent pore water pressure (1 mm water pile correponds to 0.01 KPa) of concrete with w/b = 0.30 and 5 % silica fume, at 5 mm and 50 mm depth, when exposed to air of 20°C and 50 % RH

The rate of shrinkage for a given paste-mortar-concrete is influenced by the evaporation rate, which is controlled by the climate over the top surface and the area of the water surface. In general, evaporation from a water surface occurs when the vapor concentration in the surrounding air becomes lower than that at the water surface. Then, the rate of evaporation is the product of vapor concentration difference and convection coefficient. The vapor concentration difference increases with increasing temperature difference between pore water and air, and decreasing RH. The convection coefficient is influenced by the fluid properties, but first of all the wind velocity (increasing with increasing wind velocity).

Whether or not bleeding rate is higher or lower than evaporation rate at a given external condition depends on the permeability of the sample. The permeability is therefore, a critical parameter that is discussed below.

3.4.2 Influence of permeability

Permeability is influenced by particle spacing, i.e. water-powder ratio, surface area of powder and degree of dispersion (influenced by interparticle forces). It is opportune to distinguish between the "initial permeability", as the permeability at the time of placing/finishing, and the "instantaneous permeability", as the permeability at any time considered. The first one is mainly influenced by degree of particle packing, and the second one is influenced by degree of hydration. Thus, a sample with insignificant bleeding means that its initial permeability is lower than that corresponding to the pressure head applied (here gravity, only). Then, Darcy's law can be used to find the initial rate of bleeding, **Q**.

$$Q = K \cdot \Delta h/L \ (m/s) \qquad \text{(eq. 3.2)}$$

where **K** is the coefficient of permeability (m/s) and **Δh/L** is the pressure head corresponding to the weight of the solids in water per unit area:

$$\Delta h/L = [(\rho_c - \rho_w) \cdot g/\rho_w \cdot g] \cdot (1- \varepsilon) \qquad \text{(eq. 3.3)}$$

where $\boldsymbol{\rho_c}$ and $\boldsymbol{\rho_w}$ is density of cement and water (kg/m^3), resepctively, **g** is gravity (m/s^2) and **ε** is porosity.

Radocea (1992) has calculated the permeability coefficient of fresh cement pastes with w/c between 0.3 and 0.4 and with cement fineness of 400 m^2/kg, to be in the range $0.5 \cdot 10^{-6}$ to $1 \cdot 10^{-6}$m/s, according the eq. 3.4 presented by Kozeny and Carman and supported by his own tests.

$$K = [\rho_w \cdot g \cdot \varepsilon^3] / [k_c \cdot \eta \cdot s^2 (1- \varepsilon)^2] \ (m/s) \qquad \text{(eq. 3.4)}$$

where $\boldsymbol{\rho_w}$ is density of water (kg/m^3), **g** is gravity (m/s^2), **ε** is porosity, $\mathbf{k_c}$ is Carman constant, **η** is viscosity of water (Pa·s) and **s** is specific surface area of wetted material (m^2/m^3).

This can be used to calculate the maximum evaporation rate at which the surface is still wet (no menisci are formed), i.e. when bleeding rate (Q) equals evaporation rate. Assuming w/c to be 0.3 ($\varepsilon = 0.5$), and K to be $1 \cdot 10^{-6}$ m/s as in the above mentioned example, and ρ_c to be 3000 kg/m^3, Q will correspond to 3.6 kg/m^2/h. It can be seen from Fig. 4.11 that the number corresponds to an unexpectedly high evaporation rate. This is probably an effect of hydration blocking the channels: It is commonly known that the surface of cement grains changes considerably in the first minutes/hours of hydration, which results in a significantly change of geometry from spheres (assumed) to irregular particles, which bridges particles and gives increased surface area. Note that the calculation is based on initial quantities before hydration starts (solid particles in suspension) and those presented in the Fig. 4.11 on "real" quantities (cast concrete), i.e. after some hydration has taken place, and that K (eq. 3.4) is particularly sensitive to porosity and specific surface area in that they appear in third and second power. It strongly indicates that the permeability changes considerably within the first minutes/hours and that calculated permeability of fresh concrete is not an easy task.

3.5 Volume change due to temperature changes

Normally, heat of hydration does not generate significant temperature change during the plastic and early hardening age of concrete. If any, it gives expansion which in most cases

contributes to reduce cracking tendency. Cooling and subsequent contraction of the concrete may arise from the surrounding air and from a cold formwork. The latter is probably not important since the mass of concrete is normally much more than the mass of formwork skin. A lower air temperature than concrete temperature gives two effects:

- Thermal contraction, and
- Increased evaporation if the surface is not sufficiently protected

It is conceivable that thermal contraction may constitute an additional driving force for deformation of the meniscus system (the skin) in the liquid phase, because the strain capacity of this system is so low (see chapter 8). Furthermore, coefficient of thermal contraction (CTE) changes by age and is relatively high in the plastic age (dominated by CTE of water which is approx. $60 \cdot 10^{-6}$) as demonstrated by Bjøntegaard (2000) who tested CTE of the "basic concrete", see Fig 3.21.

Thermal contraction is definitely an important contributor in the early hardening phase, as demonstrated in chapter 9.

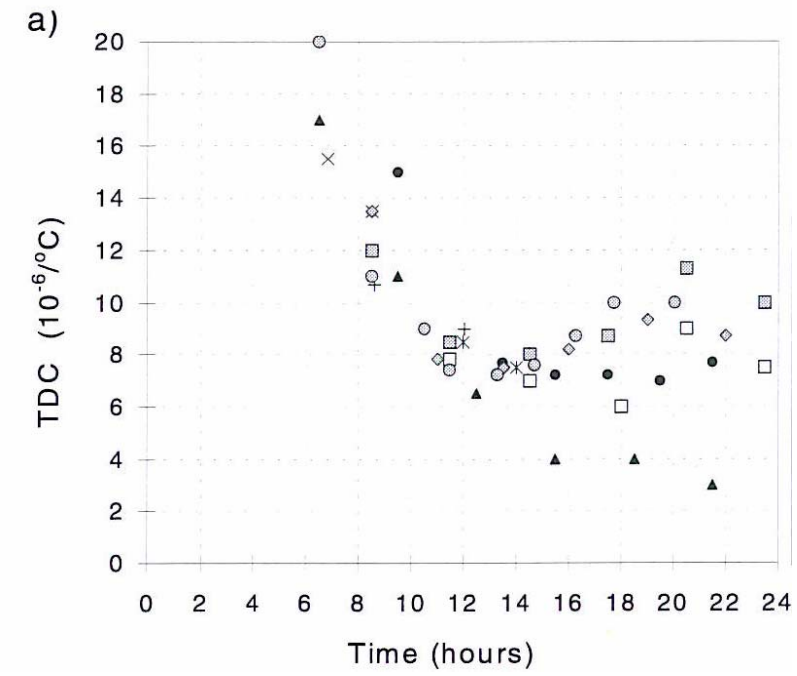

Fig 3.21 Coefficient of thermal expansion, CTE (called TDC on the y-axis) versus age (Bjøntegaard, 2000)

If the concrete surface is insufficiently protected, decreasing temperature of surrounding air will contribute to increased evaporation. It is because the vapour pressure decreases with temperature, and thus, results in larger difference between the vapour pressure of the surrounding air and that over the pore water meniscus. For instance, air temperature of 20 ºC corresponds to a vapour pressure of **8.8 torr** at 50 % RH, and air temperature of 10 ºC corresponds to **4.6 torr** at 50 % RH, while it is **17 torr** over the pore water meniscus at the top surface, at 20 ºC.

Consequently, one should strive to keep the concrete temperature as much lower than the air temperature as possible. In fact, this is a "tool" (but of course not always very practical/economical) to prevent evaporation. For instance, if the concrete temperature is 10 ºC and air temperature is 20 ºC (50% RH), the vapour pressure over the pore water is **9.2 torr** (10 ºC and ~100 % RH), while it is **8.8 torr** in the air at 50% RH, i.e. roughly 1 to 1. Hence, there is no driving force for evaporation.

3.6 Summary - the driving forces to cracking

The driving forces to cracking in the plastic and early hardening age are deformations caused by self generated **volume change** and any **externally imposed deformation**. The latter may originate from unwanted movement of the concrete after placing/finishing caused by e.g. formwork movement (settlement, vibration, etc.) or from gentle flow of a sloping slab (e.g. parking places, bridge decks, road pavements) which may occur if the concrete has high viscosity and low yield shear strength. The volume change that appears after casting is mainly result of:

- autogenous deformation, AD, (resulting from chemical shrinkage, CS),
- evaporation and
- temperature changes

The volume change is basically a volumetric deformation, but from a practical point of view it is convenient to consider linear deformations, commonly referred to as "plastic settlement" and "plastic shrinkage". The shrinkage rate –settlement rate ratio changes basically from 0 to 1 in the period, as the stiffness of the paste changes from that of a liquid to that of a solid in the hardening age (with isotropic properties). The early age as considered here, is divided in to three consecutive phases (visualized in Fig. 3.22):

1. "**Liquid phase"**: Until formation of mineral skeleton, i.e. until paste/mortar/concrete can support its own weight (point of self-support, PSS). It is the phase when AD equals chemical shrinkage, CS, and manifests it self in settlement, only (i.e. no horizontal deformation).

2. **"Semi-liquid phase"**: Until significant stiffness starts to develop, i.e. around initial setting time. The start of the phase is associated with time when pore water pressure becomes tension and horizontal deformation (shrinkage) starts to develop. The phase coincides probably with the time when the paste/mortar/concrete can be brought back to liquid phase with agitation.

3. **"Early hardening phase"**: Through final setting and the following few hours. The phase is associated with significant stiffness development and minimum strain capacity of the hardening paste/mortar/concrete.

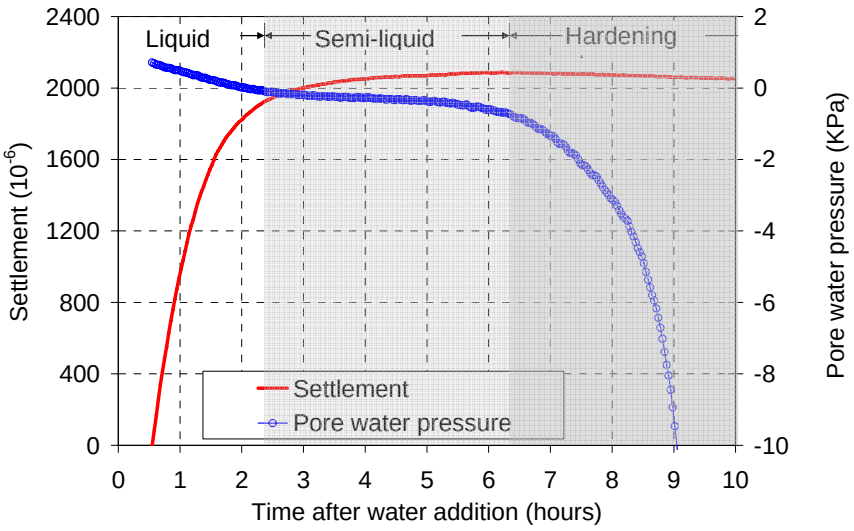

Fig 3.22 Correlation between pore water pressure, settlement and the three stiffening phases; liquid - semi-liquid - hardening, of the "basic" concrete (sealed condition).

As long as the paste behaves like a liquid, gravity makes AD equal CS. From a practical point of view AD is then seen as part of settlement. Apparently, it may constitute the main contributor to settlement (the only one if there is no air evacuation, bleeding, evaporation or thermal dilation). The rate of AD is of course influenced by the hydration rate of various cements and by the use of accelerating or retarding admixtures, but the paste (and cement) composition is considered to be of minor importance with respect to AD as driving force to cracking in the liquid phases.

Later, in the semi-liquid phase, when the hydration has created a skeleton with stiffness that needs a higher force than that caused by gravity to collapse, AD becomes significantly lower than CS and new empty pore space occurs, probably as expansion of existing air voids and/or formation of new pores. Accordingly, the settlement rate is significantly reduced. This deviation point appears to occur much earlier in linear test methods than in the widely used volumetric "condom test method". The reason can be that CS generates a vacuum effect in the condom, which constitutes an additional force to the gravitational force that compacts the sample, and which results in compaction for a longer time. The surrounding air in the linear tests, relieves the vacuum effect and allows water to suck in from the surface (i.e. emptying of surface pores as the "formation new empty pore space"). It follows that linear (and non air tight) measurement is better suited for evaluation of the practical consequence of AD, i.e. on settlement of equivalent mortars or concretes. Deviation point from condom test may be used as a rough measure for final setting time of pastes (but the relation to Vicat-measure is not clear).

AD is often expansion in the semi-liquid phase and early hardening phase (seen in both settlement and "shrinkage") caused by re-absorption of bleed water/chemical reactions, which of course contributes to reduce cracking tendency. The expansion is seldom observed in condom-test (probably because it is overshadowed by the vacuum effect). Air voids in the

paste (e.g. formed by the use of air entraining admixture) seems to increase AD in the liquid phase. It is suggested, but not verified, that the reasons could be lower stiffness of the pastes with air and/or capillary tension of pore water caused by menisci formed by the air voids. Anyway, AD is considered not to be an important contributor to the driving force to cracking in the semi-liquid phase, because it is small relative to strain capacity and other deformations. But AD may be an important contributor to contraction in the early hardening age of mortars or concretes with very low w/b-ratios.

Evaporation is the most important driving force in all the three phases. It results in capillary tension of the pore water if evaporation rate is higher than bleeding rate, which results in increased settlement and shrinkage. The result of evaporation is influenced by the particle size and spacing, mainly. Hence, factors like w/b and surface area of the binder are important factors (and more important than the chemistry of the binder).

An important point is the very early formation of capillary tension, and thus shrinkage, at the top surface which appears as a skin formation, which typically occurs in systems with low permeability (e.g. low w/b) relative to the evaporation rate. This surface skin may be a reason for cracking in the liquid phase.

Temperature changes may give thermal deformation and influence evaporation. It is particularly important in the early hardening age, when the tensile strain capacity is at its minimum. If the concrete surface is insufficiently protected, decreasing temperature of surrounding air may contribute to increased evaporation. It is because the vapour pressure decreases with temperature, and thus, results in larger difference between the vapour pressure of the surrounding air and that over the pore water meniscus. And opposite, a lower concrete temperature than air temperature reduces evaporation.

4. Development of Experimental System for Testing of Settlement, Shrinkage, Pore Water Pressure and Water loss due to Evaporation

4.1 Introduction and test systems found in the literature

Most tests methods found in the literature are designed for measuring the autogenous and/or drying shrinkage of hardening concrete. In principle, the design are quite similar to those used for testing on paste, see section 3.2.2.4: A common feature for test methods designed to handle the initial phase, is that the specimens stay in the mould during testing. The friction between the specimen and the mould may, in combination with the low stiffness of the paste-mortar-concrete in this phase, hinder the movement of the specimen. The efforts to prevent the friction differ in the test methods: In some methods the mould surface is treated with oil, wax or asphalt, while other tests use double set of plastic with talcum in between or sheets of Teflon between the specimen and the mould. The third group uses flexible tubes, i.e. corrugated tubes of metal, plastic or rubber to prevent the friction. Metal discs and oil film has also been used as under layer for pastes cast in thin plastic sheets.

A concrete dilatometer is presented by Jensen et al (1997), based on measurement of the vertical deformation in a flexible tube via metal plates on the top. Thus, in the initial phase the autogenous shrinkage equals the settlement and the linear shrinkage in this phase can, therefore, not be found. It is not clear how the possible bleed water appears on the top, whether it occurs as a layer between the concrete and the top plate or squeezes out between the tube and the top plate. Anyway, the re-absorption may cause expansion. Some of the results presented show expansion in a period around setting, but the authors do not discuss re-absorption of bleeding water as a reason, but suggest that it is thermal expansion (due to a temperature rise of ½ ºC). They say, however, that the thermal expansion can not account for the total expansion. The dilatometer is submerged in a temperature controlled water bath.

Kasai et al (1982) measured the horizontal length change of a 100x100x400 mm beam under external drying, via 30 mm anchor pins inserted in the centre of both ends of the beam. The measurements started 2 or 3 hours after casting. The temperature was controlled by the air temperature. This may have given a hydration generated temperature rise of some degrees Celsius, which in turn caused a thermal expansion in the early hardening age. Friction is taken care of by the use of paraffin paper and Teflon sheets.

A similar set up, in principle, has been used by Brüll and Komloš (1980 and 1982). They measured the linear shrinkage, as the horizontal length change, of cement pastes and mortars in a 40x40x160 mm (1980) or in a 70x70x280 mm steel mould and concretes in a 150x150x700 mm mould (1982). No temperature control is mentioned. The results did not show any deformation in the initial phase other than some thermal expansion. It is not found whether this is a material property or due to friction, fixing of the measuring points or other.

Ravina (1986) used a 70x70x280 mm mould to determine the linear drying shrinkage (T = 30 ºC, 50 % RH in a wind tunnel) of mortars with OPC and different amounts of fly ash (w/b ~ 0.45). He measured the movement of studs inserted in both ends of the beam, just 7 mm below the top surface. The measurements were started one hour after mixing, corresponding to the time of wind application. The results show always a very high expansion within the first hour of measuring (i.e. before setting), i.e. from 0.7 ‰ (without fly ash) to 1.8 ‰,

depending on the type and amount of fly ash. He explains the expansion as a “chemically-induced swelling”, probably connected to the early ettringite formation. Especially the magnitude of the expansion is very different from other results as discussed above. The author says that bleeding outweighs the evaporation in this period. Hence, re-absorption may have contributed to the expansion. Some thermal expansion may have contributed, also. Still, these contributions are probably less than 10 % of the measured values.

The systems to measure the length change of beams, slabs or cylinders, may be put into six groups:

- “Cast in nails” through a hole in the middle of the end plates with the nail heads embedded in a concrete beam, e.g. Fig. 4.1 (Bjøntegaard, 2000)
- Moveable endplates with “plugs” in a concrete beam, e.g. Fig. 4.2 (Morioka et al, 1998)
- Horizontal transverse cast-in-bars through a concrete beam, e.g. Fig. 4.3 (Takada et al, 1999)
- Vertical cast in bars in a concrete slab, e.g. Fig. 4.4 (Holt and Leivo, 1999)
- Cast in strain gage, e.g. Hanehara et al (1998)
- Metal plates placed on top of cylinders, e.g. Fig. 4.5 (Jensen et al, 1997)

The movement has been measured using inductive displacement transducers (IDT) or linear variable differential transformers (LVDT). But also “non-contact” transducers like reflection of electronic pulses or laser against a metal chip on the concrete have been used (Morioka et al, 1998) and (Holt and Leivo, 1999).

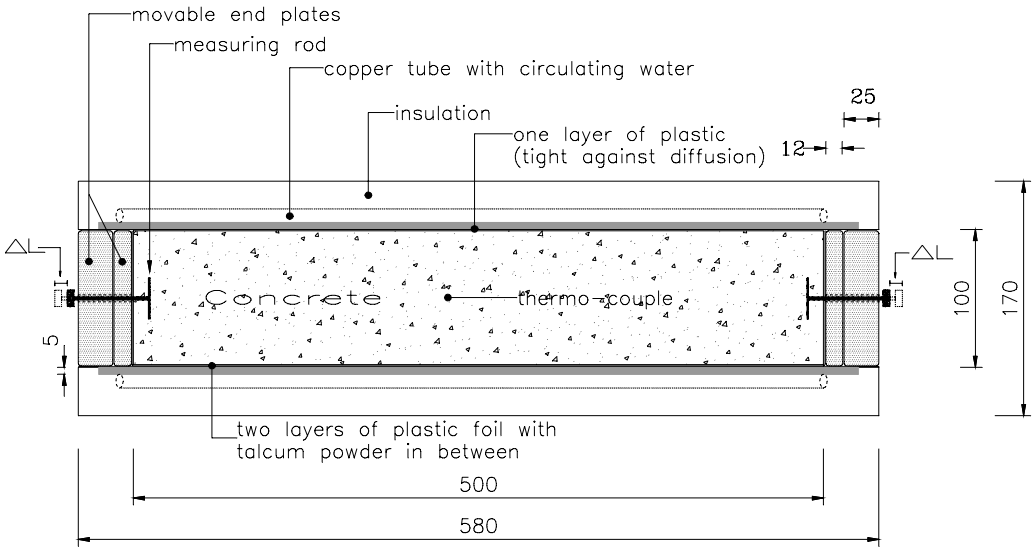

Fig. 4.1 Measuring system with “cast in nails” 100•100•500 mm beam (Bjøntegaard, 2000)

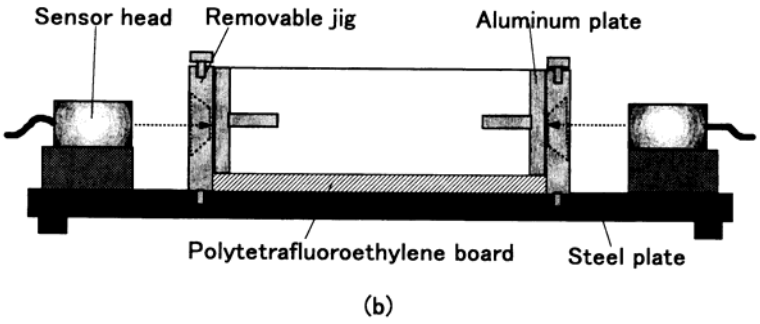

Fig. 4.2 Measuring system with moveable end plates in a 40•·40•160 mm beam (Morioka et al, 1998)

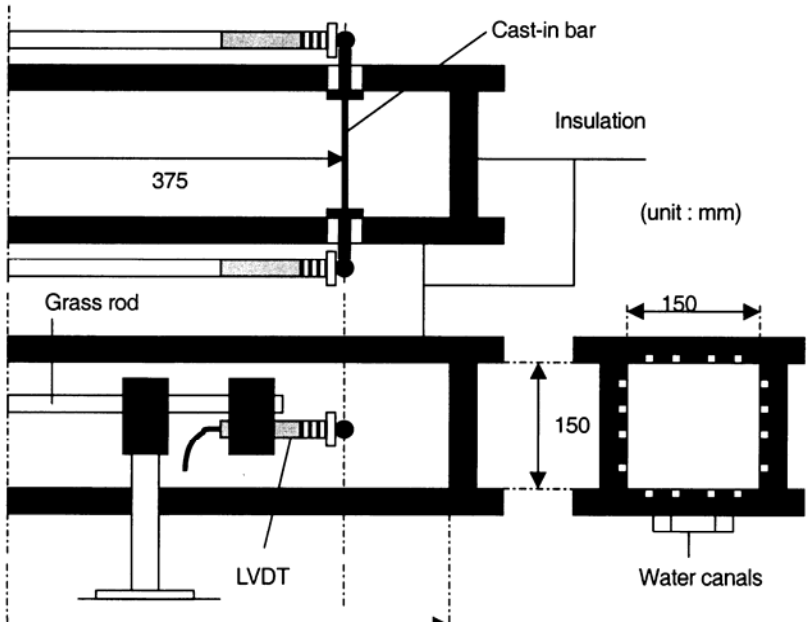

Fig. 4.3 Measuring system with horizontal "cast in bars" in a 150•150•500 mm beam (Takada et al, 1999)

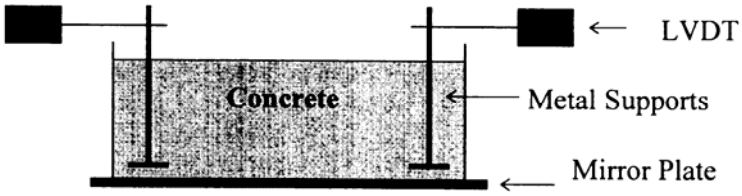

Fig. 4.4 Measuring system with vertical cast in bars in a 270•270•100 mm slab (Holt and Leivo, 1999)

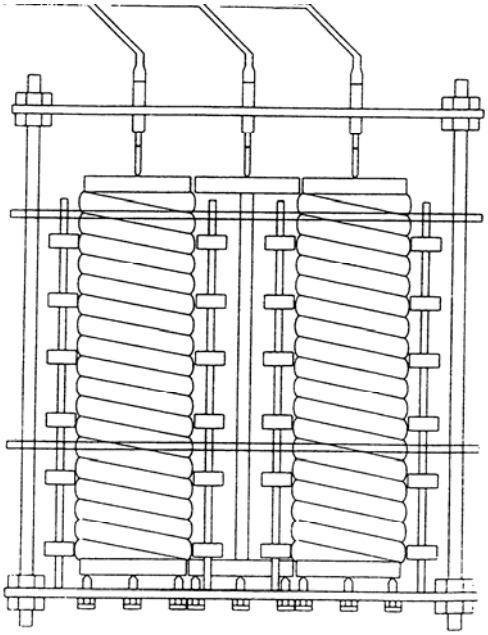

Fig. 4.5 Measuring system with concrete in 100 • 375 mm flexible tubes and vertical length measurement with displacement transducers on top (Jensen et al, 1997)

Holt and Leivo (1999) used two vertical metal supports being suspended from 150 mm above a concrete slab, and attached to LVDTs, see Fig. 4.4. They reported that false shrinkage may occur in the beginning of the test exerted by the settlement, and that this was accounted for by zeroing the shrinkage data after settlement. Hence, the suitability of the method for measurements in the whole plastic age, is uncertain. A double layer with plastic with talc powder in between was used to prevent friction. The method show good repeatability.

I consider the principle with cast in strain gages not to be of current interest because it represents a system that is too stiff to transfer the deformations of the soft concrete.

Based on this review a set of requirements were set for a suited test system, see next section.

4.2 Requirements and Description

The following requirements were set:

- Simplicity in preparation, testing and demoulding
- As low friction as possible
- Avoid wall effect on settlement
- Flexible in order to handle both paste, mortar and concrete
- Allow measurement of settlement, shrinkage, pore water pressure, weight loss and temperature on the same sample.
- Allow measurement under sealed conditions as well as unsealed and with wind
- Temperature control

The set up is shown in Fig 4.6. The rig is built on a triple 100 mm cube mould of steel. This base was chosen because of the simplicity requirement, mainly; the sides of the mould are

hinged and the end plates are loose. The height and thickness when used for concrete is 100 mm and the length is 280 mm. The dimension is a compromise, i.e. small enough for easy handling, but still large enough to represent a concrete body. The end plates are modified with braces for IDTs (inductive displacement transducer) used for shrinkage measurements, and holes for the measuring rod. Heat of hydration is not considered to be significant in the time period considered here. Therefore, special efforts to control temperature were not made, other than the utilizing the heat capacity of the relatively thick sides and the bottom of steel, 12 and 10 mm respectively, to reduce the temperature increase caused by heat of hydration. Thus, sufficient temperature control is achieved by controlling the temperature of the air in the room in which the rig is placed. In the present study, the air temperature was kept at 21 +/- 0.5 °C. See chapter 5 for typical temperature developments.

The shrinkage is measured as the horizontal movement of two “nails” placed centric in both ends of the specimen, see Fig 4.6. This “nail system” was judged to be sufficiently simple and reliable (based on the test method review presented above). The nails are made of 3 mm thick steel rods with a 15 x 15 mm steel plate soldered to the end. The length of the nail is 80 mm, and the end (steel plate) is placed 30 mm into the sample. The other end of the rod is wedged and screwed into the IDTs through a hole in the end plates of the mould. A sheet of 5 mm thick “bubble plastic” is placed inside the end plates, on order to allow any expansion of the sample.

Friction occurs between the sample and the mould sides and bottom, but also in the connection between IDT and sample. A simple test was carried out in order to find the best antifriction material between concrete and mould: Freshly made concrete was placed on tables prepared with the materials. Then, the tables were tilted until the concrete slid off. The materials used were single sheets of polyethylene (“regular plastic”) and Teflon, Teflon paste, and double sheet of polyethylene with talc powder in between. The latter gave by far the lowest friction, and was therefore chosen. The one sheet is “contact paper” applied on the mould side. It may last for 20 to 30 tests before replacement is necessary. Talc powder is then brushed on the contact paper as well as on the back side of the other sheet before placement in the mould before casting.

Friction in the connection between IDT and sample may occur either due to friction in the IDT caused by a bending, or as friction between the rod and the support. The bending is resulting from the weight of the sample on the rod. Using rods without support showed to give unreliable results, as shrinkage were recorded sometimes and sometimes not in repeated tests. Therefore, “low friction” supports were introduced in the end plates, as a Teflon plug with a 3 mm hole, together with a moment free connection to the IDT (set up by a few turns only). To further reduce friction Teflon paste is applied in the hole as well as on the rod.

Another point is to seal the transfer through the bubble plastic thoroughly with Teflon paste in order to hinder paste to penetrate to the hole in the Teflon plug. A third point is connected to the placement of the concrete and subsequent adjustment of the IDT. Placement must be done gently from the middle of the mould towards the ends, so that the nails also move towards the ends, and without hitting the nails with the placing tool or vibrator. Then, after placing, the IDTs are adjusted by loosing them and then pulling them to a position corresponding to their measuring range.

The settlement is measured as the vertical movement of two circular plastic meshes with diameter of 50 mm, placed with its centre approximately 70 mm from the ends of the mould.

In order to prevent any external load from the inductive displacement transducer, the movable part of it resting on the mesh was very light (less than 6 gram). The meshes penetrate any bleed water to rest on the concrete surface.

The pore water pressure is measured by pressure transducer connected to a water filled tube with inner diameter of 3 mm, see Figs 3.5, 4.6 and section 3.2.2.5. Two tubes are placed vertically in the concrete with the ends normally at 5 mm and 50 mm depths, respectively. The tubes are fixed in a rack, as shown in Fig 4.6.

When tested in sealed condition, the sample is covered with a plastic cover with holes for the settlement, pore water pressure devices and temperature gauge.

Wind is applied by the use of a fan connected to a channel as shown in Fig 4.7. The air stream goes towards the fan (suction) which has shown to give less turbulence than blowing. The wind velocity is normally approximately 5 m/s.

The room temperature 21 +/- 0.5 °C, and RH normally between 47 and 50 %.

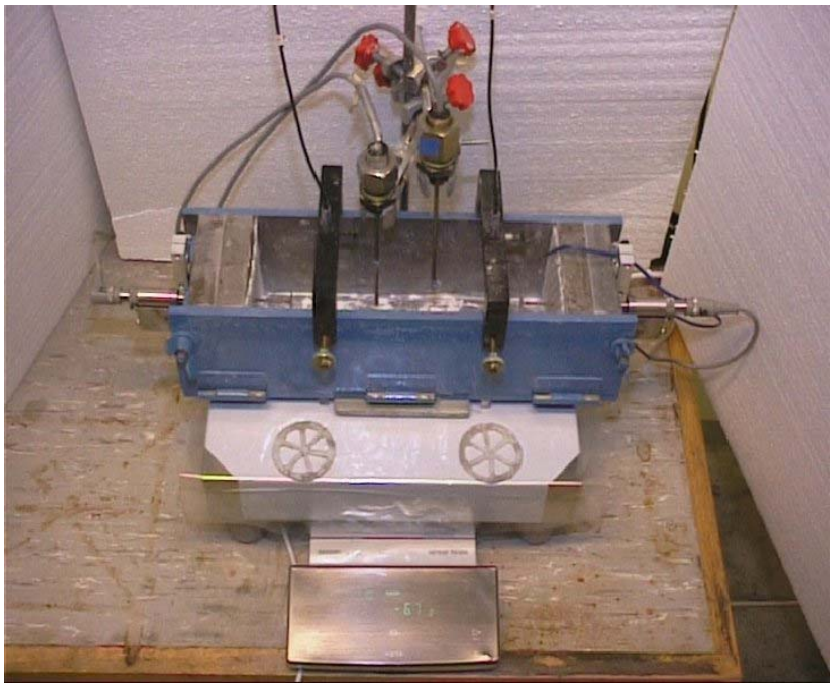

Fig. 4.6 Picture of the rig with devices used to measure settlement, shrinkage, pore water pressure and weight loss in concrete before and during setting.

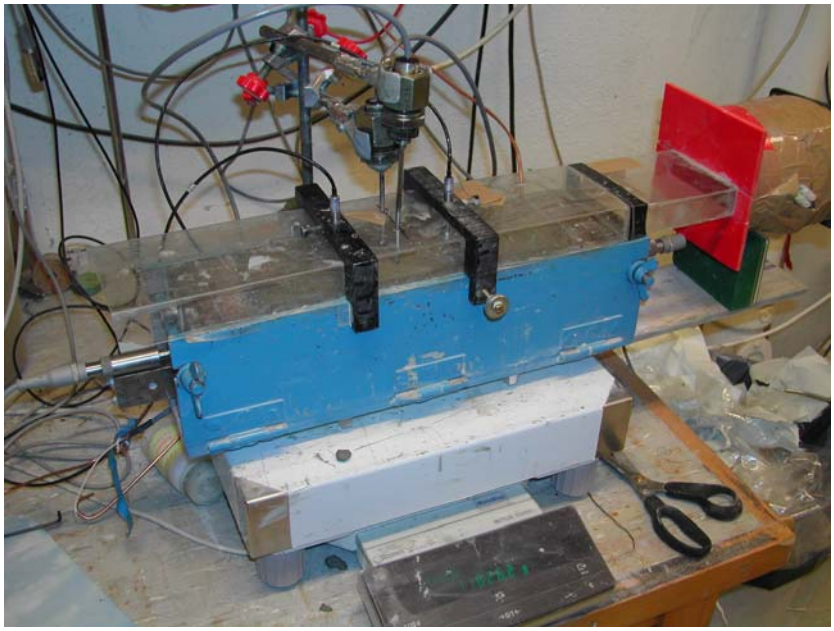

Fig. 4.7 Picture of the rig with fan and wind channel

The rig is placed on a balance so that the water loss may be recorded (in tests with external drying). All data (settlement, shrinkage, pore water pressure, temperature and weight) are recorded every second minute, by the use of an electronic data logger.

4.3 Repeatability

4.3.1 General

A repeatability evaluation includes repeated tests on equal batches. Then, of course the repeatability evaluation will be influenced by a possible batch to batch variation caused by unintended variation in mixture composition, concrete temperature and casting procedure. Furthermore, the complexity related to testing at the early age brings in several pitfalls which challenge the reliability evaluation: The concrete changes from a liquid, where water may flow rather freely to the surface and all volume change appears as settlement, to a solid where the water transport is hindered due to blocking, and the volume change appears both as emptying of surface pores (and internal pores at the end), and bulk shrinkage in all directions. Furthermore, the properties are given as curves rather than discrete values, and the evolution is characterised with “phase shifts”, which are influenced by interacting material parameters and evaporation rate.

The experimental system includes several measurable quantities, and I will assume that there exists a consistent relationship between them, which can be used in the repeatability evaluation, also. These are:

- Water loss, by recording weight change
- Settlement, two measures
- Shrinkage, measured on both ends of the specimen

- Pore water pressure, measured at 5 mm depth and at 50 mm depth
- Temperature evolution in the middle of the specimen

Therefore, a second part of the reliability evaluation is to consider the repeatability of this relationship.

Firstly, each measure is discussed separately, and then the relationship between them. The reliability is evaluated in the following based on results from ten test series (batches) on equivalent concretes; "the basic concrete", (w/b = 0.4) ANL0405, see APPENDIX 1. Six test series were performed with a wind velocity of 5 m/s, two with 3.3 m/s, and two with 0 m/s.

4.3.2 Evaporation rate

The evaporation rates in repeated tests were quite similar as shown in Figs 4.8, 4.9 and 4.10, and have monotone shapes. The scatter seen for the 5 m/s results is partly due to different starting ages (25 to 56 minutes after water addition). Note that the maximum difference between the six batches at 56 minutes is 0.31 kg/m^2, and that it is rather constant in following few hours, and then increasing to 0.49 kg/m^2 at 18 hours of age. It indicates that the evaporation rate is not considerably influenced by the present differences in age at exposure, and thus, that the curves may be normalised to have the same starting point (corresponding to that of the "latest" one), see Fig 4.9. Then it can be seen that the maximum difference in evaporation is less than 8 % between the six batches, which gives acceptable reliability.

The weight loss recording in one of the two tests at 3.3 m/s was lost, and the one measured is not shown here, but in Fig 4.10, which shows the influence of evaporation rate.

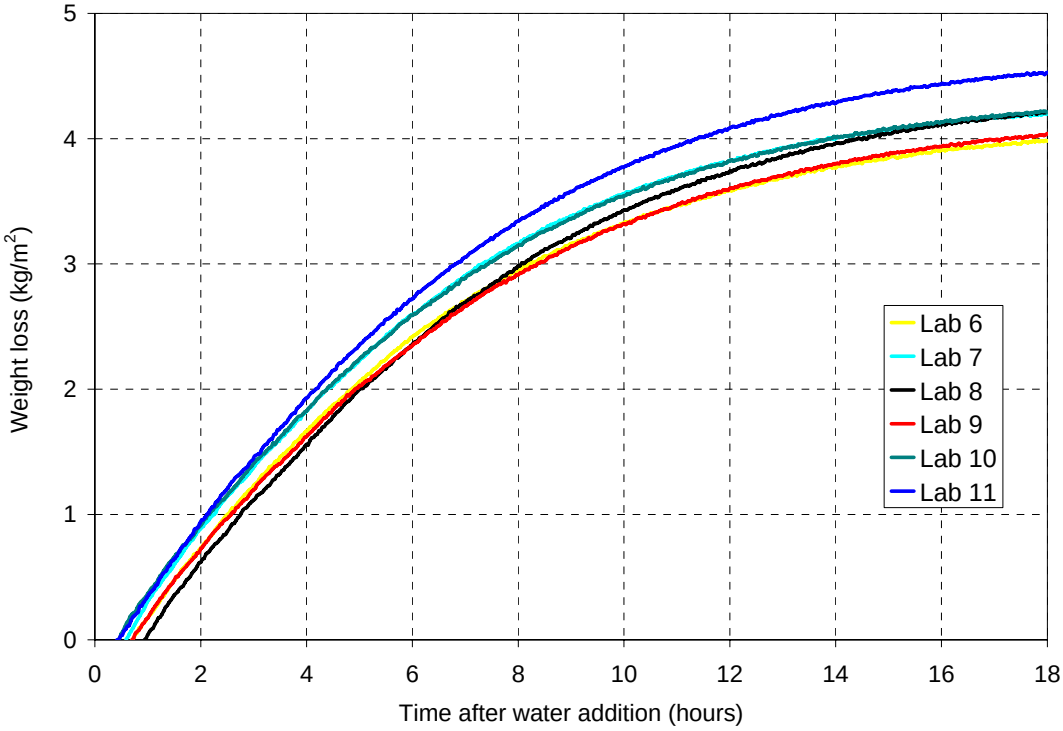

Fig. 4.8 Weight loss due to water evaporation of six equivalent "basic concretes",

when exposed to wind velocity of 5 m/s.

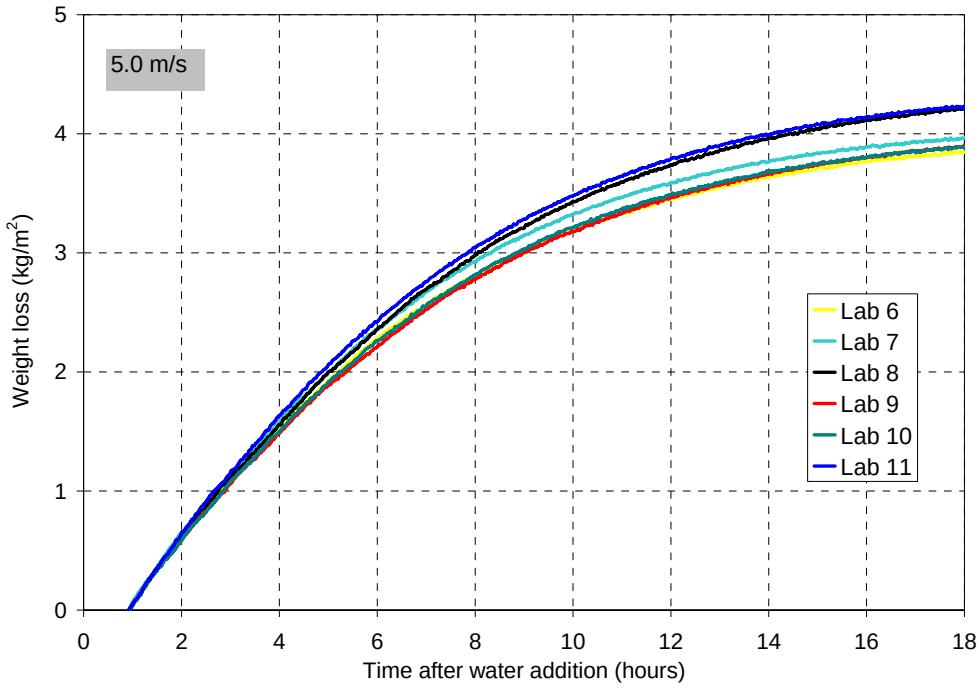

Fig. 4.9 As Fig 4.8, but normalised to have the equal starting point

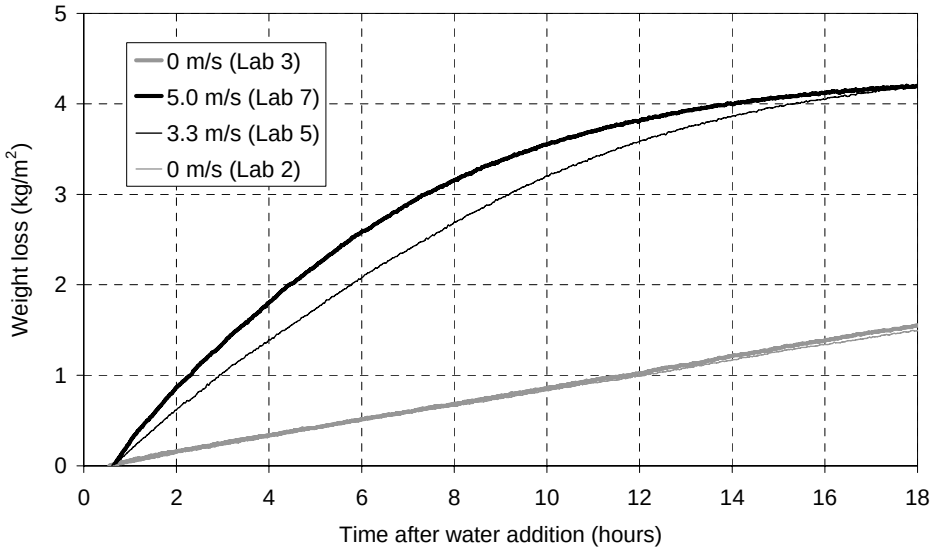

Fig.4.10 Weight loss due to water evaporation of four equivalent "basic concretes". Ttwo were exposed 0 m/s and the two others to 3.3 m/s and 5.0 m/s, respectively

It can be seen that the evaporation rate at the beginning is approximately 0.6 kg/m^2/h at 5 m/s, which corresponds fairly well with that found from the diagram in Fig. 4.11, made by PCA (1964) (assuming air and concrete temperature of 21 ºC and RH of 50 %). The corresponding rate at 3.3 m/s and 0 m/s is approximately 0.45 kg/m^2/h and 0.13 kg/m^2/h, respectively, which both corresponds fairly well to that found from Fig. 4.11, also.

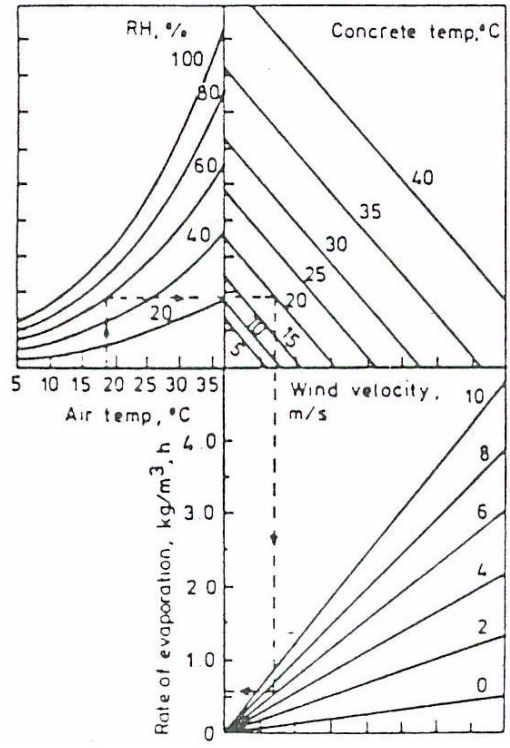

Fig.4.11 Diagram for estimation of rate of evaporation from a horizontal concrete surface in the plastic phase (PCA, 1963).

4.3.3 Temperature evolution

The temperature evolutions for the tests (measured in the middle of the specimens) were quite similar, also, see Figs. 4.12-4.14. The rather similar temperature decrease due to the evaporation, of about 2 ºC at 5 m/s, also supports the small scatter in evaporation.

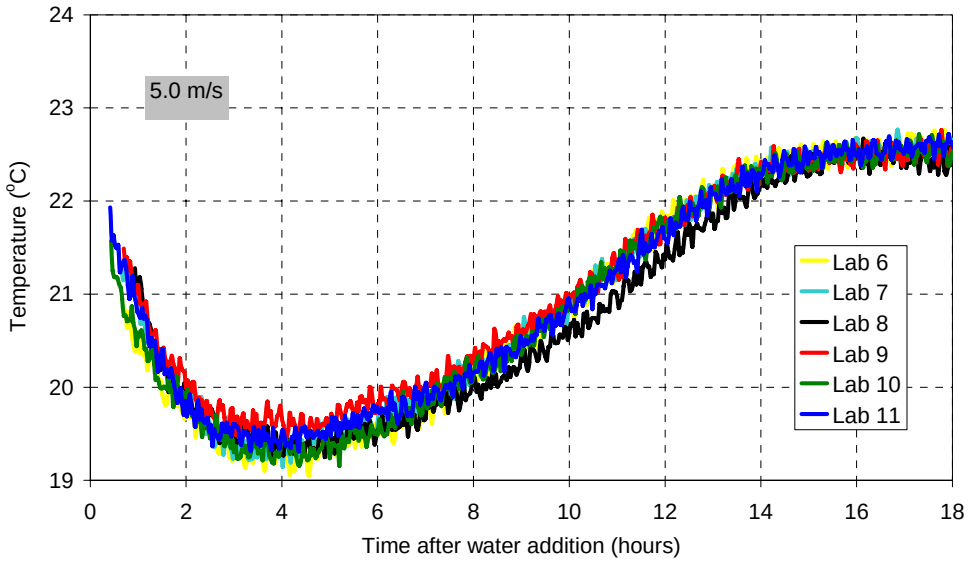

Fig. 4.12 Temperature evolution of six equivalent "basic concretes", when exposed to air with wind velocity of 5 m/s.

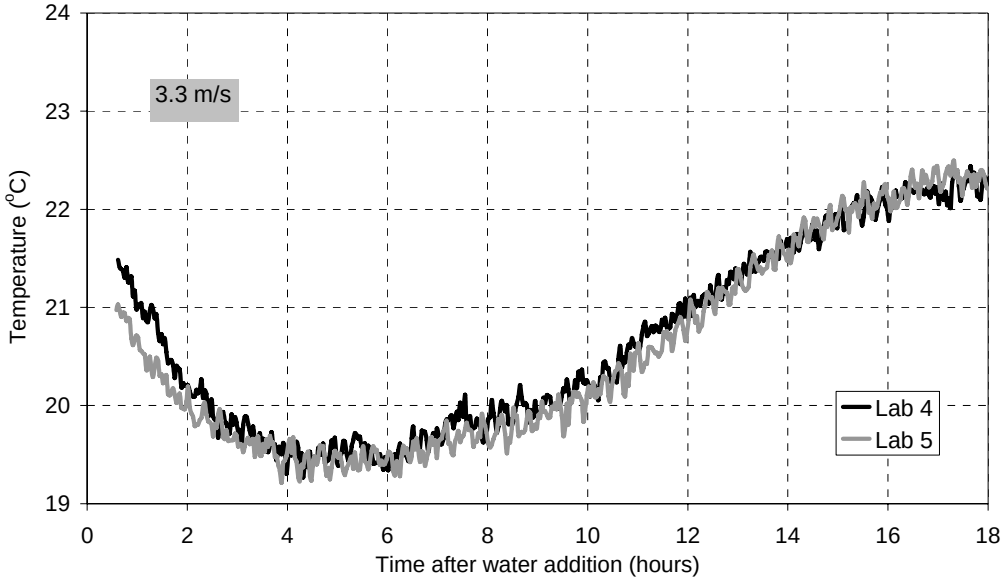

Fig. 4.13 Temperature evolution of two equivalent "basic concretes", when exposed to air with wind velocity of 3.3 m/s.

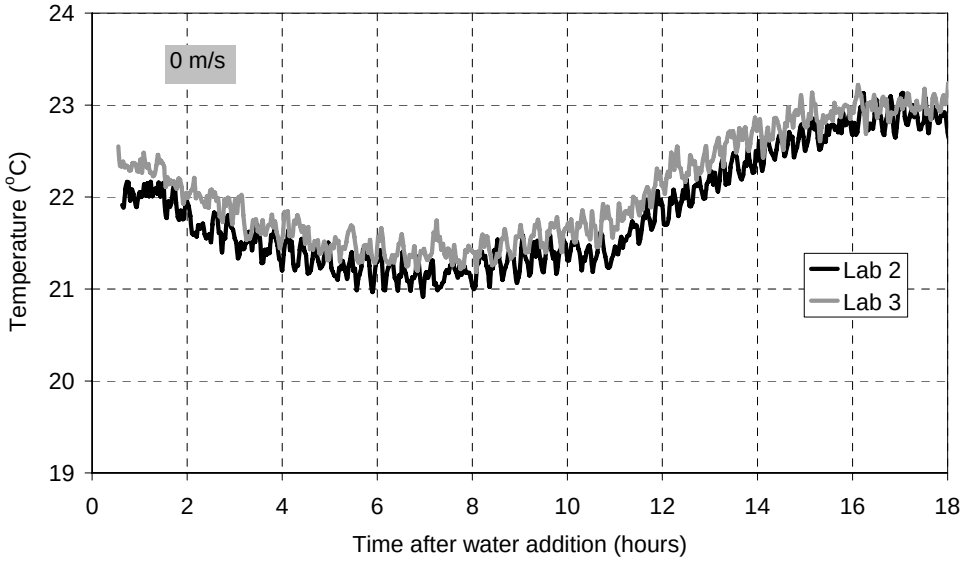

Fig. 4.14 Temperature evolution of two equivalent "basic concretes", when exposed to stagnant air.

4.3.4 Settlement

Settlement also, seems to have rather good reproducibility. The scatter seen in Fig. 4.15 is partly due to different starting ages (25 to 56 minutes after water addition), which is quite clear in the steep part. This is confirmed in Fig. 4.16, where the curves are normalised to have the same starting time. The rates in the steep part and in the flat part are fairly similar for all

batches, for the 3.3 m/s and 0 m/s batches, also, see Figs. 4.17 and 4.18. An abrupt transfer to the flat part ("knee point"), can be seen when exposed to wind. However, the abruptness varies between the batches, and "Lab 6" deviates the most. Such variation in abruptness is also sometimes seen between the two measures on a given batch, see Figs. 4.19 and 4.20. But note that the two measures on "Lab 6" are nearly the same. Note also that the two measures change being the lower and higher curve (gray and thick black lines), which implies that the differences are not related to systematic errors in the measuring device. A plausible reason for these variations may be inhomogeneities in the specimen, e.g. variable local paste-aggregate ratio and/or variable local compaction by the vibrator under the two measuring meshes. It is likely to believe that such inhomogeneities have insignificant influence as long as the concrete is fluid/soft, i.e. in the steep part, and when it becomes stiff, i.e. in the flat part. This is however, not investigated here (for instance by testing stable self-compacting mortars).

It is interesting to note that the "final" settlement (given here as the settlement at 18 hours of age) appears not to be considerably influenced by the evaporation rate. However, the total volume change is, since the corresponding "final" shrinkage is clearly influenced by evaporation rate, see next section.

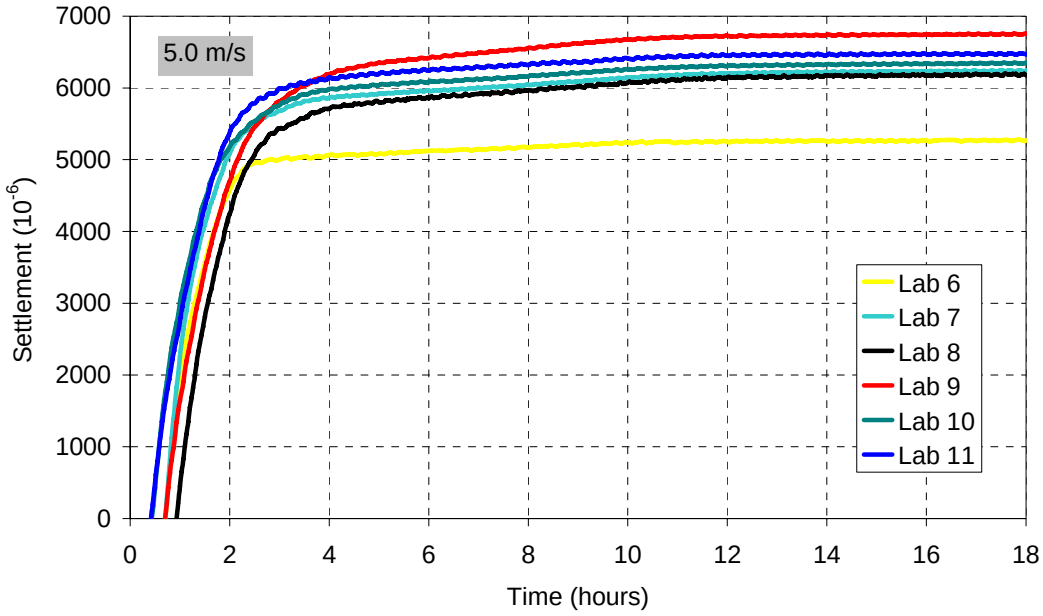

Fig. 4.15 Settlement of equivalent "basic concretes" when exposed to air with wind velocity of 5.0 m/s

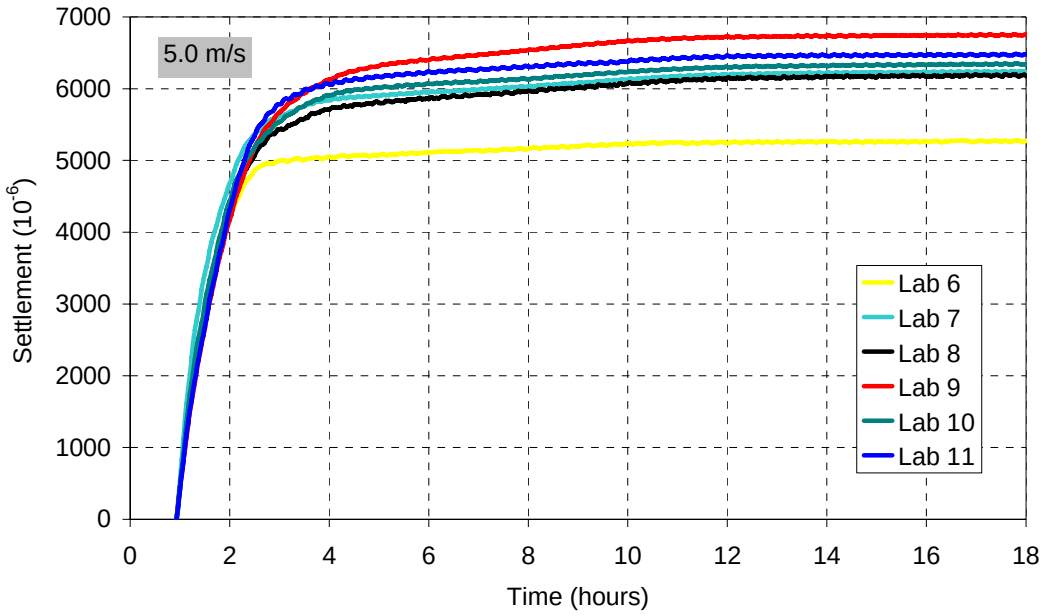

Fig. 4.16 As Fig. 4.15, but normalised to have the equal starting point

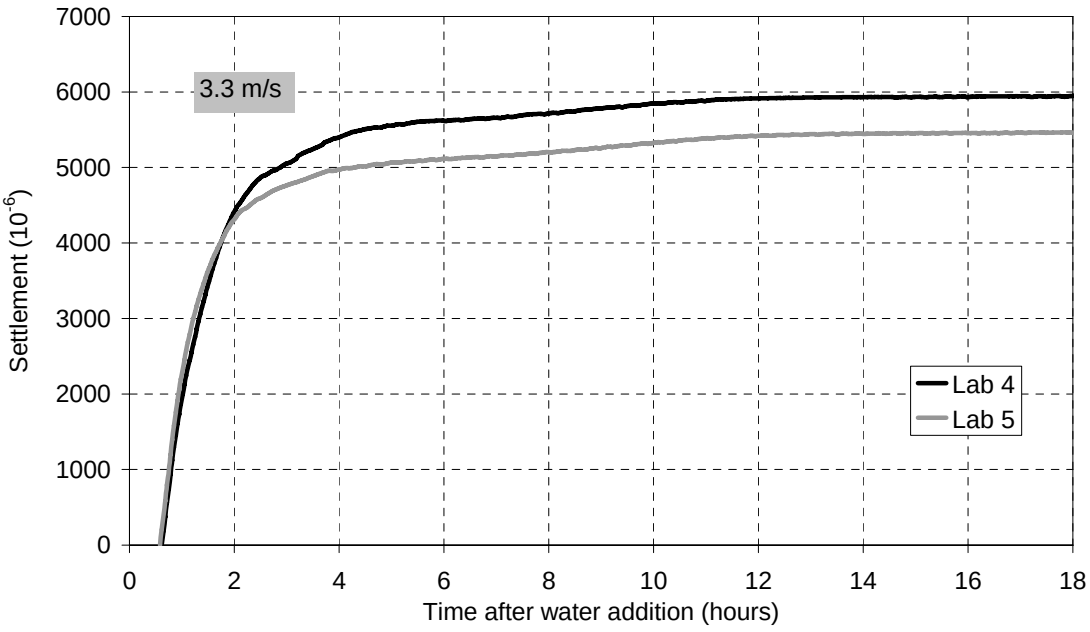

Fig. 4.17 Settlement of equivalent "basic concretes" when exposed to air with wind velocity of 3.3 m/s

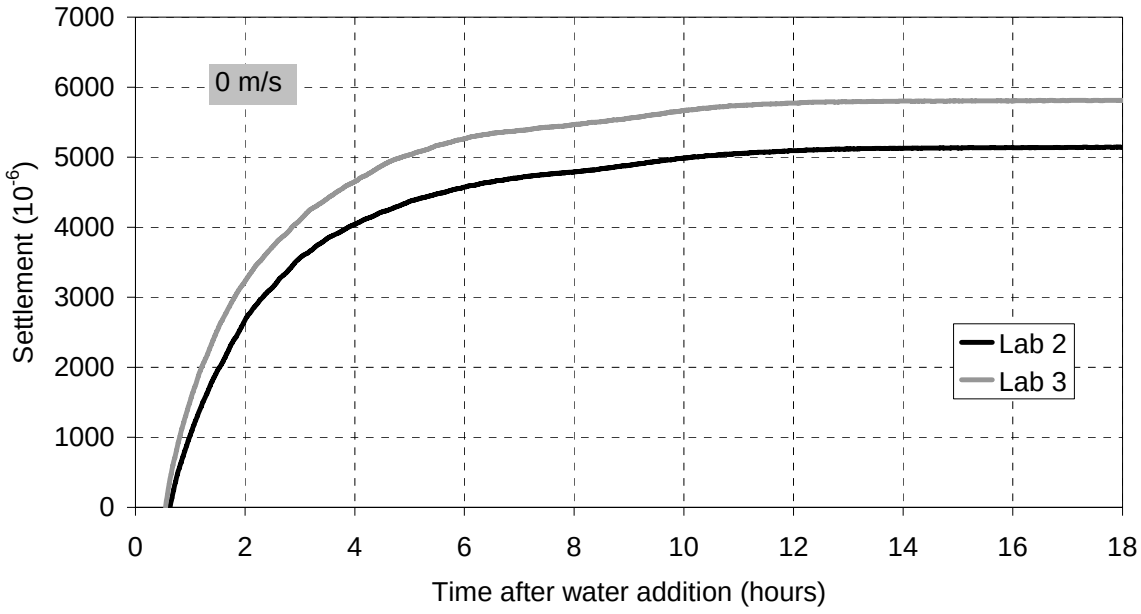

Fig. 4.18 Settlement of equivalent "basic concretes" when exposed to stagnant air

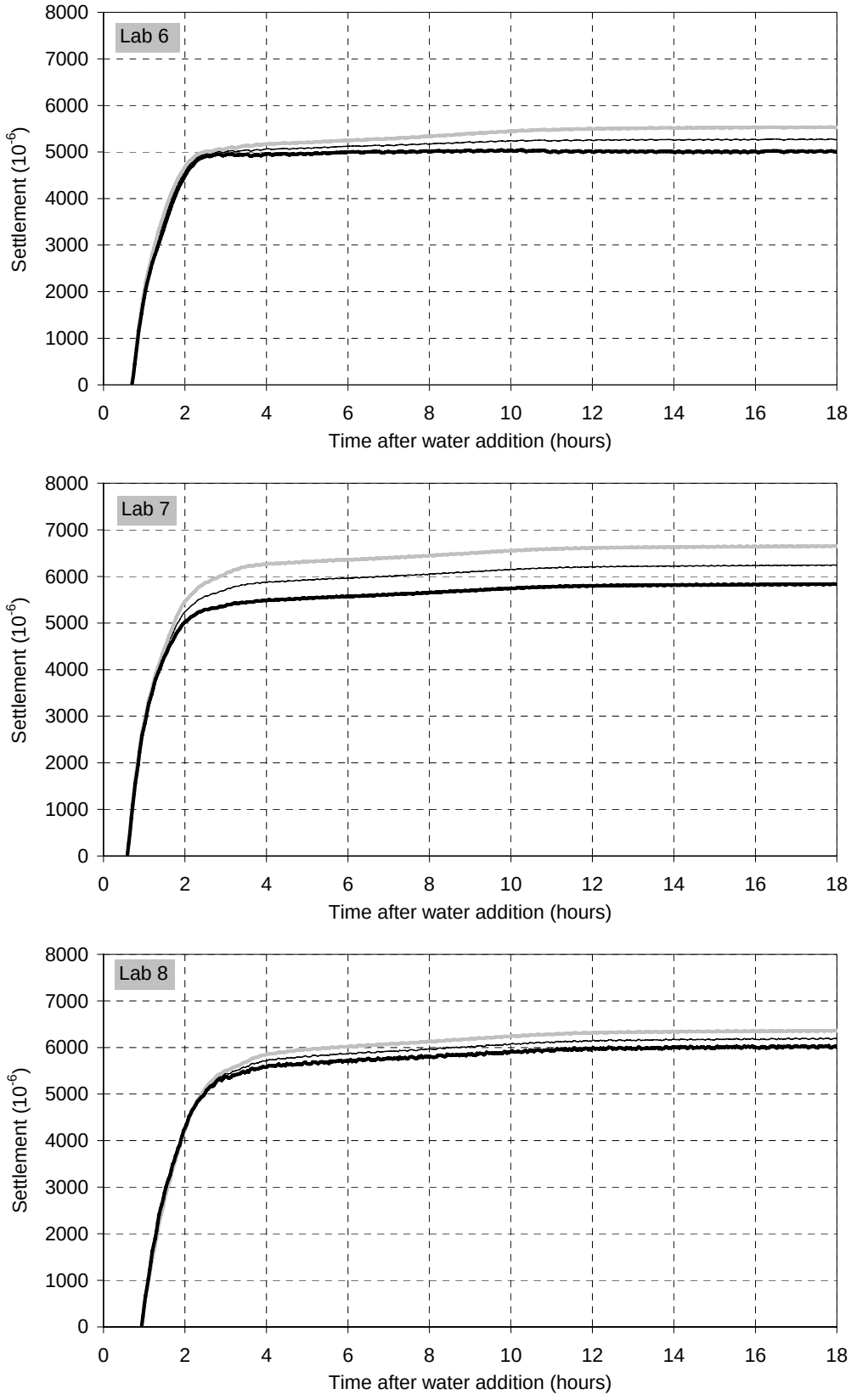

Fig. 4.19 Settlement of the single measures and average (thin line) in test series 6, 7 and 8

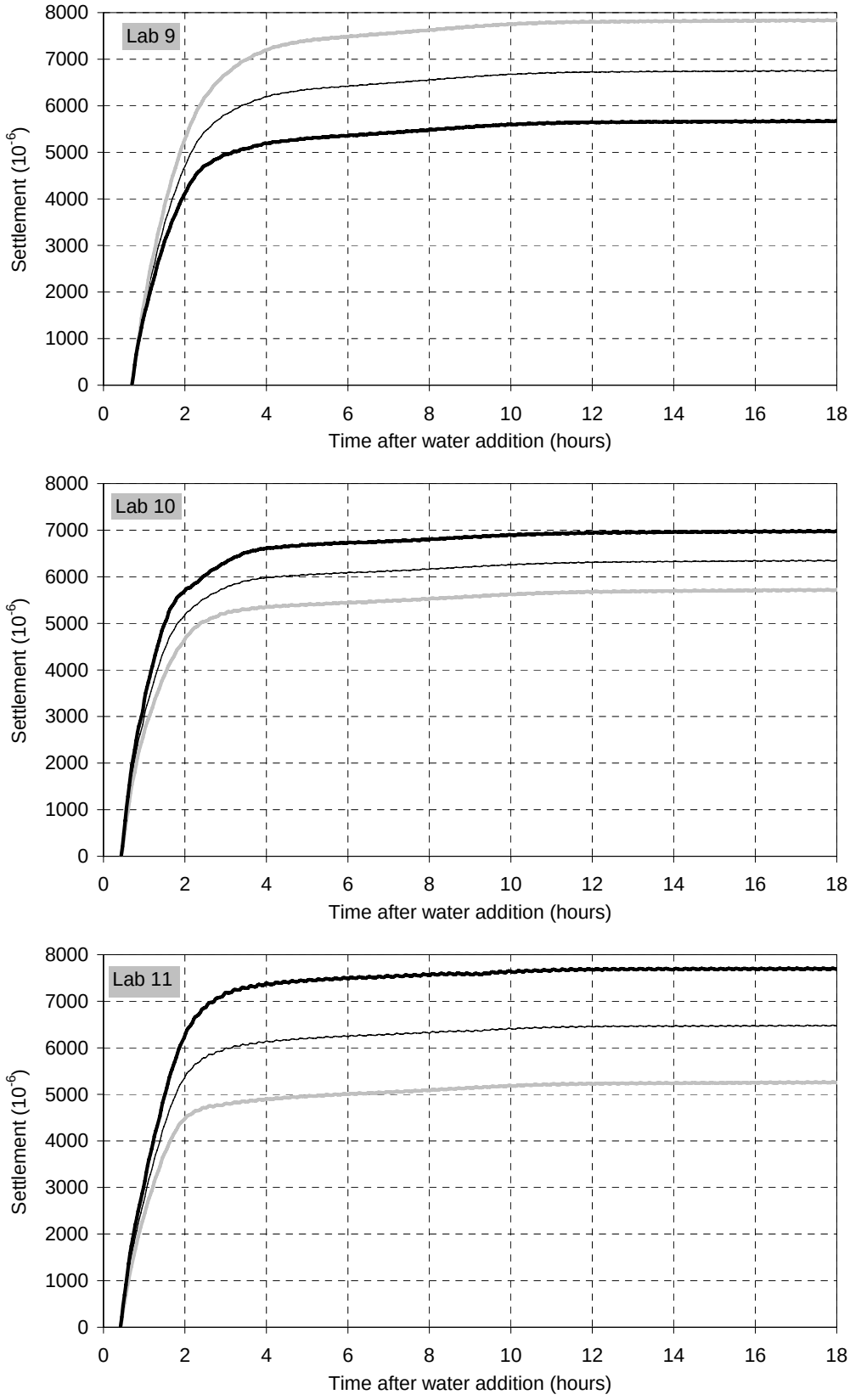

Fig. 4.20 Settlement of the single measures and average (thin line) in test series 9, 10 and 11

4.3.5 Shrinkage

As for settlement rates, shrinkage rates are rather similar in the steep part and in the flat part see Figs. 4.21-4.23 ("Lab 9" is excluded because one of the two measures failed). But, as for the settlement results, the way shrinkage flattens off is not consistent. Also, it seems that the liquid phase (time from test starts to shrinkage starts) is not significantly influenced by the variation of the time of test start (25 to 56 minutes). This is as expected since shrinkage in this period is caused by water loss (evaporation), mainly, which is not significantly influenced by time of test start, see Figs. 4.8 and 4.9.

Figs. 4.24 and 4.25 show the shrinkage at 5.0 m/s wind velocity, measured on each side of the sample and added. Variations can be seen in time when shrinkage first appears, rate in the steep part and in the following abruptness in the flattening out, but not significantly in rate beyond approximately 10 hours. It follows that the scatter occurs when the concrete is soft, which implies that he main reason for it is friction, in the measuring rod/support/IDT-system in particular (see section 4.2). It suggest that the solution to prevent friction should be improved.

Note that the two measures change between being the lower and upper curve, which implies that the differences are not caused by a systematic difference in the measuring device.

Also, it can be seen that there are three stages of shrinkage rate when exposed to wind; the first one until 3-4 hours of age, the second one until approximately 10 hours of age, and the third one beyond 10 hours of age. The three steps can be seen in the settlement, too, if shown in the same scale as shrinkage, see Figs 4.40, 4.41 and 4.47-4.51. It is probably related to two "shifts" in stiffness, i.e. the first relating to point of self-support (PSS), and the second one to the point when the E-modulus becomes significant (around final setting).

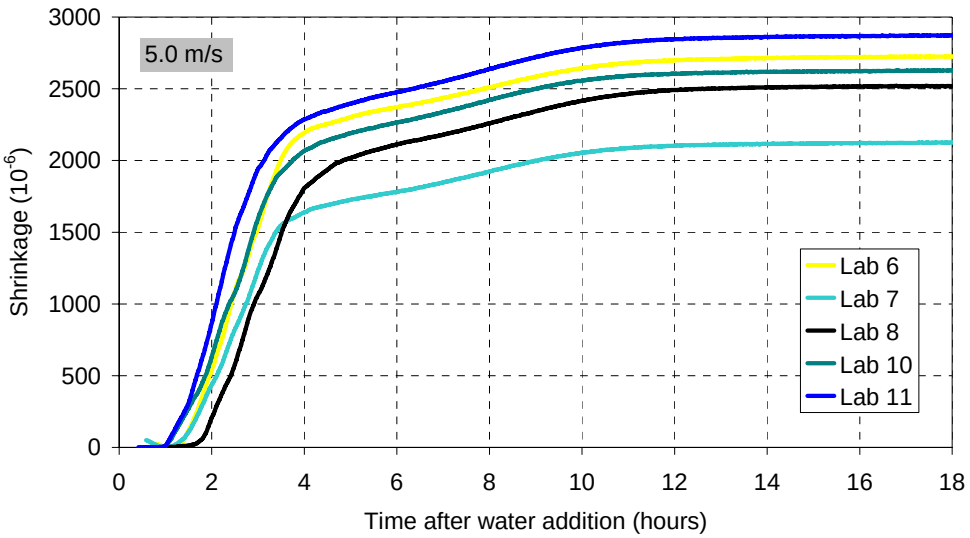

Fig. 4.21 Shrinkage of equivalent "basic concretes" when exposed to air with wind velocity of 5.0 m/s

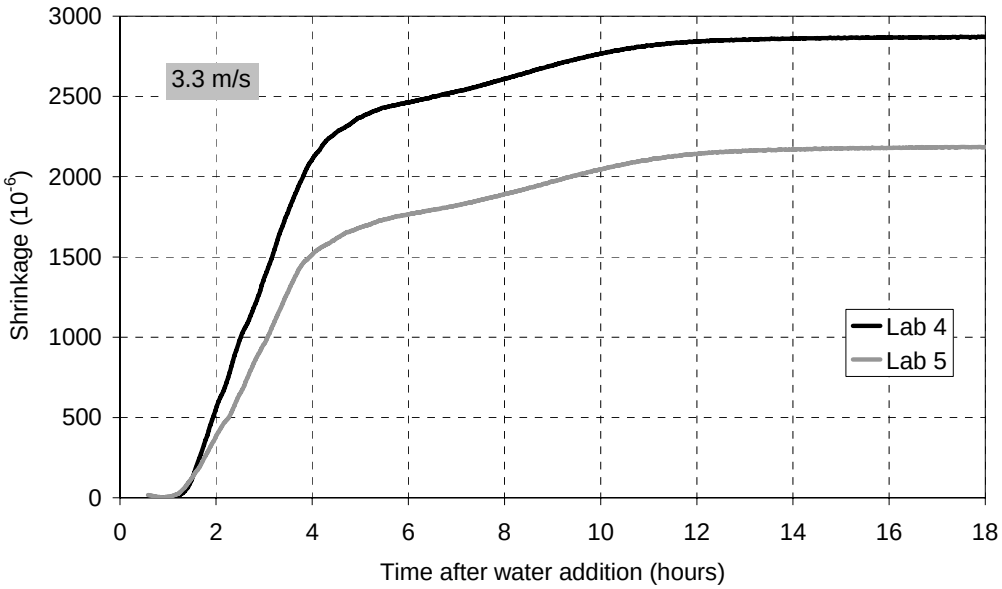

Fig. 4.22 Shrinkage of equivalent "basic concretes" when exposed to air with wind velocity of 3.3 m/s

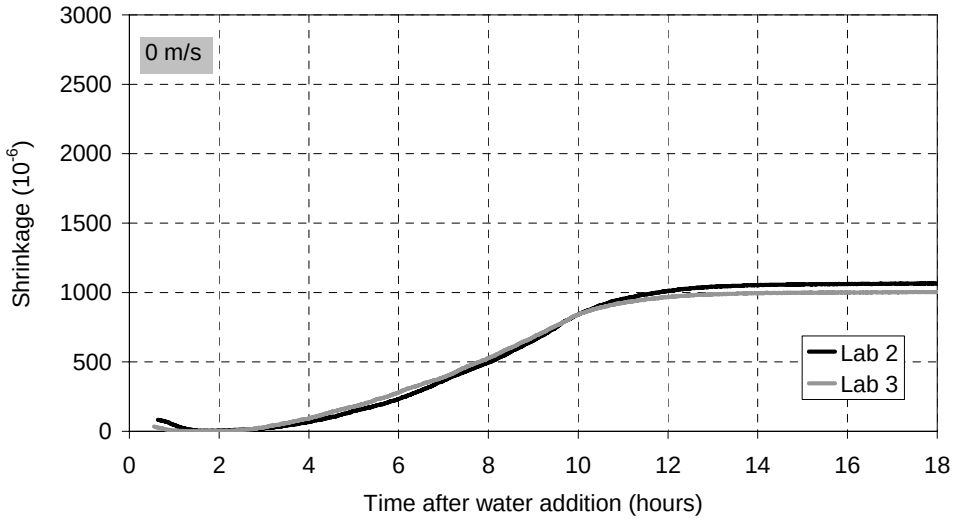

Fig. 4.23 Shrinkage of equivalent "basic concretes" when exposed to stagnant air

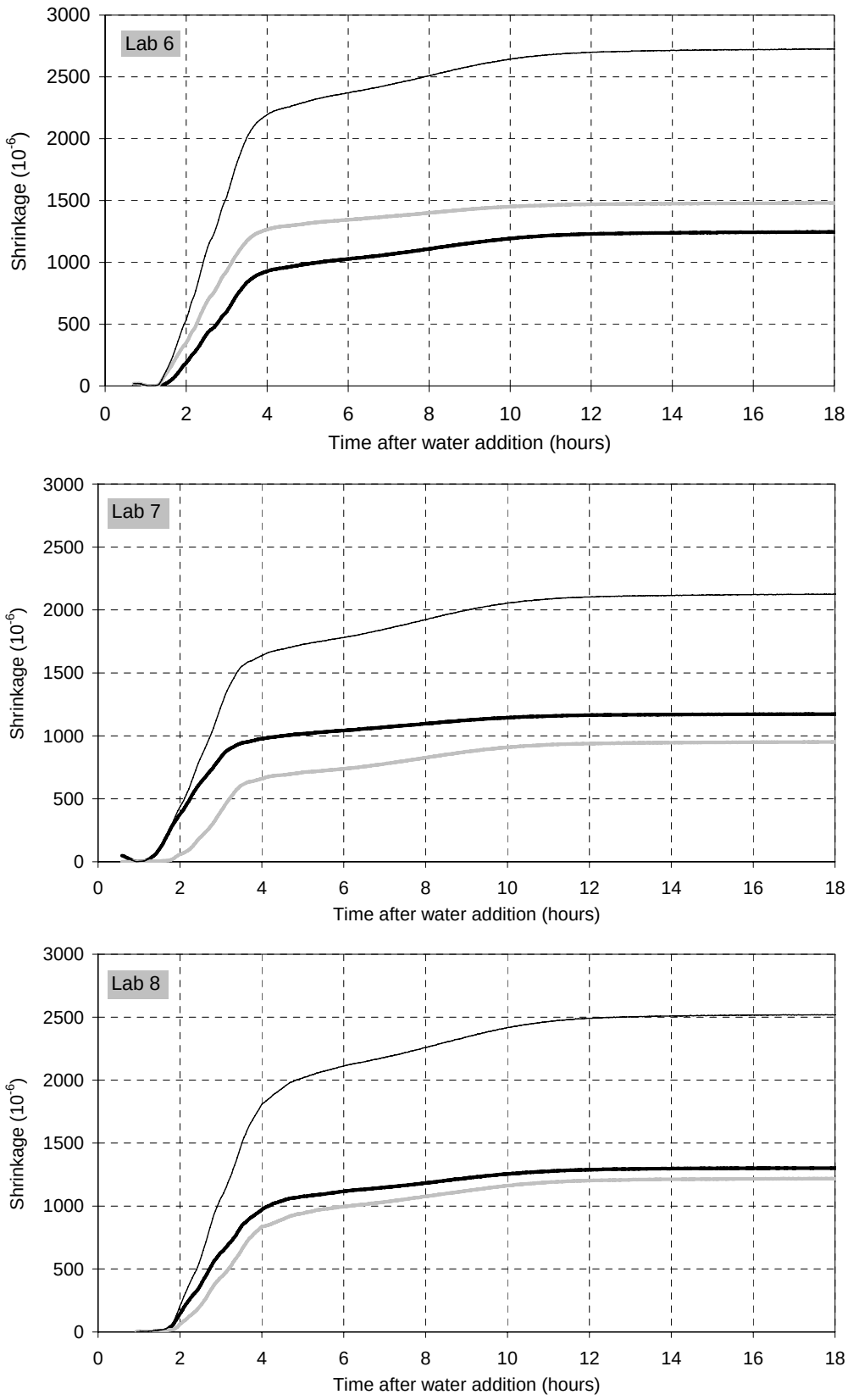

Fig. 4.24 Shrinkage measured on each side of the sample and the sum of it (thin line), in test series 6, 7 and 8.

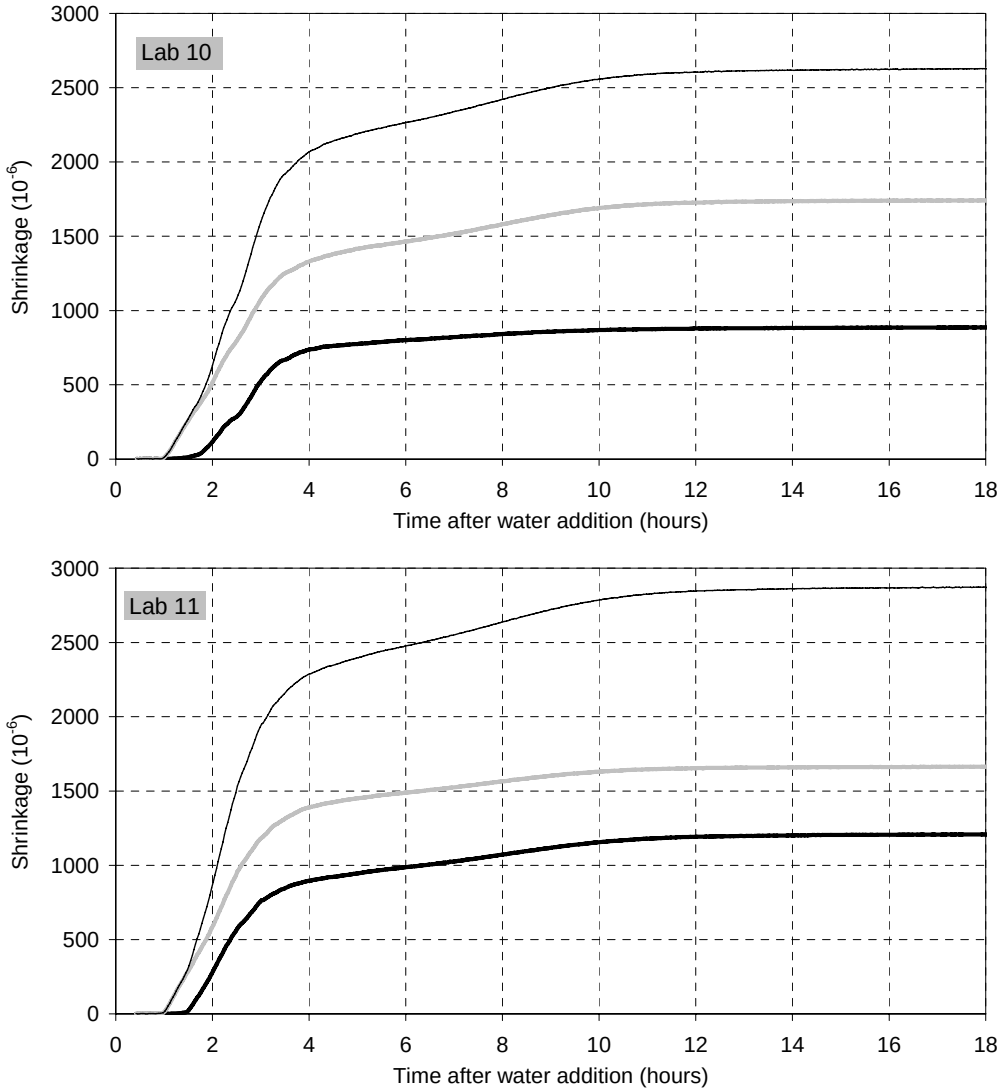

Fig. 4.25 Shrinkage measured on each side of the sample and the sum of it (thin line), in test series 10 and 11

4.3.6 Pore water pressure

Again, the different starting times are clearly reflected, both at 5 and 50 mm depth, see Figs. 4.26-4.28. If normalised to have equal starting point (which can be done since PWP evolution is result of water loss, mainly, which is not significantly influenced by time of test start, see Figs. 4.8 and 4.9), it becomes clearer that the rates vary to some extent. Differences in evaporation rate should directly influence PWP rate. Although the measured evaporation rates differed less than PWP rates in the first couple of hours (Fig. 4.9), it is noteworthy that the tests having the highest evaporation rate ("Lab 11") and the lowest one ("Lab 9"), have correspondingly the highest and the lowest PWP rate. A reason for the scatter is small variations in measuring depths, because it was difficult to place the tubes exactly at the target depths every time when using the given rack system. A more accurate system is possible and should be built for future work.

The results from testing at 3.3 and 0 m/s showed nearly no difference between the two test series at each wind velocity, see Figs. 4.29-4.30 (and correspondingly nearly no difference in evaporation rate, see Fig. 4.10).

At 5 mm depth PWP often “breaks through” at a few KPa, only, when exposed to wind, see Fig. 4.28. This is probably because the pore water becomes discontinuous at this depth (may be as result of air leakage along the tube). Still, the rates are nearly the same before this happens. Note that the PWP rate drops immediately and is practically linear until break through. The difference between PWP at 5 and 50 mm is discussed in chapter 3.3.

It is noticeable that PWP jumps one or two times in nearly all tests in this test series, before the values reaches minimum set by the transducers and amplifier (at 28-29 KPa). Such jumps were not seen in other tests series, see chapter 5. The first jump occurs at approximately -5 KPa. It happens abruptly and reaches an infinite negative value in most of the cases, remains at this level for some minutes and then returns to its natural curve after some minutes. It is noticeable that the phenomenon appears to be independent of evaporation rate and depth. Furthermore it does not seem to coincide consistently with any of the phase shifts that have been pointed out. Thus, it appears to be a “built in” measuring error, which reason has not been found. I assume that it is not important since PWP apparently returns to its natural curve after some minutes.

The second jump occurs when exposed to wind, only, and it results in a less monotone curve afterwards. Since it is recognizable with the curves at 5 mm depth it seems plausible that phenomenon is related to leakage of air along the tube, which contributes to discontinuity in the pore water system.

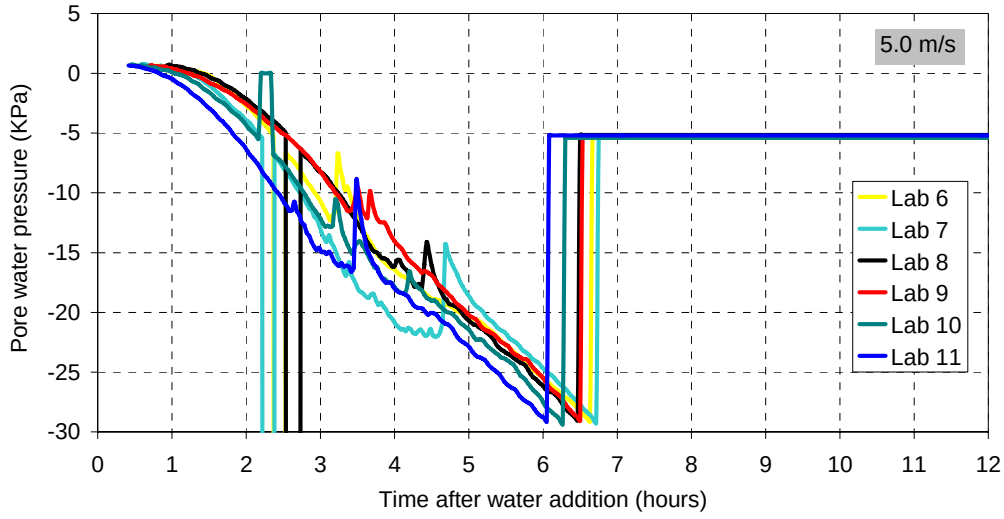

Fig. 4.26 Pore water pressure at 50 mm depth of equivalent “basic concretes” when exposed to air with wind velocity 5.0 m/s

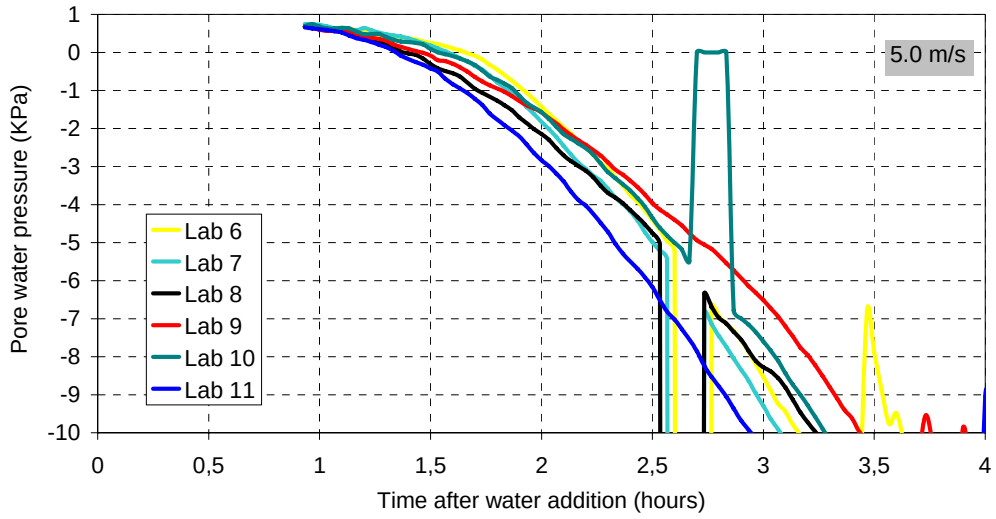

Fig. 4.27 As Fig 4.26, but normalised to have the same starting point

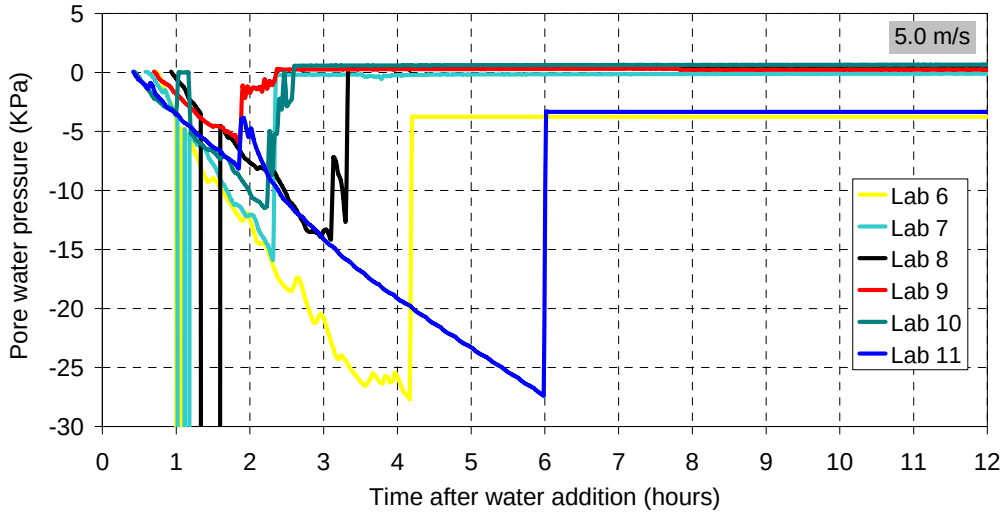

Fig. 4.28 Pore water pressure at 5 mm depth of equivalent "basic concretes" when exposed to air with wind velocity 5.0 m/s

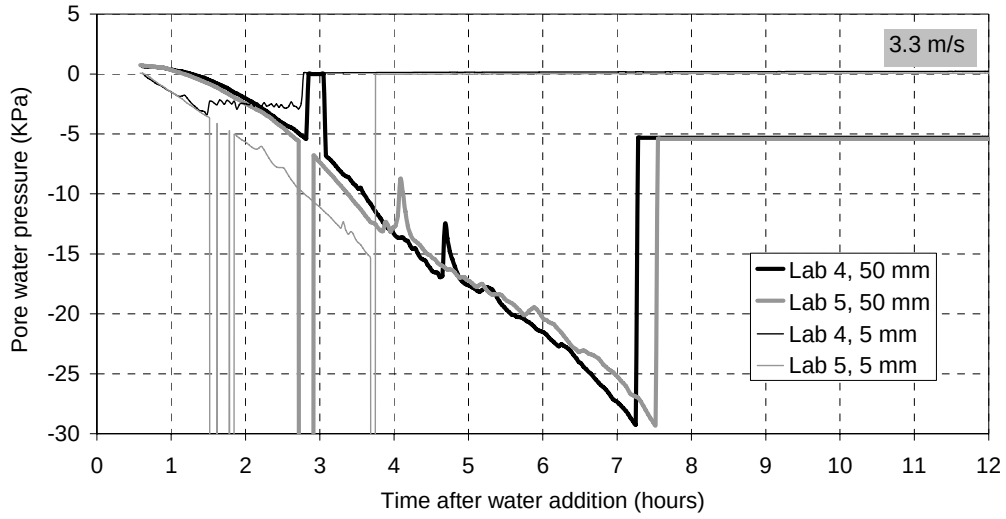

Fig. 4.29 Pore water pressure at 5 and 50 mm depth of equivalent "basic concretes" when exposed to air with wind velocity 3.3 m/s

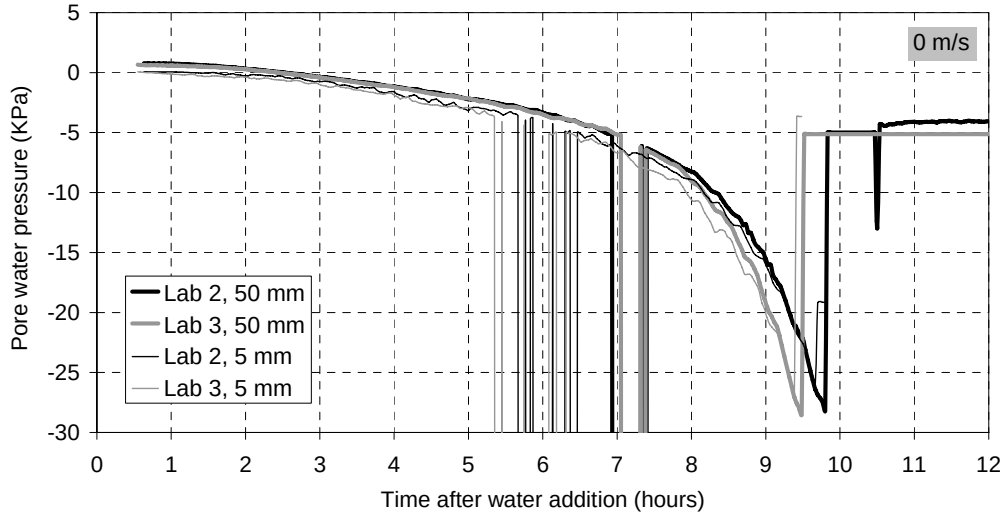

Fig. 4.30 Pore water pressure at 5 mm and 50 mm depth of equivalent "basic concretes" when exposed to stagnant air

4.3.7 Relationship between the measures

As discussed in section 4.3.1, the repeatability of the results is also assessed with respect to the relationship between water loss (given in volume units), settlement, shrinkage and PWP at 50 mm depth (equal to the depth of shrinkage measurement). This is done below, partly based on the four measures on each batch assembled in the same figure, starting with consideration of the sealed condition.

Sealed condition

The volume change is driven by CS and bleeding (assuming that the influence of temperature change and loss of air is insignificant). All volume change appears then as settlement in the time before point of self support (PSS), as discussed earlier. Settlement, shrinkage and pore water pressure at sealed condition is shown in Fig. 4.3.2. PSS is seen as the point where PWP becomes tension, here at 2.4 hours, followed by a slight decrease until approximately 6 hours of age. Shrinkage (autogenous) is insignificant in this period. From this age the stiffness of the concrete becomes significant, seen as measurable stress generation at restraint (Bjøntegaard, 2000), which reflects a progressing rate of PWP evolution. The volume change turns into expansion (both vertically and horizontally) at this point. The expansion phenomenon is discussed in section 3.2.4 and will not be repeated here.

Ideally, the measured settlement should correspond to CS + bleeding until empty pore space occurs. This may be shown if the bleeding of the same batch is measured and CS of equivalent paste is measured (it was concluded in section 3.3.7 that aggregate (filler included) does not influence CS rate significantly in this early age). The bleeding of the "basic concrete" from approximately 1 hour of age has been measured by Bjøntegaard (2000). It shows a nearly linear development and ended at approximately 5 hours of age, at approximately 0.8 ‰ of the concrete volume (i.e. $800 \cdot 10^{-6}$), which corresponds to a rate of $200 \cdot 10^{-6}$/h. CS is not measured of the equivalent paste, but Justnes et al (2000) measured CS on paste with the same type of cement, silica fume content and w/b, both with and without the admixtures used in the "basic concrete" (lignosulphonate, LS, and sulphonated naftalene formaldehyd, SNF). The result (Fig. 4.32) show a rather linear shrinkage in the 5 hour period, and with a rate corresponding to approximately $1600 \cdot 10^{-6}$/h (with LS and LS + SNF), which comes to approximately $500 \cdot 10^{-6}$/h of the equivalent concrete having 30 % paste volume, air included. The sum of CS + bleeding amounts then to approximately $\mathbf{700 \cdot 10^{-6}/h}$. The measured initial settlement rate is higher; approximately $\mathbf{1000 \cdot 10^{-6}/h}$ at 1 hour of age (deduced from Fig. 4.31). The fact that the concrete temperature was 2-3 °C higher than the paste temperature, may have contributed to higher CS rate in the concrete. Nevertheless, considering the uncertainties related to the fact that measurements were done on non-equivalent batches, I think the comparison confirms fairly well that measured settlement is the sum of CS + bleeding.

Settlement levels out within a couple of hours (Fig. 4.31), while CS continues with a nearly linear rate (Fig. 4.33) and corresponds to approximately $2500 \cdot 10^{-6}$ at six hours of age. The gap between CS and settlement is probably expanded air pores already in the concrete. It can hardly be surface pores since it has been found that bleed water is on top at least until 5 hours of age.

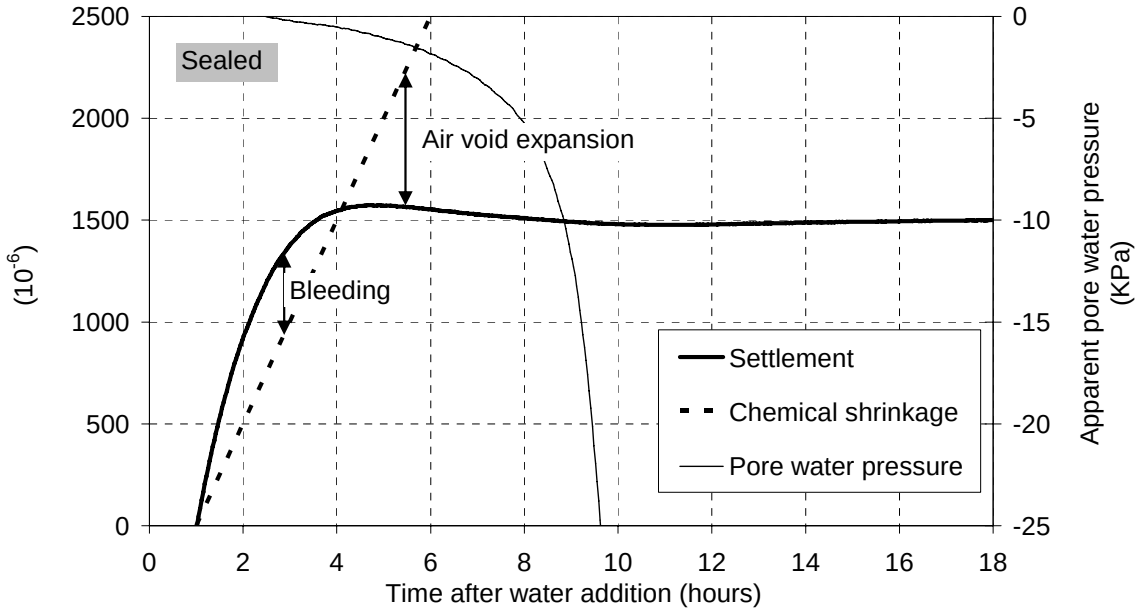

Fig. 4.31 Settlement, chemical shrinkage (deduced from Fig. 4.32) and pore water pressure of the "basic concrete" when protected against evaporation with plastic sheet

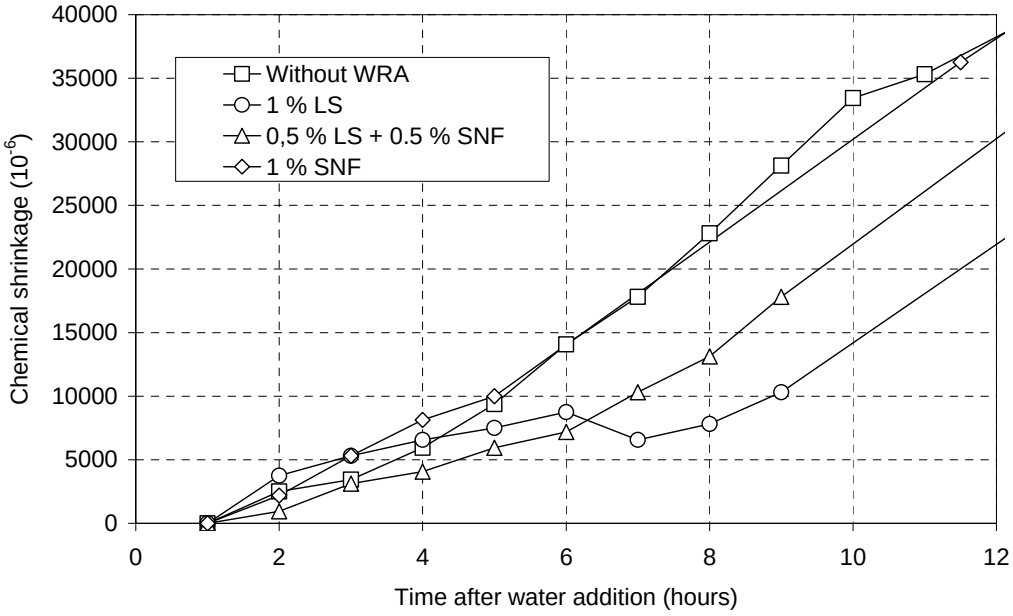

Fig. 4.32 Chemical shrinkage of cement paste with "Norcem Anlegg"-cement, w/b = 0.40 and 5 % silica fume. After Justnes et al (2000)

Top surface exposed to 21 ºC and 50 % RH ("0 m/s"):
With external drying, the total volume change in the liquid phase is the sum of water loss (evaporated water including bleeding) and CS. CS equals settlement minus bleeding in this phase, as demonstrated above. Then, the measured "0 m/s" settlement (CS + evaporated water) should equal the sum of measured "sealed" settlement (minus bleeding) and water loss

(found in the 0 m/s tests, see Figs 4.34 and 4.35). Fig 4.33 shows that this agree fairly well until approximately 3 hours of age.

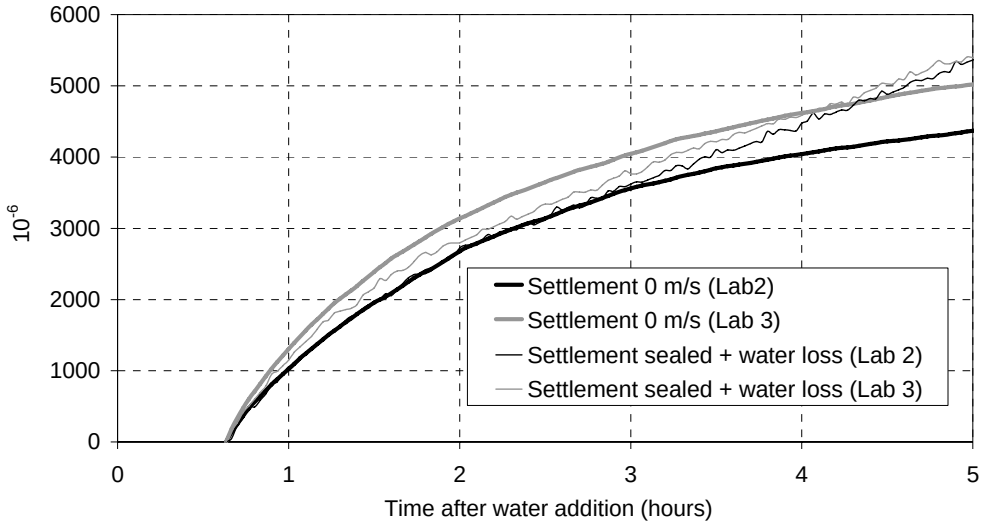

Fig. 4.33 Settlement measured with evaporation at 0 m/s and the sum of settlement measured in sealed condition (minus bleeding) and water loss measured at 0 m/s

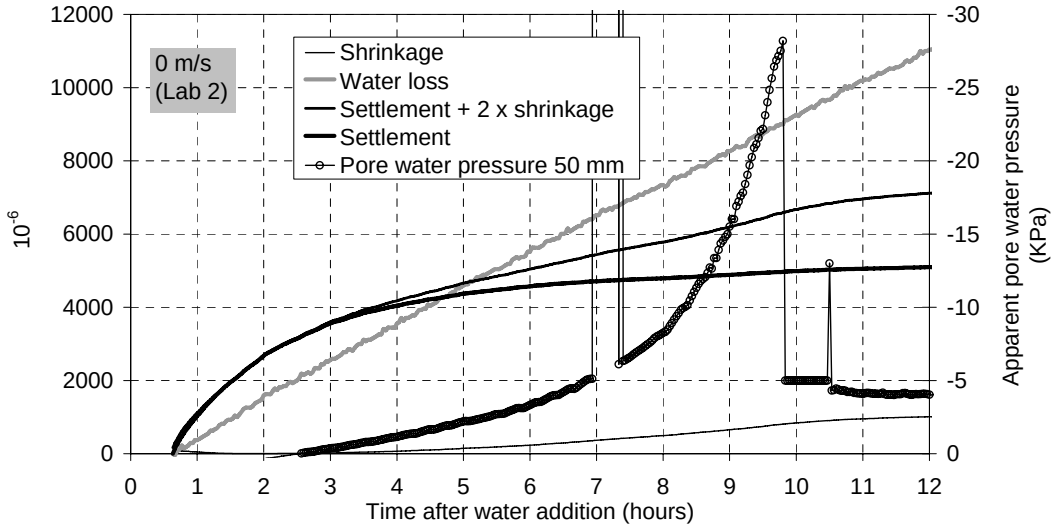

Fig. 4.34 Settlement, shrinkage, water loss and pore water pressure of the "basic concrete" no 2 when exposed to stagnant air

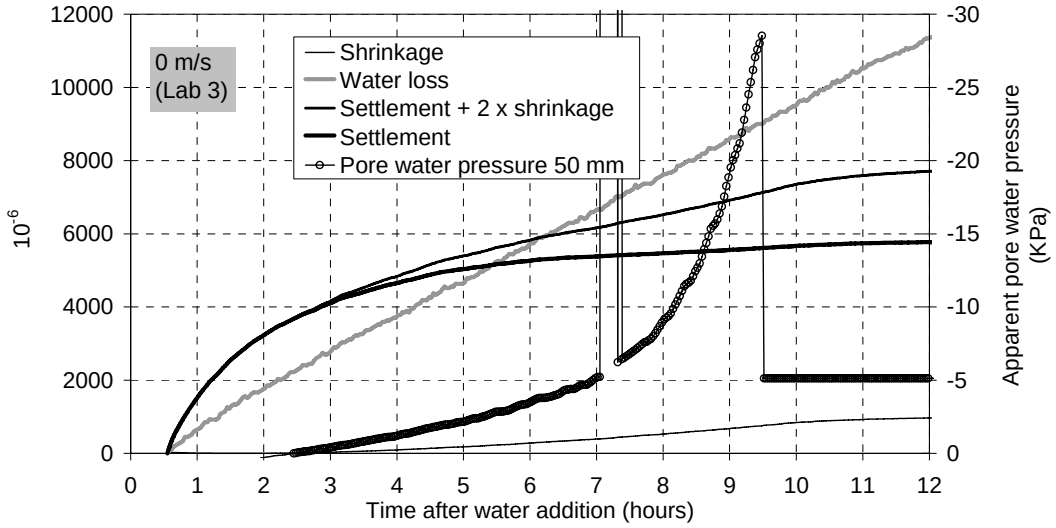

Fig. 4.35 Settlement, shrinkage, water loss and pore water pressure of the "basic concrete" no 3 when exposed to stagnant air

Figs. 4.34 and 4.35 show also that shrinkage starts when PWP turns into tension for both tests, as expected. In the next period (beyond approximately 2.5 hours of age), rate of water loss exceeds rate of measured total external deformation, i.e. settlement + 2 x shrinkage. The main reason must be that the water surface move downwards, which leave empty surface pores.

Settlement rate and shrinkage rate becomes fairly equal beyond approximately 5 hours of age, see Figs. 4.36 and 4.39. It is however noticeable that shrinkage rate is higher than settlement rate between 6-7 hours and 10-11 hours. This is the case for the 3.3 and 5.0 m/s cases, too (presented later in this section). I have not found the reason for this, but assume that it may be a result of the emptying of surface pores, which may results in a "dead" surface with respect to shrinkage (no pore water – no pore water tension). If so, the "active" height is less than 100 mm which is used to calculate the settlement (10^{-6}), resulting in too low values.

The two rates are quite similar in the time beyond 10-11 hours, as expected since the concrete then is in the hardening phase, and thus, should behave isotropic. The latter contributes to strengthen the reliability of the measuring system.

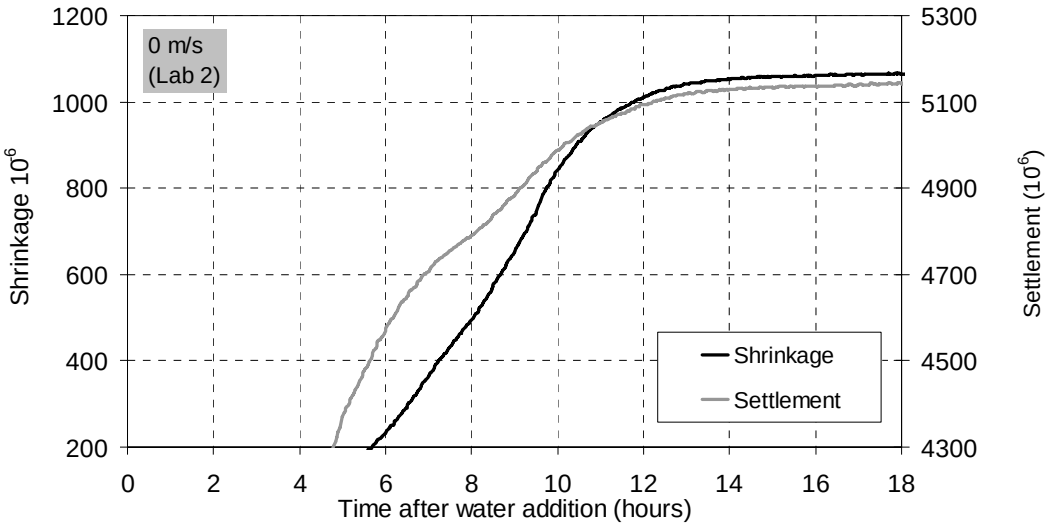

Fig. 4.36 Shrinkage and settlement for "basic concrete" no 2 when exposed to 0 m/s

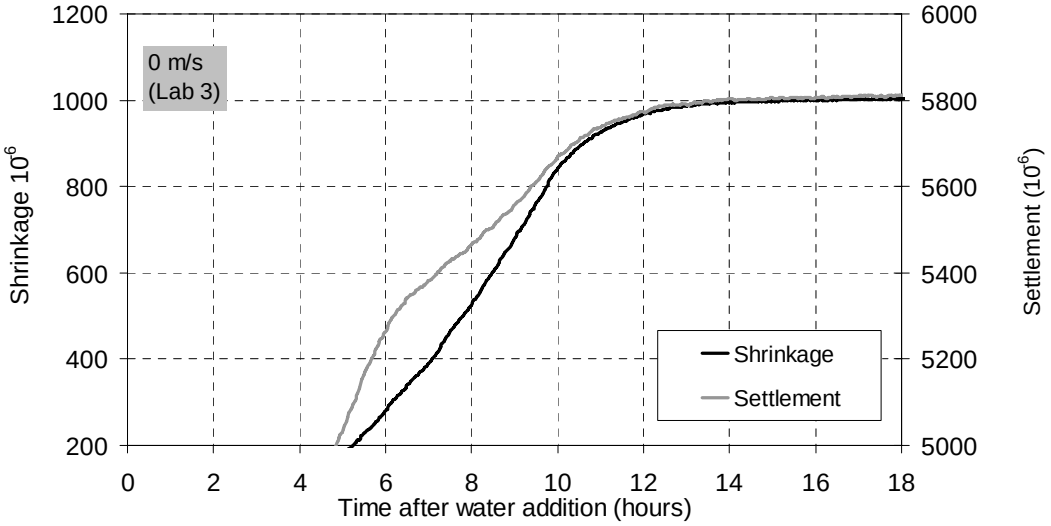

Fig. 4.37 Shrinkage and settlement for "basic concrete" no 3 when exposed to 0 m/s

Top surface exposed to 21 ºC, 50 % RH and 3.3 m/s:
The significantly increased evaporation rate, caused by the wind, contributes to considerably higher rates of settlement, shrinkage and PWP, as well decreased PSS, see Figs. 4.38 and 4.39. The fact that PWP at 5 mm becomes negative immediately implies that surface shrinkage starts immediately (Fig. 4.29), while at approximately 30 minutes later at 50 mm depth. Also, the difference between settlement and water loss is hardly visible. It follows that the water surface starts to move downwards earlier, i.e. at approximately 1 hour, following the discussion of results obtained without wind (see above).

Again, it can be seen that shrinkage starts when PWP turns into tension in both test series, as expected.

There is a rather good correspondence between shrinkage and settlement evolution in the time beyond approximately 4 hours of age when exposed to wind, and in particular beyond 10 hours of age, as commented upon above, see Figs. 4.40 and 4.41.

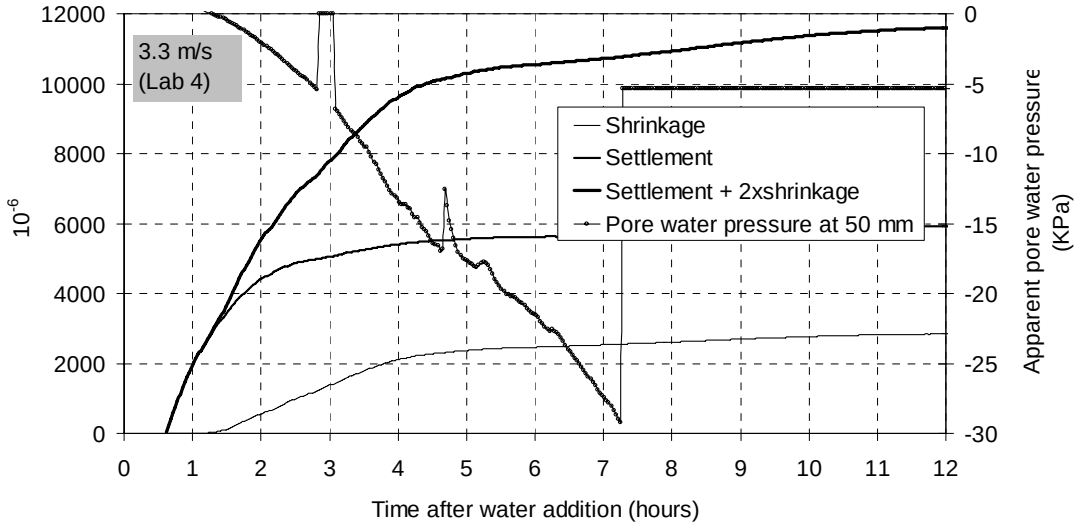

Fig. 4.38 Settlement, shrinkage, water loss and pore water pressure of the "basic concrete" no 4 when exposed to 3.3 m/s (water loss is not available)

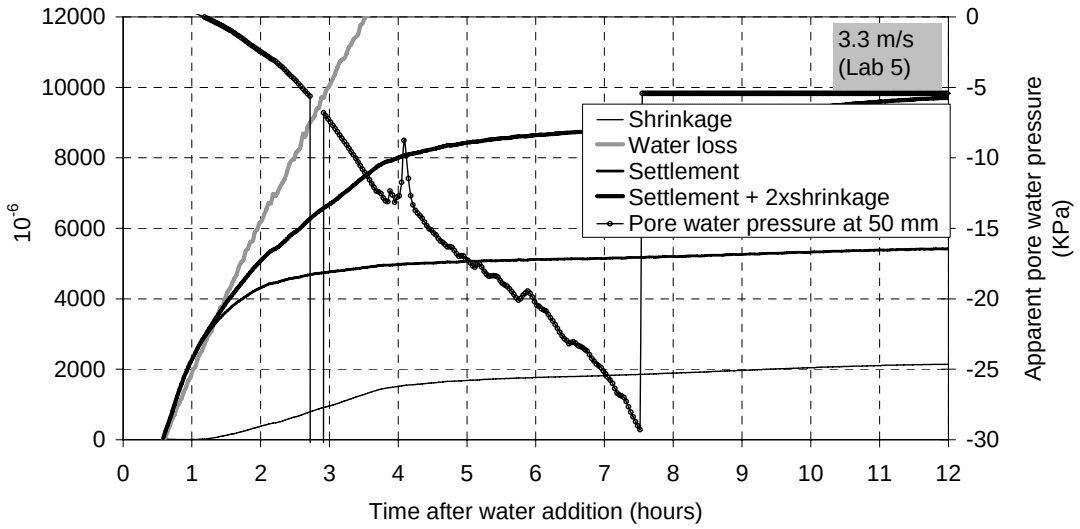

Fig. 4.39 Settlement, shrinkage, water loss and pore water pressure of the "basic concrete" no 4 when exposed to 3.3 m/s

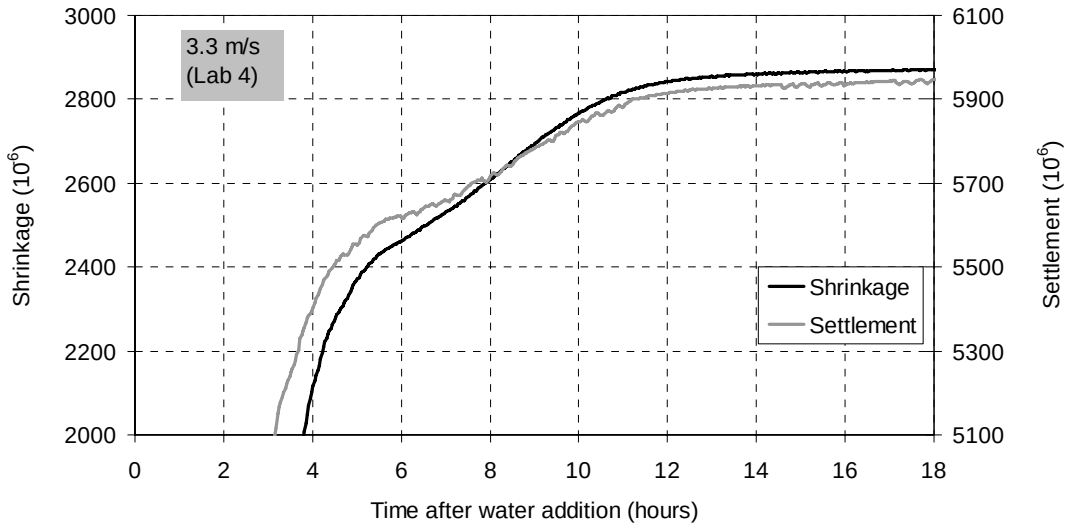

Fig. 4.40 Shrinkage and settlement for "basic concrete" no 4 when exposed to 3.3 m/s

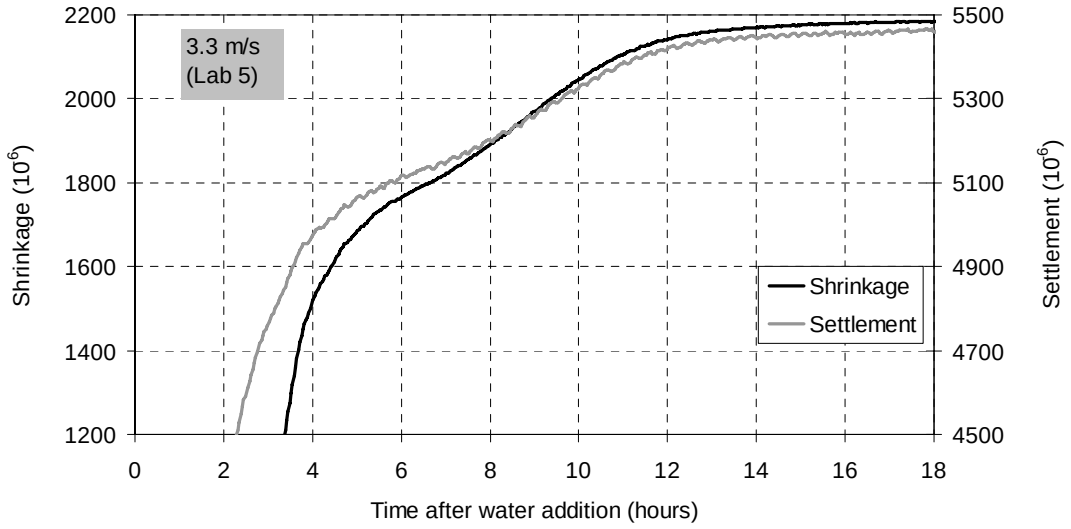

Fig. 4.41 Shrinkage and settlement for "basic concrete" no 5 when exposed to 3.3 m/s

Top surface exposed to 21 ºC, 50 % RH and 5.0 m/s:
Figs. 4.43-4.50 demonstrate that further increase of evaporation rate results in still higher rates of settlement, shrinkage and PWP, as well decreased PSS. Also, it can be seen that shrinkage starts when PWP turns into tension in all test series, and that settlement rate and shrinkage rate coincide fairly well and is in accordance with the pattern discussed above.

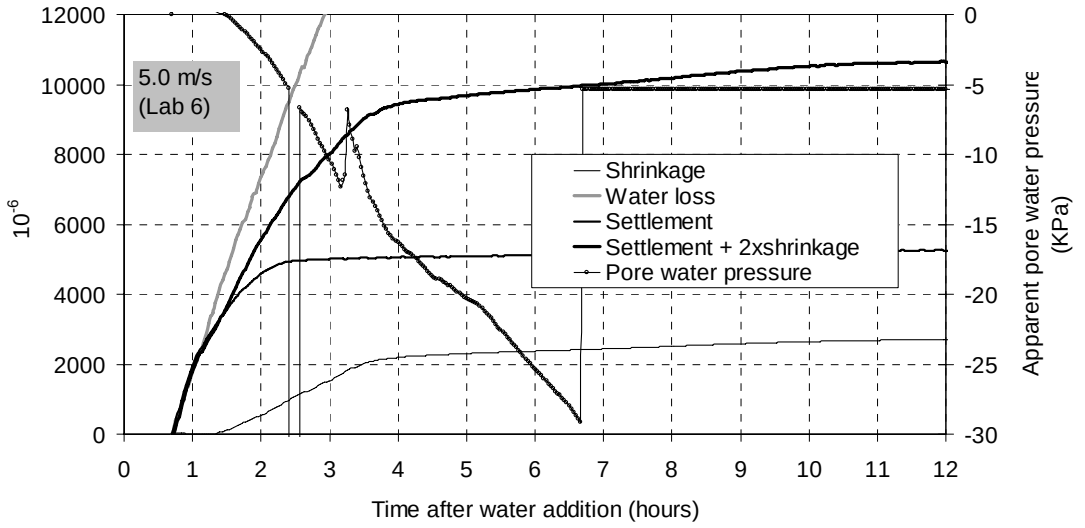

Fig. 4.42 Settlement, shrinkage, water loss and pore water pressure of the "basic concrete" no 6 when exposed to 5.0 m/s

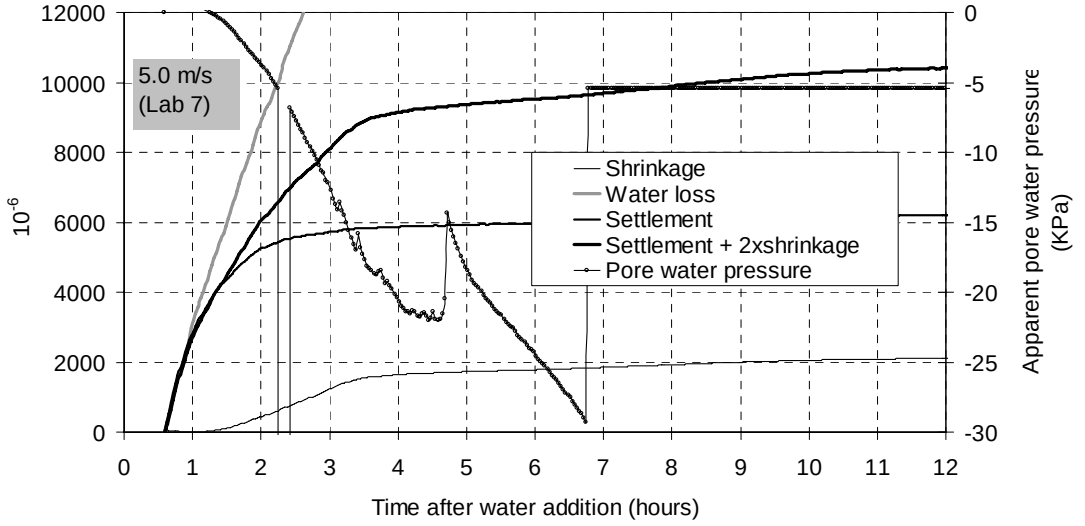

Fig. 4.43 Settlement, shrinkage, water loss and pore water pressure of the "basic concrete" no 7 when exposed to 5.0 m/s

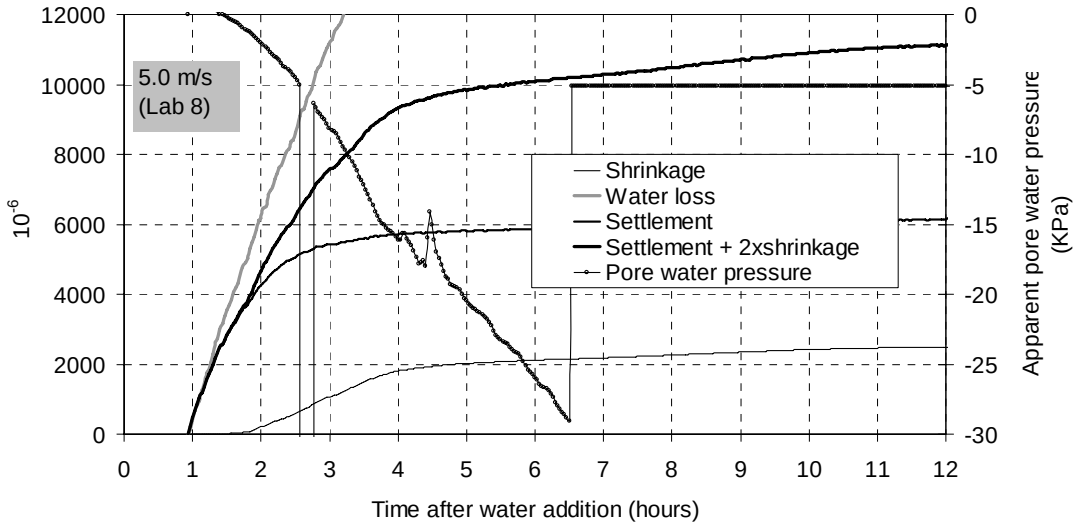

Fig. 4.44 Settlement, shrinkage, water loss and pore water pressure of the "basic concrete" no 8 when exposed to 5.0 m/s

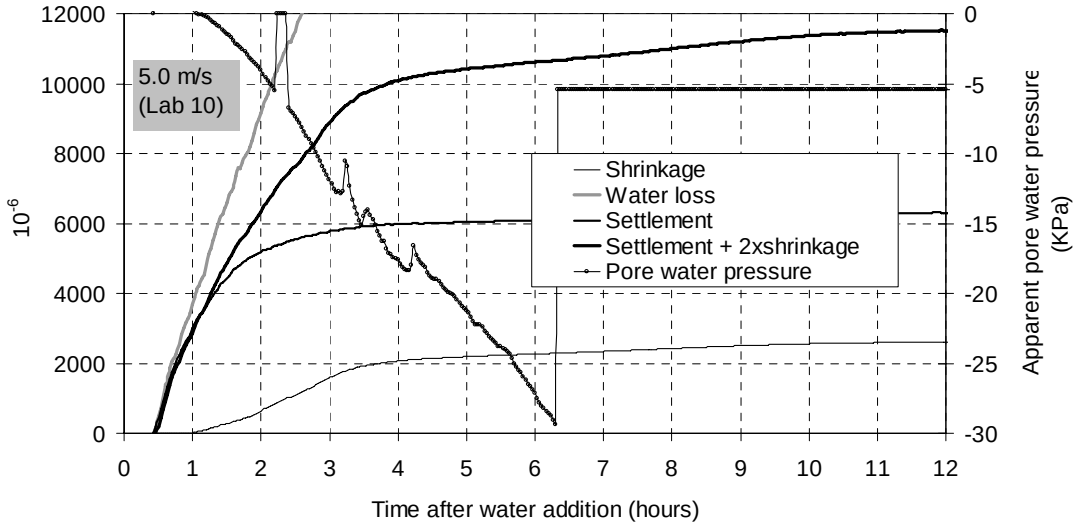

Fig. 4.45 Settlement, shrinkage, water loss and pore water pressure of the "basic concrete" no 9 when exposed to 5.0 m/s

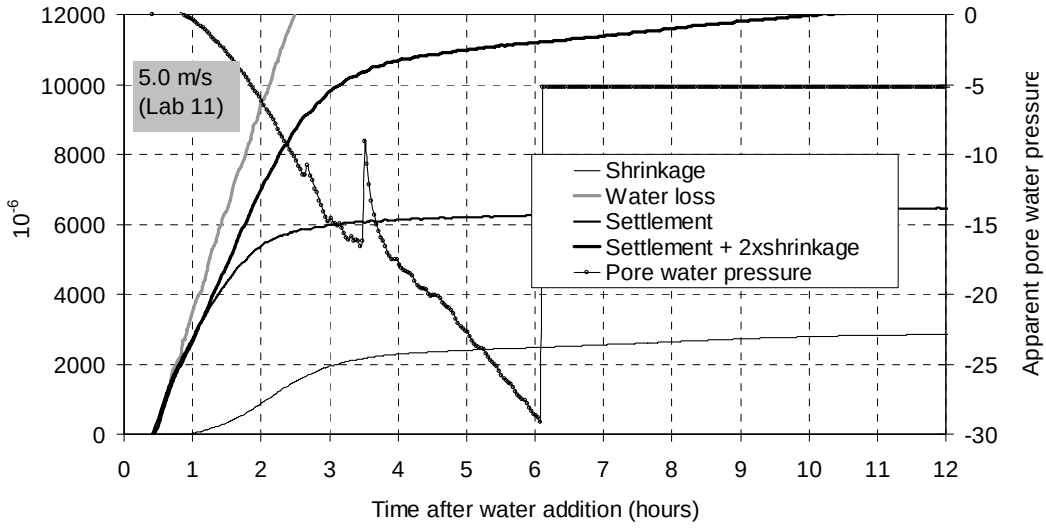

Fig. 4.46 Settlement, shrinkage, water loss and pore water pressure of the "basic concrete" no 11 when exposed to 5.0 m/s

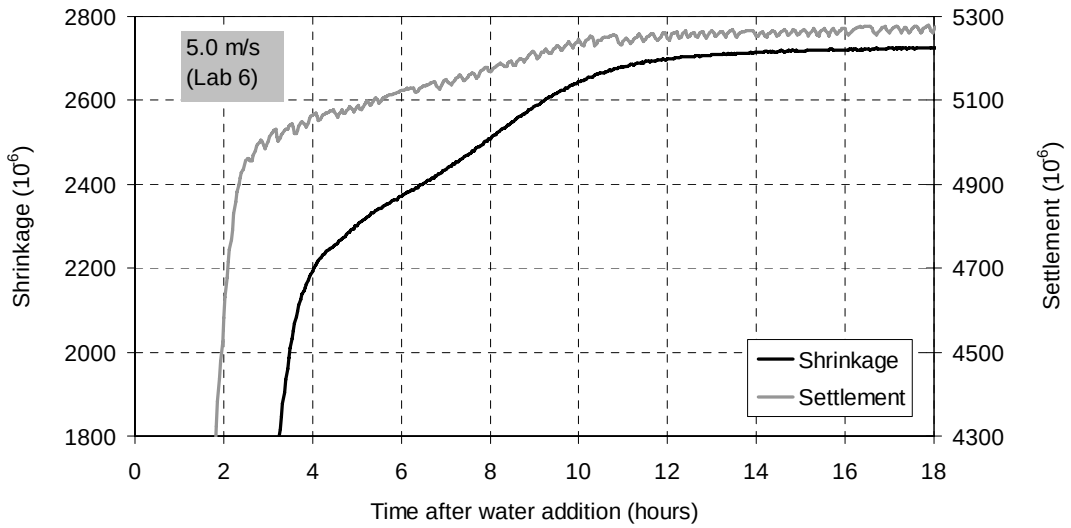

Fig. 4.47 Shrinkage and settlement for "basic concrete" no 6 when exposed to 5.0 m/s

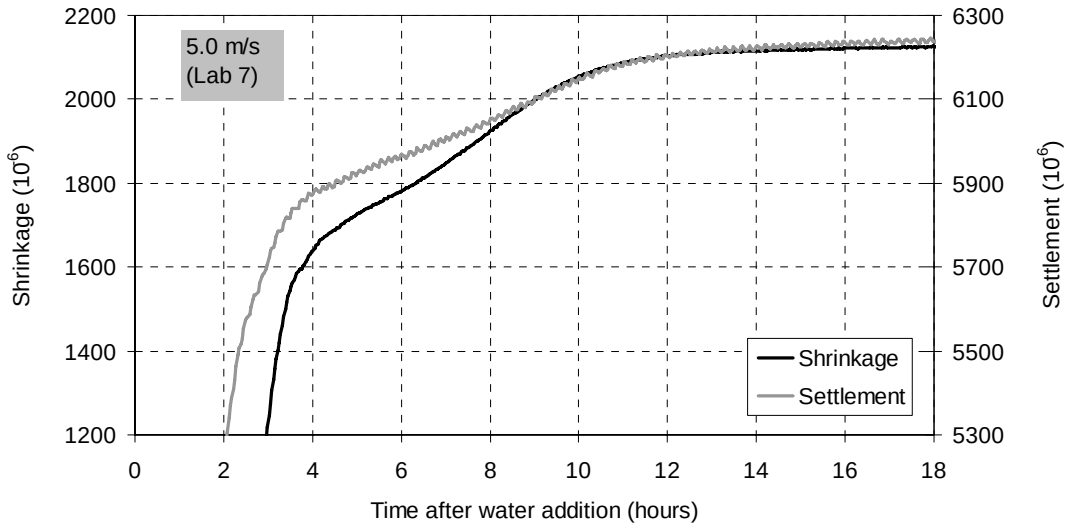

Fig. 4.48 Shrinkage and settlement for "basic concrete" no 7 when exposed to 5.0 m/s

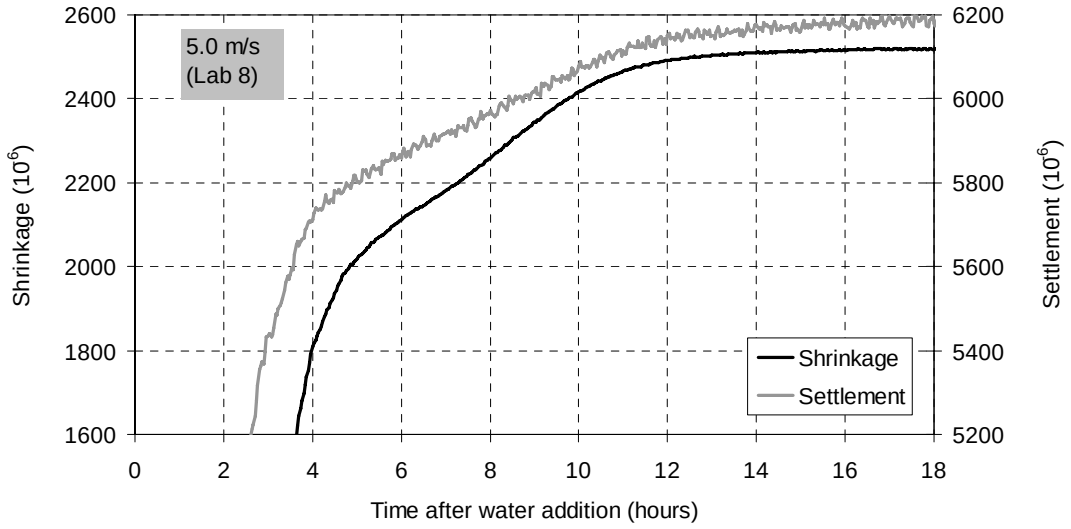

Fig. 4.49 Shrinkage and settlement for "basic concrete" no 8 when exposed to 5.0 m/s

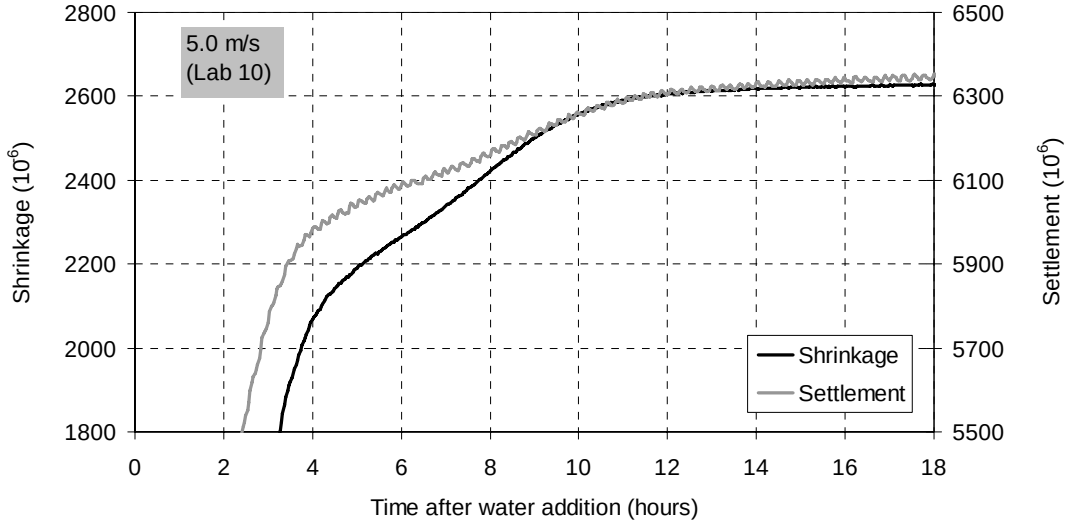

Fig. 4.50 Shrinkage and settlement for "basic concrete" no 10 when exposed to 5.0 m/s

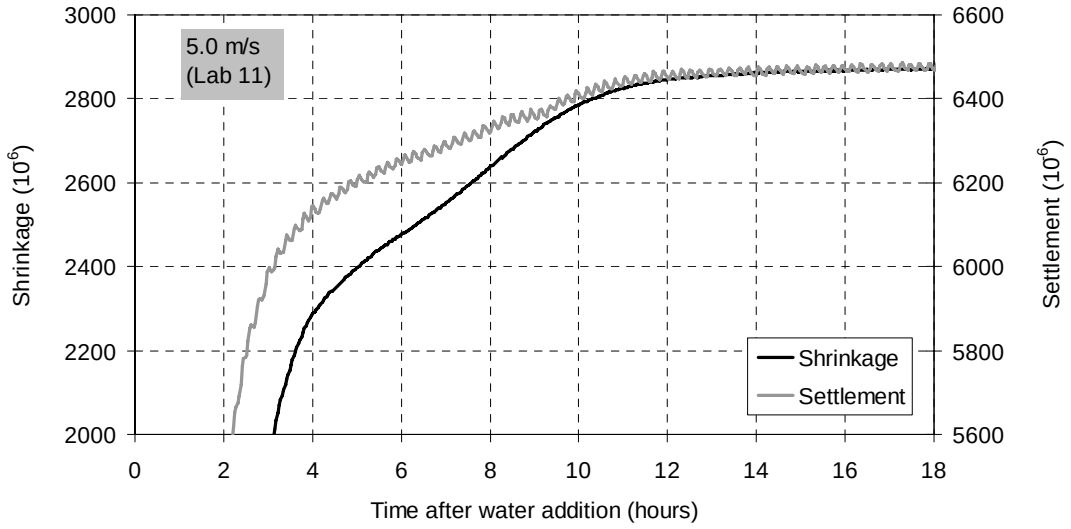

Fig. 4.51 Shrinkage and settlement for "basic concrete" no 11 when exposed to 5.0 m/s

4.3.8 Conclusion – repeatability

In general, I consider the repeatability to be acceptable with regard to the purpose of the present study. However, the measuring system can be improved to increase the repeatability. One important part of the system is that it consists of several different measures on one sample, which may be used to reveal inconsistencies in one or more of the measures. Also, the fact that small variations in time of start testing is insignificant, contributes to robustness of the system. There seems to be five different sources influencing the repeatability (order of importance):

- Friction in the measuring rod with connections for shrinkage measurements. Can be improved by using other type of measuring rod and connection.

- Inhomogeneities in the concrete sample (influences settlement mainly). Can be improved by using larger and stiffer mesh as base for settlement measuring
- Small variations in depth of PWP-measurement may occur hence the given measuring system. Can be improved by building a special rack for the pressure measuring device.
- Minor climate variation, and thus, some variation in evaporation rate
- Batch to batch variation (concrete temperature and water content, mainly)

Consistency between the different measures in the system has been confirmed. This includes:

- In sealed conditions, settlement in the liquid phase is the sum of chemical shrinkage (CS) and bleeding. Pore water pressure (PWP) is still compression. Beyond liquid phase, settlement flattens out, while CS continues at high rate resulting in an increasing gap between the two. Horizontal deformation (autogenous deformation, AD) is still insignificant. The gap in volume between settlement and CS is probably expansion of air voids, which is supported by the fact that PWP is tension.

- At relatively moderate drying rates, settlement in the liquid phase is the sum of CS + volume of evaporated water, which means that pore water is still on top of the concrete surface. The water surface starts to move downwards at the end of the liquid phase, accompanied by PWP shifting to tension and the start of plastic shrinkage. Relatively high drying rates give shorter liquid phases. The result is faster and higher settlement, that water starts to move downwards earlier as well as earlier appearance and faster evolution of PWP tension and shrinkage.

5. Deformations - influence of mix design and execution

5.1 General

The work presented in the previous chapters reveals that the deformations in the plastic and early hardening age is influenced mainly by evaporation rate, particle spacing, hydration rate, air content, surface tension of water and possibly absorbed water in aggregates. There are of course many factors influencing these basic parameters. Some examples are given in this chapter, grouped in:

- Mix design parameters: w/b, cement type, silica fume content, type of admixtures, filler amount and absorbed water in light weight aggregate
- Execution parameters: Sealed condition, exposure to stagnant air or to air with wind velocity of 5 m/s, and concrete temperature

Interpretation of the influence of mix design on each measure (e.g. settlement, shrinkage, evaporation and pore water pressure) is quite complicated because there are several interacting and counteracting effects of the above mentioned basic parameters, which makes the net result hard to predict (and thus explain). Furthermore, the influence of the exposure condition may completely overshadow the influence of other parameters, if it is sufficiently harsh. A thorough discussion of all results is therefore not done, but the rationality of the results is judged partly based on the expected consistent relationship between the different measures.

Many of the tests were run in moderate climate (to avoid the dominance of the exposure condition, as mentioned above), i.e. at stagnant air with 21 °C and 50 % RH. The “basic concrete” is the reference, and one mix design parameter at a time was investigated by keeping all other unchanged, except for the content of SNF-based WRA which was adjusted to give the target slump of 150 – 200 mm (if not other mentioned).

5.2 Influence of w/b

5.2.1 Sealed condition

When the concrete is protected against evaporation, the influence of w/b (or any other material parameter) is expected to reflect differences in initial particle spacing, hydration rate and any bleeding (see chapter 3). Hydration rate is not influenced directly by w/b, but indirectly if the w/b change includes a change of amount water reducing admixture (WRA) with a retarding side effect, as in the present study. In order to demonstrate the influence of reducing w/b, the “basic concrete” was compared with an equivalent concrete with w/b of 0.3 (“ANL 0305). The paste content and aggregate composition were similar. The amount of LS-based WRA was 0.5 % of cement weight in both concretes. However, the amount of SNF-based WRA was increased from 3.1 to 7.0 kg/m^3, in order to achieve the target slump of 150 - 200 mm.

The PWP and temperature evolution is shown in Fig. 5.1. Apparently, the SNF has a retarding influence also, as the point of temperature rise (indicating time of setting, roughly)

arrive approximately 3 hours later for the 0.30 concrete. It implies that the retarding effect overshadow the influence of reduced particle spacing (which is expected to give faster PWP evolution. The point of temperature rise appears to coincide with the points when PWP rates starts to increase rapidly. The 3 hour difference is also then seen in following PWP evolution.

PWP at 5 and 50 mm coincides for both concretes, as expected since there are no significant forces present to set up gradients. This contributes to the reliability of measurements.

Settlement is the sum of CS and bleeding in sealed condition. It can be seen in Fig. 5.2 that the 0.30 concrete has lower settlement rate than the 0.40 concrete in the beginning, probably as a result of lack of bleeding and lower hydration rate (and thus CS rate). Later, re-absorption of bleed water contributes to swelling of the 0.40 concrete, seen from the shrinkage measurements, too, see Fig. 5.3.

The commonly known influence of reduced w/b on AD of hardening concrete is demonstrated in Fig 5.3: w/b of 0.30 gives much higher rate beyond final setting time (11-12 hours). Note, however that some AD is present also before setting of this concrete.

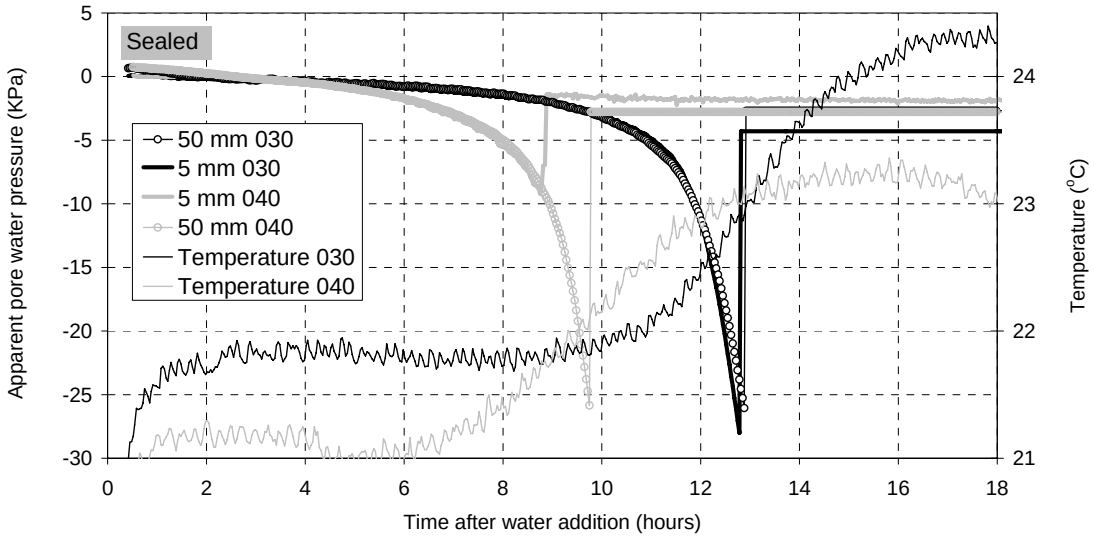

Fig. 5.1 Pore water pressure (at 5 and 50 mm depth) and temperature evolution of sealed concretes with w/b 0.30 and 0.40, respectively

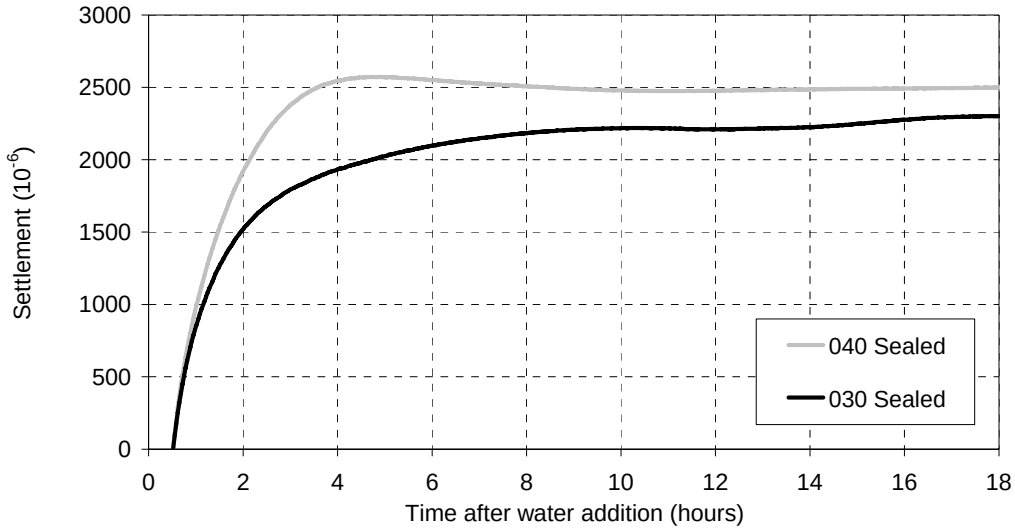

Fig. 5.2 Settlement of sealed concretes with w/b 0.30 and 0.40, respectively

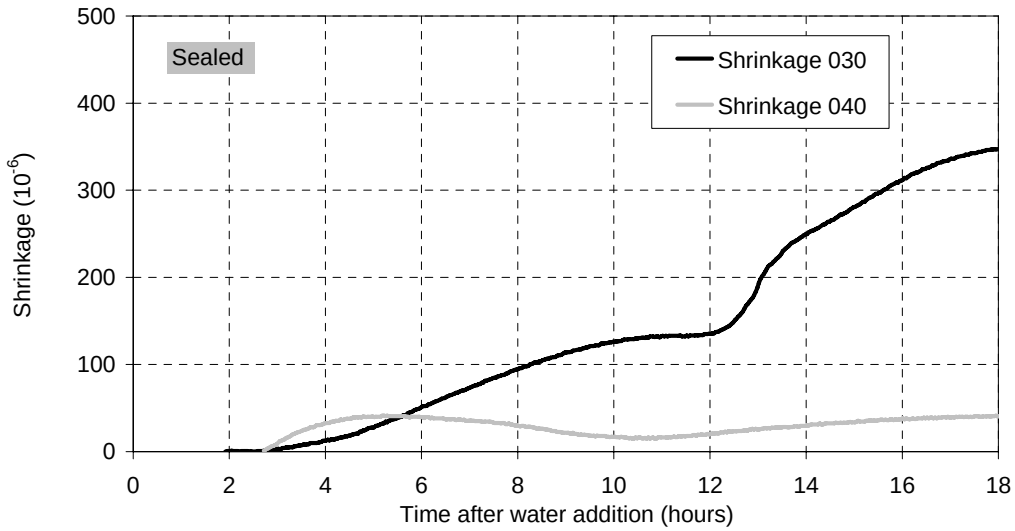

Fig. 5.3 Shrinkage of sealed concretes with w/b 0.30 and 0.40, respectively

5.2.2 Exposed to 50 % RH (0 m/s)

In addition to reduction of w/b to 0.30 as above, an increase to 0.60 (0605) was included in this series (a w/b of 0.60 was used because it complies with a typical Norwegian floor concrete). Furthermore, a second cement type was added to the program; Norcem Standard (STD), since it is more relevant for floors than "Anlegg" (ANL). It gives a total of six mixes. The recipes are given in APPENDIX 1.

Evaporation

There were no significant differences in water loss, se Figs. 5.4 and 5.5, except for the ANL 0605 concrete which showed somewhat higher water loss. The higher water loss is supported by the fact that ANL 0605 also show higher initial settlement than the others. In fact, the difference in water loss at approximately one hour of age corresponds to nearly $1000 \cdot 10^{-6}$,

which is fairly close to the difference in settlement (Fig. 5.6). I have not found a specific reason for the higher water loss (e.g. that the climate in the testing room was significantly worse).

Except for the first hour, the rates are quite linear at least until 18 hours of age for the series with ANL, which implies a rather open porosity in the period. The evaporation from STD 0305 and STD 0405 concretes flattens out before 18 hours, which probably is the result of a higher hydration rate of this cement, and thus, a lower permeability at the same point in time.

Settlement

Except for the ANL0605 (see above) there was no significant influence of w/b in the liquid phase, see Figs 5.6 and 5.7, which was expected since little difference in evaporation was seen and the influence of cement type on CS is rather little in this period. The settlement bends of into the semi-liquid phase slower and increases for a longer time (i.e. semi-liquid for a longer time) the lower the w/b is. This is probably result of lower CS rate and lower stiffness development due to the retarding side effect of WRA.

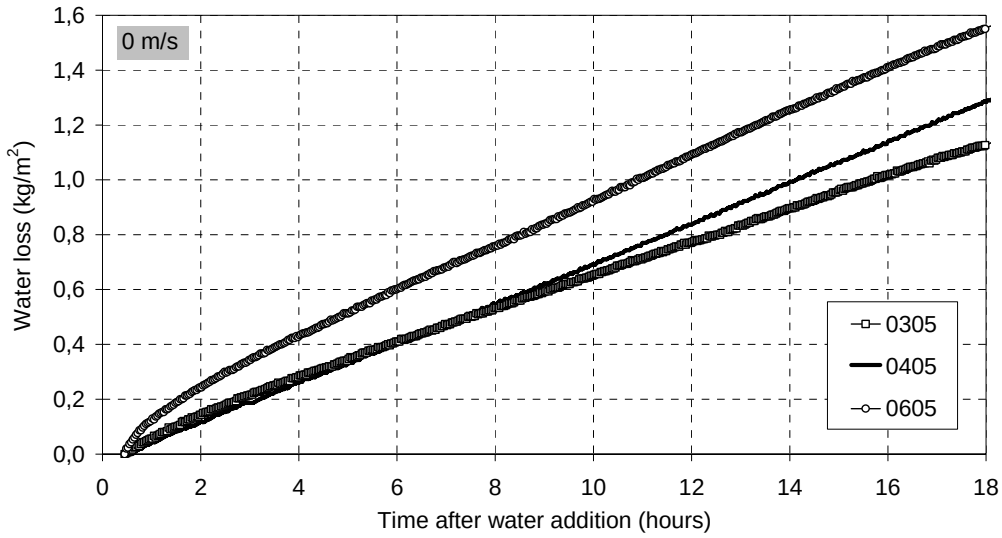

Fig. 5.4 Water loss at from Anlegg-cement concretes with different w/b, when exposed to stagnant air of 50 % RH

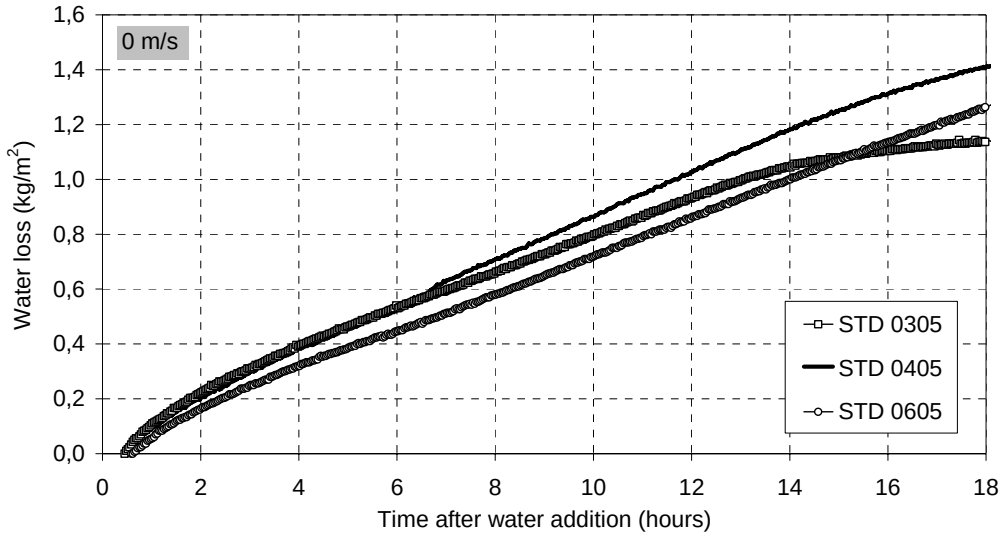

Fig. 5.5 Water loss from Standard-cement concretes with different w/b, when exposed to stagnant air of 50 % RH

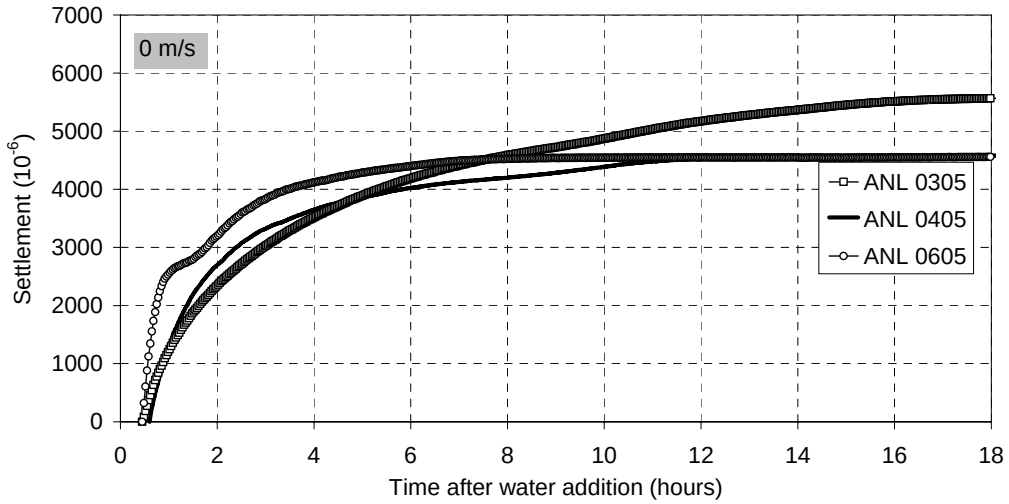

Fig. 5.6 Settlement of Anlegg-cement concretes with different w/b, when exposed to stagnant air of 50 % RH

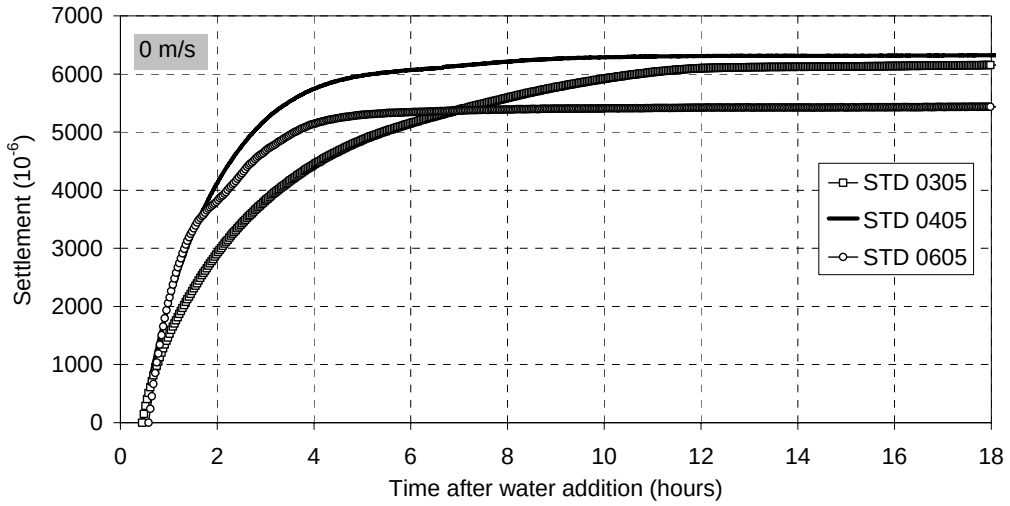

Fig. 5.7 Settlement of Standard-cement concretes with different w/b, when exposed to stagnant air of 50 % RH

Pore water pressure

The PWP evolutions at 5 mm and 50 mm, shown in Figs. 5.8 - 5.11, are quite similar both for the concrete with w/b of 0.40 and for the one with w/b of 0.60. It implies sufficient water transport from the interior to the surface, and no significant thickening zone at the top. The PWP of the w/b = 0.30 concrete, however, drops much faster at 5 mm than at 50 mm, which implies a thickening zone (skin formation) and thus shrinkage at the top. Apparently, the steep part of the PWP evolution is not consistently influence by w/b. This is probably result of the counteracting effects of reducing w/b: PWP rate increases because of decreasing interparticle space, but decreases due to retarded hydration caused by increasing WRA-content.

Shrinkage

Shrinkage rate was not considerably influenced by w/b in the first few hours, which is supported by the insignificant influence on PWP rates in the same time. But, the shrinkage "bends off" smoother and continues for a longer time, as for settlement (retardation effect), with decreasing w/b. When a lowering of w/b involves an increasing WRA content with retarding side effect (most WRA have, but with varying effect), the PWP evolution at the top is probably even more important, and it can be seen that the concrete with the lowest w/b experiences faster PWP drop, and thus earlier shrinkage start.

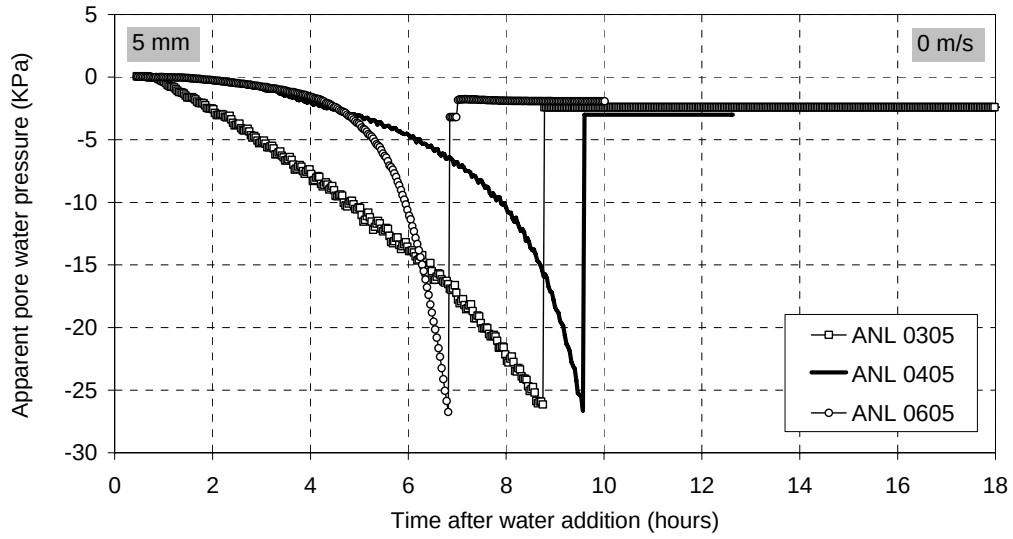

Fig. 5.8 Pore water pressure at 5 mm depth of Anlegg-cement concretes with different w/b, when exposed to stagnant air of 50 % RH

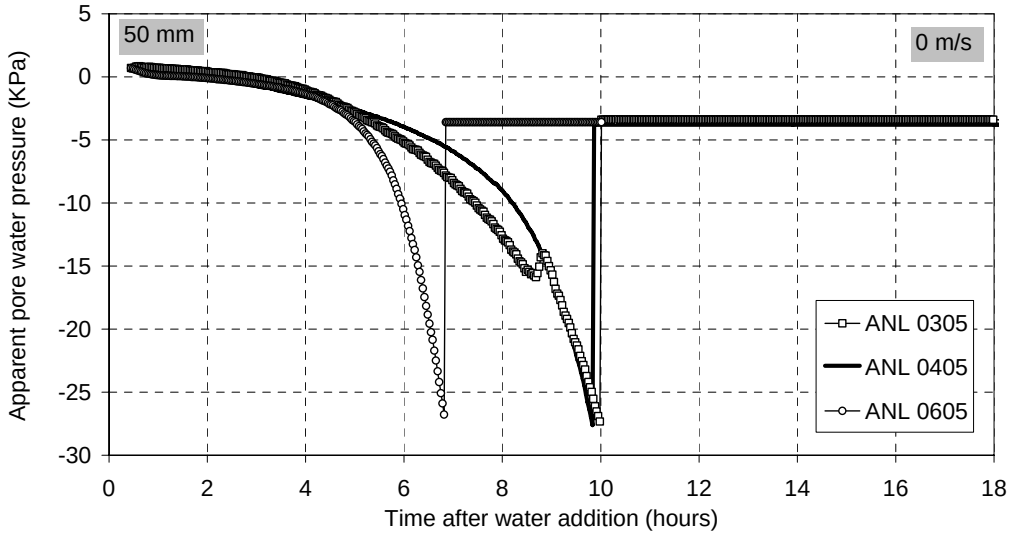

Fig. 5.9 Pore water pressure at 50 mm depth of Anlegg-cement concretes with different w/b, when exposed to stagnant air of 50 % RH

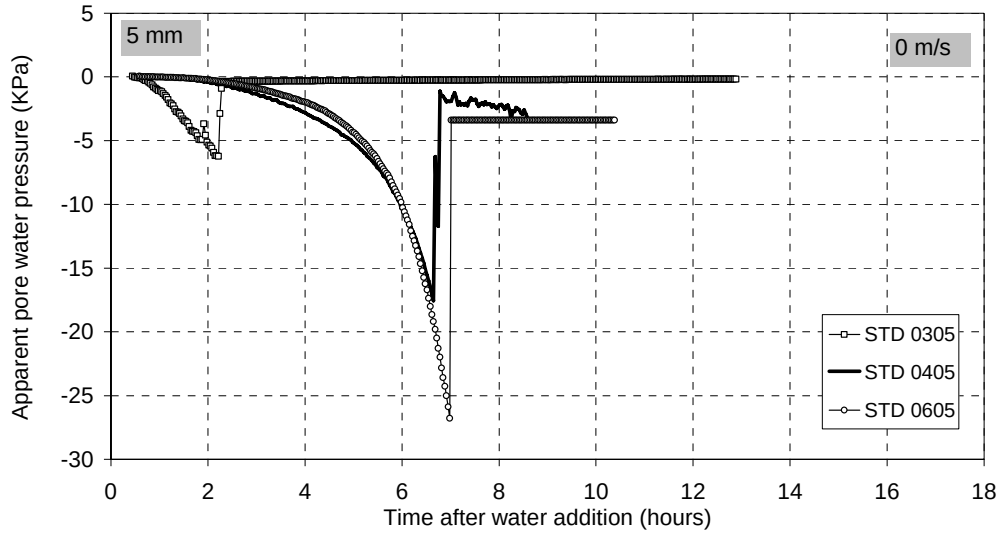

Fig. 5.10 Pore water pressure at 5 mm depth of Standard-cement concretes with different w/b, when exposed to stagnant air of 50 % RH

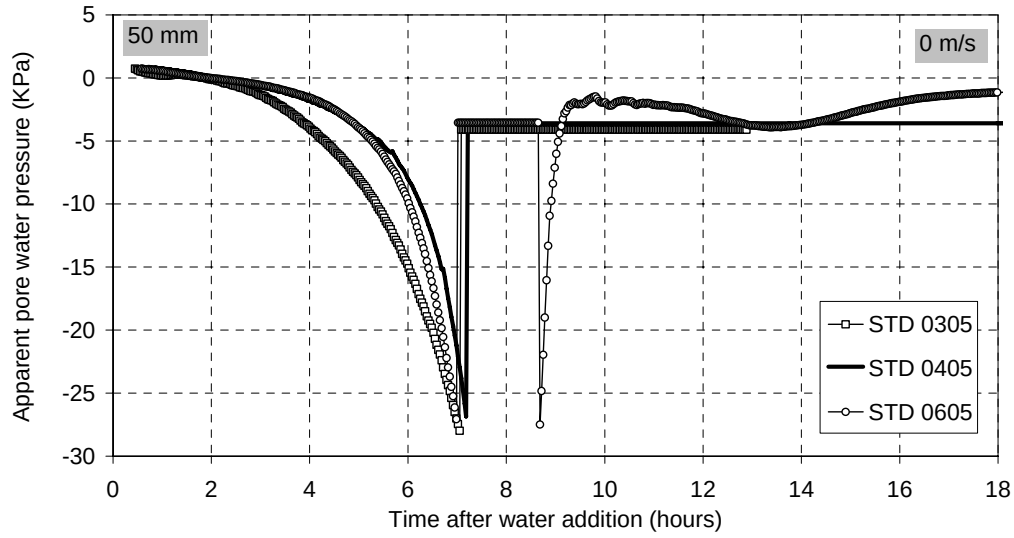

Fig. 5.11 Pore water pressure at 50 mm depth of Standard-cement concretes with different w/b, when exposed to stagnant air of 50 % RH

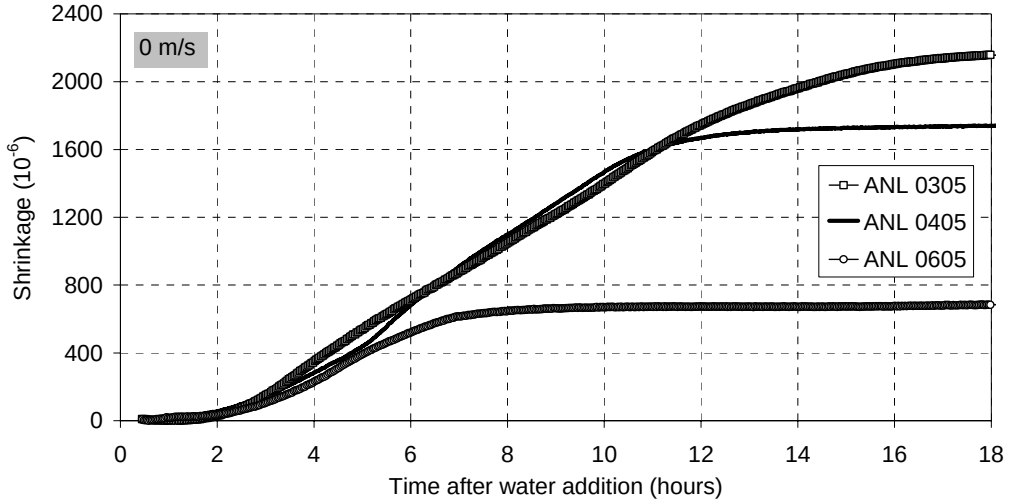

Fig. 5.12 Shrinkage of Anlegg-cement concretes with different w/b, when exposed to stagnant air of 50 % RH

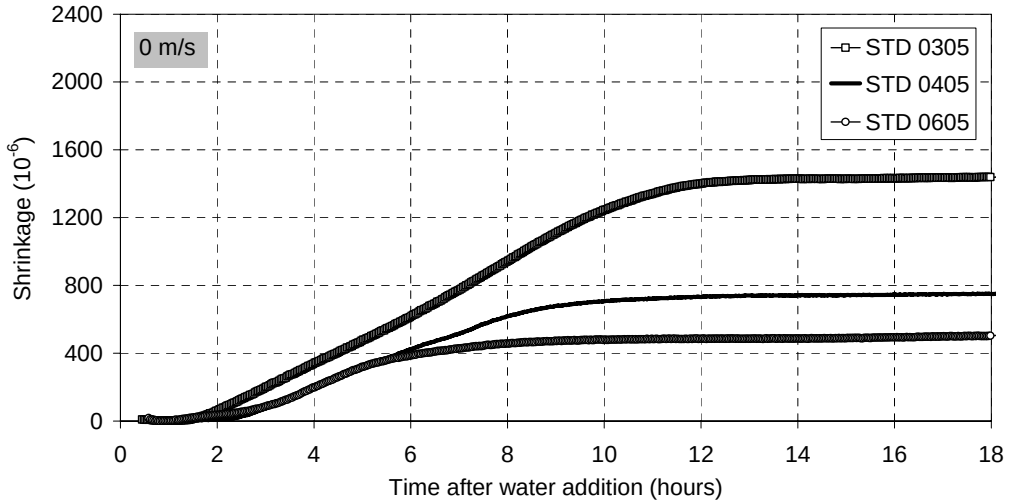

Fig. 5.13 Shrinkage of Standard-cement concretes with different w/b, when exposed to stagnant air of 50 % RH

5.2.3 Conclusion – influence of w/b on deformations

One should expect that the influence of reducing the w/b, i.e. of reducing the interparticle space, would be an increase of deformation rate, since the driving force is pore water tension which is geometry controlled (Laplace equation). This is probably also the case when considering the shrinkage of the top "skin" of a horizontal surface, as indicated by the PWP measurements at 5 mm depth. I.e. the surfaces of concretes with low w/b may experience

quite immediate shrinkage and at high rate. In fact, this is probably the most important effect of w/b (see chapter 8).

When considering the deformations of the "bulk" concrete, the expected direct influence of reduced w/b seems to be overshadowed by an indirect effect, namely decreased hydration rate as a result of the retarding side effect of WRA. The net result of the two is "smoother" transition from liquid phase to semi-liquid phase and an increasing semi-liquid phase with decreasing w/b. The latter results in increased total plastic shrinkage (i.e. longer period with plastic shrinkage), which constitute another negative influence of reducing w/b. Further work should include tests on concretes with various w/b without admixtures with retarding effect.

5.3 Influence of cement type

Four types of cements from Norcem AS have been tested: "Anlegg" (ANL), CEM I 52,5 N-LA, "Industri" (IND), CEM I 42,5 RR, "Standard" (STD) CEM I 42,5 R, and Standard FA (STDFA) CEM II/A-V 42,5 R. Characteristic data are found in APPENDIX 1. All four were tested with w/b = 0.60 and all except Standard FA with w/b = 0.40.

Following the discussion in chapter 3, the fineness of the cement is expected to be the most important parameter as it contributes both to increased CS rate (increased hydration rate) and to reduced permeability (through reduced initial particle spacing and increased hydration rate). It follows that IND is expected to give the highest deformation rates and PWP rates. However, since the fineness influences the water demand to achieve equal slump, different amounts of the WRA with retarding side effect is used, which reduces hydration rate.

5.3.1 Exposed to 50 % RH and 0 m/s

For both w/b numbers the finest cement (IND) showed the highest evaporation rates, see Figs 5.14 and 5.15, and the earliest flattening out level. The first point can be a result of slightly higher concrete temperature using this cement (contributes to higher evaporation rate). The second point was expected since it has the highest hydration rate, and thus the fastest permeability decrease.

Figs. 5.16 and 5.17 show that the ANL cement had the lowest settlement rates in the liquid phase, and a smoother transition to the semi-liquid phase. It may be a result of lower hydration rate (giving lower rate of CS and stiffness evolution), which is confirmed by the PWP measurements (Figs 5.18 – 5.21). Note that STDFA-curve levels out smoother than the curves representing the other concretes (Fig. 5.17). This indicates a slower stiffness evolution, and is supported by slower PWP (Fig. 5.20) and shrinkage evolution (Fig. 5.23). The latter is quite distinct and a repetition of the tests with STDFA concrete gave the same results.

The PWP at 5 and 50 mm depth are quite similar for all cements and with both w/b ratios, but PWP of the IND cement with w/b = 0.40 shows a slightly higher rate at 5 mm than at 50 mm in the beginning, which implies a skin formation, although probably not of great importance. However, this and the fact that PWP both at 5 and 50 mm depth have considerably higher rates than that of the other cements, confirms that IND exhibit a potentially higher driving force to cracking than the other cements.

Again, it can be seen a consistent relationship between PWP and shrinkage: The earlier and faster the PWP drops, the earlier the shrinkage starts and levels off. The IND cement being the fastest one.

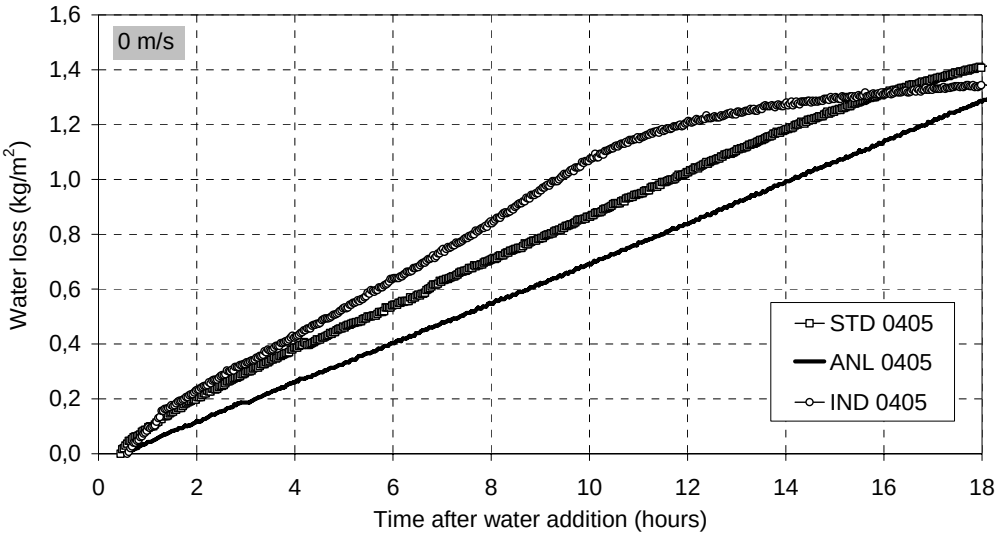

Fig. 5.14 Water loss from concretes with w/b = 0.40 and with different cement types, when exposed to stagnant air of 50 % RH

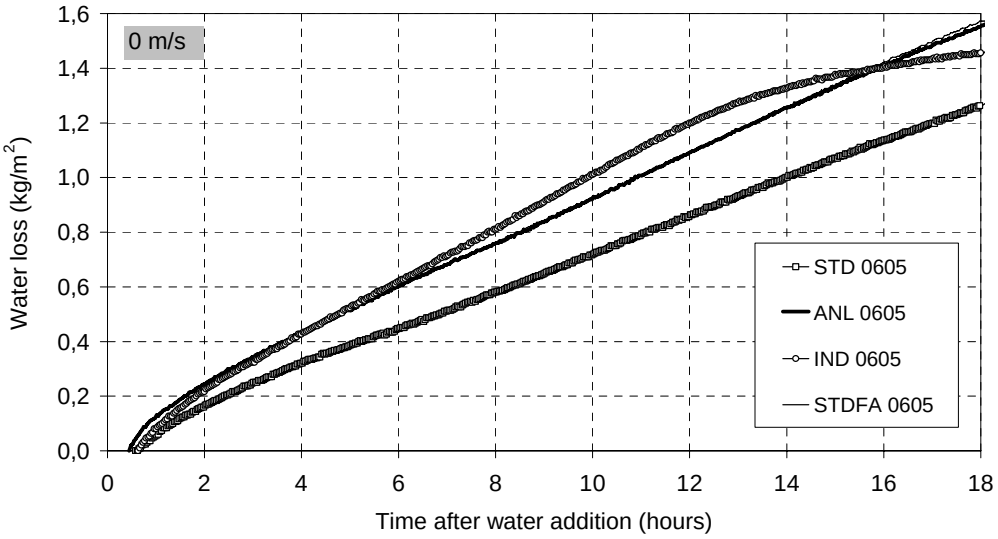

Fig. 5.15 Water loss from concretes with w/b = 0.60 and with different cement types, when exposed to stagnant air of 50 % RH

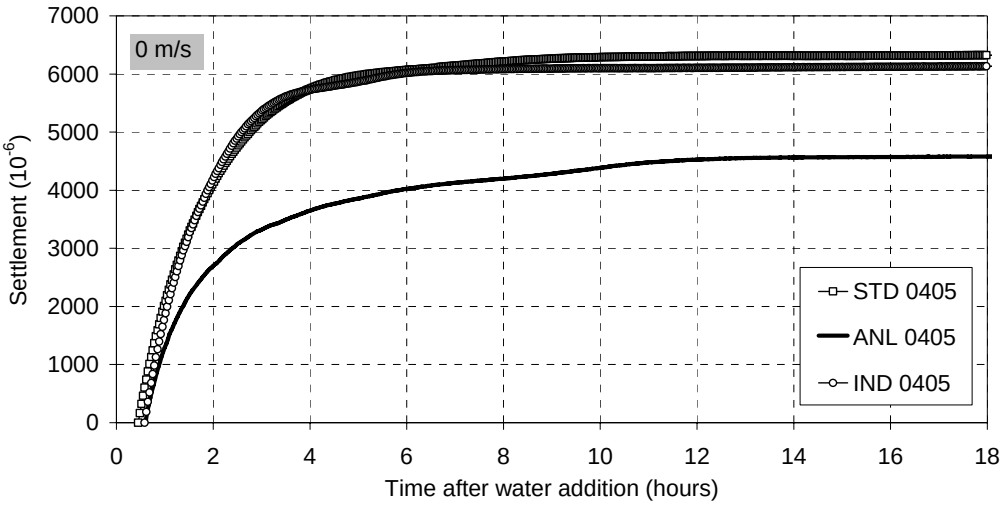

Fig. 5.16 Settlement of concretes with w/b = 0.40 and with different cement types, when exposed to stagnant air of 50 % RH

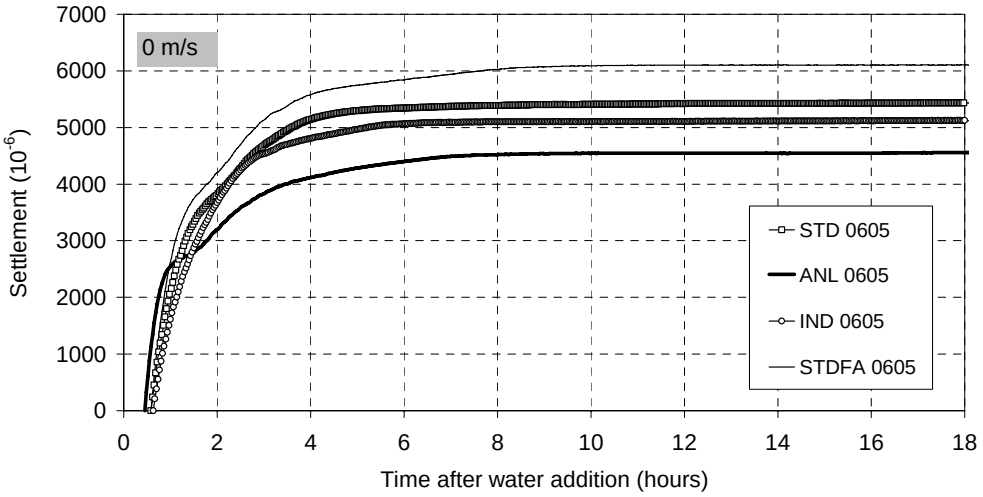

Fig. 5.17 Settlement of concretes with w/b = 0.60 and with different cement types, when exposed to stagnant air of 50 % RH

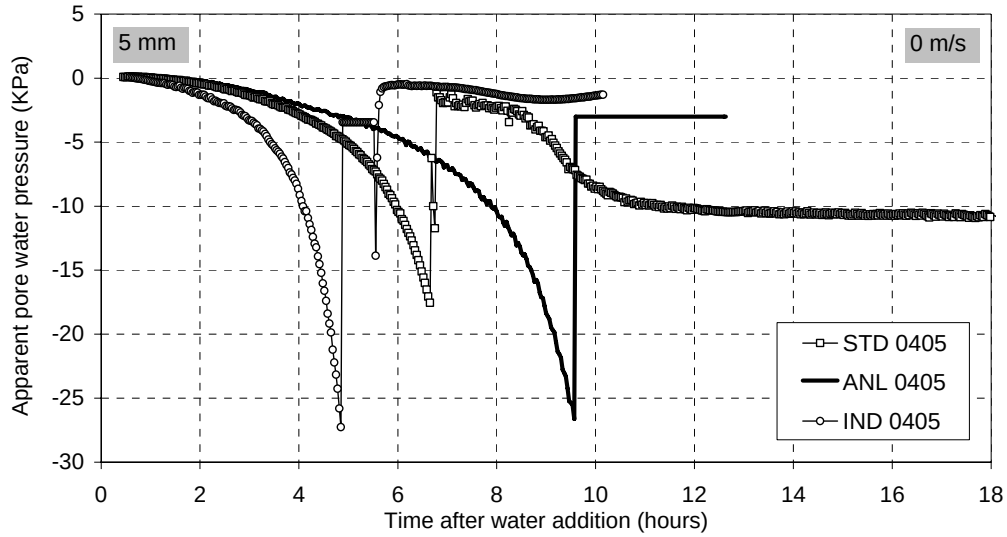

Fig. 5.18 Pore water pressure at 5 mm depth of concretes with w/b = 0.40 and with different cement types, when exposed to stagnant air of 50 % RH

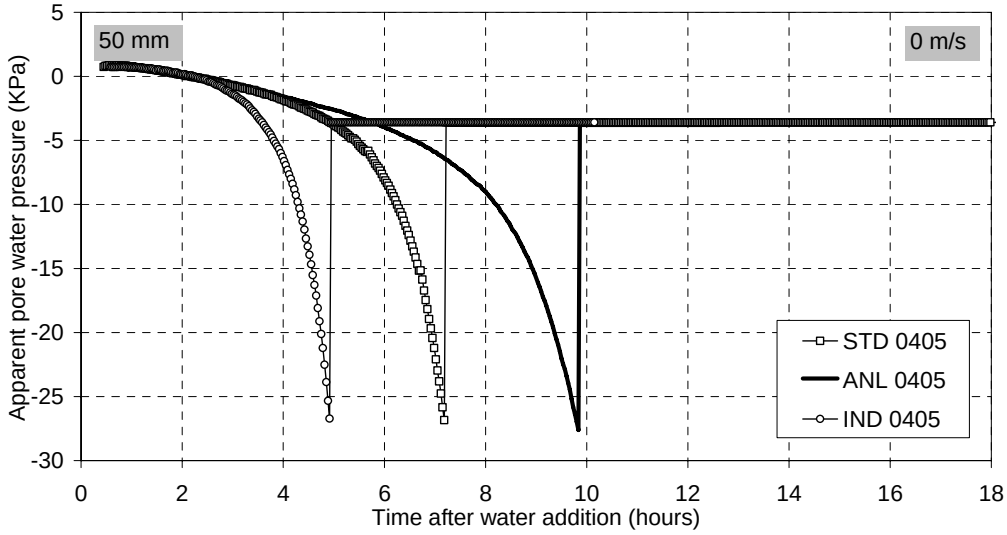

Fig. 5.19 Pore water pressure at 50 mm depth of concretes with w/b = 0.40 and with different cement types, when exposed to stagnant air of 50 % RH

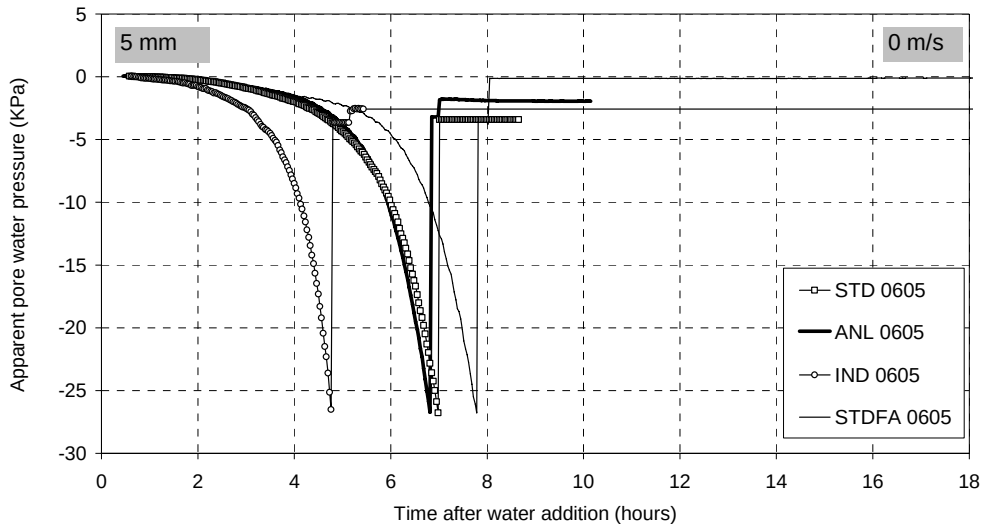

Fig. 5.20 Pore water pressure at 5 mm depth of concretes with w/b = 0.60 and with different cement types, when exposed to stagnant air of 50 % RH

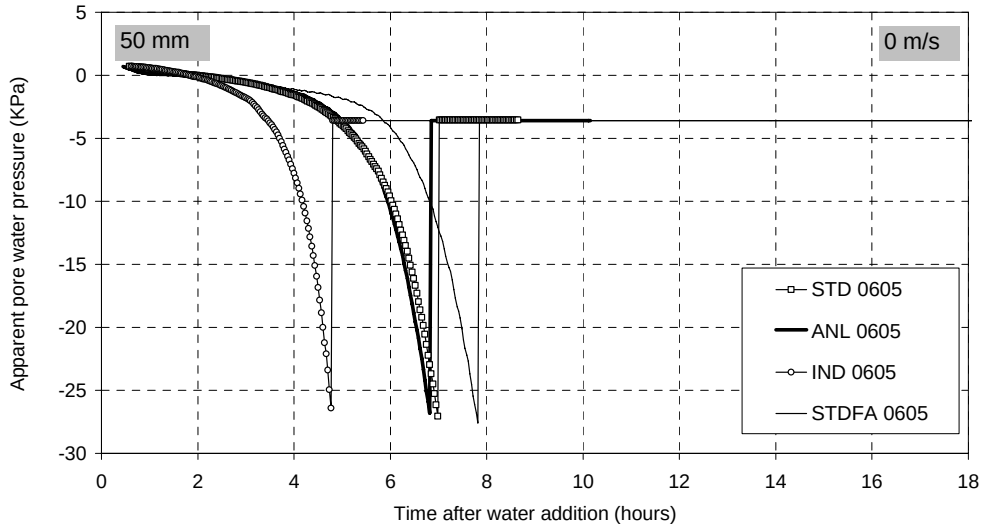

Fig. 5.21 Pore water pressure at 50 mm depth of concretes with w/b = 0.60 and with different cement types, when exposed to stagnant air of 50 % RH

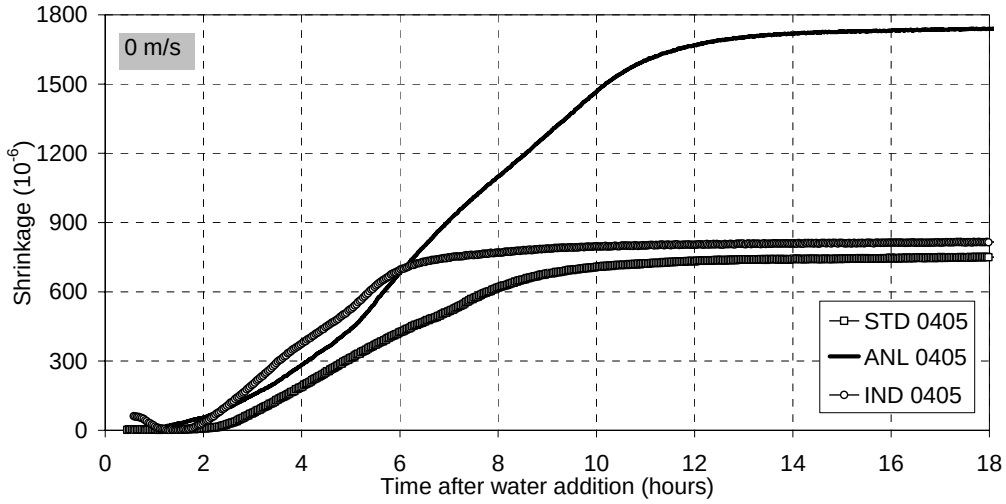

Fig. 5.22 Shrinkage of concretes with w/b = 0.40 and with different cement types, when exposed to stagnant air of 50 % RH

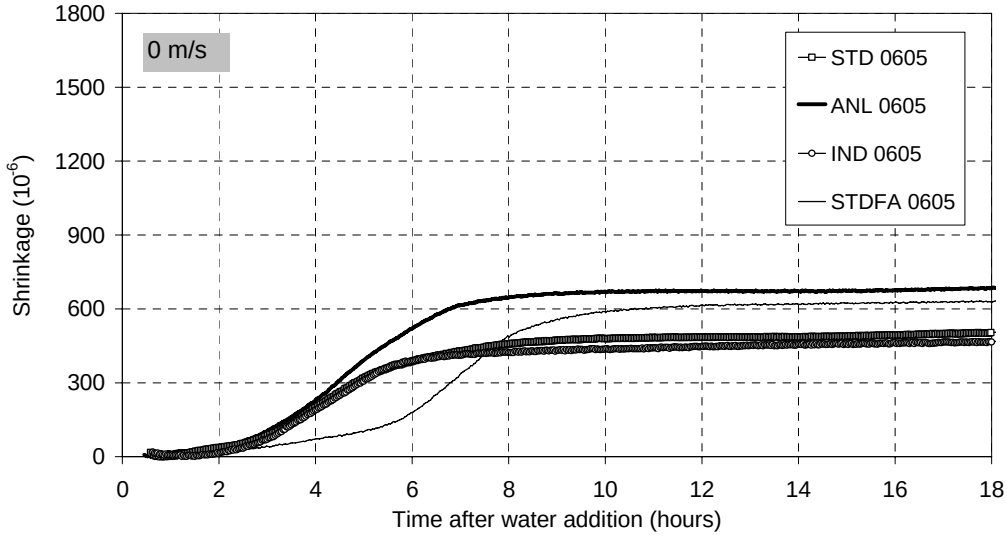

Fig. 5.23 Shrinkage of concretes with w/b = 0.60 and with different cement types, when exposed to stagnant air of 50 % RH

5.3.2 Exposed to 50 % RH and 5 m/s

Exposure without wind, as above, gives a quite low evaporation rate which do not challenge considerably the permeability evolution of the concretes. The coarsest (and "slowest") and finest (and "fastest") cements were therefore tested when exposed to 5 m/s, in order to test the influence of permeability.

The difference in water loss seen in Fig. 5.24 clearly shows the influence of initial permeability and its evolution as the evaporation rate of IND is lower than that of ANL in the

whole period. In fact, the total water loss of IND at 18 hours is only approximately 0.3 kg/m^2 higher than that at 0 m/s, while the corresponding difference for ANL is 2.3 kg/m^2. The considerably increased evaporation compared to exposure to 0 m/s resulted in corresponding increase of settlement rate for ANL, but not for the IND, see Figs. 5.16 and 5.25. The latter implies that the increased water loss of IND corresponds to emptying of surface pores, mainly, as pointed out in chapter 3. It seems that there is a physical limit (particle contact) for contraction and that IND is closer to this limit already before the extra water loss. Thus, the influence of increased evaporation is less for IND than for ANL. It suggests that the influence of cement type at high evaporation rate is less than at low evaporation rate.

Note that there is no significant difference in PWP evolution and corresponding shrinkage between the ANL and IND, see Figs. 5.26 and 5.27. Both show skin formation as PWP at 5 mm drops faster than at 50 mm depth. Note also that the total shrinkage and total settlement is quite the same. Again, the high drying load overshadows the influence of material parameters.

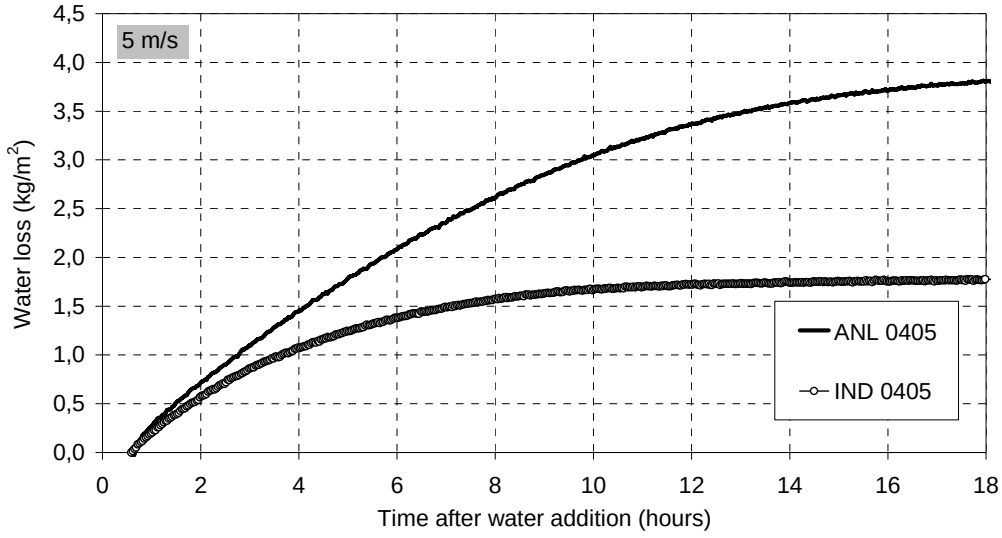

Fig. 5.24 Water loss from concretes with w/b = 0.40 and with different cement types, when exposed to air of 50 % RH and wind velocity 5 m/s

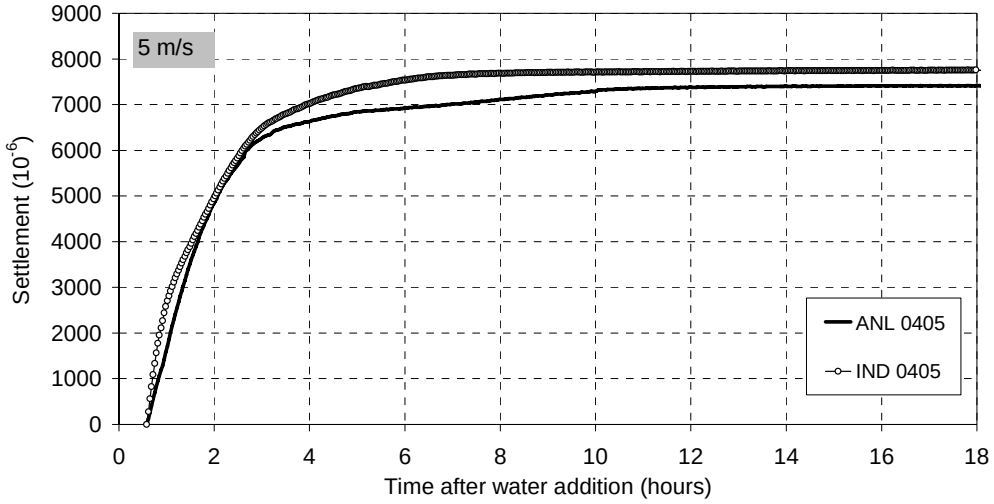

Fig. 5.25 Settlement of concretes with w/b = 0.40 and with different cement types, when exposed to air of 50 % RH and wind velocity 5 m/s

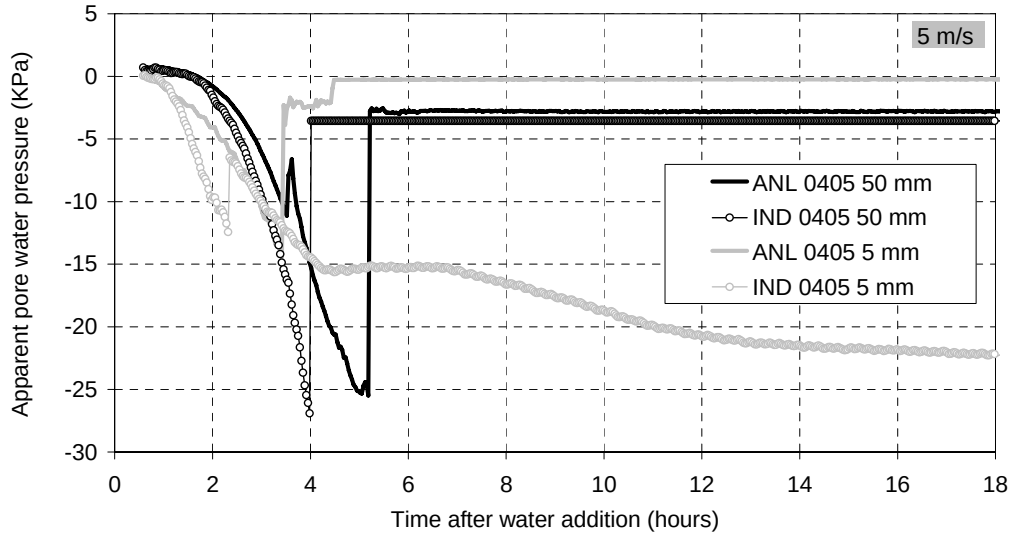

Fig. 5.26 Pore water pressure at 5 and 50 mm depth of concretes with w/b = 0.40 and with different cement types, when exposed to air of 50 % RH and wind velocity 5 m/s

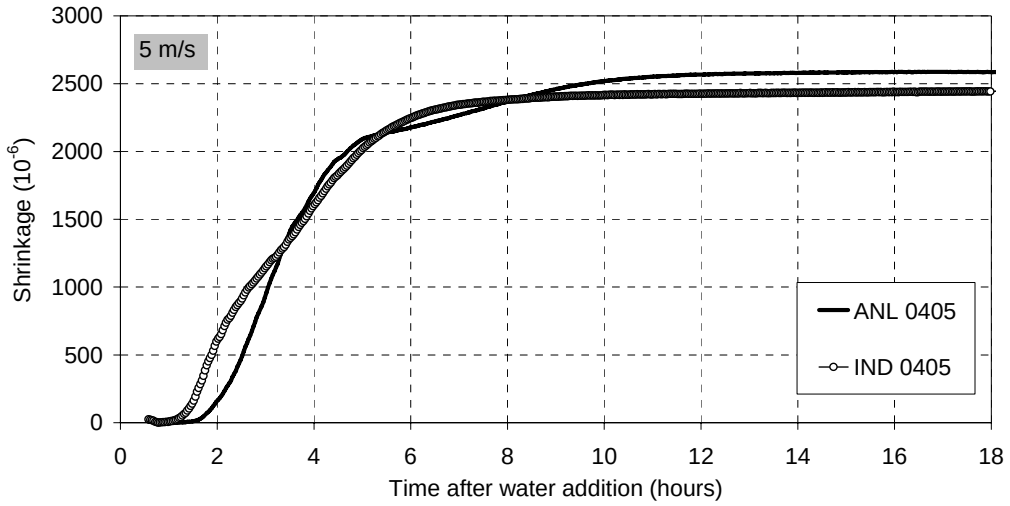

Fig. 5.27 Shrinkage of concretes with w/b = 0.40 and with different cement types, when exposed to air of 50 % RH and wind velocity 5 m/s

5.4 Influence of water reducing admixtures

As pointed out in section 3.3.5, it seems obvious that there are mainly two types of admixtures that influence the deformations: Those which influence hydration rate (i.e. accelerators and retarders) and those which influence surface tension of water. It is claimed that some WRA may reduce surface tension of water, and thus, decrease PWP rate. But it is assumed to have a secondary effect compared to the retarding effect that WRA may have, as discussed in the two previous chapters. Special surface tension reducing admixtures are discussed in section 5.7.

In order to support the retardation assumption two tests were performed with the "basic concrete" where the LS/SNF combination was replaced with the LS and the SNF, respectively. The LS is known to have a large retarding effect and the SNF to have less retarding effect. Another series was performed using a co-polymer based WRA, known to have less retarding effect than the LS/SNF.

The retarding effect of LS is confirmed by the temperature measurements of the samples, see Fig. 5.28: The temperature rise of the SNF concrete starts at approximately 5 hours while at approximately 10 hours for the LS concrete.

The PWP measurements reflect nicely the retardation, showing a slower evolution. It confirms the implication from temperature recordings of 5 hours difference in setting time, as it coincides fairly well with the time difference at "minimum" PWP, see Fig. 5.29.

The main consequence of the retardation on settlement and shrinkage is that the time before leveling out increases (with approximately 5 hours), resulting in increased total deformation in the period, see Fig. 5.29.

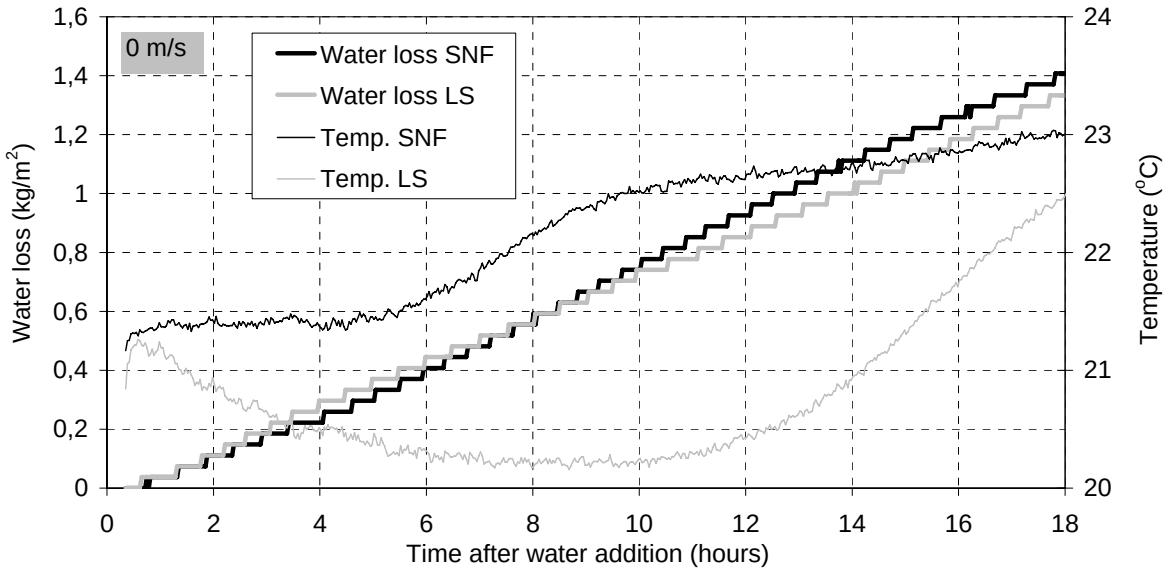

Fig 5.28 Water loss and temperature evolution of concretes with w/b = 0.40 and with different water reducing admixtures, when exposed to stagnant air of 50 % RH

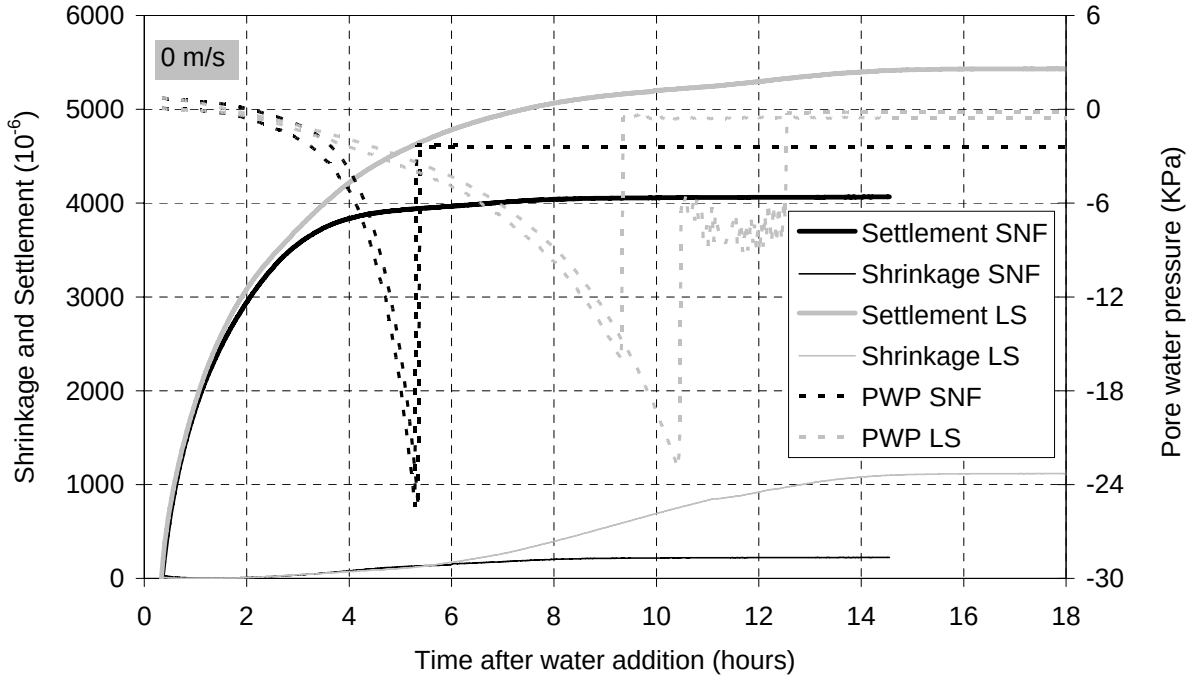

Fig 5.29 Pore water pressure (at 5 and 50 mm depths), settlement and shrinkage of concretes with w/b = 0.40 and with different water reducing admixtures, when exposed to stagnant air of 50 % RH

Two “co-polymer concretes” were made with 0,75 % (copol 2) 1,26 % (copol 1) of cement weight, respectively, giving a slump of 180 mm and 210 mm, respectively. The latter concrete showed significant bleeding.

The water loss was not significantly influenced as expected, see Fig. 5.30. The settlement of the copol 1 concrete progressed quite different from the other two concretes until approximately 2 hours of age, see Fig. 5.31. The difference is probably due to the higher bleeding of this concrete, which is supported by eye observation (but not measured). The settlement of the two co-polymer concretes is quite similar beyond 2 hours of age. The result of less retardation is reflected in that PWP of the co-polymer concretes turns into the steep part earlier. The PWP measurements also support the statement that the first co-polymer concrete had more bleeding, in that PWP of this concrete remains close to zero for a longer period of time, see Figs. 5.32 and 5.33. Furthermore, the latter is supported by a subsequent slower shrinkage rate of this concrete, see Fig. 5.33.

The PWP of the second co-polymer reached tension quite early and progressed at a relatively high rate. This is reflected in earlier and faster shrinkage (Fig. 5.34). However, the total shrinkage is still less because less retardation causes an earlier leveling out.

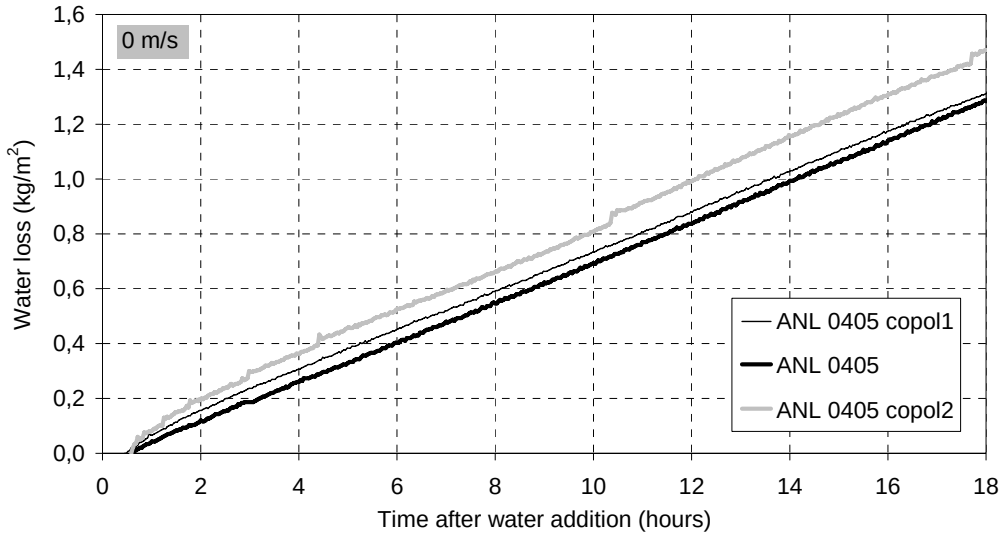

Fig 5.30 Water loss of concretes with w/b = 0.40 and with different amount of co-polymer based water reducing admixtures, when exposed to stagnant air of 50 % RH

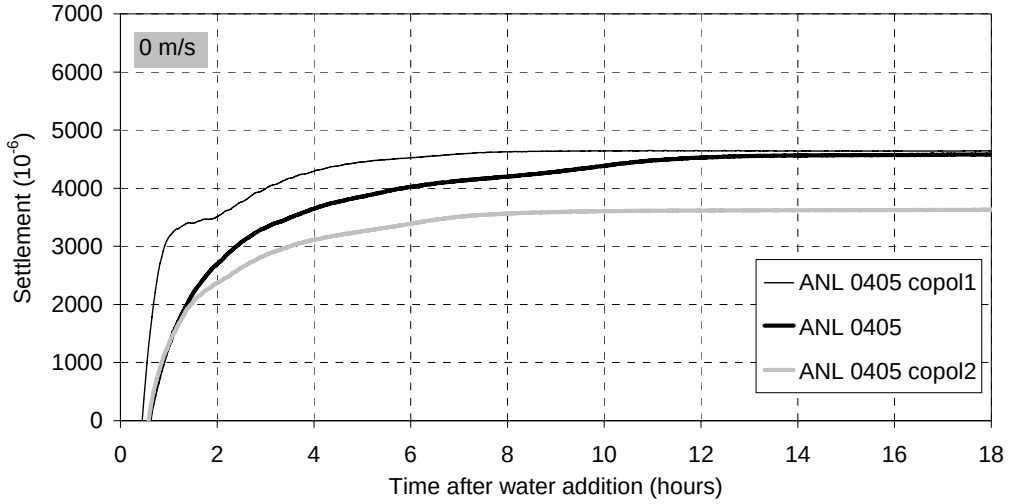

Fig 5.31 Settlement of concretes with w/b = 0.40 and with different amount of co-polymer based water reducing admixtures, when exposed to stagnant air of 50 % RH

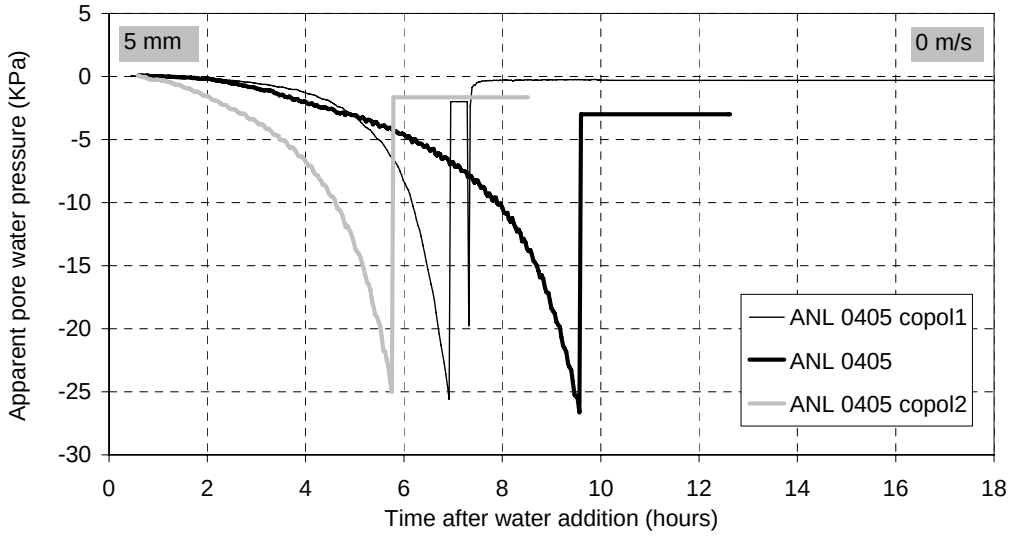

Fig 5.32 Pore water pressure at 5 mm depth of concretes with w/b = 0.40 and with different amount of co-polymer based water reducing admixtures, when exposed to stagnant air of 50 % RH

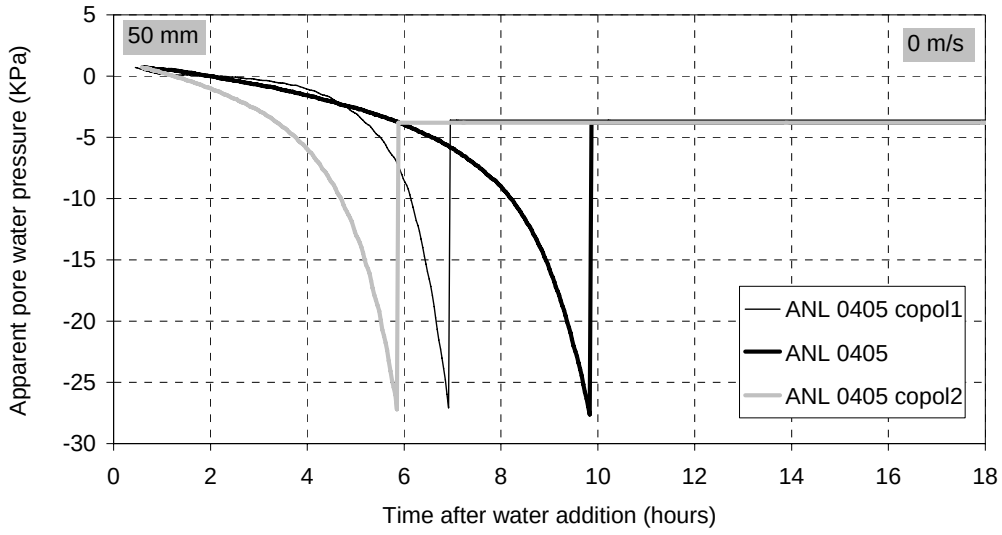

Fig 5.33 Pore water pressure at 50 mm depth of concretes with w/b = 0.40 and with different amount of co-polymer based water reducing admixtures, when exposed to stagnant air of 50 % RH

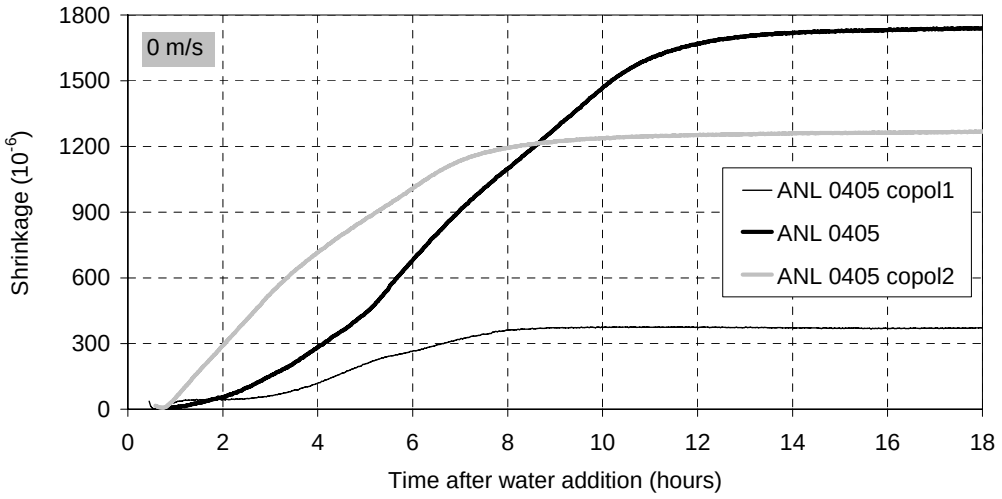

Fig 5.34 Shrinkage of concretes with w/b = 0.40 and with different amount of co-polymer based water reducing admixtures, when exposed to stagnant air of 50 % RH

5.5 Influence of silica fume

Four test series were performed based on the basic concrete with different silica fume (SF) content (replacement for cement). I.e. the 5 % SF in the basic concrete was replaced with 0, 10 and 15 % silica fume, without changing the paste amount and LS amount. As slump decreases with increasing SF amount, the amount of SNF was from 3.1 to 4.6 kg/m^3 in order to achieve the target slump of 150 – 200 mm.

The evaporation rate was not significantly influenced by SF amount as expected, see Fig. 5.35. This and the fact that CS is not significantly influenced (see chapter 3) suggest that

settlement is not influenced in the liquid phase. The results in Fig 5.36, confirm this, except that the 15 % concrete had considerably lower settlement rate than that of the others, until approximately 4 hours of age. It suggests faster stiffening of the 15 % concrete, as indicated bt the PWP measurements, also (see below).

The PWP at sealed condition show that the PWP rate increases somewhat with increasing SF content (0 % SF was not tested), see Fig. 5.37, as expected since SF contributes to less bleeding and probably to earlier bridging of cement particles (earlier stiffening). The same ranking is seen in the air exposed condition, too, see Figs 5.38 and 5.39. Unfortunately, PWP at 5 mm depth broke through very early for three of the concretes, but it can still be seen that 0 %-curves at 5 and 50 mm coincide roughly until break through at nearly 6 KPa, implying no significant skin formation. However, the equivalent relationship for the 15 % concrete is that PWP drops considerably faster at 5 mm than at 50 mm, which implies skin formation.

Again, shrinkage progresses roughly in accordance with the PWP evolution in the first hours, see Figs 5.40 and 5.38. It can be seen that the point in time when shrinkage levels off decreases with increasing SF content. Correspondingly, the point in time when PWP runs into the steep part decreases with increasing SF content.

It can be concluded that there is no significant influence of SF amount up to 10 % in the present situation. Field experience show, however, that SF contributes to increased cracking susceptibility (Kompen, 1994). There are probably two major reasons for the apparent inconsistency: One is related to the influence of SF on bleeding. Reduced bleeding (and thus less surface wetting) is commonly used as the explanation of the SF influence. The present concretes all show relatively low or no bleeding, due to the low w/b, which results in a rapid drying of the surface irrespective of SF content. The other reason is that field climate is often tougher than the one used here. Therefore, new tests should be performed with wind, which is expected to reveal the influence of lower initial permeability and probably a faster permeability evolution of the SF concretes. The results of the 15 % concrete support it since a skin formation was observed. However, the tests with coarse and fine cement revealed a relatively little influence of fineness, so the answer is not obvious.

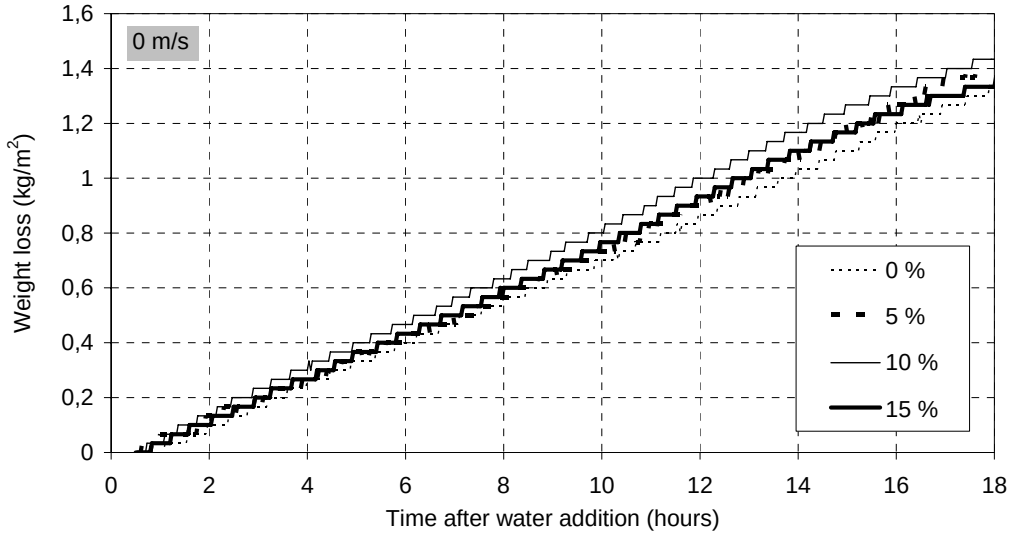

Fig. 5.35 Water loss of concretes with w/b = 0.40 and with different amount of silica fume, when exposed to stagnant air of 50 % RH

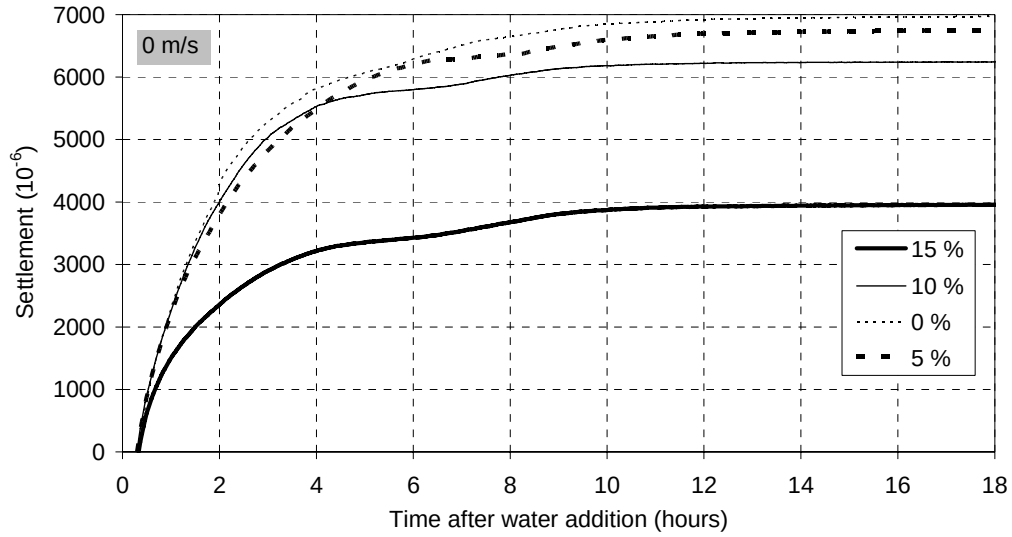

Fig. 5.36 Settlement of concretes with w/b = 0.40 and with different amount of silica fume, when exposed to stagnant air of 50 % RH

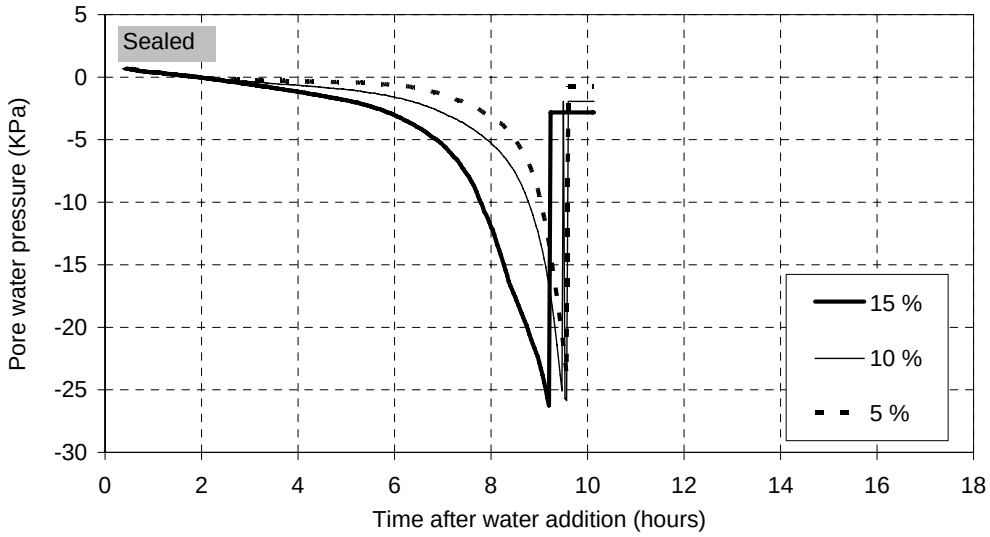

Fig. 5.37 Pore water pressure at 50 mm depth of sealed concretes with w/b = 0.40 and with different amount of silica fume

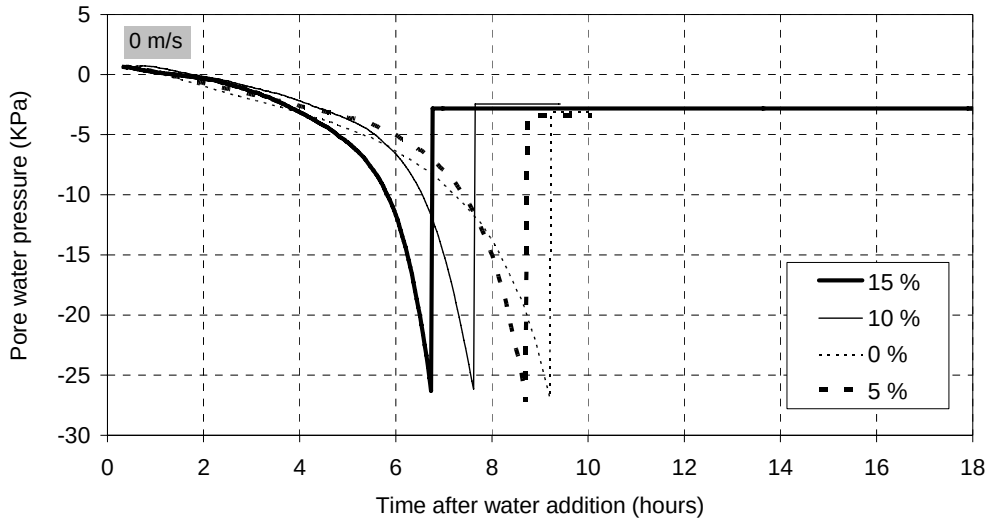

Fig. 5.38 Pore water pressure at 50 mm depth of concretes with w/b = 0.40 and with different amount of silica fume, when exposed to stagnant air of 50 % RH

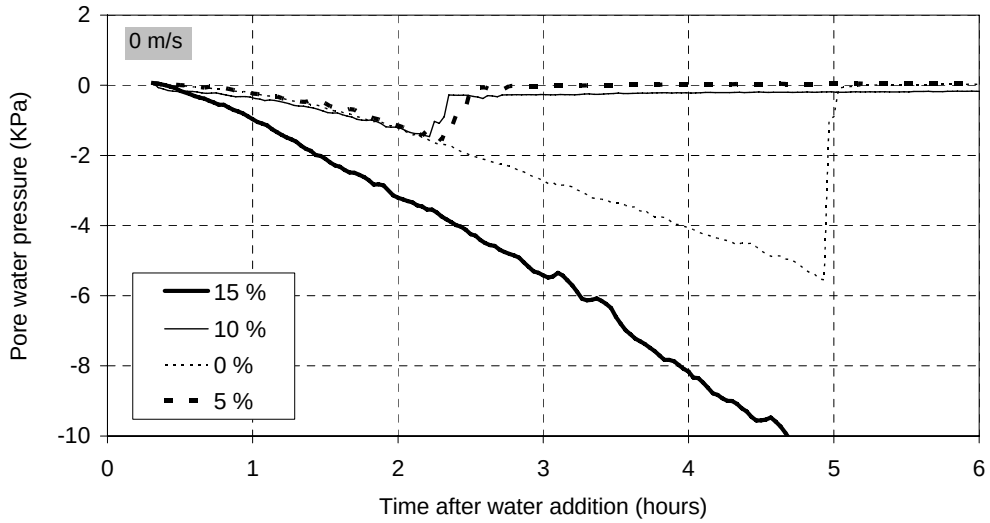

Fig. 5.39 Pore water pressure at 5 mm depth of concretes with w/b = 0.40 and with different amount of silica fume, when exposed to stagnant air of 50 % RH

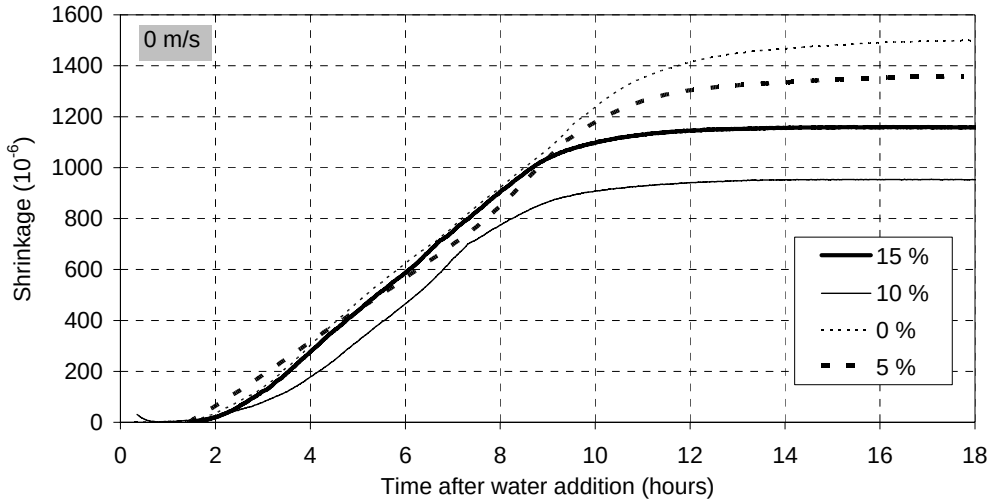

Fig. 5.40 Shrinkage of concretes with w/b = 0.40 and with different amount of silica fume, when exposed to stagnant air of 50 % RH

5.6 Influence of shrinkage reducing admixture (SRA)

SRA reduces surface tension of water. The expected results of reduced surface tension of water are increased water loss, decreased PWP rate and subsequent reduced shrinkage rate. SRA is used mainly to reduce drying shrinkage. One test was made here on the basic concrete, in order to see to what extent it may reduce deformations in the present age.

Fig. 5.41 confirms apparently higher rate of water loss until 5-6 hours of age (i.e. until time of initial setting), but it appears to decrease with age beyond this point, which is not the case for the concrete without SRA. It indicates faster reduction of permeability, i.e. increased hydration rate, but the temperature, settlement, PWP and shrinkage results indicate the opposite (Figs. 5.42-5.45) which suggest that there is another reason. This is not further discussed here.

The temperature measurements indicate that the SRA concrete is somewhat retarded (slower temperature rise, seen in Fig 5.42). This is indicated also in the settlement results in that the leveling off period is very long.

The PWP measurements imply that SRA delays PSS and PWP evolution (as expected), see Fig 5.44. This is reflected in corresponding delay of shrinkage start and reduced shrinkage rate, see Fig. 5.45. Note, however, that this may not be results of lower surface tension alone, but also partly due to some retardation, as indicated by the temperature and settlement results.

Nevertheless, the results strongly indicate that SRA contribute to reduce the driving forces to plastic shrinkage cracking. However, more tests at higher evaporation rates should be performed in order to verify it.

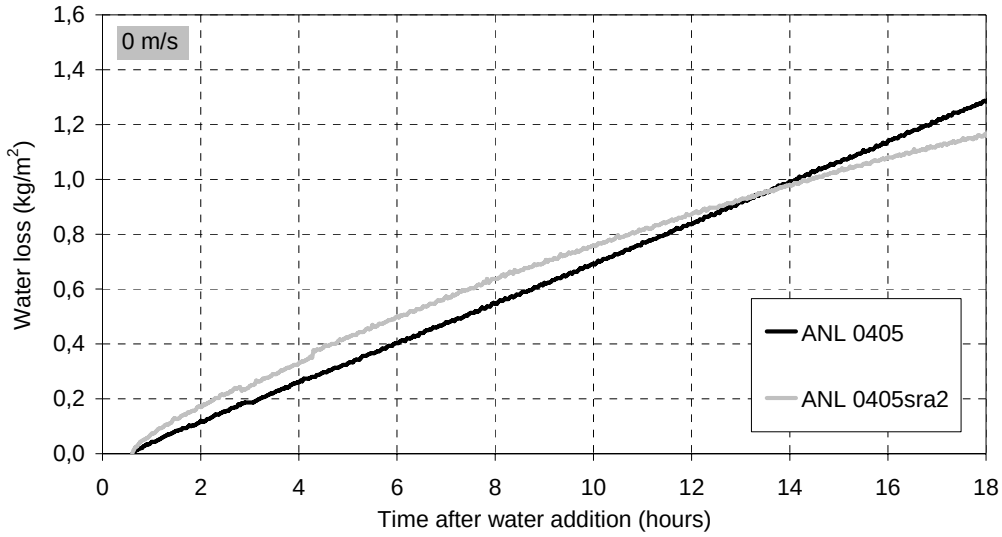

Fig. 5.41 Water loss of concretes with w/b = 0.40 with and without shrinkage reducing admixture, when exposed to stagnant air of 50 % RH

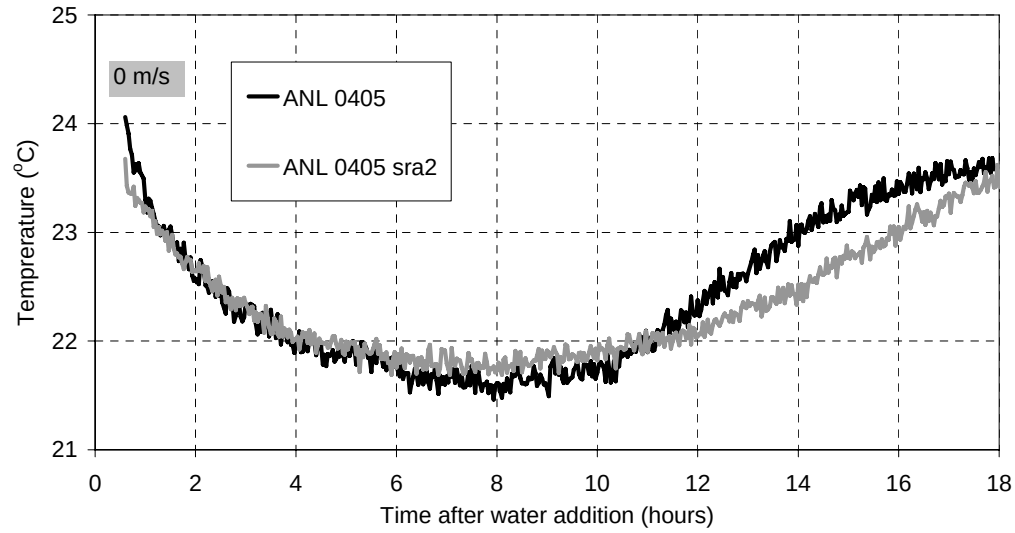

Fig. 5.42 Temperature evolution of concretes with w/b = 0.40 with and without shrinkage reducing admixture, when exposed to stagnant air of 50 % RH

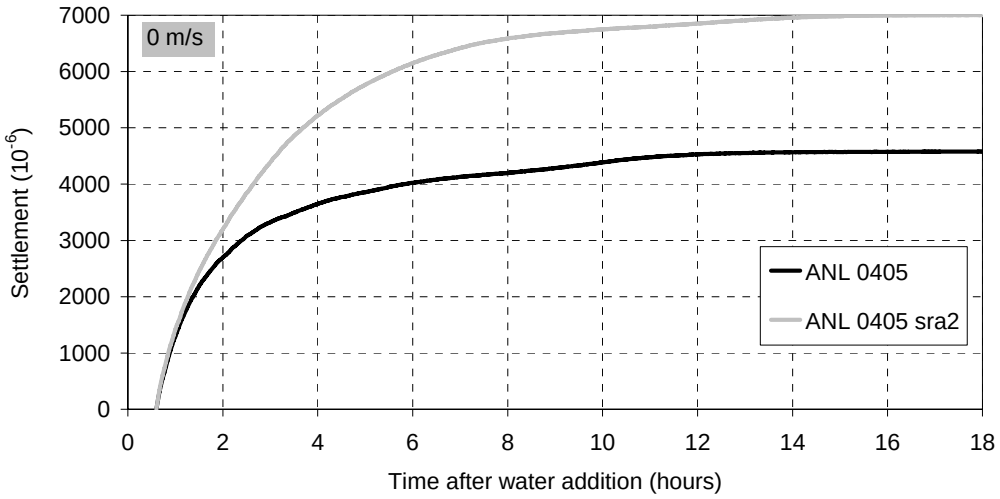

Fig. 5.43 Settlement of concretes with w/b = 0.40 with and without shrinkage reducing admixture, when exposed to stagnant air of 50 % RH

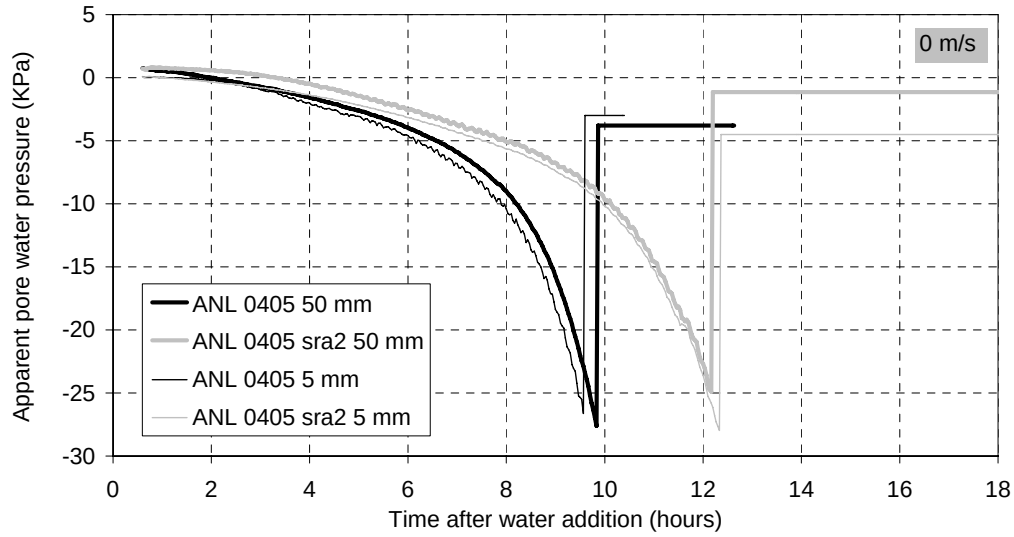

Fig. 5.44 Pore water evolution at 5 and 50 mm depth of concretes with w/b = 0.40 with and without shrinkage reducing admixture, when exposed to stagnant air of 50 % RH

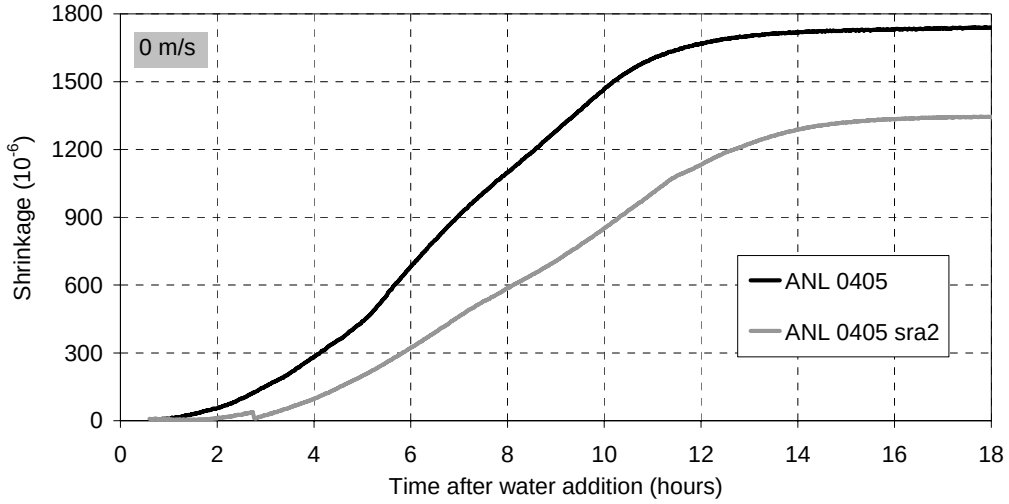

Fig. 5.45 Shrinkage of concretes with w/b = 0.40 with and without shrinkage reducing admixture, when exposed to stagnant air of 50 % RH

5.7 Influence of internal water source

Internal water is here water absorbed in aggregates ("bleeding pockets" and artificial superabsorbent material are other sources). Such water may be absorbed in the aggregate prior to mixing or it may be mix water which is being absorbed during mixing and shortly after if the aggregate is dry prior to mixing. Lightweight aggregate (LWA) is an effective source since the porosity is considerably higher than and normally coarser than that of normal aggregate. The idea is that the capillary tension of pore water in the paste pulls water from the aggregate. The mechanisms are discussed by Hammer et al (2004). Extensive work has been performed on the subject of using LWA as internal curing, to reduce autogenous shrinkage in particular, and a state-of-the-art-report is presently being prepared by RILEM TC 196 ICC (chairman K. Kovler).

The following work was performed in order to investigate the influence of internal water on volume changes in the present age:

The 8-16 mm aggregate and some sand of the basic concrete was replaced with initially dry and pre-soaked LWA, respectively. The LWA is "Leca 700" 4 - 12 mm (expanded clay) with a particle density of approx. 1300 kg/m^3. It has been shown that the total mix water absorption corresponds to the amount of water which the LWA in equivalent moisture state, absorbs in 1 hour soaked in pure water (Smeplass et al, 1992). The present LWA absorbs 7 % water in this period, which corresponds to 40 litres per m^3 of concrete as stated above. Therefore, this mix was added 40 litres per m^3 more mixing water in order to have the same effective w/b as the basic concrete. The LWA used in the other concrete was soaked in pure water for 24 hours and the surface dried (by a damp cloth) before mixing. The water absorption was 13 % corresponding to 75 litres of internal water.

Note that a mix water absorption of 40 litres per m^3 of concrete corresponds to a volumetric shrinkage of 40 000 μstrain! Although most of it occurs in the time before the start of testing, it will certainly constitute a potential additional settlement. On the other hand, if the LWA

contains a sufficient amount of water prior to mixing, it may constitute an internal water reservoir which compensates internal and external drying, as for hardening concrete.

The rate of water loss is not significantly influenced by LWA, as expected, see Fig 5.46. Still, the settlement of the LWA concrete is considerably higher than that of the reference concrete, see Fig 5.47. For the concrete with dry LWA it is easy to accept that the difference in settlement at 2 hours of age is approximately $4000 \cdot 10^{-6}$, because it corresponds to 4 litre of mix water absorption, only (the potential is 40 litre). But it is not easy to accept that the concrete with wet LWA (pre-wetted) showed so much higher settlement. The latter indicates that even wet LWA absorbs mix water, which is possible of course if it is in a drying state when added to the mixer. However, neither PWP measurements nor shrinkage measurements indicated any absorption (or bleeding), in the way they did for the concrete with dry LWA, see Figs. 5.48-5.50. So the reason is unclear.

Note that the LWA-curves levels out more abrupt and has a lower rate beyond approximately 4 hours of age. This is in line with the “internal curing” theory further discussed below, based on PWP and plastic shrinkage measurements.

As expected, the mix water absorption contributes to earlier PSS (when PWP turns into tension) of the dry LWA concrete and higher PWP rate in the time before initial setting (approximately 7 hours), see Figs. 5.48 and 5.49. It results in earlier shrinkage start and higher shrinkage rate in the same period, see Fig. 5.50. Note, however, that the time when PWP reaches “minimum” does not coincide with the point when shrinkage of the two LWAC starts to level out, as seen in the previous chapters. The two LWAC starts to level out at approximately 6 hours of age, which coincides roughly with the point when PWP rate of the normal concrete exceeds that of the two LWAC. This, and the fact that PWP rates of the two LWACs are quite similar beyond this point, suggest that the paste sucks water from the LWA beyond this point. As can be seen, both LWACs expand beyond approximately 10 hours of age, i.e. in the hardening phase, which is a well known effect when using LWA with high initial moisture content.

It can be concluded that initially dry LWA contributes to increase the driving force to plastic shrinkage cracking in the plastic phase, but to reduce it in the hardening phase. Furthermore, the internal water reservoir made by pre-wetted LWA does not seem to have any significant influence on the plastic shrinkage at moderate drying in the plastic phase, but contribute to reduce the driving force in the early hardening phase. Another results may however be seen at more severe drying i.e. if the evaporation rate is very high compared to the maximum water flow to the surface (controlled by permeability). Then the internal water may help by reducing the transport distance of water. This was not confirmed by tests.

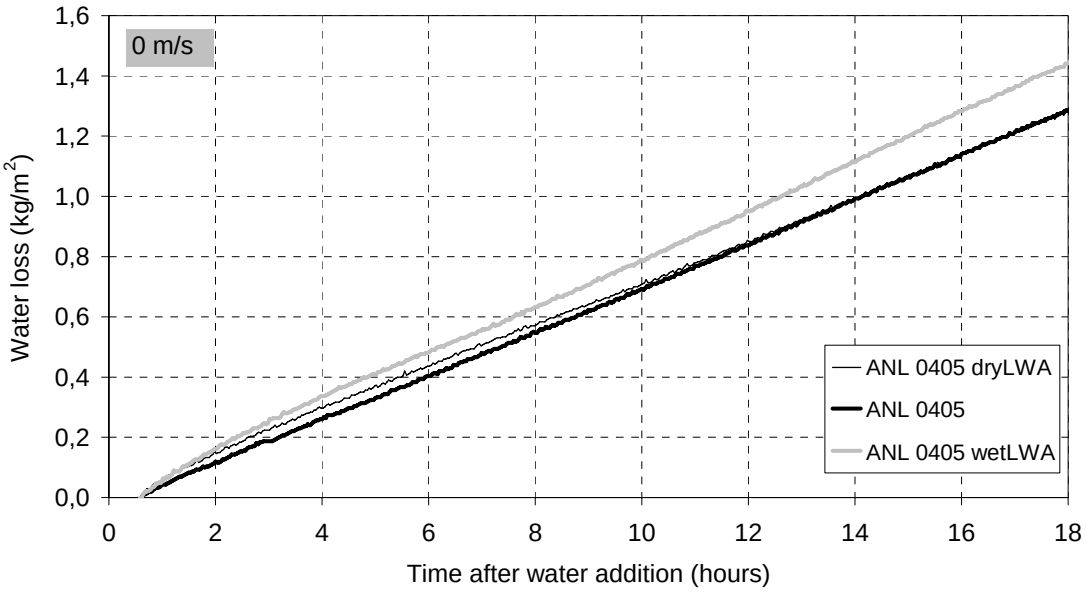

Fig. 5.46 Water loss of concretes with w/b = 0.40 with and without lightweight aggregate, initially dry or prewetted, when exposed to stagnant air of 50 % RH

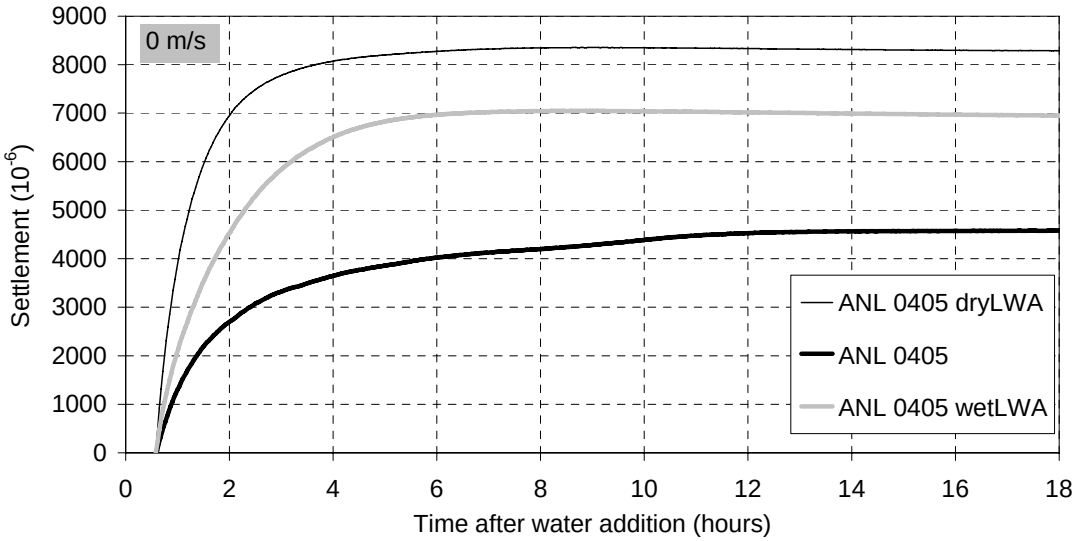

Fig. 5.47 Settlement of concretes with w/b = 0.40 with and without lightweight aggregate, initially dry or prewetted, when exposed to stagnant air of 50 % RH

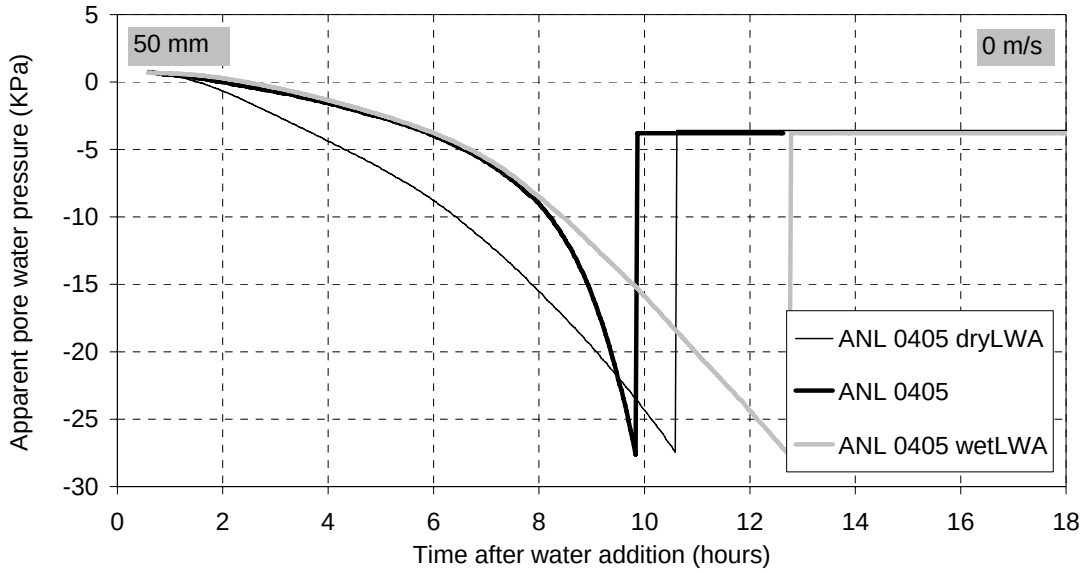

Fig. 5.48 Pore water pressure at 50 mm depth of concretes with w/b = 0.40 with and without lightweight aggregate, initially dry or prewetted, when exposed to stagnant air of 50 % RH

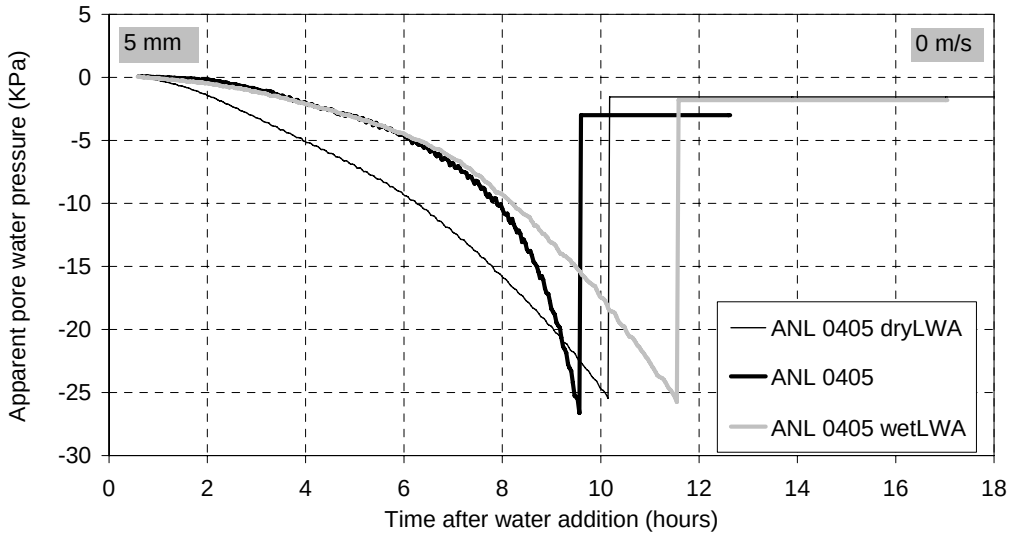

Fig. 5.49 Pore water pressure at 5 mm depth of concretes with w/b = 0.40 with and without lightweight aggregate, initially dry or prewetted, when exposed to stagnant air of 50 % RH

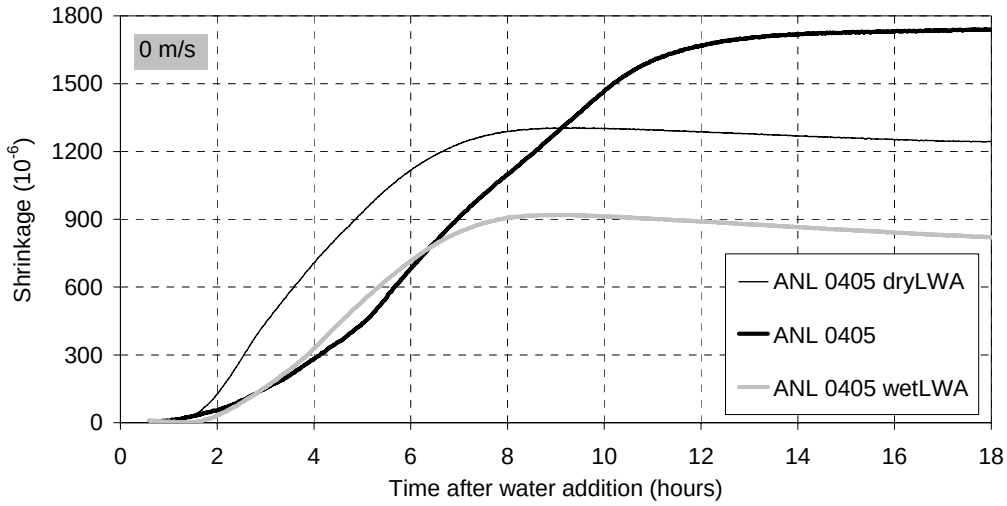

Fig. 5.50 Shrinkage of concretes with w/b = 0.40 with and without lightweight aggregate, initially dry or prewetted, when exposed to stagnant air of 50 % RH

5.8 Influence of air content

Since it is a matter of air pores in a liquid or semi-liquid (very soft) material in tension it is expected that the air pores act as a buffer that reduces the pressure evolution.

The tests were performed on basic concretes with w/b = 0.35 (ANL3505 in APPENDIX). An air entraining admixture (AEA) was used and the air content was measured to be 9 % (while approx 2.5 % in the reference concrete). Tests were run at sealed condition, as well as at external drying at 0 m/s and 5 m/s wind velocity.

The results show that the air content influences the PWP in two ways, seen in all present exposure conditions, see Figs 5.51-5.55: One is the expected **decrease** of PWP rate and subsequent deformation rate (shrinkage and settlement), appearing relatively late in the period. The other way is an **increase** of PWP rate and a subsequent increase of deformation rates in the plastic phase (about 7 hours). Similar results were seen in a repeated test. Note that early shrinkage is seen in the sealed condition, too, see Fig. 5.54, which complies with results from the paste investigations showing that AD increased when adding air to the paste (section 3.3.6). A hypothesis is that the air voids set up a meniscus system that induces capillary tension in the pore water (Laplace-equation), and thus, contraction. Air pores of 0.1 mm size corresponds to meniscus radius of 0.05 mm, which results in a capillary tension of about 1 KPa. This is close to the difference in PWP between the air entrained and non air entrained concrete (Figs. 5.51 and 5.52, “sealed”), which supports the hypotheses. This effect is not further investigated here.

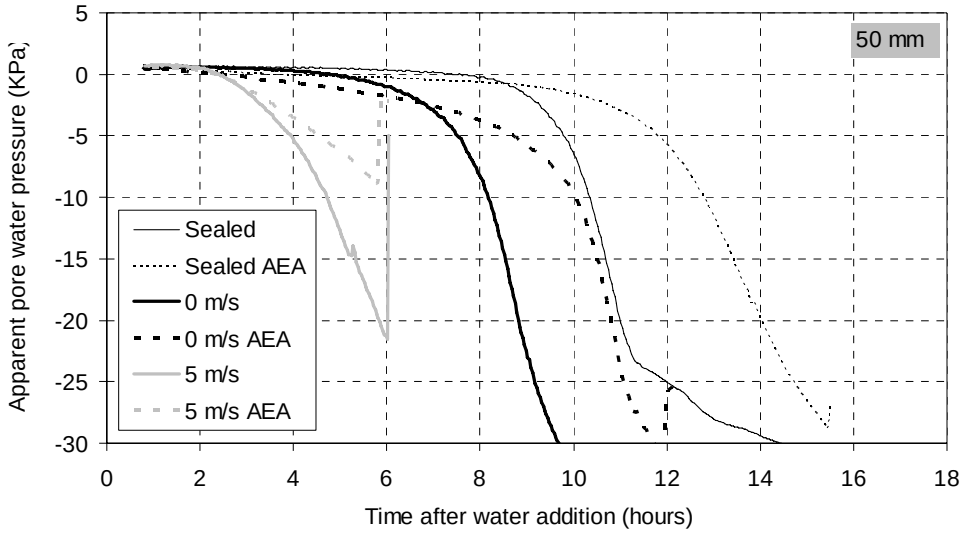

Fig. 5.51 Pore water pressure at 50 mm depth of concretes with w/b = 0.35 with and without air entraining admixture,, when exposed to various conditions

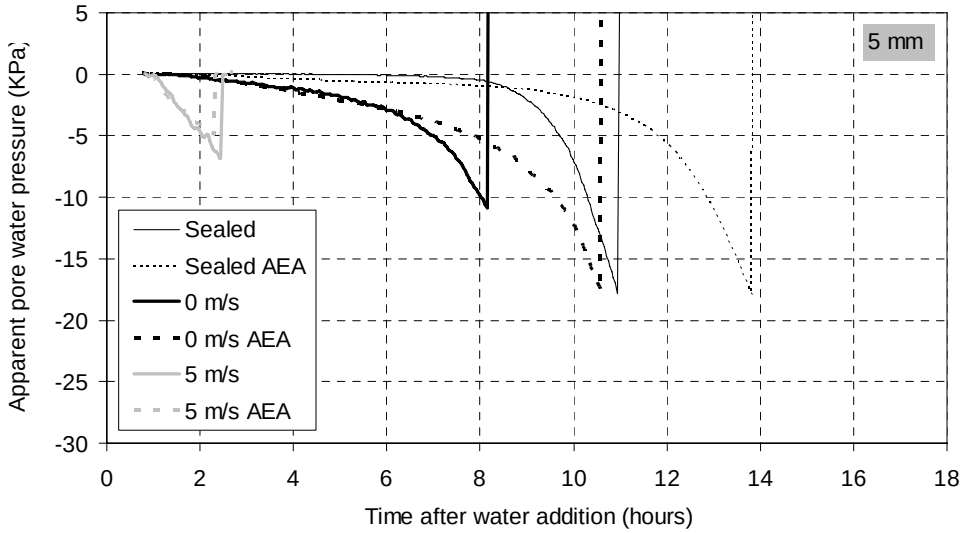

Fig. 5.52 Pore water pressure at 5 mm depth of concretes with w/b = 0.35 with and without air entraining admixture, when exposed to various conditions

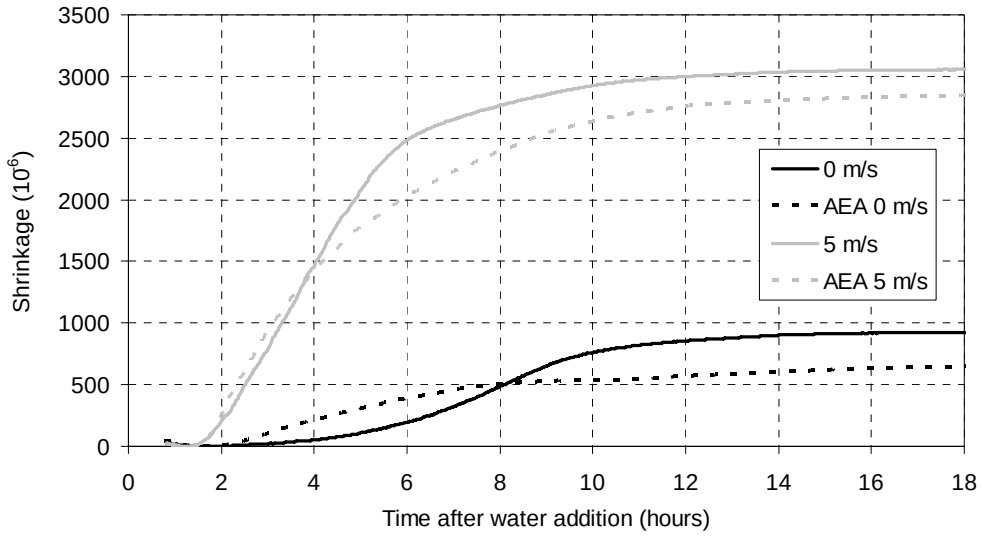

Fig. 5.53 Shrinkage of concretes with w/b = 0.35 with and without air entraining admixture, when exposed to various conditions

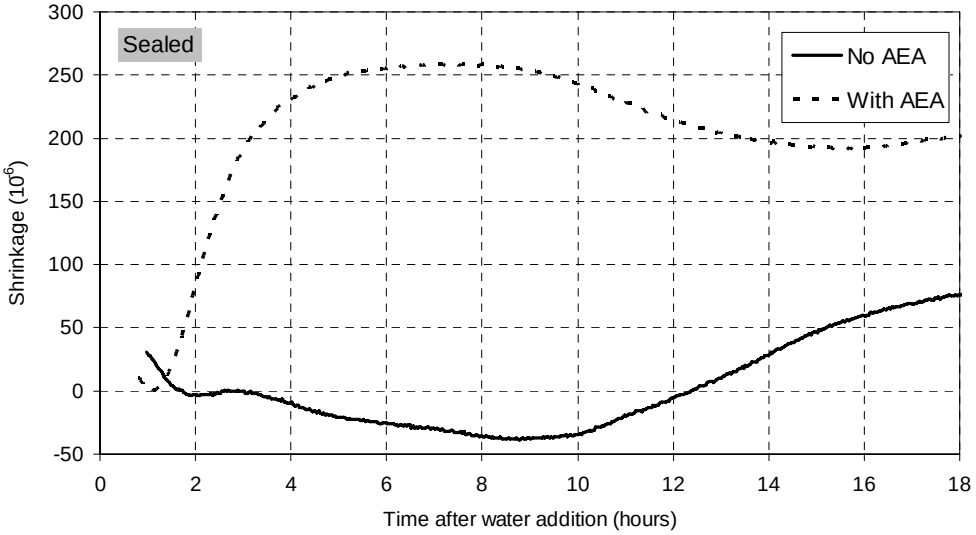

Fig. 5.54 Shrinkage of concretes with w/b = 0.35 with and without air entraining admixture, when exposed to sealed condition

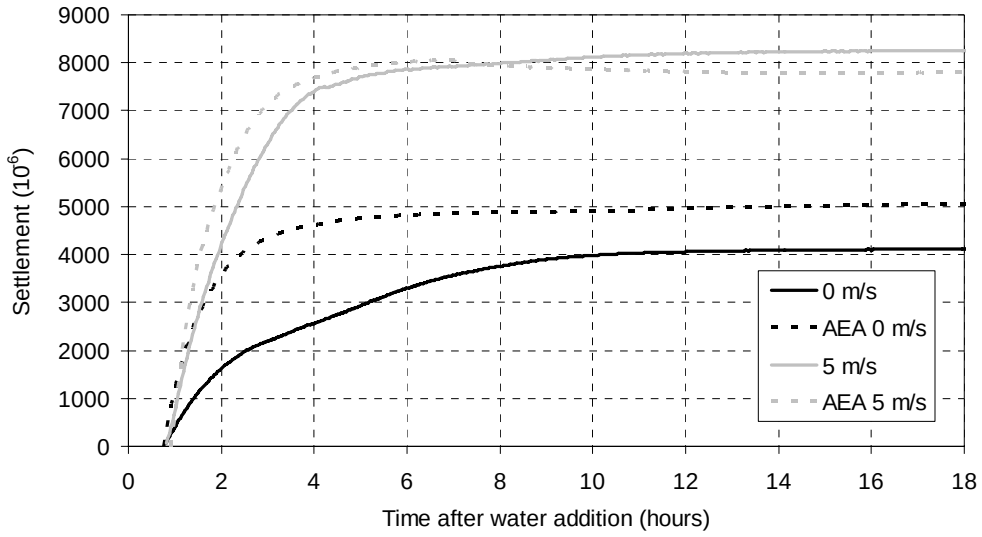

Fig. 5.55 Settlement of concretes with w/b = 0.35 with and without air entraining admixture, when exposed to various conditions

5.9 Self compacting concrete

The two main tools used to convert a normal concrete to a self compacting concrete (SCC) in Norway are normally to replace traditional WRA with co-polymer based ones to improve the flow properties and to add more filler to stabilize against segregation. Other possible tools are finer cements, increased cement content, lower w/b and stabilizing admixtures. Even AEA is used as stabilizing agent.

The influence of filler is investigated here. The influence of cement type, w/b, co-polymer and AEA is investigated in previous chapters.

Stability, of SCC in particular, is often associated with the water to powder ratio, w/p, where the powder consists of all particles with diameter equal to or lower than e.g. 0.125 mm. Here, the powder is cement, natural filler of the sand plus "extra filler" which is limestone filler with fineness in the same range as the present cement.

As previously discussed decreased particle spacing is an important factor for the deformation. An interesting question is how the influence of the inert filler particles is in comparison with cement particles. Three of the four concretes in the present investigation were therefore designed to have equal w/p = 0.35, all with equal amount of natural filler, but different cement-extra filler ratio. It resulted in:

- two concretes with w/b of 0.60, one reference without extra filler, i.e. with natural filler only, giving w/p = 0.55 (not SCC), and one with extra filler to give w/p = 0.35
- one concrete with a combination of increased cement content and extra filler to give w/p = 0.35, resulting in w/b of 0.50
- one with increased cement to give w/p = 0.35, resulting in w/b of 0.40 (i.e. no extra filler)

The recipes are given in the APPENDIX. The slumpflow was in the range of 600 – 650 mm for the three SCCs.

The concretes were expected to have different bleeding rates, as replacement of cement by limestone filler gives increased bleeding. Therefore, the tests were performed with wind in order to ensure that evaporation rate was always higher than bleeding rate.

The initial water loss was not significantly different between the concretes, but the water loss of the w/b = 0.40 concrete leveled out earlier than that of the other concretes, see Fig. 5.56. It follows that permeability decreases faster for this concrete, which is reasonable since the initial spacing of cement particles is lower.

Settlement of the two SCCs with limestone as extra filler (w/p = 0.35) was rather low as result of lower rate in the first 1.5 hour, compared with the third SCC with cement as extra filler (w/p = 0.35). It can be seen that the water loss is not significantly different. Neither is the point in time when the leveling of occurs. It suggest lower CS rate for these two concretes. The cement content is some lower in these concretes, which gives lower CS per unit volume of concrete, but it can not explain the whole difference. So this is still unclear.

The concrete without extra filler (w/p = 0.55) showed quite large settlement, see Fig. 5.57, probably because of higher initial particle spacing which means that more water must evaporate before interparticle contact, and thus leveling off, occurs.

The influence of reduced particle spacing is clearly seen in that PWP drops considerably earlier in the 0.60 concrete when extra filler is added, see Figs 5.57 and 5.58. Also, the results imply that the cement has greater influence than the limestone filler: The partly and full replacement of limestone filler with cement in the 0.50 and 0.40 concretes, respectively, resulted in decreasing age of PWP drop.

The results reveal also the influence on initial permeability as well as permeability development: The addition of filler in the 0.60 concrete leads to a slightly slower PWP drop at 50 mm than at 5 mm. However, the influence of cement as filler is more pronounced as the difference between 5 and 50 mm increases with decreasing w/b (i.e. increasing cement content). The latter is probably a result of both decreased initial permeability and that cement contributes to reduced permeability by time, while the limestone filler does not (significantly).

The shrinkage evolution reflects fairly well the PWP evolution (at 50 mm depth); the 0.60 concrete without extra filler starts to shrink later than the others, see Fig. 5.60.

The main conclusion that can be drawn from this work with respect to deformations in the plastic age, is that water-powder ratio is probably more important than water-binder-ratio, but cement is a more “dangerous” powder than fillers of approximately the same particle sizes as cement.

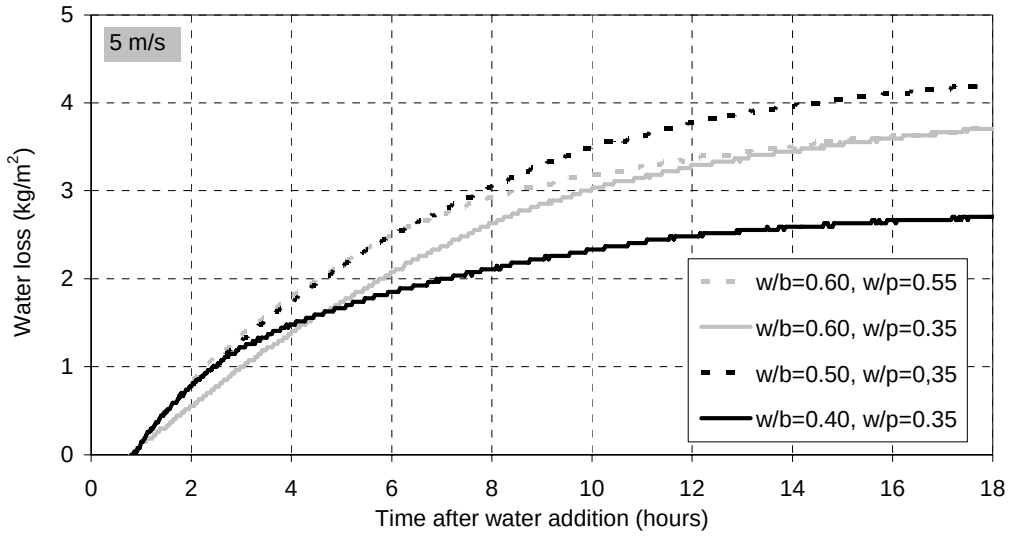

Fig. 5.56 Water loss of concretes with various w/b and w/p (p = cement + filler) when exposed to air of 50 % RH and wind velocity 5 m/s

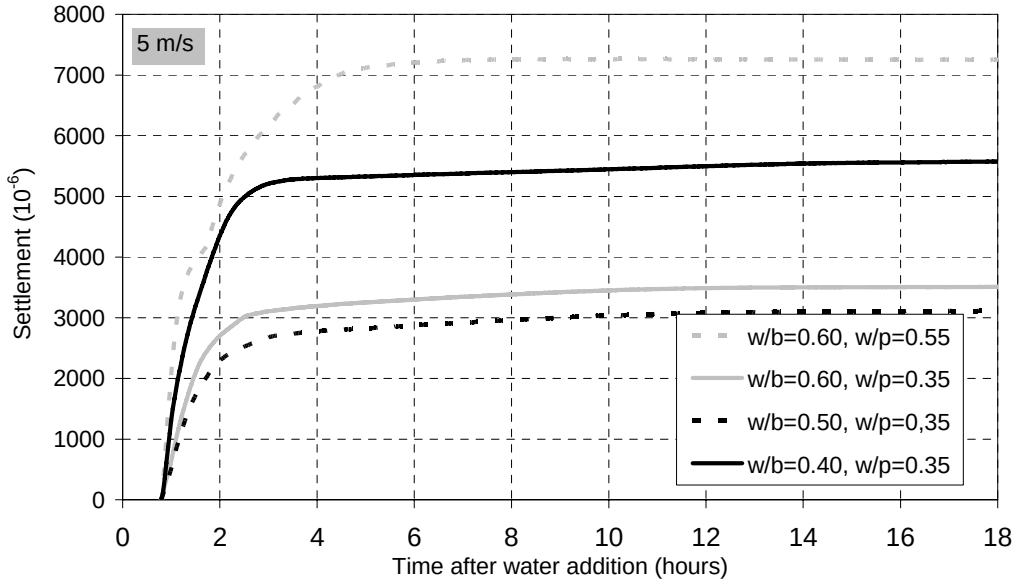

Fig. 5.57 Settlement of concretes with various w/b and w/p (p = cement + filler) when exposed to air of 50 % RH and wind velocity 5 m/s

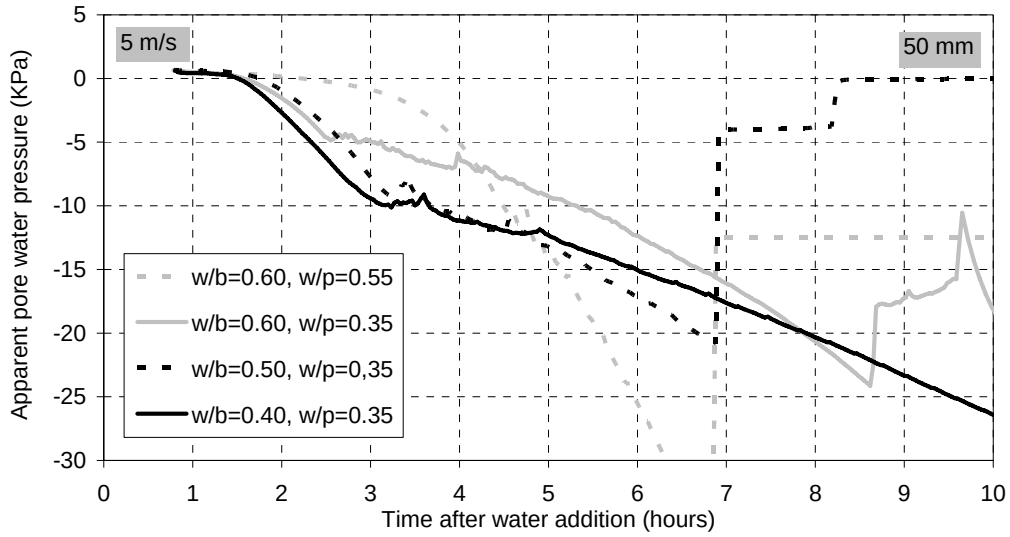

Fig. 5.58 Pore water pressure at 50 mm depth of concretes with various w/b and w/p (p = cement + filler) when exposed to air of 50 % RH and wind velocity 5 m/s

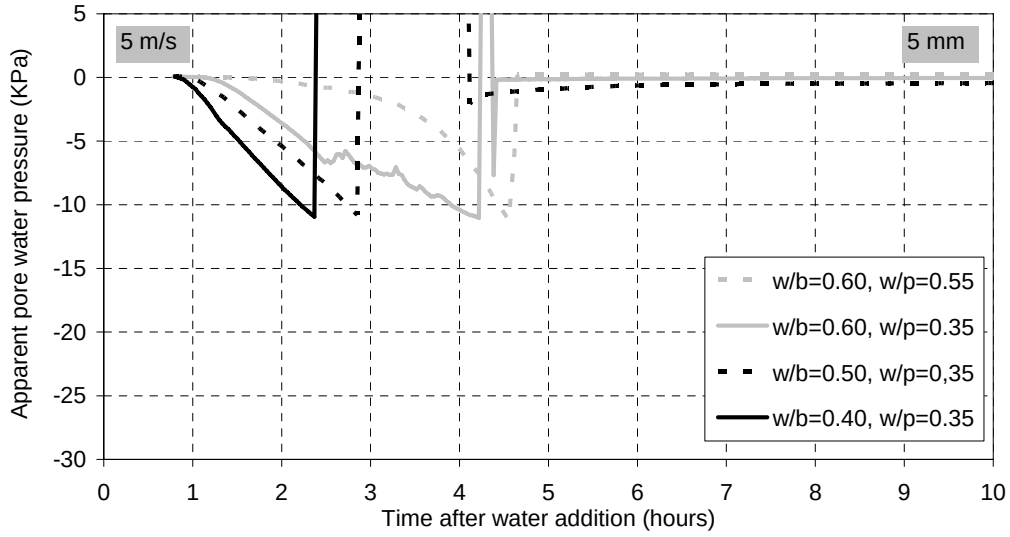

Fig. 5.59 Pore water pressure at 5 mm depth of concretes with various w/b and w/p (p = cement + filler) when exposed to air of 50 % RH and wind velocity 5 m/s

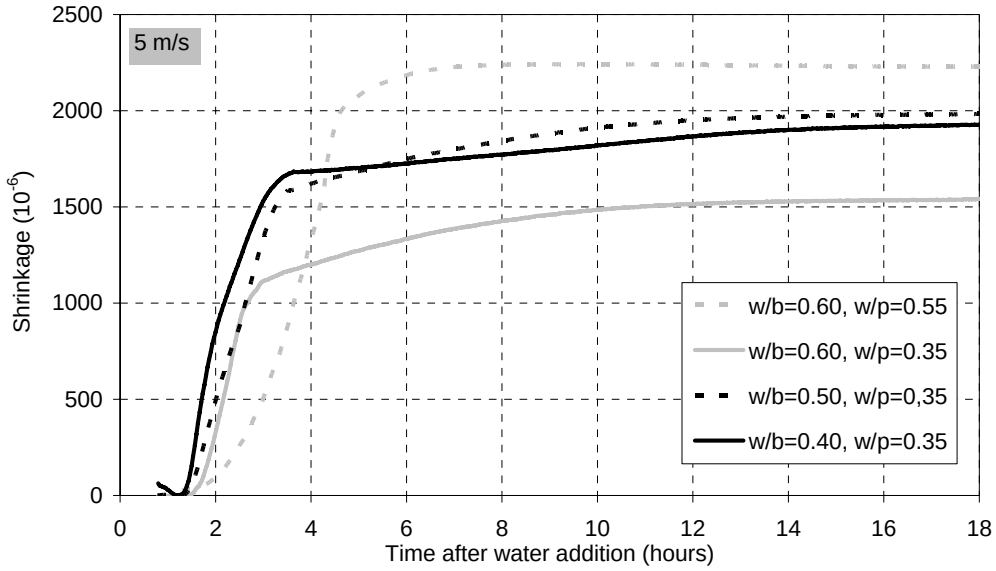

Fig. 5.60 Shrinkage of concretes with various w/b and w/p (p = cement + filler) when exposed to air of 50 % RH and wind velocity 5 m/s

5.10 Influence of initial concrete temperature

Three basic concretes with different target initial temperatures of 15, 20 and 35 ^{o}C, respectively, were tested in order to provide information about the influence of concrete temperature. It was expected influence of both increasing evaporation and increasing hydration rate as results of increasing concrete temperature. All materials were heated/cooled prior to mixing to attain the target temperatures. The concretes were exposed to 5 m/s wind at approximately 21 ^{o}C.

The temperature of the cold and warm concretes reached the temperature of the reference concrete at approximately 3 hours, already (Fig 5.61), due to the heavy wind and relatively small specimen. It resulted in relatively small differences in evaporation rate (Fig. 5.62), although the ranking was as expected (i.e. rate increases with increasing concrete temperature).

The relatively small difference in temperature between the cold concrete and the reference concrete did not influence settlement, PWP and shrinkage significantly (Figs. 5.63-5.66). The warm concrete, however, showed higher settlement rate, faster PWP reduction and subsequently earlier plastic shrinkage. Obviously, this is results of higher hydration rate, mainly, since the evaporation rate was not considerably different.

Nevertheless, the results confirm that high concrete temperature increases the deformation which indicates increased risk of cracking in the plastic age.

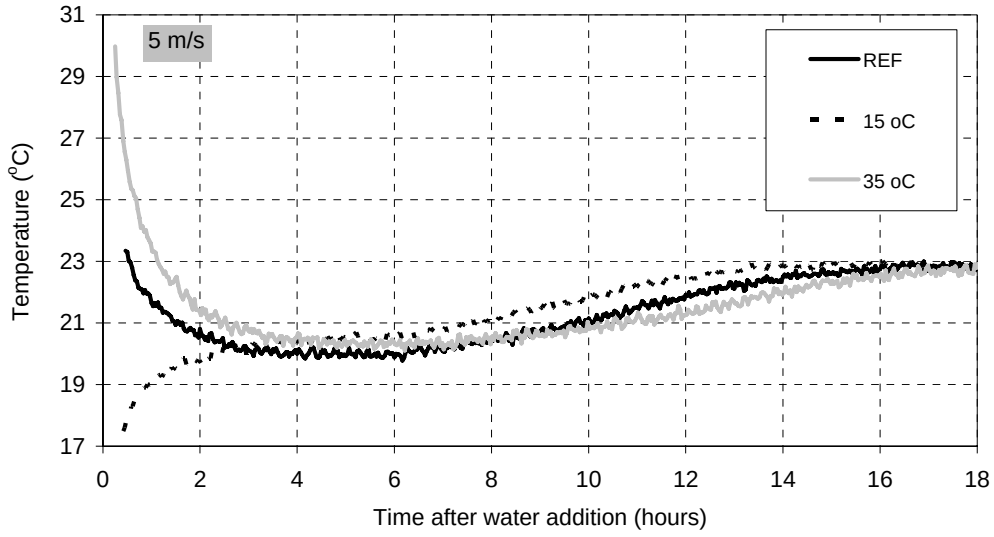

Fig. 5.61 Temperature evolution of basic concretes with various initial temperature, when exposed to air of 50 % RH and wind velocity 5 m/s

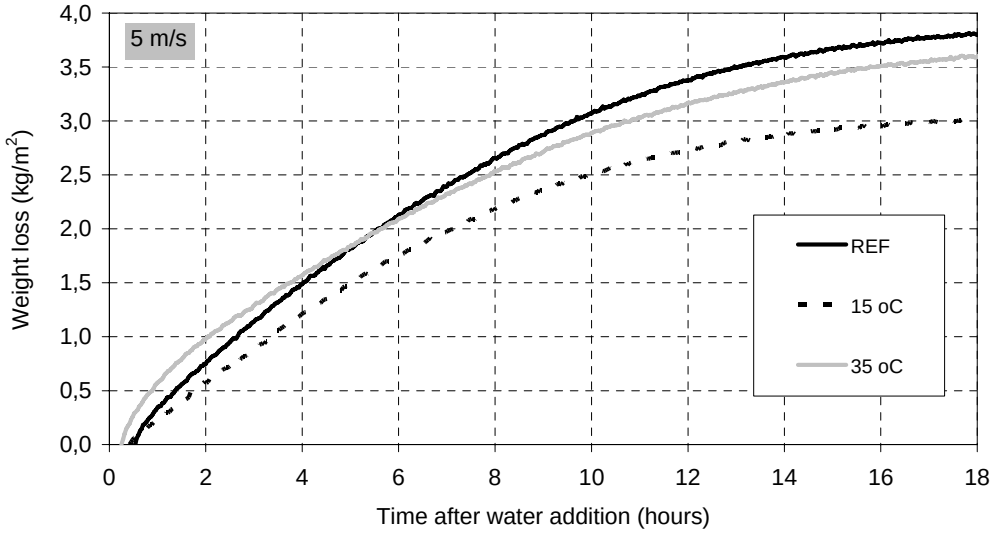

Fig. 5.62 Water loss of basic concretes with various initial temperature, when exposed to air of 50 % RH and wind velocity 5 m/s

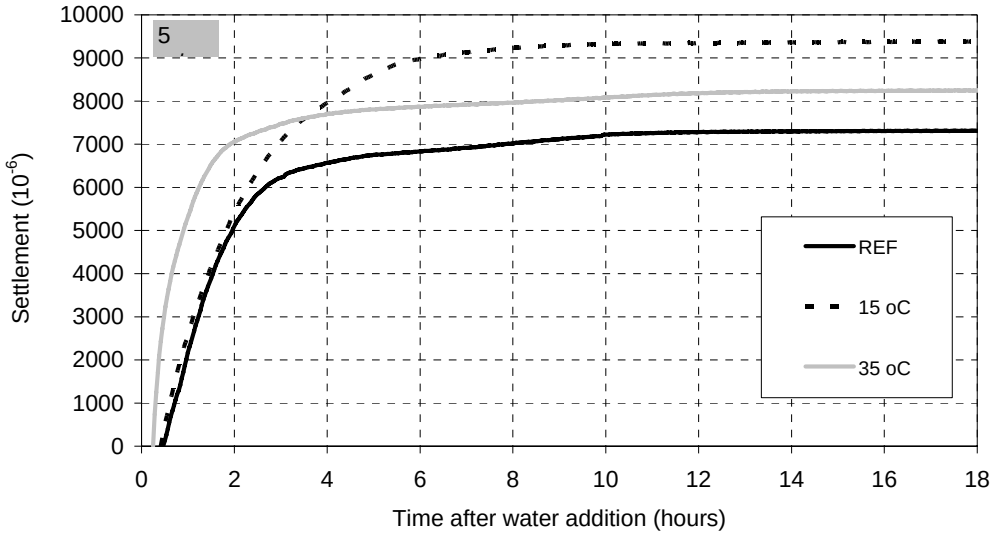

Fig. 5.63 Settlement of basic concretes with various initial temperature, when exposed to air of 50 % RH and wind velocity 5 m/s

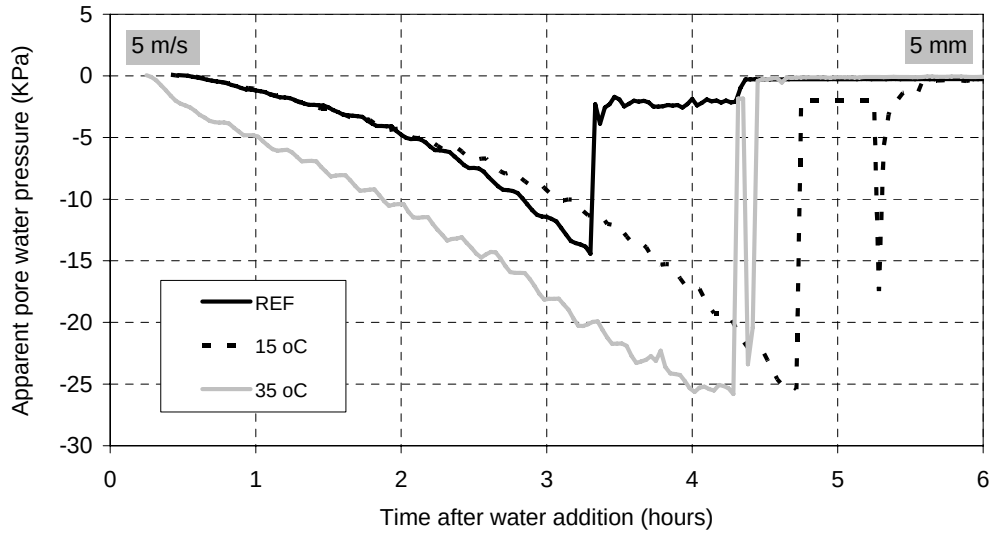

Fig. 5.64 Pore water pressure at 5 mm depth of basic concretes with various initial temperature, when exposed to air of 50 % RH and wind velocity 5 m/s

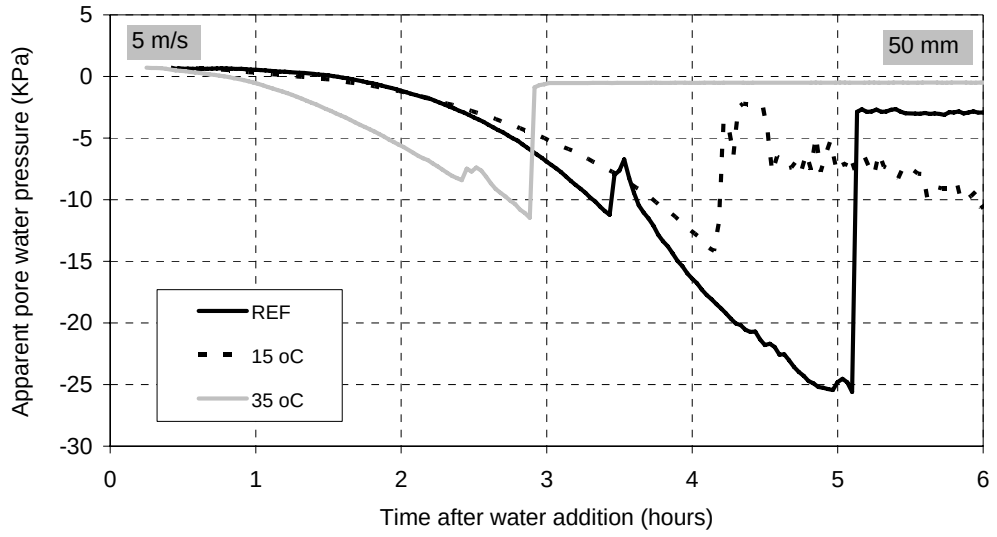

Fig. 5.65 Pore water pressure at 50 mm depth of basic concretes with various initial temperature, when exposed to air of 50 % RH and wind velocity 5 m/s

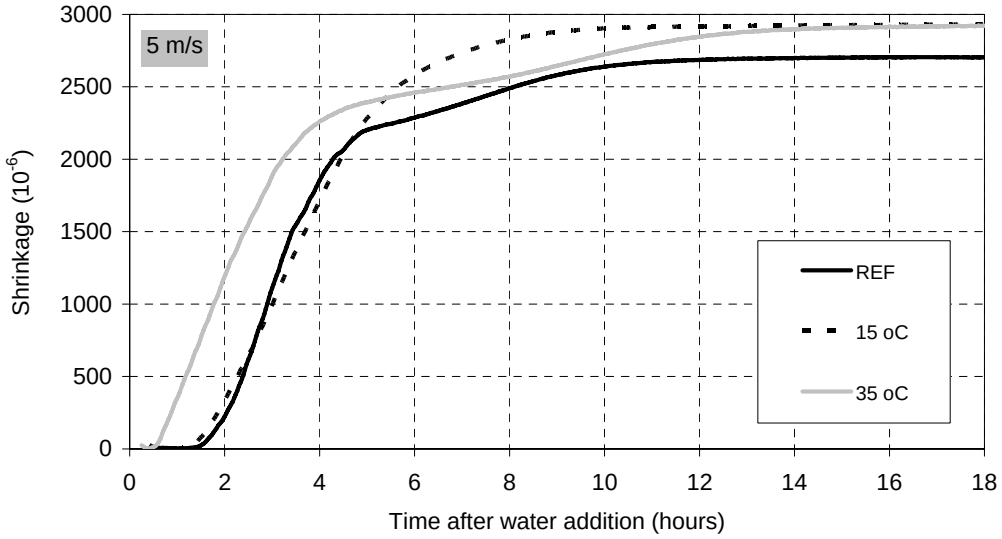

Fig. 5.66 Shrinkage of basic concretes with various initial temperature, when exposed to air of 50 % RH and wind velocity 5 m/s

6. Tensile Strain and Stress Capacity: State-of-the-art, Test Methods and Hypothesis

6.1 State-of-the-art and white spots

Not many authors have reported on testing of the tensile properties of concrete during the initial phase. One reason is probably difficulties related to design of good testing methods. Testing of concrete in uniaxial tension is generally considered to be complicated. Testing in the initial phase brings further complexity associated with the soft body, e.g. related to load transfer and friction because testing must be performed on the sample while still in the mould, see section 6.4.

Byfors (1980) compiled results from several authors. They all show a tensile strain capacity of concrete that goes through a minimum value as function of age and function of tensile strength, see Figs. 6.1 and 6.2. It appears that that minimum tensile strain capacity is approximately 0.05 ‰, i.e. approximately 1/3 of the strain capacity of the hardened concrete, and that corresponding strength is in the range of 0.1 – 0.5 MPa. By looking more thoroughly on the strain capacity results of Kasai et al, see Fig. 6.3, it appears that minimum strain capacity remain low for several hours (note that some of the trend lines may be a bit misleading). Hence, this period of time is considered to be potentially critical with respect to cracking. It would be convenient to identify when this period starts compared to time of setting, but it is not easy since time of setting may be found according to several methods, and which gives different setting times. It seems obvious, however, that the period is in the early hardening phase. This is further discussed in chapter 9.

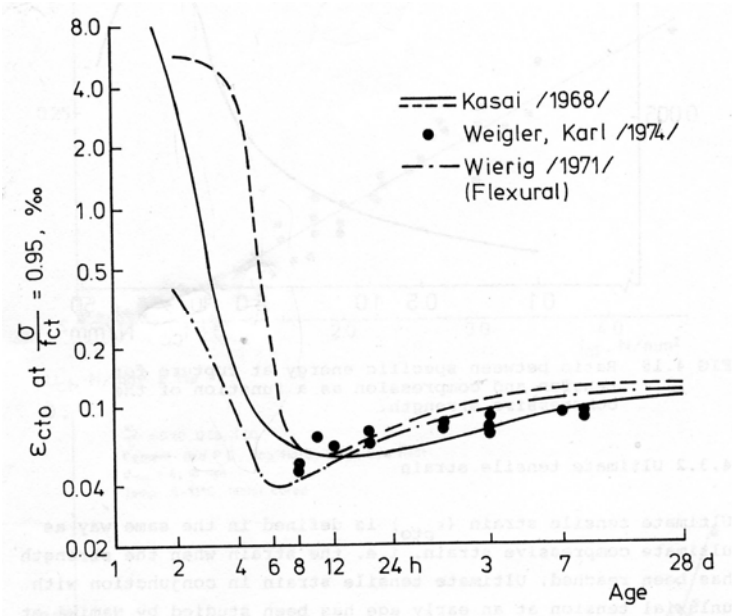

Fig. 6.1 Tensile strain at 95 % of ultimate tensile stress versus age (Byfors 1980)

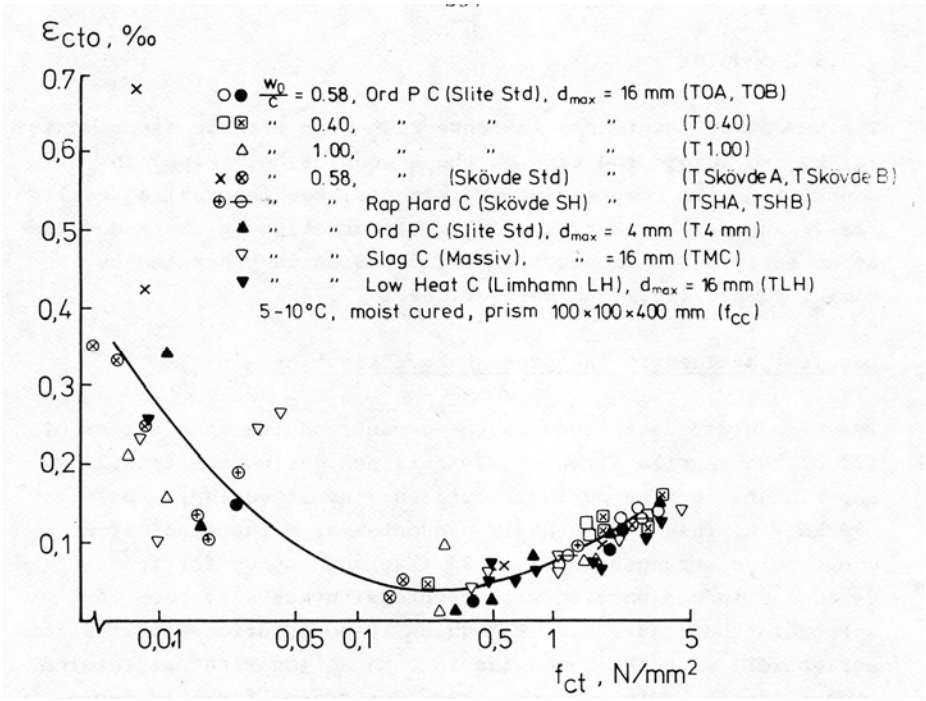

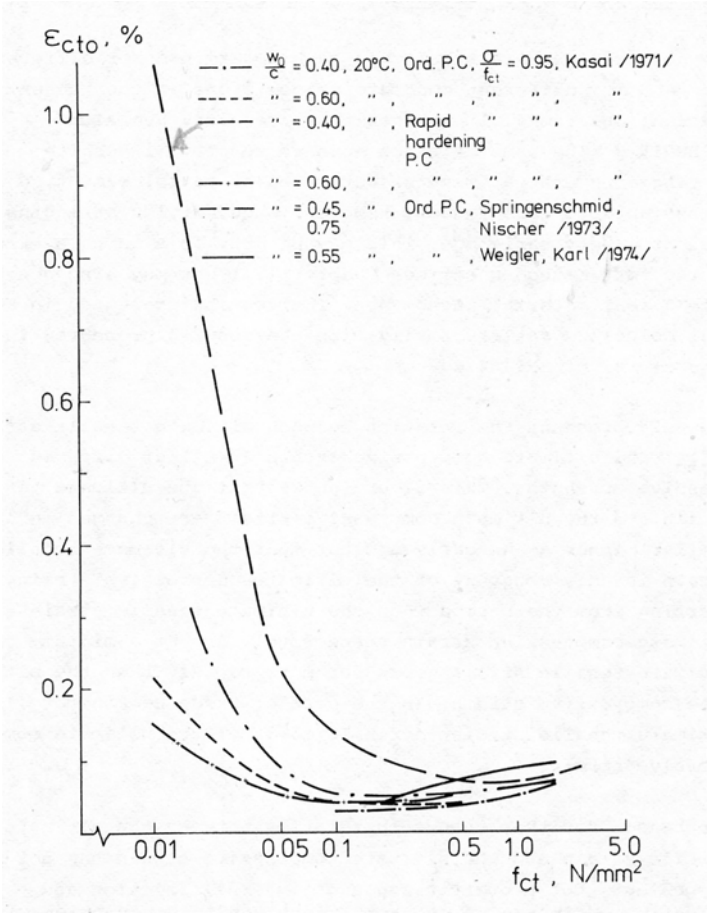

Fig. 6.2 Tensile strain versus tensile strength of concrete with age varying from the plastic phase to hardened phase (Byfors 1980)

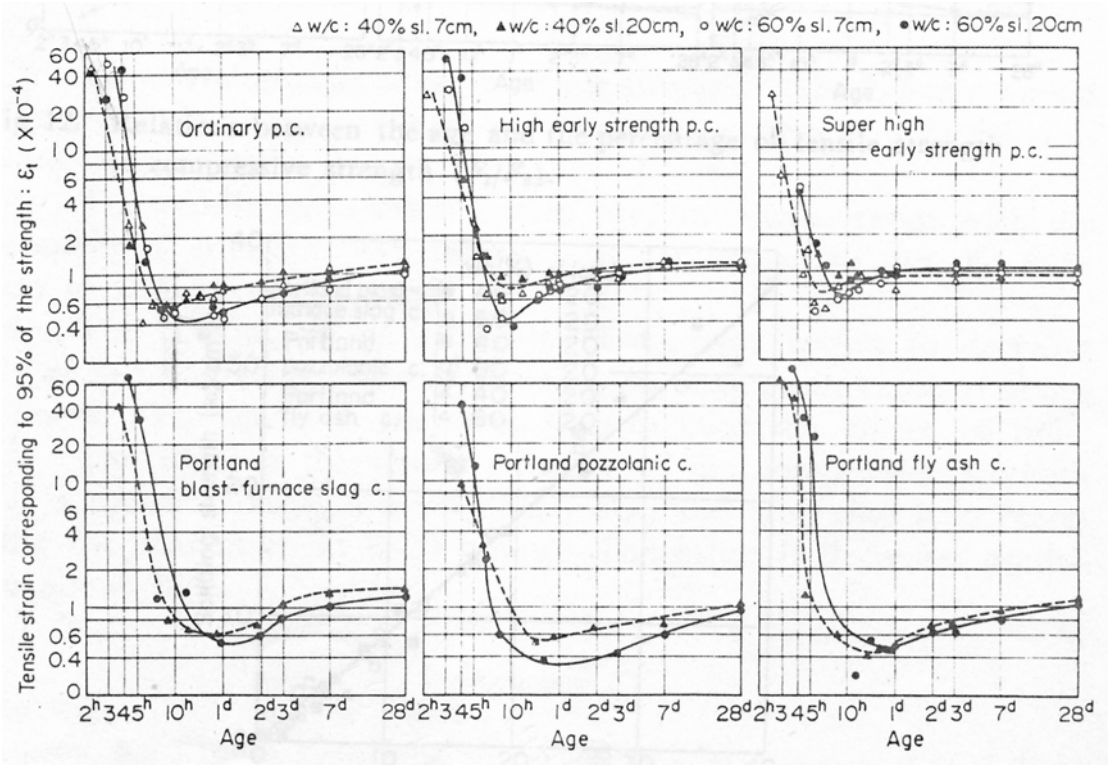

Fig. 6.3 Tensile strain at 95 % of ultimate tensile stress versus age of various concretes (Kasai et al, 1972)

Note that the tensile strain capacity is rather high until some hours of age, i.e. higher than expected deformation in the period (see chapters 4 and 5), which suggests that the period is harmless with respect to cracking risk. This appears to be in conflict with results from qualitative laboratory tests and in situ experience, which shows that concrete may crack already before an hour of age (Kompen, 1994). The strain capacity is assessed from the strain at ultimate load or close to it (e.g. 95 % of it), but nobody discusses the failure mode or crack propagation. Although not always stated, it seems that the stress-strain behaviour has been tested after moist curing or moderate drying (in “lab air”). This may constitute an important difference, which will be discussed in chapter 8.

Kasai et al (1974) demonstrated that portion of plastic deformation relative to total deformation decreased from practically 100 % at “initial setting” (they do, however, not state how initial setting was determined) when the strain capacity still was rather high, to around 20 % at the time when the strain capacity is minimum (compare Figs. 6.4 and 6.5). They found the two by cyclic loading in the rig sketched in Fig. 6.12. They consider the elastic strain as the recovery strain during every unloading, and plastic strain as the difference between maximum strain before every unloading and the elastic strain, see Fig. 6.6.

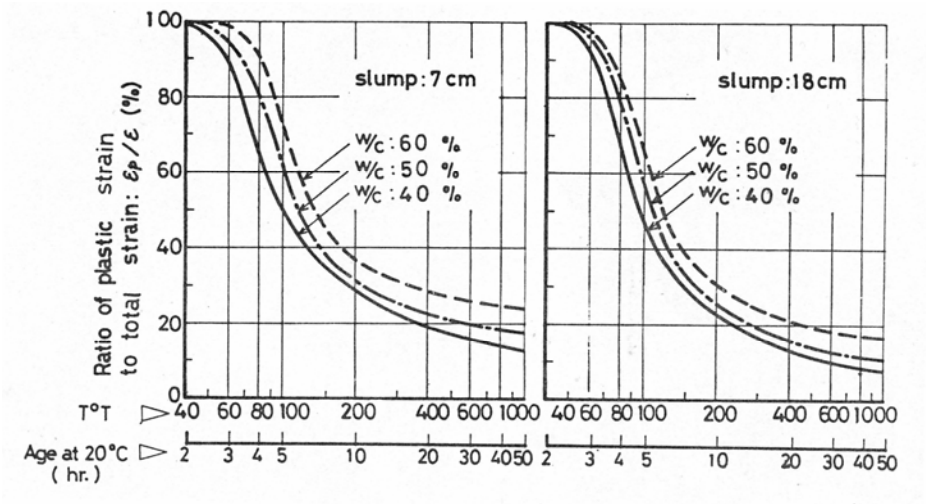

Fig. 6.4 Ratio of plastic strain to total strain versus age of various concretes (Kasai et al, 1974)

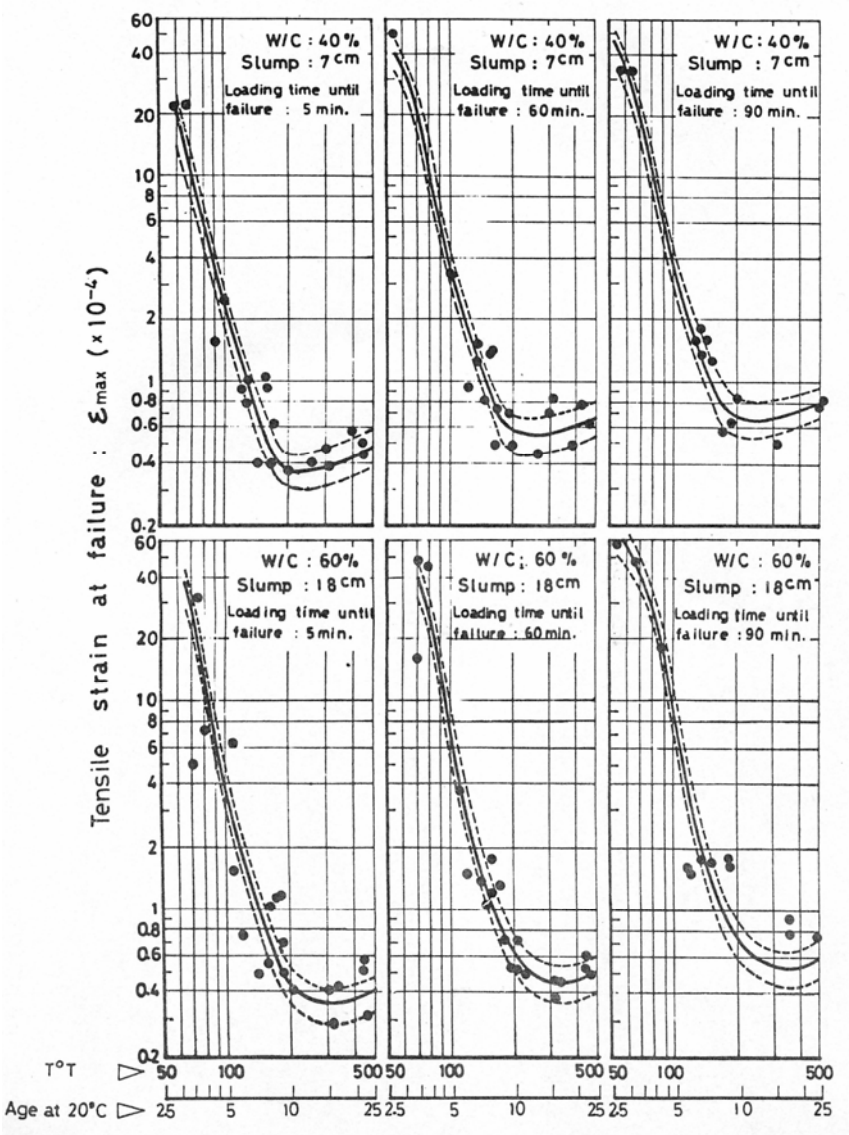

Fig. 6.5 Tensile strain at failure using different strain rates (loading time) versus age of various concretes (Kasai et al, 1974)

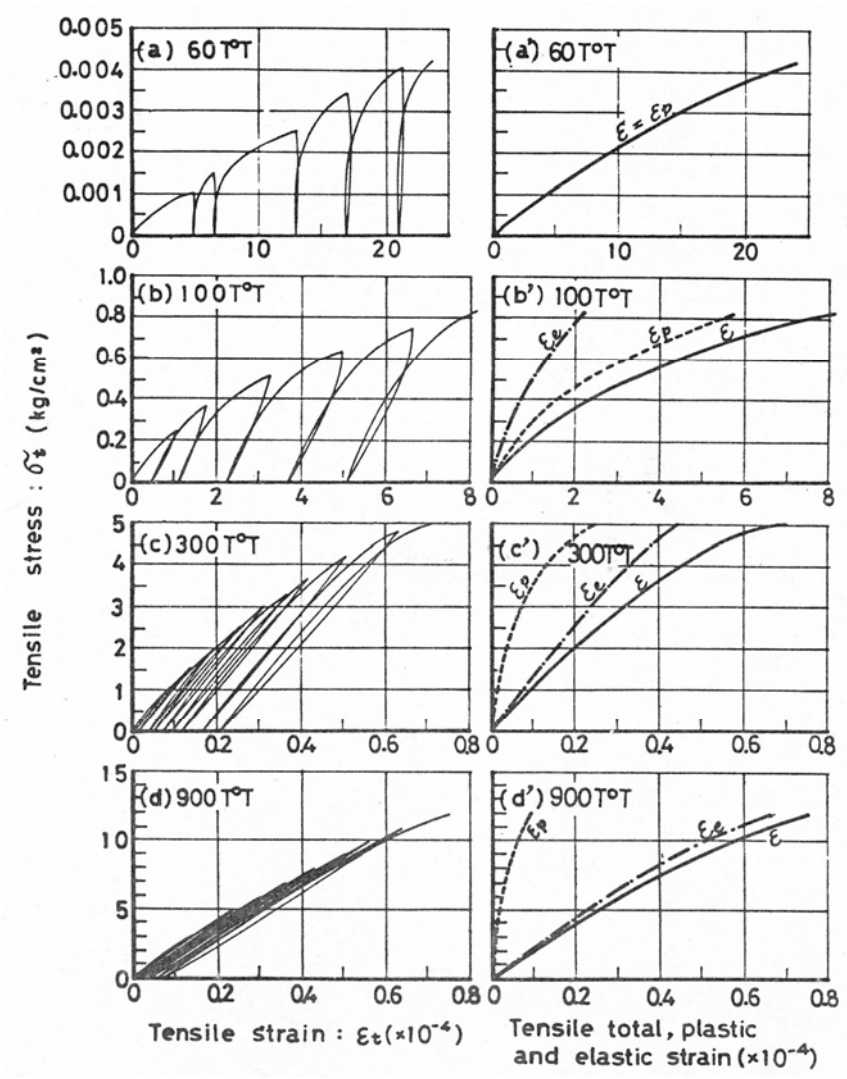

Fig. 6.6 Tensile stress versus tensile strain after cycling loading at different ages (equivalent times) in order to separate plastic and elastic strain (Kasai et al, 1974)

Creep is significant in the present age period, and contributes to increase the realistic strain capacity. Kasai et al also investigated the influence of strain rate on strain at failure by varying the time from start of loading until failure, from 5 to 90 minutes (details on how this was arranged are not given). The results from testing of two different concretes, given in Fig. 6.7 show some scatter, but the trend is an increase of strain at failure with decreasing strain rate, as expected. In fact, it can be seen from Fig. 6.7, that the strain capacity increased approximately 100 % between the highest and lowest strain rate at low ages and less than 50 % at the higher ages. It confirms that strain rate is an important parameter that has to be considered if crack risk is being assessed by strain/strain capacity. They do not say anything about the influence of strain rate on the failure stress. Realistic strain rate is the one that corresponds to the rate of deformation, which means that it may be anything between zero and that corresponding to heavy evaporation. External loads like formwork settlement, etc, may however be at high rates. So, it seems sensible to use relatively high strain rates in testing and bear in mind that it results in an underestimation of the tensile strain capacity in many cases.

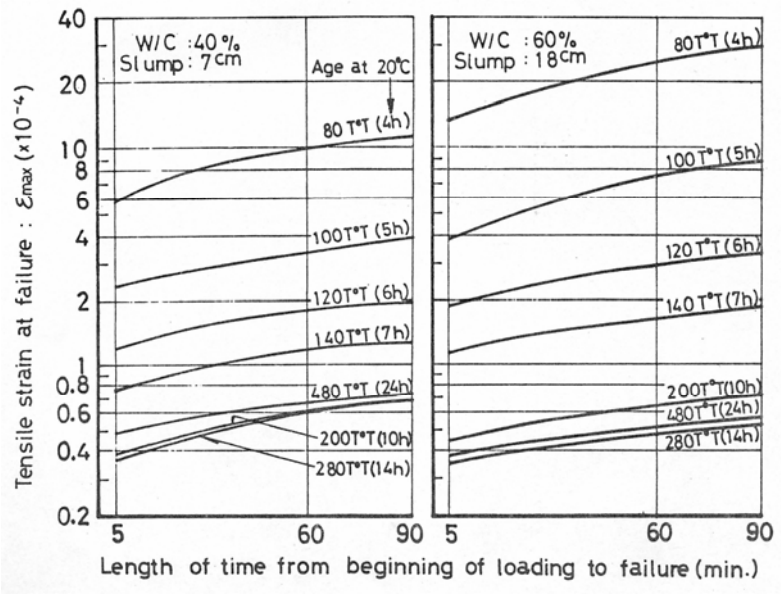

Fig. 6.7 Tensile strain at failure versus strain rate of concretes with varying ages (Kasai et al, 1972)

The conclusions that can be drawn from the above discussion are, under the assumption that the concrete is covered against considerable evaporation:

- The short term strain capacity determined as strain at maximum load reaches a minimum value that is approximately 1/3 of that of hardened concrete, at the age corresponding to when significant strength may be measured, i.e. commonly referred to as the time of final setting. The strain capacity remains at its minimum for some hours
- The real strain capacity is, in most cases, expected to be considerably higher than the strain capacity found from testing, because strain capacity increases significantly with decreasing strain rate, and realistic strain rate is normally low (corresponds to shrinkage rate). Thus, creep is an important parameter
- The strain capacity determined as strain at maximim load is considerably higher than the expected deformation in the first hours of age, which appears to be in conflict with both practical experience and laboratory results showing that cracking occurs in this time period

The latter point suggests that strain capacity is considerably influenced by drying. It seems sensible therefore to discuss, as done below, stress-strain behaviour without external drying and with external drying separately. Furthermore, it seems sensible to divide into an early age (plastic phase) and late age (early hardening phase).

6.2 Influence of drying on strain and stress capacity

It is quite obvious that external drying reduces the tensile strain capacity in this period of time, since concrete may crack minutes after placing (i.e. at less than an hour of age), while the measured tensile strain capacity in sealed condition is “infinite”. A possible explanation of how this can be is presented in the following.

As demonstrated in previous chapters, a result of external drying is a rapid evolution of capillary tension of pore water accompanied with shrinkage. In low w/b concretes in particular, this causes a skin formation. The skin may be considered to be a structure made of particles with water menisci in between, which is controlled by the Laplace equation, see section 3.4:

$$\Delta P = 2\sigma/r$$

where ΔP is the capillary tension in the pore water given relative to atmospheric pressure of the air and in the water, σ is the surface tension of water, and r is the meniscus radius.

Evaporation causes emptying of the pores bounded by the particles and menisci (causing reduced r and accordingly more tension). The water loss may be compensated for by suction of water from internal and movement of particles towards each other (appears as settlement and shrinkage). Assuming that the permeability of the mass is sufficiently low to prevent water flow to the surface, and that the body is restrained, surface included, so that the particles are hindered to approach each other, the pores must empty. The coarsest pores will empty first and new menisci will form between particles below the top ones. Then, there are no menisci to bind these top grains and they will move to the opposite direction due to the capillary tension on the other side of the grains, where the menisci are intact - a “crack” has been initiated. This may be a mechanism of crack initiation of a homogeneous and smooth surface. Progressing shrinkage will probably both extend the crack in length and widths and create new cracks.

However, a more plausible mechanism is crack initiation at inhomogeneities, like cavities and aggregate-paste interfaces where the menisci-particle structure is “weaker” and may act as wall effect. E.g. the gap between an aggregate and the paste is probably relatively wide (and long) and will therefore empty before the pores between cement grains; a crack has been initiated. Thus, surface finishing is probably an important parameter.

Since this is local phenomena at the surface, it will probably not be significantly reflected in the stress/strain behaviour of the bulk mass. One obvious way of finding the tensile strain capacity, defined as the strain at first crack, is then to observe the surface during testing at a given strain rate (ε/unit time) and record the time (t) at which the first crack appears. Then, the strain capacity (ε_t) can be calculated simply as (ε/unit time) $\cdot$ (t). This approach has been used in the present work, see chapter 8.

In the early hardening period the strain and stress capacity is expected to be influenced by drying as for hardened concrete, in principle; moisture gradients may cause additional tension at the surface, and thus, contribute to lower tensile strength and subsequent strain capacity. However, the gradients are probably much less in the early hardening period than in hardened period, because of both lower stiffness to set up the stress gradients and the short drying period.

6.3 Test methods

A review of relevant test methods is presented in the following, first of all to provide a basis for design of the "tension rig" to be used in the present study, see chapter 7.

Methods with both vertically applied load and with horizontally applied load have been presented. Weigler and Karl (1974) built a rig for vertical load application, see Fig. 6.8, consisting of a mould (560x120x120 mm) in a frame. The deformation was measured with extensometers connected to rods embedded in the sample. They used stronger concrete as "heads" in order to impose failure in the tested concrete. Failure seemed to occur quite often in the upper part of the sample, probably due to the influence of the dead load of the concrete which constitute a large part of the total failure load in the initial phase.

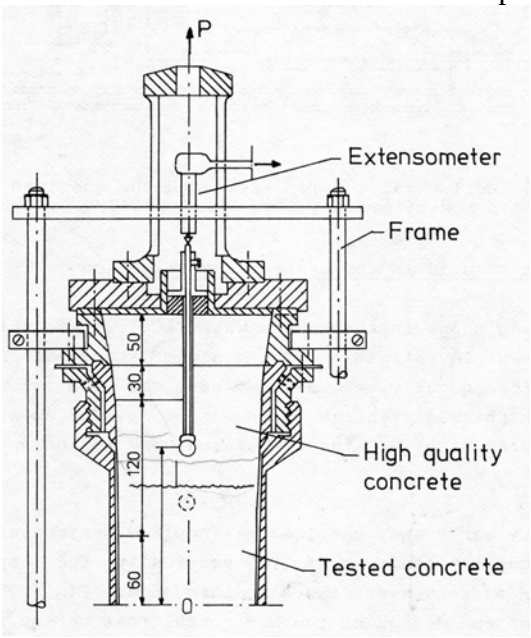

Fig. 6.8 Rig for testing of measurement load-deformation of early age concrete. Weigler and Karl (1974)

Testing horizontally brings friction between the sample and mould, bottom in particular, as an important parameter. Orr and Haig (1971) solved the problem by applying the sample on a Mercury bed, see Fig. 6.9.

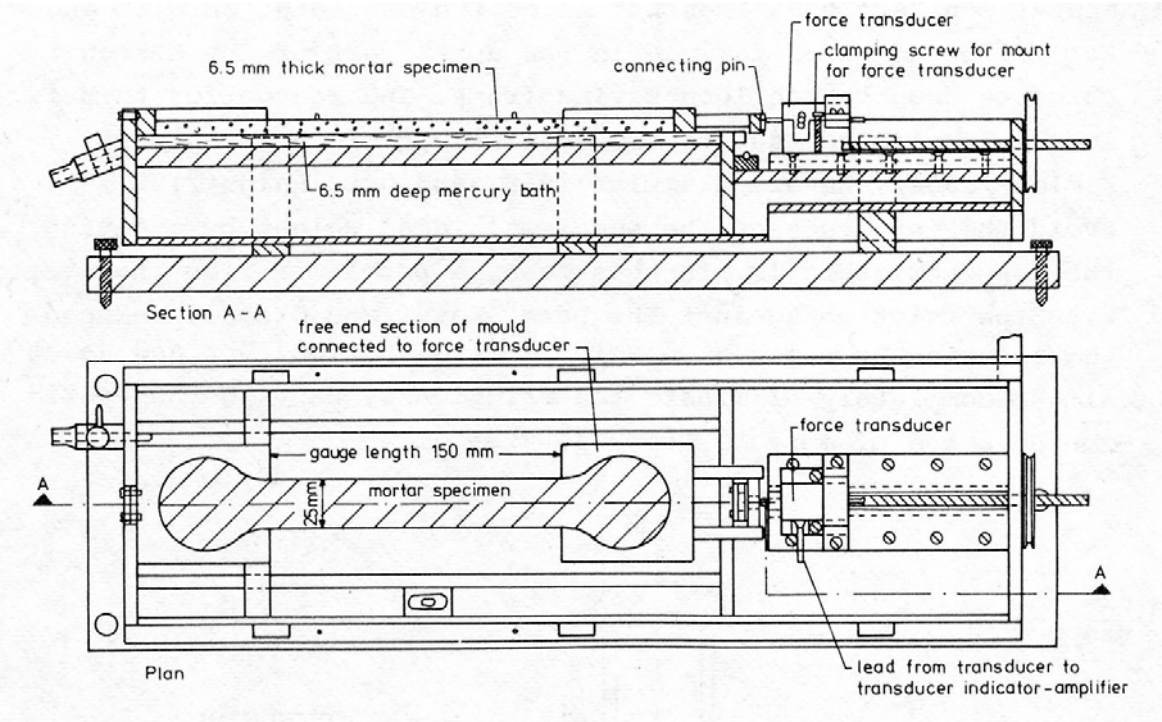

Fig. 6.9 Rig for testing of measurement load-deformation of early age concrete. Orr and Haig (1971)

Hannant et al (1999) made a prototype with two air bearing plates with a small gap in between, on which the concrete is cast, see Fig. 6.10. The deformation is measured over 50 mm on top of the 100 mm thick slab. They reported results apparently in line with those presented using other methods. The method seems to be good to avoid friction. However, the influence of different deformation zones at the bottom (6 mm), where the deformation is applied, and at the top (50 mm) where it is measured, is unclear (not discussed). It does not seem obvious to me that the strain should be calculated from the deformation over the top 50 mm.

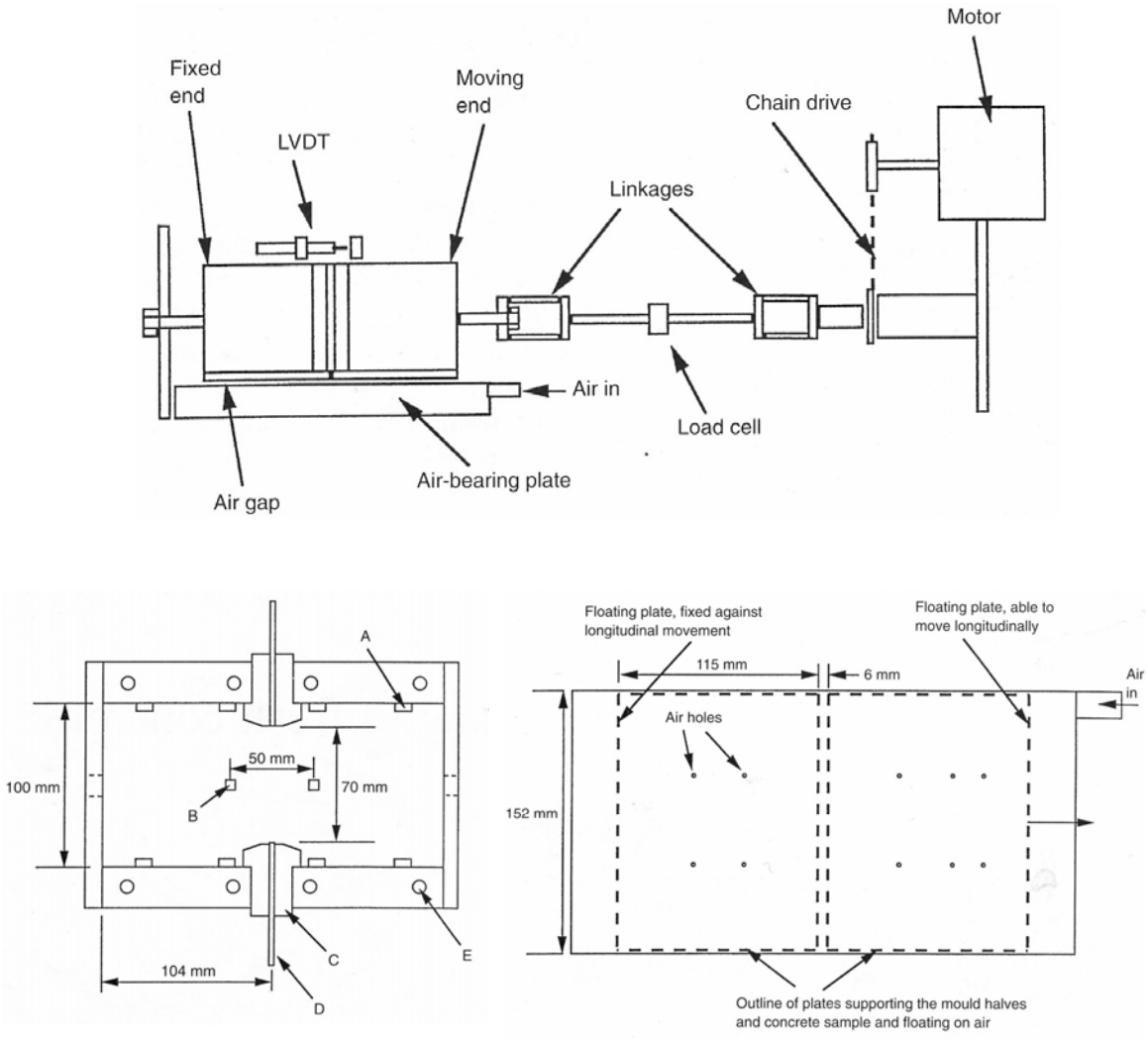

Fig. 6.10 Rig for testing of measurement load-deformation of early age concrete. Hannant et al (1999)

Komlos (1964), Kasai et al (1972), and Byfors (1980) used sheets of Teflon to reduce friction. As pointed out in chapter 4, the friction is actually suction due to capillary tension of the pore water. Such suction will occur even if Teflon is used (see also section 4.2) Kasai et al omitted this by using many cuts of Teflon forming a lamella, which proved to give lower friction than an unbroken sheet gave. The magnitudes are not given. Byfors used rapid hardening concrete at the end in order to secure that failure occurred in the mid section. The cross section was 50x50 mm, see Fig. 6.11. The longitudinal mould sides could be removed at “very early age”, which enabled installation of extensometers on the sides for deformation recording. He measured a friction of 10-15 N, which corresponds to 30-50 % of the total load applied at the “earliest ages” (not given). He claimed that there were uncertainties in the determination of the friction, and thus, since it constitutes so much of the total load, that the determined stress is uncertain.

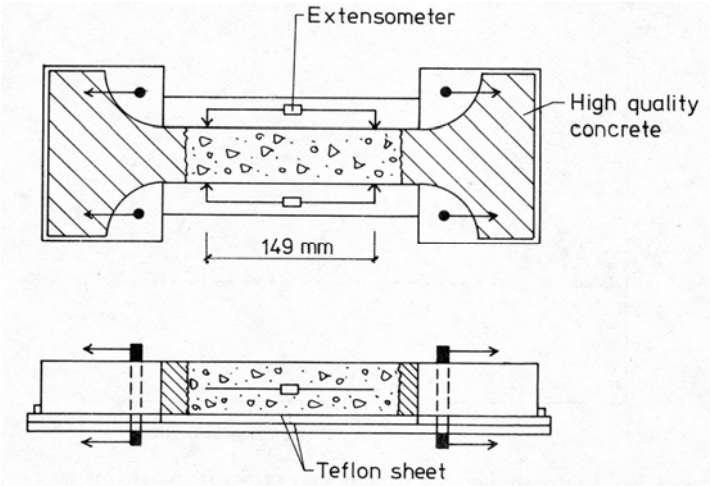

Fig. 6.11 Rig for testing of measurement load-deformation of early age concrete. Byfors (1980)

Kasai et al used a jelly-like dummy to find the friction as a function of deformation, and subtracted this curve from the total load-deformation in order to find the "true" stress-strain relation. They constructed special end plates with wedged bolts for load transfer. The mould was placed on a rolling table in order to obtain equal load action on both ends of the sample, see Fig. 6.12. The cross section is 100 x 100 mm, which is well suited for concretes. The method seems to handle the early age related testing problems, as discussed in section 6.1, in a sensible way. This impression was strengthened in a discussion with Prof. Kasai, and it was therefore used as template for construction of the rig used in the present work, see chapter 7.

None of the testing rigs have built in temperature control, but may be placed in temperature controlled rooms.

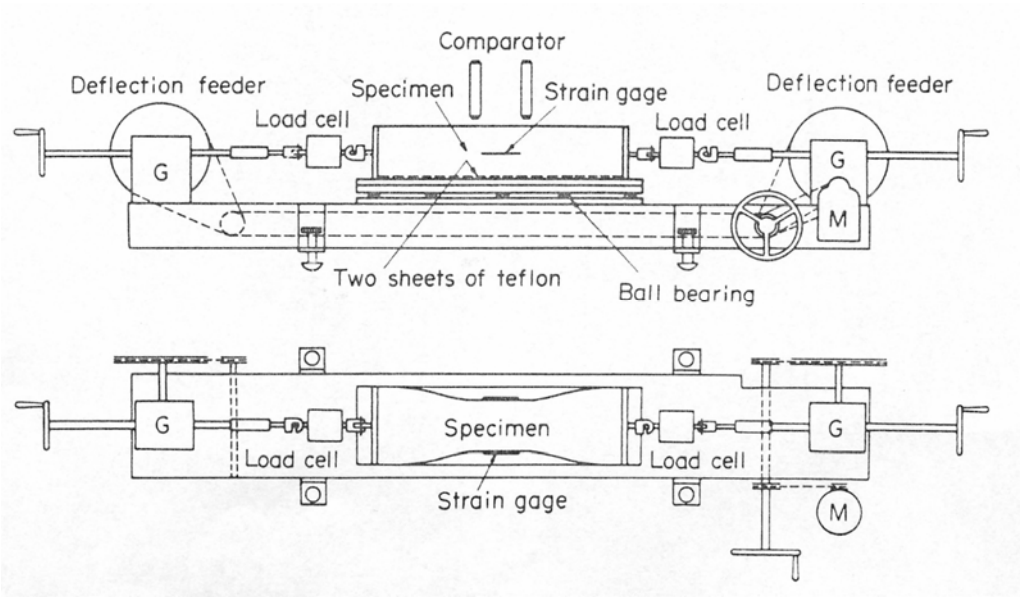

Fig. 6.12 Rig for testing of measurement load-deformation of early age concrete. Kasai et al (1972)

7. Development of the "Tension Rig" - for Testing of Strain Capacity and Tensile Strength

7.1 Basis and design

The following main requirements were used as basis for design of the tension rig:

- Simple principle allowing direct and reliable measurement of "true" stress and strain, i.a. to enable a direct comparison of deformation (from the dilation rig) and strain capacity
- Specimen size as a compromise of the requirement of representing a real slab and the requirement of easy and safe handling in laboratory scale
- Simplicity in preparation, testing and demoulding
- As low friction as possible
- Allow measurement under sealed conditions as well as unsealed and with wind
- Acceptable construction cost as well as cost of testing

Based on these requirements and the review of test methods given in chapter 6.3, the design developed by Kasai et al (1972) was chosen, see Fig. 6.12. The set up is simple, in principle; a direct tension test of a supported body allowing deformation measurement over a relatively large length, easy deformation application and load recording. Furthermore, the dimension fits the sample dimension in the deformation rig and is suitable for most mortars and concretes. The main objection against it is that friction may play an important role.

Based on discussion with Prof. Kasai, some modifications have been made in order to reduce friction between concrete and mould and to reduce the weight of the mould with respect to easy handling. The main friction reducing effort is the "rolling system" of the end sections. The weight has been reduced by the use of light materials (see below).

The rig consists of one base frame with displacement and loading device, and four moulds. The deformation is applied on both sides. The rig consists of 11 main parts, see fig 7.1 and 7.2:

- A rigid base steel frame which carries all the rest and with steering pins to secure that the mould is in centre position before testing
- Two step motors with controllers
- Two linear bearings with ball screws
- Two load cells (5KN)
- Two adjustable tension rods
- Two inductive displacement transducers (IDT), in a rack fixed to the base frame. During testing, the IDTs are connected to 1x10x100 mm steel plates of which approximately 70 mm of them is in the concrete, see Fig 7.13

The bottom of the four moulds is made of Polyoxymethylen (POM), the sides of painted aluminium, and the end plates of 6 mm thick Polycarbonate. The sides are connected to the bottom by screws. The end plates have grips made of eight 6 mm threaded steel bolts with

100 mm length, placed in a circle with diameter of 72 mm, plus four bolts with length of 50 mm placed at the corners see Fig. 7.1. Details about the design are adopted from Kasai, and are given in and fig. 7.3. The system has proven to be sufficient to transfer the deformation in to the concrete; the fracture always occurs outside the grip zone (according to personal communication with Prof. Kasai).

The end section, 100 mm in length, is made like a bearing which rests on two rollers made of 11 mm stainless steel, in a frame, see fig. 7.4. Thus, the friction between the concrete and the mould in the grip zone (corresponding to 200 mm of the concrete length) is negligible. It consists of a bottom plate which fits the horizontal cross section of the sample, see Fig 7.4. The end plate is connected to the load cell by two ball bolts, with an adjustable tension rod in between, to minimize the influence of any eccentricities.

The load cells are fixed directly to the linear bearings with bolts. The ball screws are in turn connected to the motors by the use of special connections.

The data is recorded by the use of the PC-based “Labtech Notebook”, via amplifiers and “Datascan 7250” data processor.

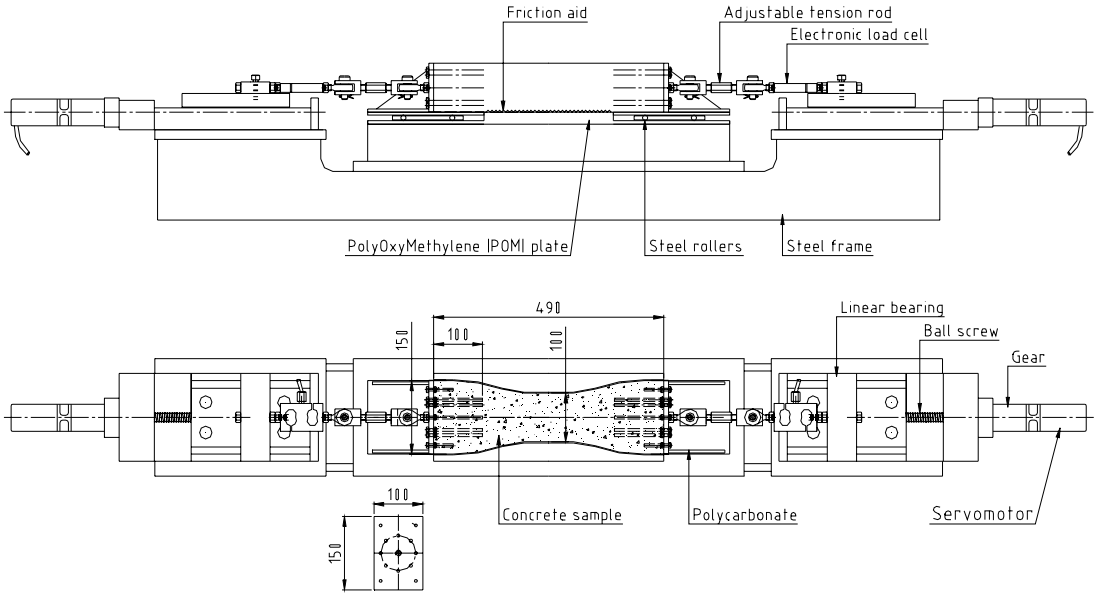

Fig 7.1 Sketch of the present “Tension Rig” for determination of tensile stress-strain relation of very young concrete

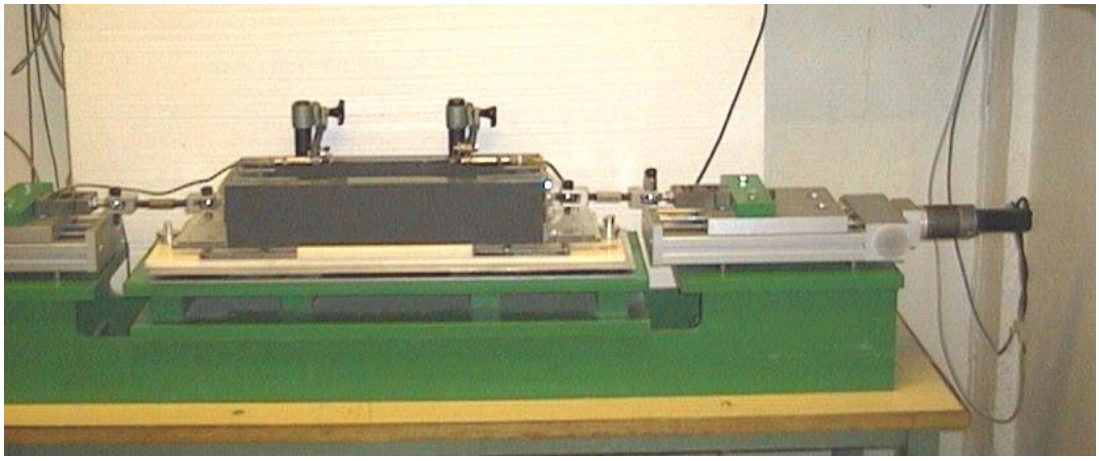

Fig. 7.2 Picture of the present "Tension Rig" for determination of tensile stress-strain relation of very young concrete

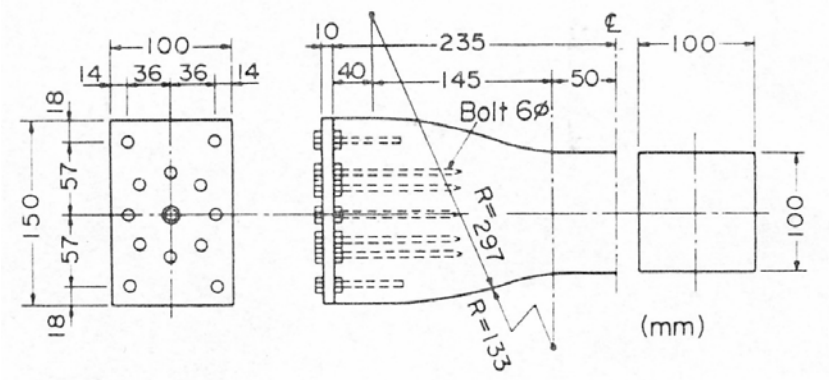

Fig. 7.3 Details of one end of the "Tension Rig" (Kasai et al, 1972)

Fig. 7.4 Picture of end section with rollers.

7.2 Deformation and Load Control

7.2.1 Deformation

The controllers of the step motors may be programmed to give a displacement rate within a wide range. Kasai used a rate between 0.005 and 0.02 mm/sec at each side (i.e. total 0.01-0.04), depending on the deformation at ultimate load. The rate of 0.005 mm/sec was used as standard in the present rig.

Fig 7.5 shows that measured deformation rate of the end sections (without concrete in the rig) complies well with the programmed rate of 0.005 mm/sec (the inclination of the curves is 0.0049 mm/sec). The non/linearity in the beginning is caused by slack in the pull line at the start of the test.

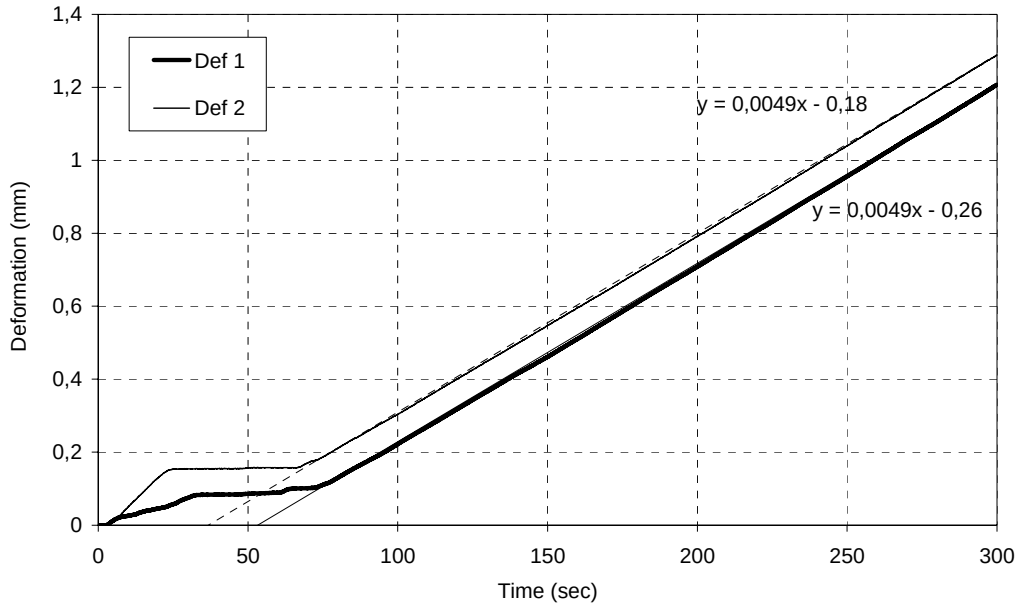

Fig. 7.5 Rate of movement of the end sections of the tension rig (without concrete) at a deformation rate of 0.005 mm/sec.

The strain rate of the concrete will, however, change with age of the concrete as demonstrated in the following Figs., based on testing of ANL 3505 concrete in sealed condition. There appears to be three periods of this change: In the very early age when the concrete is fluid like, there is almost a uniform axial deformation over the whole specimen length (490 mm). This is confirmed in Fig 7.6 by the fact that the measured deformation rate over the mid 200 mm of 0.004 mm/sec (inclination of "Def 1 + Def 2"), corresponding to a strain rate of 20 μstrain/sec, equals the strain rate calculated from the applied deformation rate of 0.01 mm ("Applied Def") over the whole length of 490 mm.

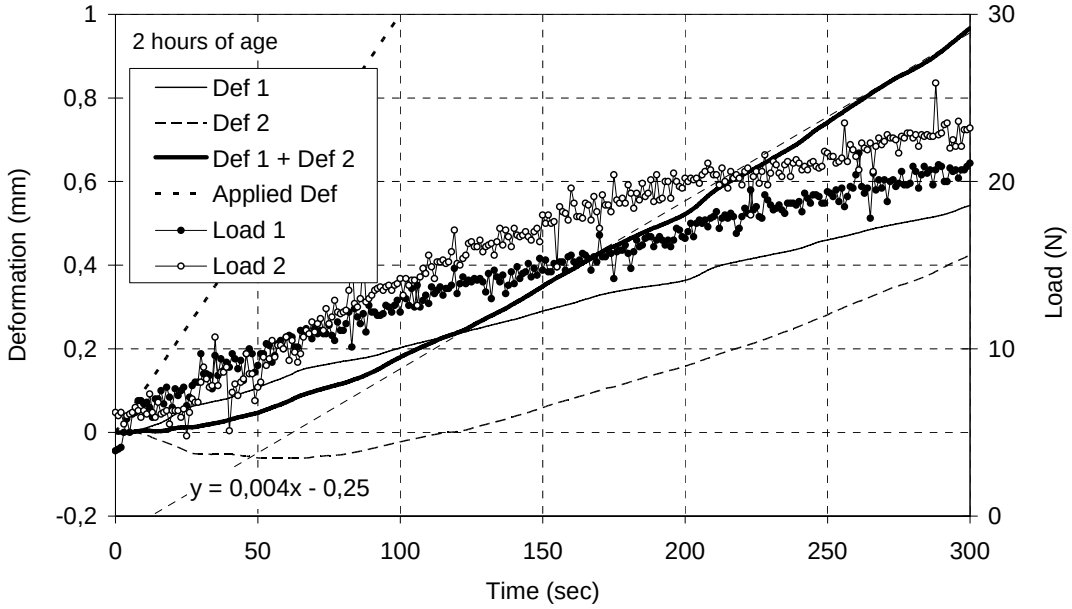

Fig. 7.6 Deformation and load development of the ANL3505 concrete, when tested at 2 hours of age (sealed)

The second period follows and is characterised with less uniform axial strain distribution because the increasing stiffness of the concrete results in less deformation in the end sections because of its larger dimension and the reinforcing action of the grip bolts: Fig. 7.7 shows that the measured deformation rate over the mid 200 mm is 0.0058 mm/sec (inclination of "Def 1 + Def 2"), corresponding to a strain rate of 29 μstrain/sec. It corresponds to a length of uniform axial strain (assuming no deformation in the pull line) of 0.01 mm • 10^6 μstrain / 29 μstrain = 345 mm, i.e. 145 mm less than the whole length.

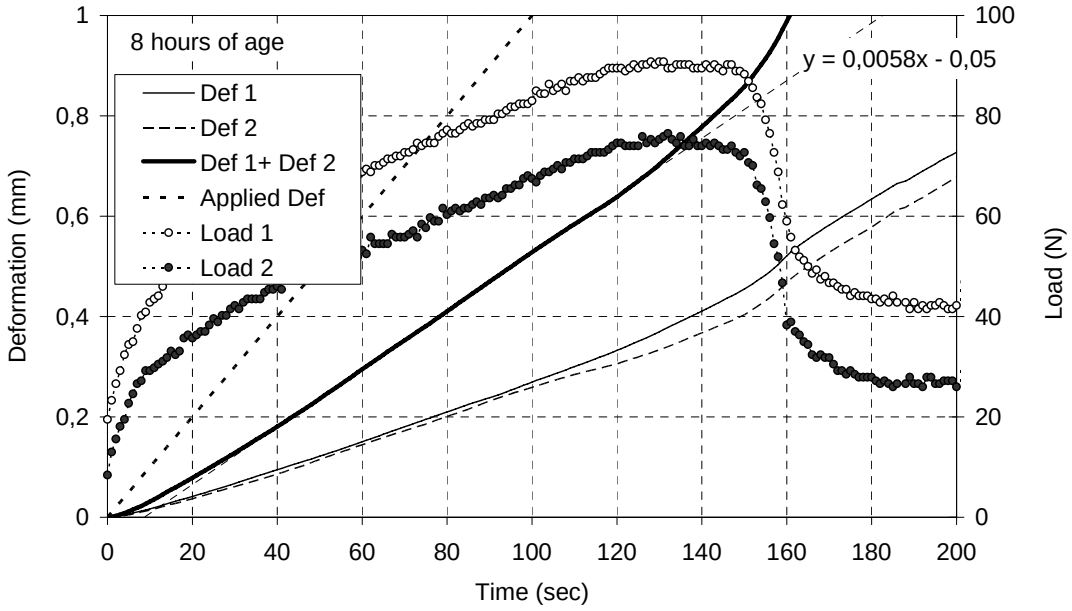

Fig. 7.7 Deformation and load development of the ANL3505 concrete, when tested at 8 hours of age (sealed)

The third period (early hardening phase) is characterised with significant deformation of the pull line at relatively high loads, as seen in Figs. 7.8 and 7.9: The measured deformation rate of approximately 0.00013 mm/sec, deduced from Fig 7.9, is significantly lower than the applied one in period 2 (0.0058 mm/sec). Most of this deformation occurs probably as bulging of the vertical end plate between the eye bolt in the pull line and the inner circle of the grip bolts (see Figs. 7.3 and 7.4), as the wall is rather soft (6 mm thick polycarbonate) compared with relatively thick steel bolts and rigid connectors in the pull line, see Figs. 7.2 and 7.4. The influence of deformation rate is not investigated explicitly here. Consequences of the strain rate variation are discussed in section 6.1.

The results show that a stiffer end plate/section should be designed in a further development of the rig, in order to avoid any influence of changing effective deformation rate. Another solution is to programme the controllers to give a constant deformation rate of the IDTs, via a feed back system (from the IDTs). This is, however, not done here.

The measured deformation rate after failure coincides well with the applied one, see Fig. 7.10. Note that "Applied Def" corresponds to total deformation from the start of the test, while the measured deformation ("Def 1 and Def 2") was nearly zero until 22 seconds later, see Fig. 7.9, due to slack in the pull line. "Applied def corr" has the zero point at 22 seconds. As can be seen, the measured deformation catches up rather nicely the applied deformation. It can also be seen that the crack width is approximately 1.5 mm, immediately after failure (at 195 seconds).

It can also be seen from Figs. 7.6-7.9 that the mould sometimes moves towards one side (seen as negative Def 1 or Def 2 values), which is possible thanks to the rolling plate under the mould (Fig. 7.4). This is result of an unintended lower pre-load on the side with negative values (i.e. more slack to catch up on this side).

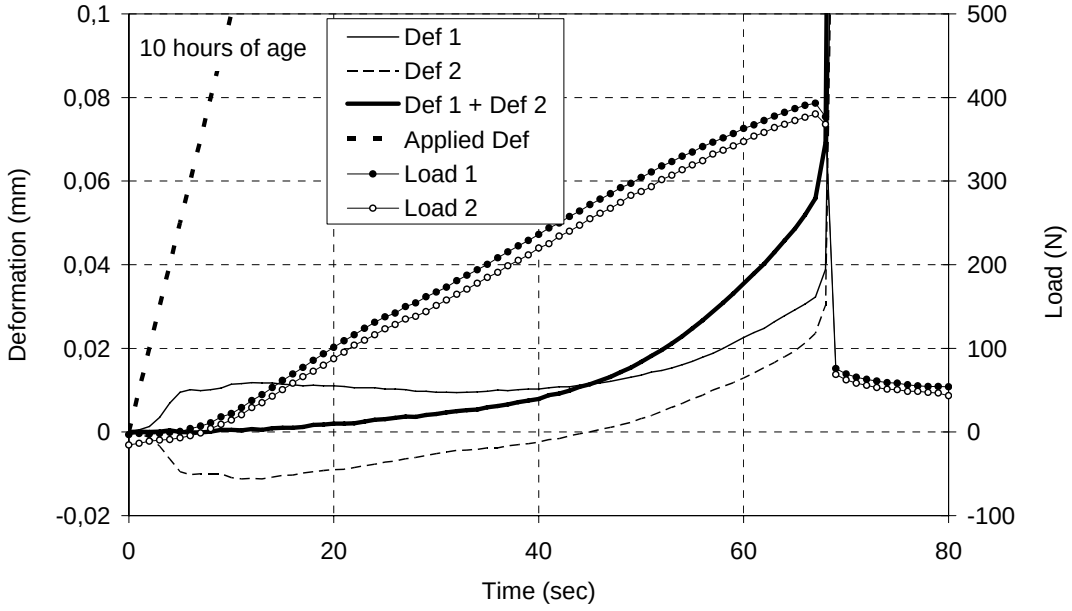

Fig. 7.8 Deformation and load development of the ANL3505 concrete, when tested at 10 hours of age

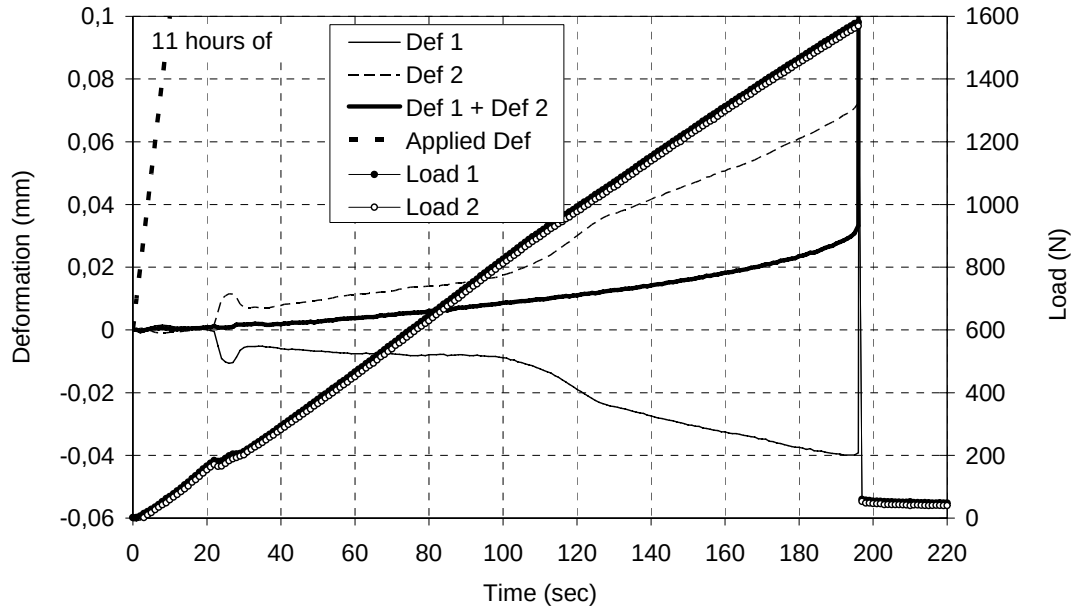

Fig. 7.9 Deformation and load development of the ANL3505 concrete, when tested at 11 hours of age

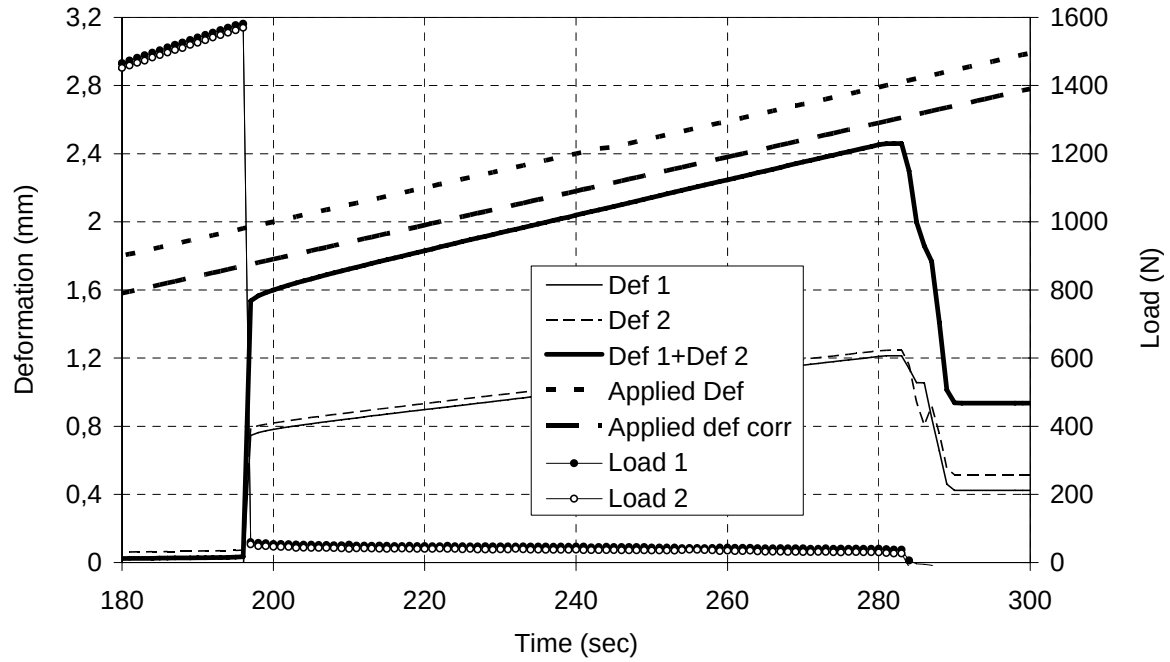

Fig. 7.10 Deformation and load development of the ANL3505 concrete, when tested at 11 hours of age (same as Fig 7.9, but with another scale)

7.2.2 Load

It can be seen from Figs 7.6 – 7.9, that there is good symmetry as the loads on both sides are quite similar, thanks to the friction suspending rolling plate under the mould, see Figs. 7.2

and 7.4 (any friction between the mould and base frame would have given lower load on the side with the most slack). Furthermore, the load development is quit linear until failure, except at the beginning of the test.

7.3 Friction

Friction is considered to be the most important source of error in the measurement since the axial load level is so low. Friction occurs between the concrete body and the mould, and between movable parts of the rig, i.e. between end sections and the mould. The friction itself may induce a deformation gradient over the specimen cross section (height in particular) in that it restrains the deformation at the bottom and sides.

Fosså (2001) demonstrated in his study of friction in slipforming, that suction due to pore water tension is the main contributor to friction before initial set, and that mechanical friction is the main contributor beyond initial set. Furthermore, he found that "static" and "sliding" friction are equal the first few hours (provided no external drying), and that both increased considerably thereafter as pore water tension increased, static more than sliding, and reached a maximum at the time around initial set. Then, both dropped to about 1/3 of the maximum. Thus, it seems to be three periods to be considered:

1. Before pore water pressure (PWP) becomes tension, which coincides with the liquid phase
2. Subsequent period with PWP as tension and until PWP disappears (percolation), which coincides with the semi-liquid phase, roughly
3. Subsequent period, when influence of PWP has disappeared, which coincides with the early hardening phase, roughly

In general, as long as the concrete is rather soft, the deformation applied will appear partly in a shear zone in the concrete closest to the mould, and partly as a sliding between concrete and mould. In the first period the shear deformation will probably dominate. Consequently, the apparent friction is low and mainly a result of the rheological properties of the concrete, and it is therefore probably not significantly influenced by the remedies used to reduce friction between concrete and mould. Results from testing at very early ages when the concrete is still fluid, e.g. those given in Fig. 7.6, confirms low loads in this period.

In the second period, friction becomes significant and PWP dependent. Since the PWP evolution is influenced by the concrete composition and any drying, friction is too. The friction-stress in Fosså´s study was typically 5 KPa (0.005 N/mm^2). Assuming that the friction area corresponds to the bottom area of the mould in the stress-rig, end sections excluded (approx. 30 000 mm^2), the friction corresponds to a tension load of about 160 N, which corresponds to an additional concrete stress of 0.015 MPa. Moreover, it corresponds to an apparent coefficient of friction of approximately 2, since the weight of the part of the specimen in the same section corresponds to approximately 75 N. It certainly demonstrates that friction-reducing aid is needed.

The friction in the third period (when suction is insignificant) is lower and mechanical, and depends therefore mainly on the surface properties of the mould.

The double plastic sheet solution used in the deformation rig can not be used because tensile load would be transferred to the plastic sheet during testing. The load evolution would then reflect the elasticity of the plastic, which is higher than that of the concrete in this period of time, or the "suction friction" if it is lower than that corresponding to the elasticity of the plastic. The following solution was developed, see Figs 7.4 and 7.11:

- The end sections, 100 mm in length, made as rolling bearings as described earlier. Hence, the friction between the concrete and the bottom of the mould in the grip zone (i.e. corresponding to 200 mm of the concrete length) is considered to be insignificant, and influenced by the adhesion between the plastic frilling over the joint between the end section and the mid section (approximately 15 mm on the mid section), only
- The friction in the remaining mid section (270 mm) is prevented by the use of a rubber sheet, 0.15 mm in thickness which has a low stiffness relative to the concrete. It is assumed that the rubber sheet slides easily on the Teflon sprayed POM
- A "bubble-plastic" along the sides in order to further prevent friction

It can be seen from Figs 7.7 that the load is rather high in the first 20 seconds of the test, up to approximately 40 N. Also, it can be seen from Figs 7.7 – 7.9 that the sliding friction in the time after failure is 30 – 40 N. It implies that the friction component of the chosen solution corresponds to a load of 30 – 40 N. Thus, this load should be subtracted from the measured load before calculating the stress of the concrete.

Fig. 7.11 Picture of mould with the remedies used to prevent friction

7.4 Casting and testing procedure

Prior to casting, one mould is placed in the rig, the other ones on a separate rolling table. In order to allow an easy and careful push and pull operation of the moulds in and out of the base frame, the height of the table is the same as the top of the base frame, and the top surface of the table and the underside of the moulds are coated with Talc powder to minimize friction.

The end plates are closed in position by the use of and eccentric knot placed behind each plate, see Fig 7.4. The knots are loosened immediately before testing.

The temperature of the fresh concrete is normally 20 – 22 ºC. The casting, storing and testing take place in a temperature controlled room at the same temperature. The rig in the present version has no temperature control it self. All the moulds are filled from the same batch and normally compacted with a 20 mm rod vibrator. Surface finishing is normally done by a casting ladle. Next, the measuring plates are put in position by the use of a special template. The distance between the plates is 200 mm, at the middle of the specimen, and they go 70 mm into the concrete. At this time the age of the concrete is about half an hour. Then, the decided exposure regime is applied (e.g. covered with plastic sheet, uncovered or wind). Fig. 7.12 shows the channel with fan used for the wind appliance. The air stream goes towards the fan (suction) which has shown to give less turbulence than blowing. The wind velocity is approximately 5 m/s.

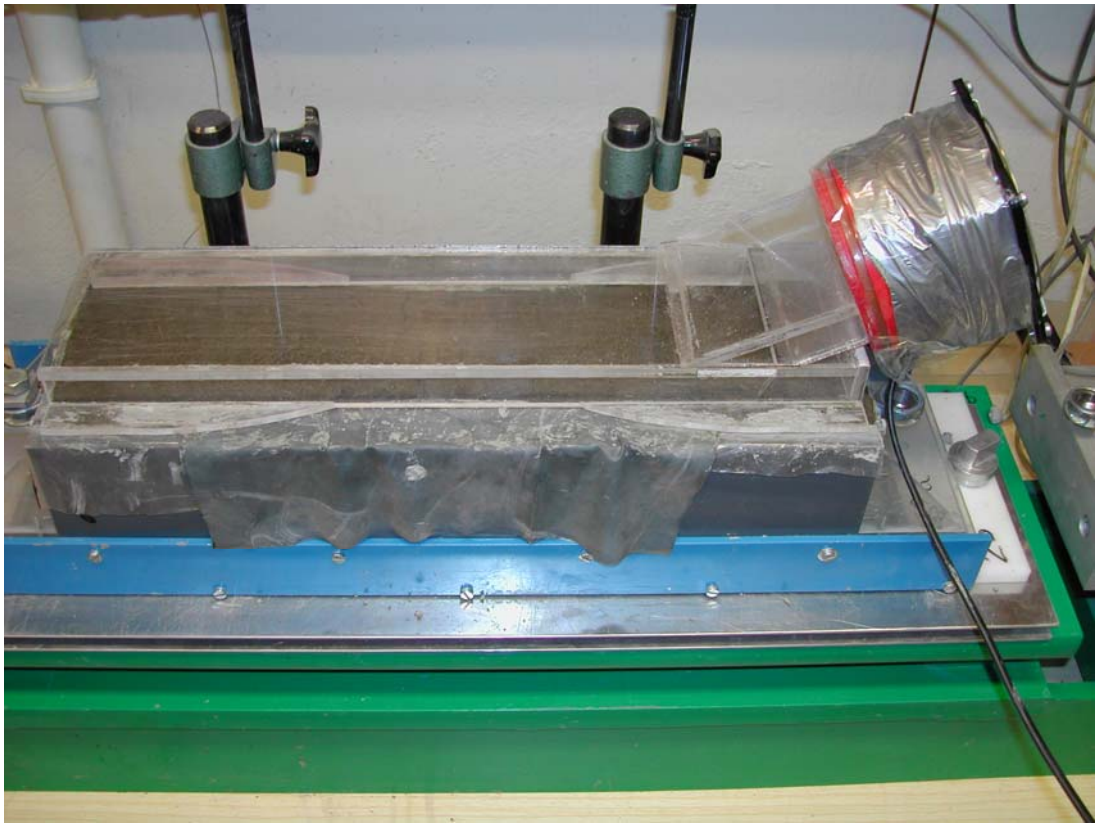

Fig 7.12 Specimen prepared for wind exposure

The specimens are normally uncovered during testing (i.e. any plastic sheets are removed and any wind stream disconnected). In order to prevent any slack in the tension line, a preload of

approximately 5 N is applied immediately before testing, by the use of the adjustable tension rods. Then, the IDTs are connected to the measuring plates and then adjusted to be in its measuring range. This process has shown to be sensitive regarding unwanted movement of the measuring plates, and several solutions have been tried. The most gentle one found is used here: The adjustment is done by moving the IDT in the clip in the rack while the actual measuring pin of the IDT is resting on the plate, see Fig. 7.13. There is a pleated rubber tube on this pin that gives just enough spring load to secure contact and without moving the plate. Then the test starts immediately after.

Fig. 7.13 Specimen prepared for tension test

7.5 Stress/strain

The strain, ε_t, is calculated as the sum of the measured deformations (mm), i.e. movement of each measuring plate, $\Delta l_1 + \Delta l_2$ (Def 1 + Def 2 in Figs 7.6 - 7.10) divided by the measuring length, l, of 200 mm between the measuring plates.

$$\varepsilon_t = (\Delta l_1 + \Delta l_2)/200 \bullet 10^6 \quad \mu\text{strain}$$

The stress, σ_t, is calculated as half the sum of loads (N) on each side, F_1 and F_2 minus friction load, F_f, divided by the mid cross section, A, of 10 000 mm^2. The friction load is considered to be 35 N, see section 7.4, and is considered to build up before the concrete starts to deform. The latter is not quite true, but the small deformation that may occur before the load reaches 35 N is insignificant compared to the many times higher deformations at maximum load.

$\sigma_t = [(F_1 + F_2)/2 - F_f]/A$ MPa

Figs. 7.14 and 7.15 show stress/strain developments calculated from the results given in Figs. 7.8 – 7.10. See chapter 9 for more results.

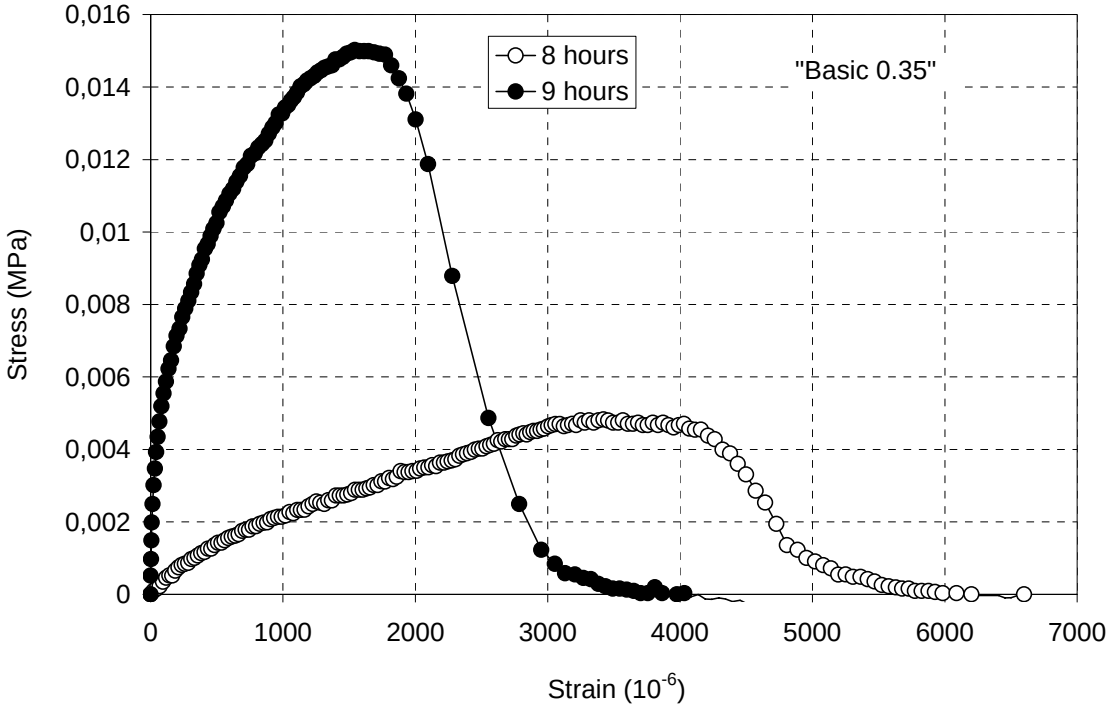

Fig. 7.14 Stress/strain in tension of the ANL3505 concrete at the age of 8 and 9 hours

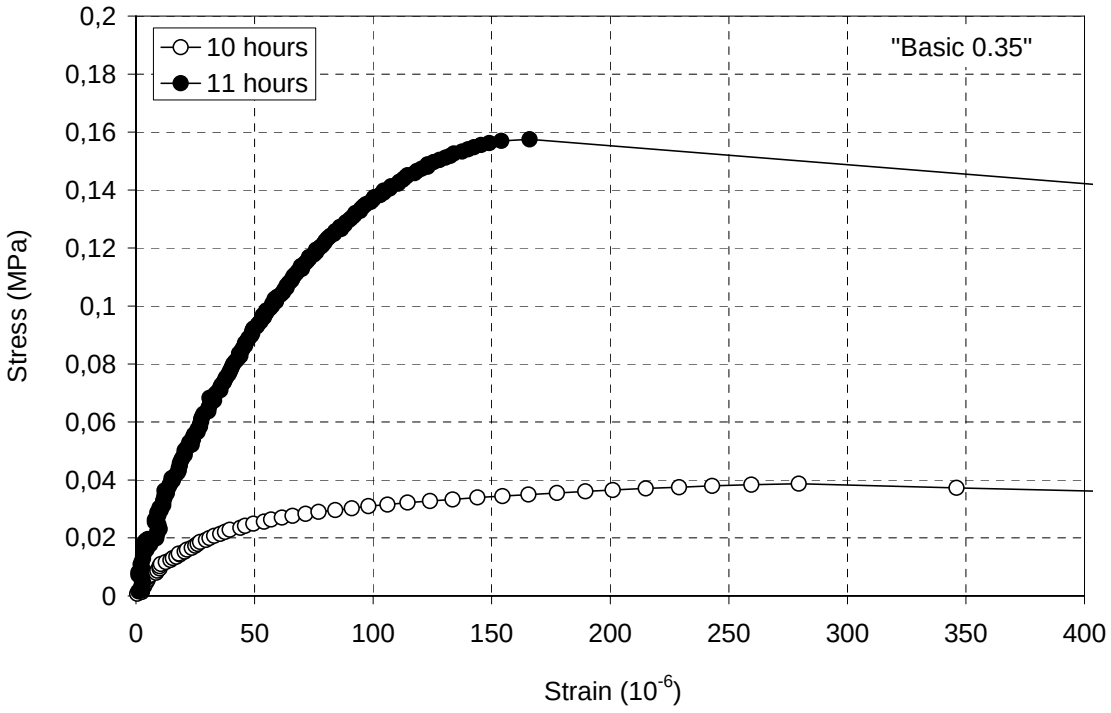

Fig. 7.15 Stress/strain in tension of the ANL3505 concrete at the age of 10 and 11 hours.

7.6 Summary

The “Tension Rig” is constructed based on a principle design by Kasai et al (1972). The set up is simple, in principle; a direct tension test of a supported body allowing deformation measurement over a relatively large length, easy deformation application and load recording. Furthermore, the dimension fits the sample dimension in the deformation rig and is suitable for most mortars and concretes.

Measurements in the plastic age has been in focus since here there is inconsistency between field experience (saying that cracking likely occurs in this age), and lab.tests (showing that the tensile strain capacity appears to be far too high to explain the cracking). Friction in the testing in the plastic age is considered to be particularly important, and therefore, much effort was put on reducing friction. The rig performs well in testing of concrete in the plastic age.

The performance in the hardening age should be improved before used in further investigations on e.g. material and execution parameters as well as of repeatability. The main thing is to increase the stiffness of the pulling line (end plates included) in particular. The present design results in a considerable variation of strain rate during the test.

8. Crack Risk Assessment in the Plastic Age

8.1 Determination of strain capacity

From the discussion in chapter 6, it follows that the short term strain capacity determined as strain at maximum load of moist cured or "lab. air" cured specimens, is considerably higher than the expected deformation (even when exposed to wind) in the first hours of age (see chapter 5). It implies that the risk of cracking is insignificant, which is in conflict with both practical experience and laboratory results showing that cracking occurs in this time period. It suggests that strain capacity is considerably influenced by drying. So the obvious thing to do was tension tests on specimens subjected to drying.

Firstly, tension tests were done on sealed specimens in order to confirm the very high strain capacity found in the literature. A typical result is shown in Fig. 7.6. As can be seen the load level is very low (20 N corresponds to 0.002 MPa) and the strain level is very high (1 mm corresponds to 5000 μstrain), and no cracks were observed (even if deformations were more than 10 000 μstrain).

Tests with drying were done on a number of the concretes tested in the deformation rig (chapter 5), see next section. Typical deformation and load results did not significantly deviate from the results from testing of sealed specimens, and can therefore, not be used to determine the strain capacity in the plastic age. But surface cracks were observed and at rather low deformations corresponding to 100 – 200 μstrain. In the following therefore, the strain capacity is in principle considered as the strain at which the first crack can be observed by eye. This strain at first crack was found from the recorded deformation versus time and the time at which the first crack was observed. For instance using Fig. 7.7, if the first crack was observed 10 seconds after starting the test, the deformation at first crack was 0.035 mm, i.e. $0.035/200 \cdot 10^6 = 175$ μstrain.

However, the method is not consistent because the very first crack is hard to catch by eye (appears to be invisible in the beginning and it may occur anywhere on the surface within few seconds). Video recording during testing as basis for image analysis would obviously improve the consistency of the method (not done here). Consequently, the method does not give a consistent strain at first crack, and the results are therefore indicative and suited to give trends, only.

More serious is the fact that cracks sometimes were observed prior to the test was started. In fact, the low strain capacity caused a problem in that the strain caused by the small deformations associated with preparation of the test sometimes obviously exceeded the strain capacity of the concrete. Such deformations may arise under movement of the mould from the base frame of the rig, but probably mostly from loosening of the end plates (see section 7.4): As tests in the plastic age often run before the self-supporting point of the concrete, the concrete still exerts a pressure on the end plates which will be transferred to a movement when loosened. It is therefore important to apply a small compression in the pull line before start of test (and not tension as recommended for tests in the early hardening age) by using the adjustable tension rod, before loosening the lock knot. The result is then a delayed start of deformation compared to start of recording, since it will take some time to catch up the slack in the line. But it does not have any consequence for the determination of strain at first crack, since the delay is visible on the graph, and thus, can be subtracted. An example is shown in

Fig 8.1: “Standard procedure” represents loosening of the lock knot prior to start of recording, i.e. the end plate has moved before start of recording and caused a slight compression in the pull line causing a delay of about 30 seconds. The same situation will occur when a small compression is applied in the pull line before start of test, as suggested above. “Loose end sections” represents loosening of the lock knots after start recording. The result is an immediate deformation (recorded over the 200 mm mid section) corresponding to a strain of approximately 300 μstrain within the first 10 seconds.

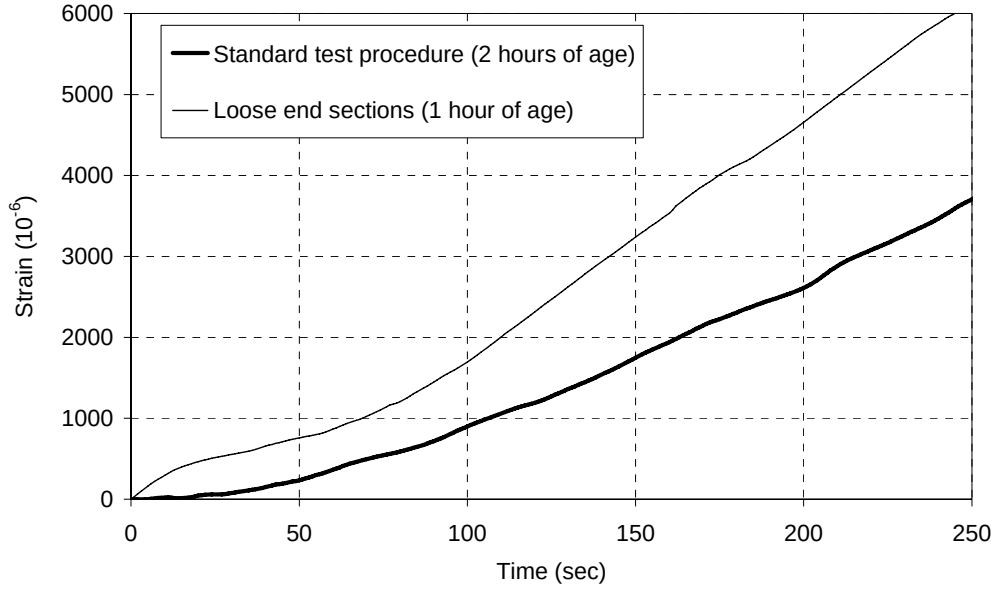

Fig 8.1 Strain development during tensile test of “Basic” concrete at very early age when loosening the end sections prior to start of deformation recording (standard test procedure) and when loosening after start of recording (“loose end sections”)

The present strain capacity is determined with a relatively high strain rate (approximately 50 μstrain/sec.) and may represent in situ cases with typically high rate deformations like accidental movement of the formwork. The settlement and shrinkage rates are much lower - in the magnitude of 1 μstrain/sec. (as deduced from results presented in chapter 4). It is suggested that the cracking mechanism is related to emptying of pores/cavities, (section 6.2). Thus, it may be expected that the strain at first crack increases with decreasing strain rate, as there will be more time for water to move from the interior and for redistribution of water at the surface, and thus, less change of emptying of pores/cavities. The “minimum” strain rate is the one corresponding to the settlement or shrinkage rate in the given case. Such rates may be established by restraining the specimens against deformation under drying, i.e. by keeping the end sections in the initial fixed position during the relevant time. The question is if 100 % restraint of the “skin” of the present specimen can be achieved, since it is relatively short and the “friction” between the skin and the fluid concrete under it is probably rather low. It is hard to measure a possible deformation of the skin due to its low thickness, in order to confirm it. It is shown in section 3.3, (Fig. 3.17) that the top (upper 5 mm) starts to shrink earlier than the middle part (50 mm depth), and shrinks several hundred μstrain before the middle starts to shrink. It shows that the skin may shrink while the body below is restrained, and thus, that full restraint of the skin can not be achieved by simply keeping the end sections fixed in its initial positions. This fact also implies that the body may deform considerably before the skin starts to deform in tension test. Consequently, the skin strain at first crack is

probably considerably lower than the strain at first crack found according to the method described above (based on deformation of the body).

Crack propagation at both the “high strain rate” (standard tension test) and the “low strain rate” (restrained) were investigated.

8.2 Tests

8.2.1 Tension tests

The hypothesis is discussed in section 6.2. It suggests that PWP is a good indicator for skin formation, i.e. that the skin starts to form when PWP turns into tension. It can be seen from Fig. 4.30 that PWP of “Basic” concrete exposed to 50 % RH and 21 °C (no wind) turns into tension (negative values) at drying time of approximately 1 hour at 5 mm depth and approximately 2 hours at 50 mm depth. The drying time before PWP turns into tension at the top is obviously shorter (the present PWP-measure method does not allow reliable measurements at depths less than 5 mm, se section 4.3.5). Therefore, tension tests were run at short drying times also, down to 10 minutes. Since the PWP development at a given drying load is influenced by the permeability of the concrete the following parameters were investigated:

- w/b: 0.30, 0.35 and 0.40,
- cement type: Norcem Anlegg and Norcem Industri,
- the plasticizer composition: LS/SNF as usual, LS only (giving larger retardation) and SNF, only (giving less retardation), and
- time of drying, from 10 minutes until 5 hours

The specimens were exposed to 50 % RH and 21 °C (no wind). The casting/surface finishing was done approximately 30 minutes after water addition. Beyond that, testing was performed according to the standard procedure, given in section 7.5, with a deformation rate of 0.01 mm/sec. Cracks were observed by eye, as described in the previous section.

Due to the difficulty related to the first crack identification (discussed in previous section) the results are indicative, only. The following trends were found from the tests:

- Cracks occurred in tests performed at very short time of drying. A test on the “Basic” concrete at 10 minutes of drying, only, showed hair cracks immediately after start of test (probably at strain of approximately 100 μstrain)

- Strain at first crack increases with increasing time of drying (i.e. increasing age): Testst on the 030 concrete showed strain capacity < 200 μstrain at 1.5 hours of drying increasing to approximately 400, 600 and 1000 μstrain at 2.5, 3,5 and 4,5 hours of drying, respectively.

- The typical crack propagation during testing was both occurrence of new cracks and opening of existing cracks. Occurrence of new cracks dominated when testing at the earliest ages and opening of cracks dominated when testing at later ages.

- The number of cracks decreased with increasing age, see Fig 8.2, and crack widths increased with increasing age.

- The tension tests of the 0305 concretes showed that hair cracks occurred already at testing 20 minutes after surface finishing (about 40 minutes after water addition) at 100 to 200 μstrain, and apparently regardless of strain rate. Further applied strain opened the cracks, but created new cracks, also. The 0405 concretes behaved differently: Hair cracks appeared always at the highest strain rate, but not always at the lowest rate (repeated tests). Neither concretes cracked in the restraint conditions. The results support the hypotheses that the crack risk is strain rate dependent.

- The point of origin for the cracks seemed to be random in most tests, but in some cases it was observed that cracks propagated from cavities, from aggregate surfaces, see Fig 8.3, or even from the measuring plates.

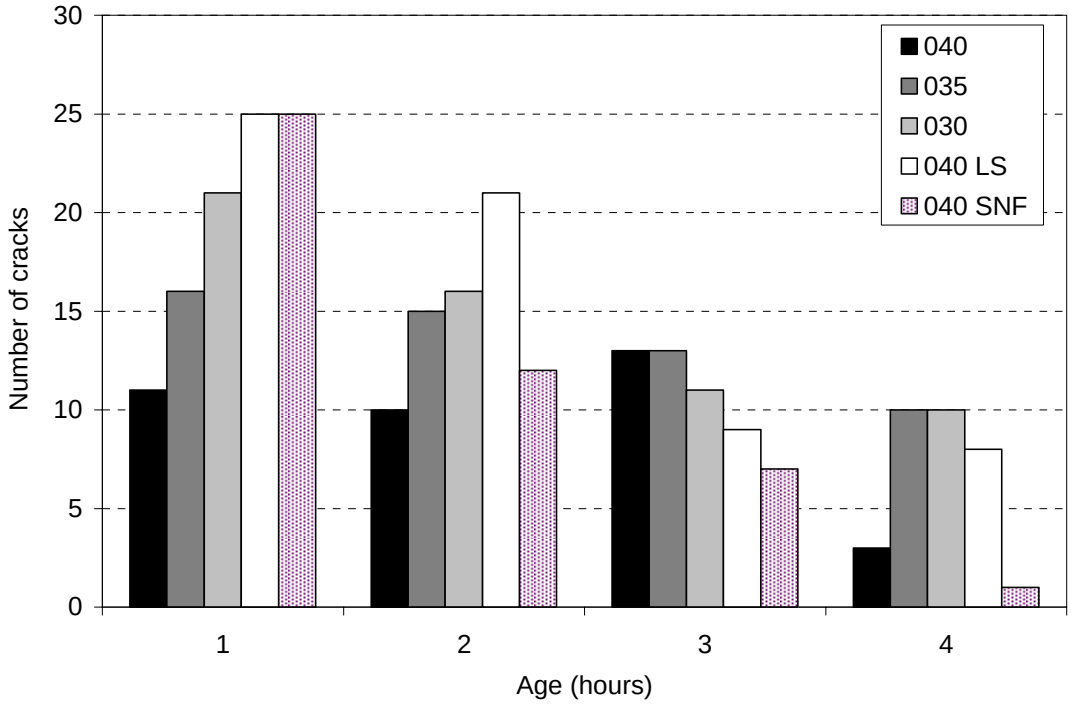

Fig. 8.2 Number of cracks after tension tests on concretes with various w/b (0.40, 0.35 and 0.30) and content of water reducing admixture (LS is based on lignosulphonate, SNF is based on sulphonated naphtalen formaldehyde)

8.2.2 Tests on restrained specimens

A number of tests with restrained specimens were performed at 50 % RH and 21 °C without wind. Neither showed cracking, even the one with Norcem Industri Cement and w/b = 0.35 (slump of 170 mm), assuming to have a high cracking tendency because of rapid PWP reduction. The test with this concrete was then tested again at 50 % RH and 21 °C, but with 5 m/s wind velocity. The wind was applied by suction through at tunnel, see Fig. 7.12. Even then, only one of the two specimens cracked. Fig. 8.3 shows the crack propagation. The crack started at approximately 10 minutes of drying, at the tip of the coarse aggregate seen, and

propagated as a continuation of (in parallel to) the side of it. No aggregates were seen at the surface of the un-cracked specimen.

The fact that cracking hardly ever occurred in these tests is in conflict with results from tests on similar concretes in the NORDTEST-method NT Build 433 (Bjøntegaard et al, 1998). The main reason may be result of different specimen geometry: As discussed in section 8.1, it is a question if 100 % restraint of the skin can be achieved in the tension rig. The specimen in NT Build 433 is a ring, see Fig. 8.4, which represents an infinite length, and thus, "full restraint" of the surface.

8.2.3 Conclusion

In the plastic age, the strain capacity seems to be related to whether or not the meniscus system has been established: If not established (i.e. if evaporation rate is lower than bleeding rate), the concrete acts like a liquid and the strain capacity is then "infinite". If established (i.e. if evaporation rate exceeds bleeding rate) the concrete seems to act like a stiff body with a very low strain capacity (probably in the order of magnitude of 100 μstrain). This is probably because the geometry controlled meniscus system means that the particles are locked in position and can not move more than that caused by the evaporation. If any external deformation is applied, or if the body it is restrained during the evaporation, the body is prone to crack. Since pore water measurement easily reveals when the menisci system occur, it is a good tool in the assessment cracking risk in the "plastic age".

Cracks probably initiate at inhomogeneities, like cavities and aggregate-paste interfaces where the menisci-particle structure is "weak" and may act as wall effect.

If the permeability of the mass is sufficiently low to prevent water flow to the surface, the surface will dry faster and form a stiff body (skin) on top, with a liquid beneath. This may happen during the first minutes of drying, and is probably the main reason why low permeable systems (i.e. low water to powder ratio systems like in HSC and SCC) are more vulnerable to such cracking.

Crack risk assessment in the plastic age can not be determined from stress-strain curves because the body is too soft to generate significant stress, so cracks must be observed by eye. Then, strain capacity can be determined as strain at first crack, where the strain is found from the recorded deformation versus time and the time at which the first crack was observed by eye. The method is not consistent because the very first crack is hard to catch by eye (appears to be invisible in the beginning and it may occur anywhere on the surface within few seconds). Hence, it is recommended to use pore water pressure measurements at the top surface as the tool for crack risk assessment in the plastic age. I.e. to consider the point in time when pore water pressure turns into tension.

Fig 8.4 Crack propagation of a restrained specimens (100 mm in width) exposed to 50 % RH and 21 °C and 5 m/s wind velocity. Upper picture taken at 10 minutes of drying, lower at 90 minutes.

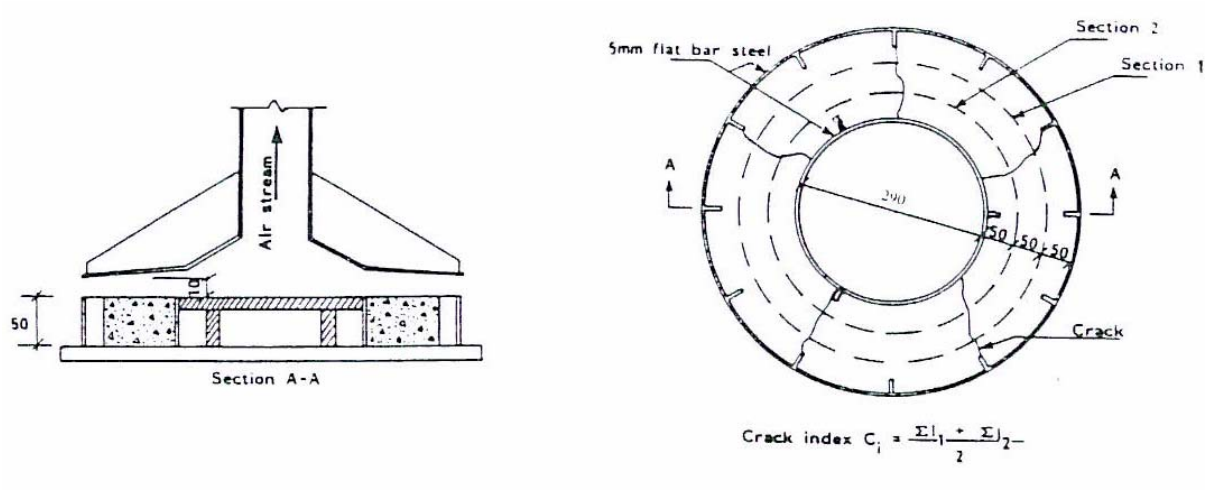

Fig 8.5 Sketch of method for determination of "plastic shrinkage cracking" tendency according to the NORDTEST method NT BUILT433.

9. Crack Risk Assessment in the Early Hardening Age

9.1 General

The early hardening age is associated with minimum tensile strain capacity which makes it a potentially risky period with regard to cracking (see chapter 6). On the other hand, the deformation in the period, if moisture sealed (i.e. AD), is usually expansion, due to expansive chemical reactions and absorption of bleed water (discussed in section 3.2.4) as well as temperature rise due to heat of hydration. Hence, the period is normally harmless with respect to cracking unless other driving forces appear. Such driving forces to cracking in the early hardening age may be:

- Drying shrinkage due to evaporation because of insufficient moisture protection of the surface (transition of plastic shrinkage)
- Contraction due to temperature decrease caused by the evaporation,
- Contraction due to temperature decrease of the surrounding air and disappearance of solar radiation on the surface. Both are often the case when concrete is cast in the morning, and thus, reaches the critical age in the evening
- Autogenous shrinkage

An obvious question is whether the crack risk assessment shall be done by comparing deformation with tensile strain capacity or by comparing self induced stress (when restraining the deformation) with tensile strength. As long as concrete is plastic, the stress built up is insignificant, and thus, the latter approach does not make sense. Moreover, the crack propagation seems to be determined by the surface strain capacity and not the bulk mass, according to the discussion in the previous chapter. Later, beyond the time of setting, restraint of the deformation will generate measurable stress, and thus the stress/strength approach may be used. The stress evolution may be found directly in a “Temperature-Stress-testing Machine” (TSTM) or indirectly by calculating the product of volume change, E-modulus and (1- creep).

A strain assessment sounds easier to perform from a testing point of view, if an “early age” tension rig is available. On the other hand it is complicated to handle the time dependency in the strain assessment. The tensile strain capacity at a certain age is normally found by a short term loading, while the volume change is accumulated over the whole age. The fundamental question is to what extent restraining of deformation in the period when the strain capacity is high, causes damage.

Both approaches are considered in the work discussed below.

9.2 Influence of autogenous deformation

As stated above, AD of normal HSC/HPC in the period is normally expansion. However, Bjøntegaard (2000) demonstrated that AD of concretes with low w/b may turn into contraction practically from time of setting, and thus, constitute a driving force that leads to cracking. He found a very high rate of autogenous shrinkage in the first hours of age of a very high strength concrete (“VHSC”, with w/b = 0.22), see Fig. 9.1, and that the corresponding

stress at 20 ºC (isothermal), under full restraint, exceeded the tensile strength, resulting in en early failure. Even at an imposed realistic temperature rise, the rate of autogenous shrinkage exceeded the rate of thermal expansion, resulting in net contraction and subsequent tension that was rather similar to those of the isothermal tests in the beginning, see Fig. 9.1. However, as the autogenous shrinkage levels off after a few hours (see “isothermal”), thermal expansion saves the concrete from cracking in this period, but it failed in the cooling period. Such special concretes or mortars are normally used in rather thin sections where the hydration generated temperature rise is relatively low. Consequently, little help can be expected from thermal expansion. On the other hand, watering applied on the surface as early as possible to prevent autogenous shrinkage, is more efficient in thin sections, and is thus expected to prevent cracking. Moreover, the results certainly demonstrate that it is of vital importance to avoid additional driving forces (listed above) of such concretes in this early, but short period in time.

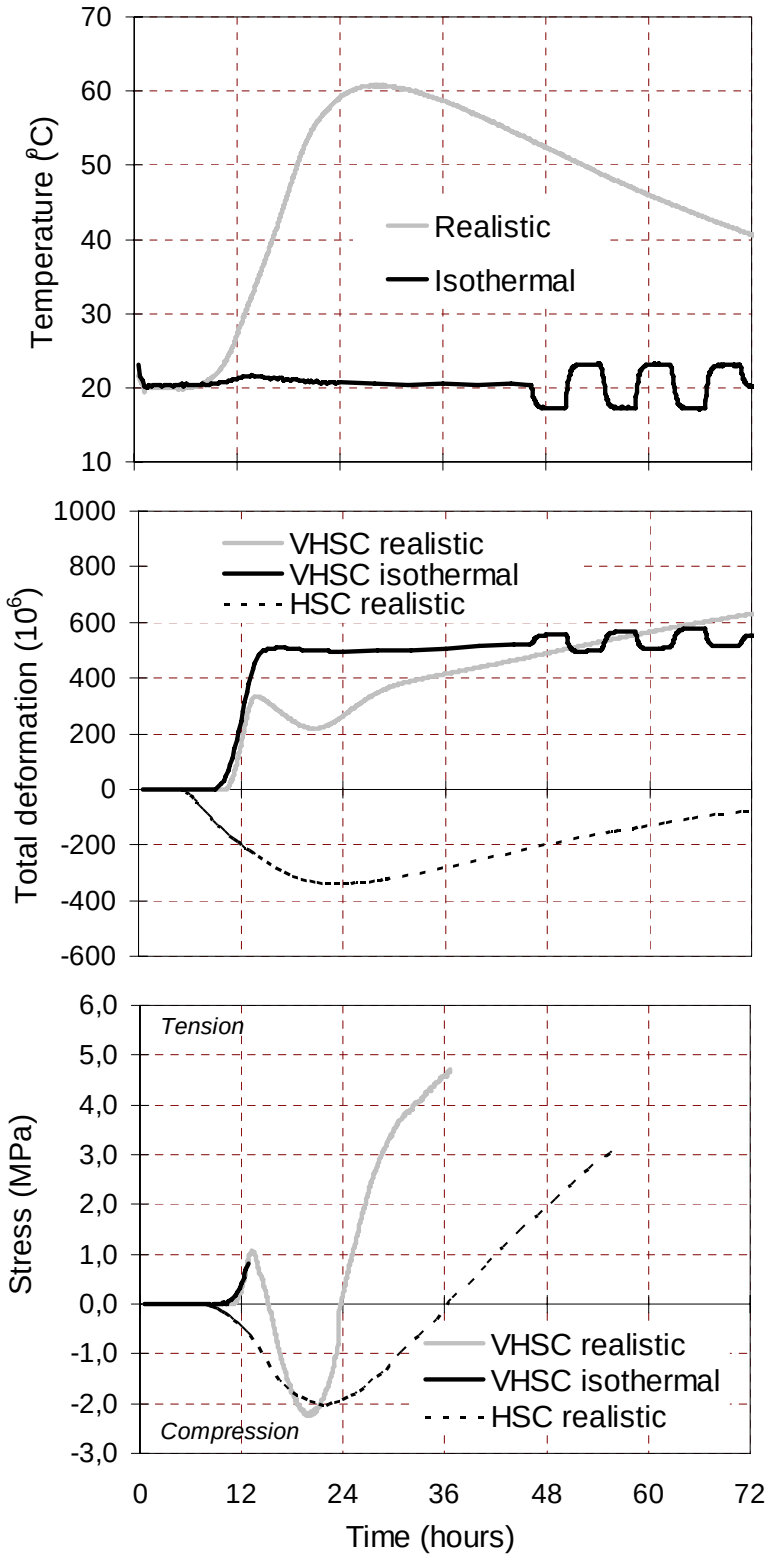

Fig.9.1 Comparison of a very high strength concrete, "VHSC", (w/b = 0.22) with a normal high strength concrete, "HSC" (w/b = 0,40), when exposed to isothermal temperature and a realistic temperature evolution (upper graph), respectively. Middle and lower graph shows the autogenous deformation plus thermal dilation, and subsequent stress evolution at 100 % restraint, respectively (Bjøntegaard, 2000)

9.3 Influence of drying and cooling

9.3.1 Experimental program

A limited investigation was conducted in order to generate some data to evaluate the importance of drying and cooling on cracking in the early hardening age, and to find a testing methodology for crack risk assessment in the period. Testing includes measuring of volume change and subsequent stress generation, tensile strain capacity and tensile strength evolution.

The "Basic" concrete was chosen, but with lower w/b, 0.35 (ANL3505 in the APPENDIX), because it was expected to give higher cracking risk (less influence counteracting chemical expansion and/or swelling from absorption of bleed water).

The deformation and subsequent stress generation were measured on specimens subjected to:

A. **Sealed** condition and 20 ºC (reference)
B. **Drying**: In air with approximately 50 % RH and 21 ºC (no wind), immediately after placing of the concrete.
C. **Cooling**: At the age of approximately 12.5 hours sealed specimens were subjected to cooling from 20 ºC to approximately 10 ºC in 1 hour, and then kept constant at 10 ºC the remaining part of the test period. The age of 12 hours was chosen because it is close to the final setting time of the present concrete, which is at the time when the tensile strain capacity goes through a minimum value.
D. **Drying and cooling**: Drying as in B. followed by cooling as in C.

The tensile strength and strain capacity was measured on sealed cured specimens, only. The influence of drying was not investigated. It is expected that drying contributes to lower strain capacity and strength in the critical period, because moisture gradients are known to induce stress gradients, i.e. tension at the surface that adds to the applied tension. Consequently, the measurements are expected to overestimate strain capacity and strength at drying. The influence of drying should be investigated in any future work.

9.3.2 Testing

Tensile strength and strain capacity
Tensile strength and strain capacity was tested in the "Tension Rig", see chapter 7.

The influence of strain rate was investigated, since pervious work shows that strain capacity increases with increasing strain rate, see chapter 6. The lowest and highest rate programmed for the rig were used, i.e. 0.002 mm/s and 0.16 mm/s corresponding to 10 μstrain/s and 800 μstrain/s, respectively. Note that both rates are rather high compared to the "natural" rate of deformation (i.e. during drying), which corresponds to less than 0.05 μstrain/s (deduced from Fig. 9.5)

The test rig is designed for a maximum load corresponding to a concrete stress of 0.5 MPa. In order to follow the strength development further, the tensile splitting strength was measured on 150 x 300 mm cylinders. The earliest measurements of splitting strength were done at

approximately the same ages as the latest measurement in the tension rig, in order to correlate the two test methods.

Kanstad et al (2003) showed that splitting strength is a good substitute for early age uniaxial tensile strength. Indirect tensile test methods like the tensile splitting test, have been widely used because of the difficulties experienced with direct tensile methods. In the present splitting test, cylinders with diameter/height = 150/300 mm, was loaded along two opposite generatrices. According to linear elastic theory a stress-field, with tensile stresses normal to the load direction, is then established. The tensile splitting strength at failure, f_{ts}, is found as:

$$f_{ts} = 2P/\pi DL, \text{ P = the failure load, D = cylinder diameter, and L = cylinder length}$$

A wooden fiber strip, 15 mm in width and 4 mm in thickness, was used to transmit the load to the concrete. Three cylinders were tested at each age.

Deformation and stress development

Volume change was measured in the "Dilation Rig" shown in Fig. 9.2a, where specimen geometry is 100 x 100 x 500 mm. Stress development during full restraint is measured in a Temperature-Stress Testing Machine (TSTM), as shown in Fig. 9.2b, where the specimen is "dog-bone shaped" and has a restraining "crosshead" at both sides and a prismatic part in the middle with geometry 1000 x 90 x 100 mm. Both rigs are temperature-controlled by water circulating in the moulds, hence both isothermal tests and tests with temperature changes can be performed. The TSTM contains a feedback-system that provides zero deformation in the specimen, i.e. the degree of restraint (R) is 100%. In both rigs the measurements are started before setting.

The specimens are generally well protected against drying (aluminium sheets and plastic sheets and surrounding mould). Drying shrinkage tests have however been performed during this test program. The top cover is then removed and the specimens exposed (from the top) to 20 °C and 50 % relative humidity (RH).

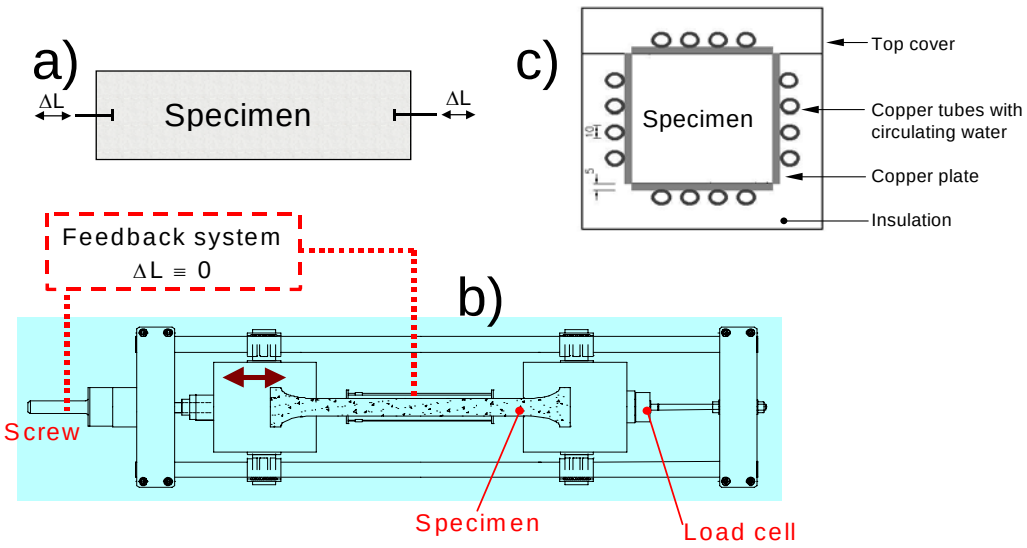

Fig. 9.2 Sketches of a) "Dilation rig" to measure deformation and b) "TSTM" to measure subsequent stress development under restraint and c) system for water circulating in the mould (Bjøntegaard, 2000)

9.4 Results and discussion

9.4.1 Setting time

The initial setting time is deduced from the heat evolution of the concrete in a semi-adiabatic calorimeter. The time of initial set is then defined as the point of time when the heat evolution reaches 12 kJ/kg cement. For the present concrete it corresponds to approximately 10 hours of age.

9.4.2 Uniaxial Tensile Strength and Strain Capacity

It can be seen from Fig. 9.3 that the tensile strain capacity (strain at maximum stress) is very high in the period before initial setting, and that the tensile strength evolution accelerates from the point of initial setting, which both are in accordance with results discussed in chapter 6. Also, note that the strain capacity continues to decrease in the time beyond setting, which suggests that minimum strain capacity is reached somewhat later, also found by Kasai et al (1972).

The strain rate did not influence the tensile strength significantly, but the strain capacity was highest for the highest strain rate, both before and after initial setting time. This is surprising since one should expect that decreasing rate leads to increasing creep since less time is available, and thus, lower failure strain. It is confirmed by Kasai et al (1972) whom showed that the strain capacity doubled when decreasing the deformation rate from that corresponding to 5 minutes to that corresponding to 90 minutes of deformation before failure, see section 6.1. More tests are needed in order to find if this is right or wrong.

The uniaxial tensile strength and splitting tensile strength are shown in Fig. 9.4. As can be seen, there is some scatter between the three parallel uniaxial test series (three separate mixtures). The splitting strength seems to be at a lower level than the uniaxial one, but this is just an indication due to few data. The main point is, however, that the tensile splitting strength seems to be an acceptable substitute for the uniaxial tensile strength in the early hardening phase. I.e. it may be used to extend the uniaxial tensile strength development.

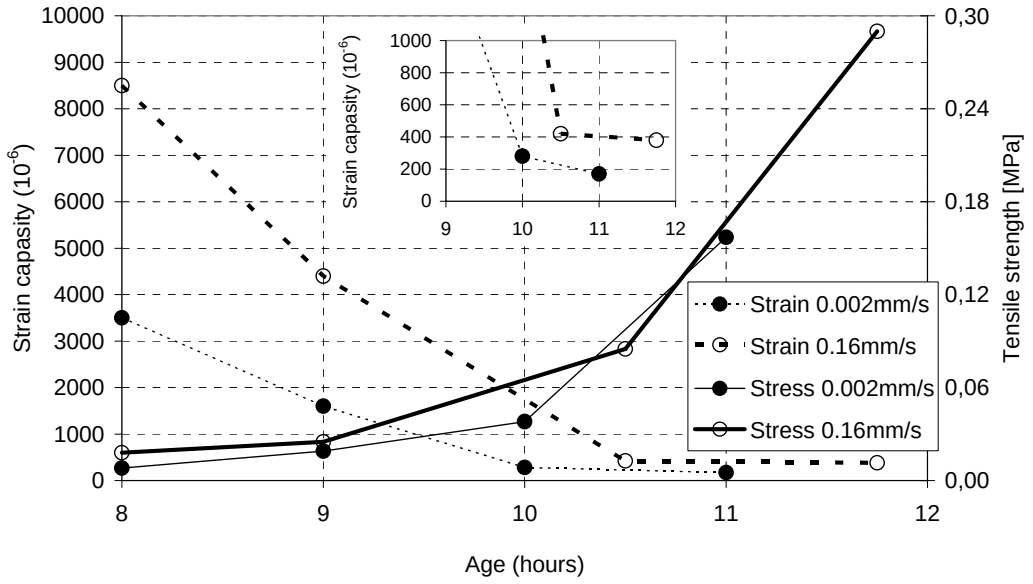

Fig. 9.3 Uniaxial tensile strength and tensile strain capacity versus age of concrete with w/b = 0.35

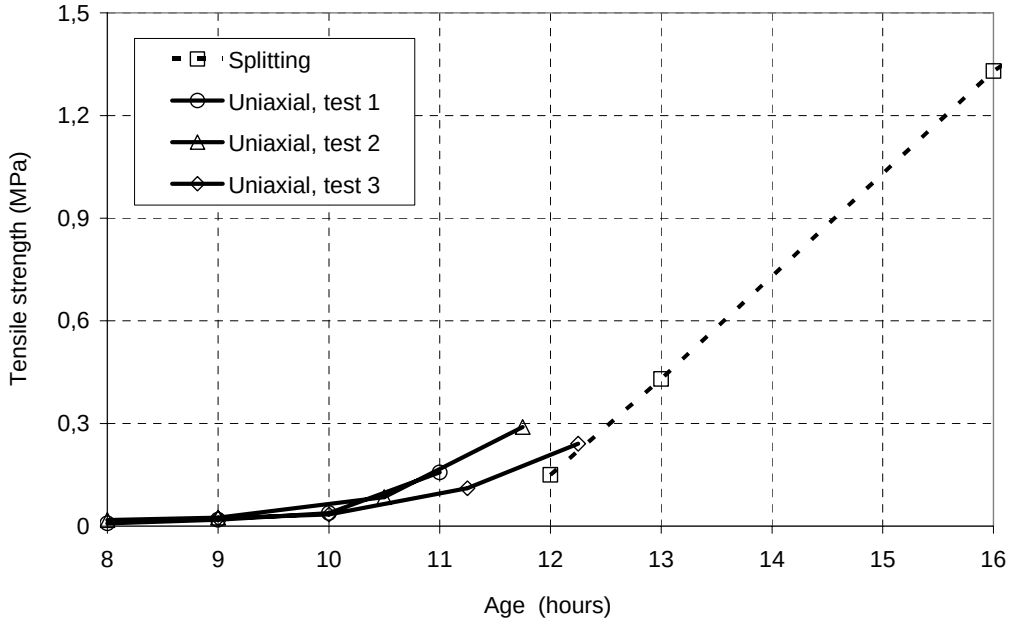

Fig. 9.4 Uniaxial and splitting tensile strength and versus age of concrete with w/b = 0.35

9.4.3 Deformation

The measurements begin immediately after placing. However, the measurements during the first hours in the this tension rig are uncertain because the measuring device "floats" in the fresh concrete, and thus, is influenced by actions caused by the large settlement of the concrete in this period (Bjøntegaard, 2000). Therefore, results before initial setting time are subtracted, see Fig. 9.5.

The sealed specimen experienced shrinkage (autogenous shrinkage) from approximately 13 hours, which coincides fairly well with the time when the drying shrinkage starts to level out. This indicates that the concrete has obtained a certain stiffness that strongly reduce the further deformation, and that empty pore space is being created.

The thermal dilation is approximately 60 μstrain (corresponds to difference between the two curves noted “S, 20-10 ºC” and “S, 20 ºC” at 13.5 hours), which corresponds to a coefficient thermal dilatation (CTE) of $6 \cdot 10^{-6}$ (i.e. 60 μstrain/10°C) which again coincides with the measured CTE of $6 \cdot 10^{-6}$ of this concrete (Bjøntegaard, 2000).

A similar deformation can also be seen for the samples with exposed surface (ES). Note that the drying shrinkage rate of the cooled specimens (“S, 20-10 ºC” beyond 13.5 hours) is lower than that of the not cooled specimens (Fig. 9.5). Different drying forces in terms of different vapour pressures may explain this: When the concrete and air temperature is equal (here 20 ºC) and the RH of the surrounding air is 50 %, the vapour pressure gradient is 2 to 1 (i.e. 17.5 torr x 100 % RH to 17.5 torr x 50 % RH). When the concrete temperature is 10 ºC and air temperature is 20 ºC (50% RH), the vapour pressure over pore water is 9.2 torr at 100 %, while it is 17.5 torr x 50 % = 8.8 torr in the air, i.e. roughly 1 to 1. Thus, there is no significant drying taking place, which is reflected in Fig 9.. in that shrinkage rate of “exposed” concretes are lower at 10 °C than at 20 °C.

Note that the strain capacity beyond 10 hours of age, which is between 170 and 420 μstrain, see Fig. 9.3, is in the same range as the maximum “free strain” (shrinkage), see Fig. 9.5. Thus, a strain vs strain capacity assessment suggests a rather high possibility of cracking.

9.4.4 Stress generation

The stress generation, shown in Fig. 9.6, reflects very well the volume change evolution, as expected. The drying of the top surface causes an additional tensile stress of approximately 0.3 MPa (“ES, 20 ºC” - “S, 20 ºC”), and the cooling (“S, 20-10 ºC“) some more. Note that the stress generation of the cooled specimen levels out (beyond 13.5 hours), which is due to low shrinkage (see previous section) and relaxation. The combined effect of drying and cooling superposes nicely until the specimen fails at 13 hours of age, except for a slight time difference (approximately 1 hour) between the “drying-curves” (“ES, 20-10 ºC” and “ES, 20 ºC”). The time difference is apparently a result of different points for activation of the feedback system of the TSTM: In the “ES, 20-10 ºC”-test, it was activated at approximately 8 hours of age, and at approximately 9 hours of age in the “ES, 20 ºC”-test. Previous results (Bjøntegaard, 2000) have shown that when the feedback system is activated around the time of setting, it may influence the stress generation shortly after erroneously. Nevertheless, the main point is that the stress generated from the given drying and cooling corresponds roughly

in magnitude and time, with the tensile strength development (note that the time of failure corresponds to only about 5 ºC cooling). This correspondence indicates that the risk of cracking of HSC in this period is high, as found in practice, if proper actions against drying/cooling are not used. Furthermore, it demonstrates that the present methodology is a good tool for studying the cracking risk in this period.

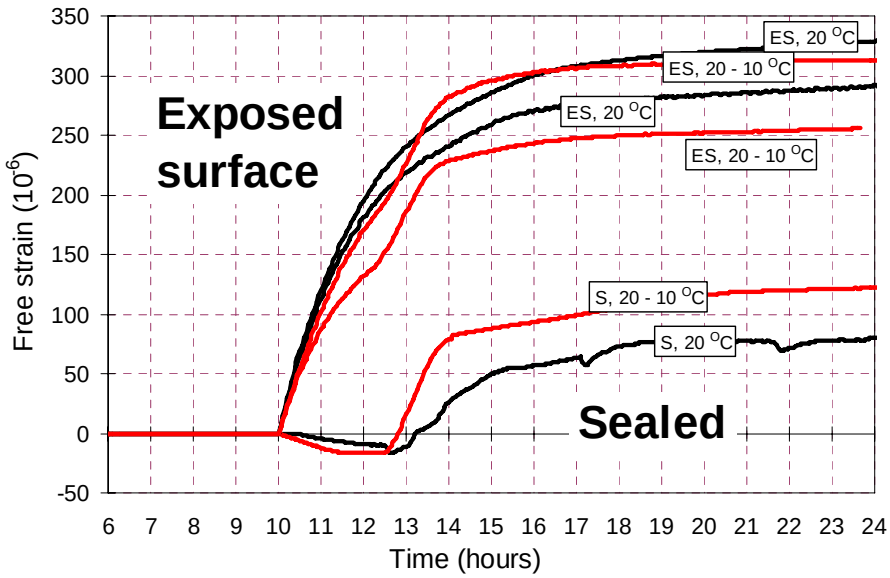

Fig. 9.5 Deformations under various exposure conditions: Sealed ("S", 20 ºC), sealed and cooled ("S, 20-10 ºC"), exposed to air ("ES, 20 ºC") and exposed to air and cooled ("ES, 20-10 ºC"). Two parallel tests are shown for "ES, 20 ºC" and for "ES, 20-10 ºC"

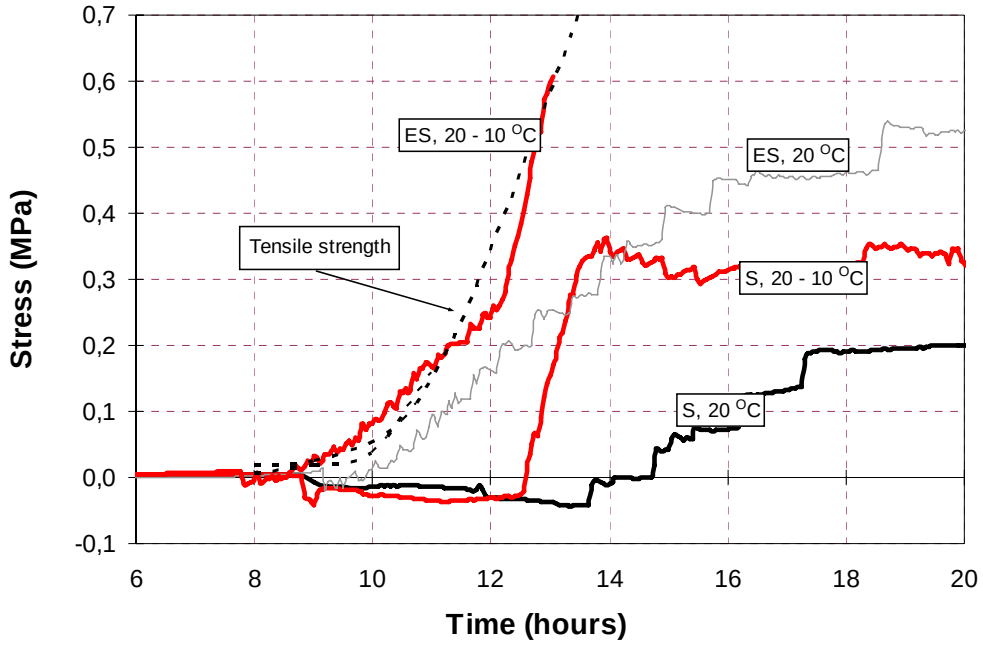

Fig. 9.6 Self generated stress and uniaxial tensile strength. Sealed ("S", 20 ºC), sealed and cooled ("S, 20-10 ºC"), exposed to air ("ES, 20 ºC") and exposed to air and cooled ("ES, 20-10 ºC"). Two parallel tests are shown for "ES, 20 ºC"and for "ES, 20-10 ºC"

9.5 Conclusion

A promising methodology has been developed to measure volume change, tensile strain capacity, stress generation and tensile strength evolution, in order to assess the risk of cracking in the period of setting and early hardening.

The results confirm that early hardening age is a critical time period for cracking of horizontal surfaces of HSC. It is shown that the deformation of HSC-surfaces in the period caused by moderate drying (here 20 ºC and 50 % RH) combined with a moderate cooling (here approximately 5 ºC), generate restraining stress that may exceed the tensile strength, and thus, generate failure.

The results indicate that crack risk assessment from stress/strength is more reliable than using strain/strain capacity.

10. References

Acker, P: Swelling, shrinkage and creep: a mechanical approach yo cement hydration. Materials and Structures, Vol. 37, May 2004, pp237-243.

Barcelo, L., Boivin, S., Acker, P., Toupin, J. and Clavaud, B., 2001: Early age shrinkage of concrete: Bach to physical mechanisms". Concrete Science and Engineering, June 2001, Vol.3 – No 10.

Barcelo, L., Boivin, S., Rigaud, S., Acker, P. and Clauvaud, B., 1999: Linear vs volumetric autogenous shrinkage measurements: Material behaviour or experimental artefact. Proceedings of the second intn. research seminar on self-desiccation and its importance in concrete technology (ed. B. Persson and G. Fagerlund). Lund, Sweden 1999.

Bjøntegaard, Ø., 2000: Thermal Dilation and Autogenous Deformation as Driving Forces to Self.Induced Stresses in High Performance Concrete. Doctor theses from the Norwegian Institute of Science and Technology, Trondheim, Norway.

Bjøntegaard, Ø., Hammer, T.A. and Sellevold, E.J., 1998: Cracking in High Performance Concrete before Setting; Presented at the International Symposium on High-Performance and Reactive Powder Concretes, Sherbrooke, Canada, 1998, Volume 1, pp. 1-18.

Brüll, L. and Komlős, K. and Majzlan, B., 1982: Early age shrinkage of cement pastes, mortars and concretes. Materials and Structures, Vol. 13 – No 73, Rilem 1980, pp. 41 – 45.

Brüll, L. and Komlős, K., 1982: Early volume change of cement pastes and cement mortars. International conference on concrete of early ages, Paris, Rilem Proceedings, April 1982, pp. 29 – 34.

Buil, M. and Baron, J., 1982: Le retrait autogène de la pâte de ciment durcissante. Bulletin de liaison des laboratoires des ponts et chaussée, No 117, Jan - Feb 1982, pp. 65 – 70.

Byfors, J., 1980: Plain concrete at early ages, CBI-report 3:80, Swedish Cement and Concrete Research Institute.

Fosså, K.T., 2001: Slipforming of Vertical Concrete Structures – Friction between concrete and slipform panel', Dr.ing thesis, Department of Structural Engineering, The Norwegian University of technology, 2001, ISBN 82-471-8325-4.

Geiker, M., 1984: Studies of Portland cement hydration. Measurements of chemical shrinkage and systematic evaluation hydration curves by means of dispersion model, Ph.D. Thesis, Technical University of Denmark, 1984.

Hammer, T.A., Bjøntegaard, Ø and Sellevold, E.J., 2004: Internal curing - role of absorbed water in aggregates. Proceedings of the symposium on High-Performance Structural Lightweight Concrete at ACI fall Convention, 2002. ACI international SP-218 (ed. J.P. Ries and T.E. Holm).

Hanehara, S., Hirao, H. and Uchikawa, H., 1999: Relationships between autogenous shrinkage, the microstructure and humidity changes at inner part of hardened cement paste at early ages. Autogenous Shrinkage of Concrete. Proceedings of an intn. workshop 1998 (ed. Ei-ichi Tazawa). E & FN Spon, London 1999.

Hannant, D.J., Branch, J. and Mulheron, M, 1999: Equipment for tensile testing of fresh concrete. Magazine of Concrete Research, No. 4, Aug. pp263-267.

Holt, E.E. and Leivo, M.T., 1999: Autogenous shrinkage at very early ages". Autogenous Shrinkage of Concrete. Proceedings of an intn. workshop 1998 (ed. Ei-ichi Tazawa). E & FN Spon, London 1999.

Jensen O.M., 1993: Autogen Deformation og RF-ændring (autogenous deformation and RH-development). Thesis for the degree of Doctor of Engineering from the Technical University of Denmark, Copenhagen, 1993.

Jensen, O.M., Christensen, S.L., Dela, B.F., Hansen, J.H., Hansen P.F. and Nielsen, A., 1997: HETEK Control of early age cracking of concrete phase 2: Shrinkage and concrete. Report No. 110 1997, Road Directorate Denmark Ministry of Transport.

Johansen, R, and dahl, P.A., 1993: Control of plastic shrinkage of cement. Proceedings of 18th Conference on Our World in Concrete and Structures, Singapore.

Justnes, H., Reyniers, B. and Sellevold, E.J., 1994: An evaluation of methods for measuring chemical shrinkage of cementitious pastes. Nordic Concrete Research, publication no. 14. 1/94, Norwegian Concrete Association, Oslo pp. 44 – 61.

Justnes, H., Hammer, T.A., Ardouille, B., Hendrix, E., Van Gemert, D., Overmeer, K. and Sellevold, E.J., 1999: "Chemical Shrinkage of Cement Paste, Mortar and Concrete", (ed. E Tazawa), E & FN Spon, London. pp. 201-211.

Justnes, H., Sellevold, E.J., Reyniers, B., van Loo, D. and Verboven, F., 1999: The influence of cement characteristics on chemical shrinkage. Proceedings of Autogenous shrinkage of concrete (ed. E Tazawa), E & FN Spon, London

Justnes, H., van Gemert, A., Verboven, F. and Sellevold, E.J., 1996: Total and External Chemical Shrinkage of low w/c Ratio Cement Pastes. Advances in Cement Research, 1996, 8, No. 31, July, pp. 121 – 126.

Justnes, H., Clemmens, F., Depuydt, P., Van Gemert, D. and Sellevold, E.J., 2000: Correlating the deviation point between external and total chemical shrinkage with setting time and other characteristics of hydrating cement pastes. RILEM proceedings Pro17; "Shrinkage of concrete", Proceedings of the International RILEM workshop Shrinkage 2000, 16-17 October 2000, Paris, France, 17 pp.

Justnes, H., Sellevold, E.J., Van Gemert, D., Van Gemert, A. and Verboven, F., 2000: Influence of Plasticizers and Super-plasticizers on Chemical Shrinkage of Cement, Proceedings of the Sixth International Conference on Superplasticizers and Other Chemical Admixtures in Concrete, Nice, France, 11-13 October 2000, CANMET/ACI SP-195, pp. 601-614.

Kanstad T., Hammer, T.A., Bjøntegaard, Ø. and Sellevold, E.J., 2003: Mechanical properties of young concrete: Part 1: Experimental results related to the test methods and temperature effects. Materials and Structures, Vol. 36, May 2003, pp218-225.

Kasai, Y., Yokoyama, K. and Matsui, I., 1972: Tensile Properties of Early-Age Concrete; Presented at the International Conference on Mechanical Behaviour of Materials, The Society of Materials Science, Japan, 1972, Volume IV, pp. 288-299.

Kasai, Y., Yokoyama, K., Matsui, I. and Tobinai, K., 1974: Tensile properties of early-age concrete. Proceedings of the 1974 Symposium on Mechanical Behaviour of Materials, The Society of Materials Science, Japan, 1974, Volume II, pp. 433-444.

Kasai, Y., Matsui, I. and Yokoyama, K., 1982: Volume change of concrete at early ages. International conference on concrete of early ages, Paris, Rilem Proceedings, April 1982, pp. 51 - 56.

Kjellsen, K.O. and Lagerblad, B., 2006: Microstructure of tricalcium and Portland cement systems at middle periods of hydration-development of Hadley grains. Article in press, to be bublished in Cement and Concrete Research Volume 37, Issue 1, January 2007, Pages 13-20.

Kompen, R., 1994: High performance concrete: Field observations of cracking tendency at early ages, in proceedings of the International Rilem Symposium: Thermal Cracking in Concrete at Early Ages, Munich, Rilem Proceedings 25, Oct. 1995, pp. 449-456.

Komlos, K: Tensile strength investigation of fresh and hardening concrete. RILEM Symposdium, October 1964, Trondheim, Norway.

Lura, P. and Jensen, O.M., 2005: Measuring techniques for autogenous strain of cement paste. Proceedings of the Knud Højgaard conference on Advanced Cement-Based Materials - Research and Teaching, Technical University of Denmark, 12-15 June.

Morioka, M., Hori, A., Hagiwara, H., Sakai, E. and Daimon, M., 1998: Measurement of autogenous length changes by laser sensors equipped with digital computer systems. Autogenous Shrinkage of Concrete. Proceedings of an intn. workshop 1998 (ed. Ei-ichi Tazawa). E & FN Spon, London 1999.

Orr and Haig: An apparatus for measuring the shrinkage characteristics of plastic mortars. Magazine of Concrete research, 23 (1971) :74, pp43-48.

Pauluni, P., 1992: A weighing method for cement hydration. 9'th international conference on the chemistry of cement, vol 3, New Dehli 1992, pp. 248 – 254.

Powers, T.C and Brownyard, T.L., 1948: Studies of the physical properties of hardened Portland cement paste. Bulletin 22, Research Laboratories of the Portland Cement Association, Chicago, 1948.

Powers, T.C., 1968: The Properties of Fresh Concrete. John Wiley & Sons Inc., 1968.

Radocea, A., 1992: A Study on the Mechanism of Plastic Shrinkage of Cement-based Materials, Thesis for the degree of Doctor of Engineering from Chalmers Technical University, Gothenburg, Sweden.

Ravina, D., 1986: Early longitudinal dimensional changes of fresh fly ash mortar exposed to drying conditions. Cement and Concrete Research, Vol. 16, 1986, pp 902 – 910.
Setter, N. and Roy, D.M.,1978: Mechanical features of chemical shrinkage of cement paste. Cement and Concrete Research, Vol 8, 1978, pp. 623 – 634.

Setter, N. and Roy, D.M., 1978: Mechanical features of chemical shrinkage of cement paste. Cement and Concrete Research, Vol 8, 1978, pp. 623 – 634.

Slate, F.O. and Matheus, R.E., 1967: Volume changes on setting and curing of cement paste and Concrete from zero to seven days. ACI Journal, 1, 1967, pp. 34 – 39.

Smeplass, S., Hammer, T.A and Narum, T, 1992: Determination of the effective composition of LWA concretes. Nordic Concrete research Publication no 11-1992. The Norwegian Concrete association, Oslo 1992.

Takada, K., van Breugel, K., Koenders, A.A.B and Kaptjin, N., 1999: Experimental evaluation of autogenous shrinkage of lightweight aggregate concrete". Autogenous Shrinkage of Concrete. Proceedings of an intn. workshop 1998 (ed. Ei-ichi Tazawa). E & FN Spon, London 1999.

Wittman, F.H., 1976: On the Action of Capillary Pressure in Fresh Concrete'. Cement and Concrete Research, Vol 6, pp 49 – 56.

Weigler, Karl: Junger Betong – Beanspruchung – Festigkeit – Verformung. Forshungsberichte as dem Institute für Massivbau der Technische Hochschule Darmstadt, 1974. Nr 20, 55p.

Ziegeldorf, S. and Hilsdorf, H.K., 1980: Early Autogenous Shrinkage of Cement Pastes. 7'th international conference on the chemistry of cement, vol 4, Paris 1980, pp. 333 – 338.

APPENDIX Materials and Recipes

Materials

Cements: From Norcem, Norway

Constituent	*Name of cement (all from Norcem, Brevik)*			
	Anlegg-sement	***Standard-sement***	***Standard-sement FA***	***Industri-sement***
C_3S	60	60	60	60
C_2S	19	15	15	14
C_3A	6	7.5	7.4	8
C_4AF	10	10	10	10
Alkalis (eqv. Na_2O)	0.55	0.95	0.85	1.15
Fly ash	0	0	20%	0
Fineness (m^2/kg)	360	345	400	520
Specific weight (kg/dm^3)	3.12	3.12	2.95	3.12
Type	CEM I-52.5 LA	CEM I-42.5 R	CEM II/A-V-42.5 R	CEM I-42.5 RR

Silica fume:
Compacted, from Elkem, Bremanger, Norway. Always added as dry material

Admixtures:
Scancem P: Lignosulfonate based plasticizer
Mighty 150: Naphtalene based superplasticizer
Viscocrete 3: Polycarboxyleter based superpalsticizer
Glenium 27: Polycarboxyleter based superpalsticizer
SIKA AER: Tensid based air entraining admixture
Scancem ScanGuard: Alcohol based shrinkage reducing admixture

Aggregate:
Gneiss/granite, mostly gravel, from Årdal, Norway. Three fractions composed to fit the target grading curve shown below

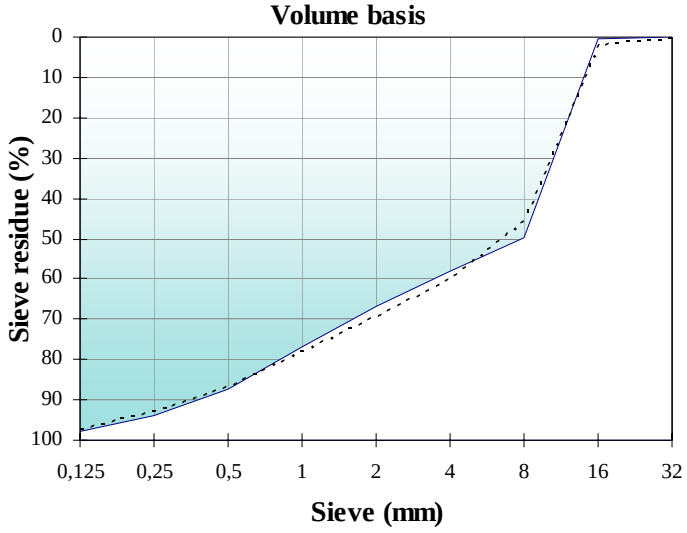

Lightweight aggregate for Leca, Norway. Grain size 4-12 mm, particle density of 1300 kg/m^3

Nominal recipes (kg/m^3) based on the ”Basic concrete (ANL0405)

Materials	Notation										
	Basic	LS	SNF	Copol 1	Copol 2	0 % SF	10 % SF	15 % SF	SRA	Dry LWA	Wet LWA
Cement	368	368	368	368	368	390	350	331	368	368	368
Silica fume	18	18	18	18	18	-	35	50	18	18	18
Water	155	155	155	155	155	156	153	152	155	155*	155
	-	-	-	-	-	-	-	-	-		-
0-2 mm aggr.	204	204	204	204	204	204	204	204	204	204	204
0-8 mm aggr.	751	751	751	751	751	751	751	751	751	466	466
8-16 mm aggr.	901	901	901	901	901	901	901	901	901	-	-
4-12 mm LWA	-	-	-	-	-	-	-	-	-	577	652
Scancem P	2.0	5.5	-	-	-	2.0	2.0	2.0	2.0	2.0	2.0
Mighty 150	3.1	-	4.5	-	-	3.1	4.2	5.5	3.1	3.1	3.1
Glenium 27	-	-	-	2.8	4.6	-	-	-	-	-	-
ScanGuard	-	-	-	-	-	-	-	-	11.0	-	-

* + 40 kg/m^3 of water to compensate mix water absorption of the dry LWA

Nominal recipes (kg/m^3) for concretes with various w/b and cement types

Materials	Notation											
	ANL 0305	ANL 0405	ANL 0605	STD 0305	STD 0405	STD 0605	STDFA 0405	STDFA 0605	IND 0405	IND 0605	ANL 3505	ANL 3505 AEA
Cement	426	368	289	426	368	289	348	273	368	289	395	384
Silica fume	21	18	14	21	18	14	18	14	18	14	20	19
Water	134	155	182	134	155	182	155	182	155	182	145	141
0-2 mm aggr.	204	204	204	204	204	204	204	204	204	204	204	204
0-8 mm aggr.	751	751	751	751	751	751	751	751	751	751	751	751
8-16 mm aggr.	901	901	901	901	901	901	901	901	901	901	901	901
Scancem P	2.2	2.0	1.5	2.2	2.0	1.5	2.0	1.5	2.0	1.5	2.0	2.0
Mighty 150	7.0	3.1	-	7.0	3.1	-	4.0	1.0	4.5	1.5	5.1	5.1
SIKA AER	-	-	-	-	-	-	-	-	-	-	-	0.8

Nominal recipes (kg/m^3) of SCC

Materials	Notation			
	REF w/b=0.60, w/p=0.55	SCC w/b=0.60, w/p=0.35	SCC w/b=0.50, w/p=0.35	SCC w/b=0.40, w/p=0.35
Norcem STDFA	319	268	323	405
Lime stone filler	-	129	77	-
Water	192	161	161	162
0-2 mm aggr.	147	147	147	147
0-8 mm aggr.	816	816	816	816
8-16 mm aggr.	854	854	854	854
Viscocrete 3	1.0	2.8	3.9	4.6

DEPARTMENT OF STRUCTURAL ENGINEERING
NORWEGIAN UNIVERSITY OF SCIENCE AND TECHNOLOGY

N–7491 TRONDHEIM, NORWAY
Telephone: +47 73 59 47 00 Telefax: +47 73 59 47 01

"Reliability Analysis of Structural Systems using Nonlinear Finite Element Methods",
C. A. Holm, 1990:23, ISBN 82-7119-178-0.

"Uniform Stratified Flow Interaction with a Submerged Horizontal Cylinder",
Ø. Arntsen, 1990:32, ISBN 82-7119-188-8.

"Large Displacement Analysis of Flexible and Rigid Systems Considering Displacement-Dependent Loads and Nonlinear Constraints", K. M. Mathisen, 1990:33, ISBN 82-7119-189-6.

"Solid Mechanics and Material Models including Large Deformations",
E. Levold, 1990:56, ISBN 82-7119-214-0, ISSN 0802-3271.

"Inelastic Deformation Capacity of Flexurally-Loaded Aluminium Alloy Structures",
T. Welo, 1990:62, ISBN 82-7119-220-5, ISSN 0802-3271.

"Visualization of Results from Mechanical Engineering Analysis",
K. Aamnes, 1990:63, ISBN 82-7119-221-3, ISSN 0802-3271.

"Object-Oriented Product Modeling for Structural Design",
S. I. Dale, 1991:6, ISBN 82-7119-258-2, ISSN 0802-3271.

"Parallel Techniques for Solving Finite Element Problems on Transputer Networks",
T. H. Hansen, 1991:19, ISBN 82-7119-273-6, ISSN 0802-3271.

"Statistical Description and Estimation of Ocean Drift Ice Environments",
R. Korsnes, 1991:24, ISBN 82-7119-278-7, ISSN 0802-3271.

“Properties of concrete related to fatigue damage: with emphasis on high strength concrete”,
G. Petkovic, 1991:35, ISBN 82-7119-290-6, ISSN 0802-3271.

"Turbidity Current Modelling",
B. Brørs, 1991:38, ISBN 82-7119-293-0, ISSN 0802-3271.

"Zero-Slump Concrete: Rheology, Degree of Compaction and Strength. Effects of Fillers as Part Cement-Replacement",
C. Sørensen, 1992:8, ISBN 82-7119-357-0, ISSN 0802-3271.

"Nonlinear Analysis of Reinforced Concrete Structures Exposed to Transient Loading",
K. V. Høiseth, 1992:15, ISBN 82-7119-364-3, ISSN 0802-3271.

"Finite Element Formulations and Solution Algorithms for Buckling and Collapse Analysis of Thin Shells", R. O. Bjærum, 1992:30, ISBN 82-7119-380-5, ISSN 0802-3271.

"Response Statistics of Nonlinear Dynamic Systems",
J. M. Johnsen, 1992:42, ISBN 82-7119-393-7, ISSN 0802-3271.

"Digital Models in Engineering. A Study on why and how engineers build and operate digital models for decisison support", J. Høyte, 1992:75, ISBN 82-7119-429-1, ISSN 0802-3271.

"Sparse Solution of Finite Element Equations",
A. C. Damhaug, 1992:76, ISBN 82-7119-430-5, ISSN 0802-3271.

"Some Aspects of Floating Ice Related to Sea Surface Operations in the Barents Sea",
S. Løset, 1992:95, ISBN 82-7119-452-6, ISSN 0802-3271.

"Modelling of Cyclic Plasticity with Application to Steel and Aluminium Structures",
O. S. Hopperstad, 1993:7, ISBN 82-7119-461-5, ISSN 0802-3271.

"The Free Formulation: Linear Theory and Extensions with Applications to Tetrahedral Elements
with Rotational Freedoms", G. Skeie, 1993:17, ISBN 82-7119-472-0, ISSN 0802-3271.

"Høyfast betongs motstand mot piggdekkslitasje. Analyse av resultater fra prøving i Veisliter'n",
T. Tveter, 1993:62, ISBN 82-7119-522-0, ISSN 0802-3271.

"A Nonlinear Finite Element Based on Free Formulation Theory for Analysis of Sandwich Structures", O. Aamlid, 1993:72, ISBN 82-7119-534-4, ISSN 0802-3271.

"The Effect of Curing Temperature and Silica Fume on Chloride Migration and Pore Structure of High Strength Concrete", C. J. Hauck, 1993:90, ISBN 82-7119-553-0, ISSN 0802-3271.

"Failure of Concrete under Compressive Strain Gradients",
G. Markeset, 1993:110, ISBN 82-7119-575-1, ISSN 0802-3271.

"An experimental study of internal tidal amphidromes in Vestfjorden",
J. H. Nilsen, 1994:39, ISBN 82-7119-640-5, ISSN 0802-3271.

"Structural analysis of oil wells with emphasis on conductor design",
H. Larsen, 1994:46, ISBN 82-7119-648-0, ISSN 0802-3271.

"Adaptive methods for non-linear finite element analysis of shell structures",
K. M. Okstad, 1994:66, ISBN 82-7119-670-7, ISSN 0802-3271.

"On constitutive modelling in nonlinear analysis of concrete structures",
O. Fyrileiv, 1994:115, ISBN 82-7119-725-8, ISSN 0802-3271.

"Fluctuating wind load and response of a line-like engineering structure with emphasis on motion-induced wind forces",

J. Bogunovic Jakobsen, 1995:62, ISBN 82-7119-809-2, ISSN 0802-3271.

"An experimental study of beam-columns subjected to combined torsion, bending and axial actions", A. Aalberg, 1995:66, ISBN 82-7119-813-0, ISSN 0802-3271.

"Scaling and cracking in unsealed freeze/thaw testing of Portland cement and silica fume concretes", S. Jacobsen, 1995:101, ISBN 82-7119-851-3, ISSN 0802-3271.

"Damping of water waves by submerged vegetation. A case study of laminaria hyperborea", A. M. Dubi, 1995:108, ISBN 82-7119-859-9, ISSN 0802-3271.

"The dynamics of a slope current in the Barents Sea",
Sheng Li, 1995:109, ISBN 82-7119-860-2, ISSN 0802-3271.

"Modellering av delmaterialenes betydning for betongens konsistens",
Ernst Mørtsell, 1996:12, ISBN 82-7119-894-7, ISSN 0802-3271.

"Bending of thin-walled aluminium extrusions",
Birgit Søvik Opheim, 1996:60, ISBN 82-7119-947-1, ISSN 0802-3271.

"Material modelling of aluminium for crashworthiness analysis",
Torodd Berstad, 1996:89, ISBN 82-7119-980-3, ISSN 0802-3271.

"Estimation of structural parameters from response measurements on submerged floating tunnels",
Rolf Magne Larssen, 1996:119, ISBN 82-471-0014-2, ISSN 0802-3271.

“Numerical modelling of plain and reinforced concrete by damage mechanics”,
Mario A. Polanco-Loria, 1997:20, ISBN 82-471-0049-5, ISSN 0802-3271.

“Nonlinear random vibrations - numerical analysis by path integration methods”,
Vibeke Moe, 1997:26, ISBN 82-471-0056-8, ISSN 0802-3271.

“Numerical prediction of vortex-induced vibration by the finite element method”,
Joar Martin Dalheim, 1997:63, ISBN 82-471-0096-7, ISSN 0802-3271.

“Time domain calculations of buffeting response for wind sensitive structures”,
Ketil Aas-Jakobsen, 1997:148, ISBN 82-471-0189-0, ISSN 0802-3271.

"A numerical study of flow about fixed and flexibly mounted circular cylinders",
Trond Stokka Meling, 1998:48, ISBN 82-471-0244-7, ISSN 0802-3271.

“Estimation of chloride penetration into concrete bridges in coastal areas”,
Per Egil Steen, 1998:89, ISBN 82-471-0290-0, ISSN 0802-3271.

“Stress-resultant material models for reinforced concrete plates and shells”,
Jan Arve Øverli, 1998:95, ISBN 82-471-0297-8, ISSN 0802-3271.

“Chloride binding in concrete. Effect of surrounding environment and concrete composition”,
Claus Kenneth Larsen, 1998:101, ISBN 82-471-0337-0, ISSN 0802-3271.

“Rotational capacity of aluminium alloy beams”,
Lars A. Moen, 1999:1, ISBN 82-471-0365-6, ISSN 0802-3271.

“Stretch Bending of Aluminium Extrusions”,
Arild H. Clausen, 1999:29, ISBN 82-471-0396-6, ISSN 0802-3271.

“Aluminium and Steel Beams under Concentrated Loading”,
Tore Tryland, 1999:30, ISBN 82-471-0397-4, ISSN 0802-3271.

"Engineering Models of Elastoplasticity and Fracture for Aluminium Alloys",
Odd-Geir Lademo, 1999:39, ISBN 82-471-0406-7, ISSN 0802-3271.

"Kapasitet og duktilitet av dybelforbindelser i trekonstruksjoner",
Jan Siem, 1999:46, ISBN 82-471-0414-8, ISSN 0802-3271.

“Etablering av distribuert ingeniørarbeid; Teknologiske og organisatoriske erfaringer fra en norsk ingeniørbedrift”, Lars Line, 1999:52, ISBN 82-471-0420-2, ISSN 0802-3271.

“Estimation of Earthquake-Induced Response”,
Símon Ólafsson, 1999:73, ISBN 82-471-0443-1, ISSN 0802-3271.

“Coastal Concrete Bridges: Moisture State, Chloride Permeability and Aging Effects”
Ragnhild Holen Relling, 1999:74, ISBN 82-471-0445-8, ISSN 0802-3271.

”Capacity Assessment of Titanium Pipes Subjected to Bending and External Pressure”,
Arve Bjørset, 1999:100, ISBN 82-471-0473-3, ISSN 0802-3271.

“Validation of Numerical Collapse Behaviour of Thin-Walled Corrugated Panels”,
Håvar Ilstad, 1999:101, ISBN 82-471-0474-1, ISSN 0802-3271.

“Strength and Ductility of Welded Structures in Aluminium Alloys”,
Miroslaw Matusiak, 1999:113, ISBN 82-471-0487-3, ISSN 0802-3271.

“Thermal Dilation and Autogenous Deformation as Driving Forces to Self-Induced Stresses in High Performance Concrete”,
Øyvind Bjøntegaard, 1999:121, ISBN 82-7984-002-8, ISSN 0802-3271.

“Some Aspects of Ski Base Sliding Friction and Ski Base Structure”,
Dag Anders Moldestad, 1999:137, ISBN 82-7984-019-2, ISSN 0802-3271.

"Electrode reactions and corrosion resistance for steel in mortar and concrete",
Roy Antonsen, 2000:10, ISBN 82-7984-030-3, ISSN 0802-3271.

"Hydro-Physical Conditions in Kelp Forests and the Effect on Wave Damping and Dune Erosion. A case study on Laminaria Hyperborea",
Stig Magnar Løvås, 2000:28, ISBN 82-7984-050-8, ISSN 0802-3271.

"Random Vibration and the Path Integral Method",
Christian Skaug, 2000:39, ISBN 82-7984-061-3, ISSN 0802-3271.

"Buckling and geometrical nonlinear beam-type analyses of timber structures",
Trond Even Eggen, 2000:56, ISBN 82-7984-081-8, ISSN 0802-3271.

”Structural Crashworthiness of Aluminium Foam-Based Components”,
Arve Grønsund Hanssen, 2000:76, ISBN 82-7984-102-4, ISSN 0809-103X.

“Measurements and simulations of the consolidation in first-year sea ice ridges, and some aspects of mechanical behaviour”, Knut V. Høyland, 2000:94, ISBN 82-7984-121-0, ISSN 0809-103X.

”Kinematics in Regular and Irregular Waves based on a Lagrangian Formulation”,
Svein Helge Gjøsund, 2000-86, ISBN 82-7984-112-1, ISSN 0809-103X.

”Self-Induced Cracking Problems in Hardening Concrete Structures”,
Daniela Bosnjak, 2000-121, ISBN 82-7984-151-2, ISSN 0809-103X.

"Ballistic Penetration and Perforation of Steel Plates",
Tore Børvik, 2000:124, ISBN 82-7984-154-7, ISSN 0809-103X.

"Freeze-Thaw resistance of Concrete. Effect of: Curing Conditions, Moisture Exchange and Materials", Terje Finnerup Rønning, 2001:14, ISBN 82-7984-165-2, ISSN 0809-103X

Structural behaviour of post tensioned concrete structures. Flat slab. Slabs on ground",
Steinar Trygstad, 2001:52, ISBN 82-471-5314-9, ISSN 0809-103X.

"Slipforming of Vertical Concrete Structures. Friction between concrete and slipform panel",
Kjell Tore Fosså, 2001:61, ISBN 82-471-5325-4, ISSN 0809-103X.

"Some numerical methods for the simulation of laminar and turbulent incompressible flows",
Jens Holmen, 2002:6, ISBN 82-471-5396-3, ISSN 0809-103X.

“Improved Fatigue Performance of Threaded Drillstring Connections by Cold Rolling”,
Steinar Kristoffersen, 2002:11, ISBN: 82-421-5402-1, ISSN 0809-103X.

"Deformations in Concrete Cantilever Bridges: Observations and Theoretical Modelling",
Peter F. Takâcs, 2002:23, ISBN 82-471-5415-3, ISSN 0809-103X.

"Stiffened aluminium plates subjected to impact loading",
Hilde Giæver Hildrum, 2002:69, ISBN 82-471-5467-6, ISSN 0809-103X.

"Full- and model scale study of wind effects on a medium-rise building in a built up area",
Jónas Thór Snæbjørnsson, 2002:95, ISBN82-471-5495-1, ISSN 0809-103X.

“Evaluation of Concepts for Loading of Hydrocarbons in Ice-infested water”,
Arnor Jensen, 2002:114, ISBN 82-417-5506-0, ISSN 0809-103X.

”Numerical and Physical Modelling of Oil Spreading in Broken Ice”,
Janne K. Økland Gjøsteen, 2002:130, ISBN 82-471-5523-0, ISSN 0809-103X.

”Diagnosis and protection of corroding steel in concrete”,
Franz Pruckner, 20002:140, ISBN 82-471-5555-4, ISSN 0809-103X.

“Tensile and Compressive Creep of Young Concrete: Testing and Modelling”,
Dawood Atrushi, 2003:17, ISBN 82-471-5565-6, ISSN 0809-103X.

“Rheology of Particle Suspensions. Fresh Concrete, Mortar and Cement Paste with Various Types of Lignosulfonates”,
Jon Elvar Wallevik, 2003:18, ISBN 82-471-5566-4, ISSN 0809-103X.

“Oblique Loading of Aluminium Crash Components”, Aase Reyes, 2003:15, ISBN 82-471-5562-1, ISSN 0809-103X.

“Utilization of Ethiopian Natural Pozzolans”, Surafel Ketema Desta, 2003:26,
ISSN 82-471-5574-5, ISSN:0809-103X.

“Behaviour and strength prediction of reinforced concrete structures with discontinuity regions”, Helge Brå, 2004:11, ISBN 82-471-6222-9, ISSN 1503-8181.

“High-strength steel plates subjected to projectile impact. An experimental and numerical study”, Sumita Dey, 2004:38, ISBN 82-471-6281-4 (elektr. Utg.), ISBN 82-471-6282-2 (trykt utg.),
ISSN 1503-8181.

“Alkali-reactive and inert fillers in concrete. Rheology of fresh mixtures and expansive reactions.”
Bård M. Pedersen, 2004:92, ISBN 82-471-6401-9 (trykt utg.), ISBN 82-471-6400-0 (elektr. utg.),
ISSN 1503-8181.

“On the Shear Capacity of Steel Girders with Large Web Openings”. Nils Christian Hagen, 2005:9 ISBN 82-471-6878-2 (trykt utg.), ISBN 82-471-6877-4 (elektr. utg.), ISSN 1503-8181.

”Behaviour of aluminium extrusions subjected to axial loading”. Østen Jensen, 2005:7, ISBN 82-471-6872-3 (elektr. utg.) , ISBN 82-471-6873-1 (trykt utg.), ISSN 1503-8181.

”Thermal Aspects of corrosion of Steel in Concrete”. Jan-Magnus Østvik, 2005:5, ISBN 82-471-6869-3 (trykt utg.) ISBN 82-471-6868 (elektr.utg), ISSN 1503-8181.

”Mechanical and adaptive behaviour of bone in relation to hip replacement.” A study of bone remodelling and bone grafting. Sébastien Muller, 2005:34, ISBN 82-471-6933-9 (trykt utg.) (ISBN 82-471-6932-0 (elektr.utg), ISSN 1503-8181.

“Analysis of geometrical nonlinearities with applications to timber structures”. Lars Wollebæk, 2005:74, ISBN 82-471-7050-5 (trykt utg.), ISBN 82-471-7019-1 (elektr. Utg.), ISSN 1503-8181.

“Pedestrian induced lateral vibrations of slender footbridges”, Anders Rönnquist, 2005:102, ISBN 82-471-7082-5 (trykt utg.), ISBN 82-471-7081-7 (elektr.utg.), ISSN 1503-8181.

“Initial Strength Development of Fly Ash and Limestone Blended Cements at Various Temperatures Predicted by Ultrasonic Pulse Velocity”, Tom Ivar Fredvik, 2005:112, ISBN 82-471-7105-8 (trykt utg.), ISBN 82-471-7103-1 (elektr.utg.), ISSN 1503-8181.

“Behaviour and modelling of thin-walled cast components”, Cato Dørum, 2005:128, ISBN 82-471-7140-6 (trykt utg.), ISBN 82-471-7139-2 (elektr. utg.), ISSN 1503-8181.

“Behaviour and modelling of selfpiercing riveted connections”, Raffaele Porcaro, 2005:165, ISBN 82-471-7219-4 (trykt utg.), ISBN 82-471-7218-6 (elektr.utg.), ISSN 1503-8181.

”Behaviour and Modelling og Aluminium Plates subjected to Compressive Load”, Lars Rønning,
2005:154, ISBN 82-471-7169-1 (trykt utg.), ISBN 82-471-7195-3 (elektr.utg.), ISSN 1503-8181

”Bumper beam-longitudinal system subjected to offset impact loading”, Satyanarayana Kokkula, 2005:193, ISBN 82-471-7280-1 (trykt utg.), ISBN 82-471-7279-8 (elektr.utg.), ISSN 1503-8181.

“Control of Chloride Penetration into Concrete Structures at Early Age”, Guofei Liu, 2006:46, ISBN 82-471-7838-9 (trykt utg.), ISBN 82-471-7837-0 (elektr. utgave), ISSN 1503-8181.

“Modelling of Welded Thin-Walled Aluminium Structures”, Ting Wang, 2006:78, ISBN 82-471-7907-5 (trykt utg.), ISBN 82-471-7906-7 (elektr.utg.), ISSN 1503-8181.

”Time-variant reliability of dynamic systems by importance sampling and probabilistic analysis of ice loads”, Anna Ivanova Olsen, 2006:139, ISBN 82-471-8041-3 (trykt utg.), ISBN 82-471-8040-5 (elektr.utg.), ISSN 1503-8181.

“Fatigue life prediction of an aluminium alloy automotive component using finite element analysis of surface topography”. Sigmund Kyrre Ås, 2006:25, ISBN 82-471-7791-9 (trykt utg.), ISBN 82-471-7791-9 (elektr.utg.), ISSN 1503-8181.

”Constitutive models of elastoplasticity and fracture for aluminium alloys under strain path change”, Dasharatha Achani, 2006:76, ISBN 82-471-7903-2 (trykt utg.), ISBN 82-471-7902-4 (elektr.utg.), ISSN 1503-8181.
“Simulations of 2D dynamic brittle fracture by the Element-free Galerkin method and linear fracture mechanics”, Tommy Karlsson, 2006:125, ISBN 82-471-8011-1 (trykt utg.), ISBN 82-471-8010-3 (elektr.utg.), ISSN 1503-8181.

“Penetration and Perforation of Granite Targets by Hard Projectiles”, Chong Chiang Seah, 2006:188, ISBN 82-471-8150-9 (printed ver.), ISBN 82-471-8149-5 (electronic ver.) ISSN 1503-8181.